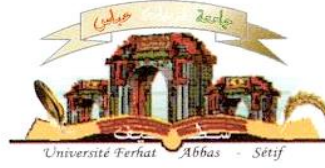


الجمهورية الجزائرية الديمقراطية الشعبية
وزارة التعليم العالي و البحث العلمي

Université Ferhat Abbas Sétif 1
Faculté des Sciences de la
Nature et de la Vie



جامعة فرحات عباس، سطيف 1
كلية علوم الطبيعة و الحياة

DEPARTMENT OF MICROBIOLOGY

N°...../SNV/2018

THESIS

Presented by

NOUMEUR Sara Raouia

For the fulfillment of the requirements for the degree of

DOCTORATE OF SCIENCES

IN BIOLOGY

Option: MICROBIOLOGY

TOPIC

**Identification of bioactive natural products from
endophytic fungi isolated from *Globularia alypum***

Presented publically in 02/07/2018

JURY

President	Mohamed Mihoub Zerroug	Pr. UFA Sétif 1
Supervisor	Daoud Harzallah	Pr. UFA Sétif 1
Examiners	Ammar Ayachi	Pr. Univ. Batna 1
	Tayeb Idoui	Pr. Univ. Jijel
	Marc Stadler	Pr. HZI (Germany)
Invited guest	Samia Mezaache-Aichour	MCA. UFA Sétif 1
	Soleiman Elsayed Helaly	Dr. Univ. Aswan (Egypt)

Laboratory of Applied Microbiology

ملخص

تعتبر الفطريات الداخلية مصدرا غنيا بالمركبات الطبيعية اكتسبتها من خلال العلاقة التكافئية بينها وبين النبات العائل، تم خلال هذه الدراسة معرفة التنوع البيولوجي للفطريات الداخلية المعزولة من جذور نبتة *Globularia alypum* (Plantaginaceae، Scrophulariales) التي تم جنيها من ولاية باتنة (الجزائر). أدت الدراسة الى عزل 17 سلالة فطرية و التي عرفت إلى مستوى النوع باستخدام خصائص مورفولوجية وتحاليل النشوء والتطور حيث مكنت هذه الأخيرة إلى انتماء الفطريات المعزولة إلى ثلاث فئات في شعبة Ascomycota: Eurotiomycetes، Dothideomycetes و Sordariomycetes و المتمثلة في تسعة أجناس: *Diaporthe*، *Dendrothyrium*، *Chaetomium*، *Aspergillus*، *Alternaria*، *Penicillium*، *Macrophomina*، *Fusarium* و *Preussia*. تم اختيار من بين الفطريات المعزولة ثمانية للتخمير على نطاق صغير في ثلاثة اوساط غذائية مختلفة. أثبتت المستخلصات المتحصل عليها نشاطا ضد ميكروبيا. بعدها تم تخمير خمسة فطريات: ثلاث سلالات من *Dendrothyrium variisporum*، *Preussia similis* و *Chaetomium madrasense* على نطاق اكبر. أدى هذا التخمير إلى عزل 28 مستقلب ثانوي من بينها 12 مركبا جديدا. تم التعرف على صيغة المركبات الكيميائية المعزولة بواسطة طرق طيفية 1D و 2D NMR spectroscopy، high-resolution mass spectrometry و CD spectroscopy. درست النشاطات البيولوجية للمركبات المعزولة سواء الجديدة منها أو المعروفة بشكل واسع. تم عزل 13 مركب من المعقد *Preussia similis* من بينها ستة مركبات جديدة: بوليكتايد ثنائية الحلقة تم تسميتها preussilides A-F ومركب جديد dimer of 2-amino benzoid acid moieties بالإضافة إلى مركبات أخرى معروفة مثل السايبتوكالازين ومشتقات الغزانتون. أظهرت A و C preussilide في اختبار preussilides A-F نشاطا مثبطا انتقائيا ضد حقيقيات النواة، تأثيرا على مورفولوجيا خلايا سرطان العظام. كما يستهدف هذا البوليكتايد إنزيم مسؤول على تنسيق دورة إنقسام الخلايا. أسفرت الدراسات التي أجريت على إنتاج المستقلبات الثانوية من فطر *Dendrothyrium variisporum* عن عزل 12 مركب، منها H و D Massarilactones كمركبين رئيسيين و2 من المشتقات الجديدة للفيرانون التي تم تسميتها (5S) و cis-gregatin B و graminin D بالإضافة إلى 3 مشتقات جديدة من حمض الأونتراليك، اثنين من نظائر حمض الأنترانيليك المعروفة وثلاثة سيكلوبنتيدس. أظهرت تجارب النشاط ضد ميكروبي أن للمركبين 2-phenylethyl-3-hydroxyanthranilate و 2-phenylethylanthranilate نشاطية تثبيطية ضد ميكروبية واسعة، في حين اظهر المركب تثبيطه لتكاثر الخلايا السرطانية HeLa أخيرا تم عزل 3 مركبات معروفة من

Chaetomium madrasense: A1، A3، xanthoquinodins و N-acetytryptamin.

كلمات مفتاحية: الفطريات الداخلية، التنوع البيولوجي، المستقلبات الثانوية، تعريف الصيغة الكيميائية،

Preussia similis، *Chaetomium madrasense*، *Dendrothyrium variisporum*

Abstract

The endophytic mycobiota constitute a prolific source of bioactive natural products that has evolved during the symbiotic endophyte–plant relationship. The diversity of fungal endophytes isolated from the roots of the plant *Globularia alypum* (Plantaginaceae, Scrophulariales) collected in Batna (Algeria) were studied in the present thesis. In total, seventeen fungal strains were isolated and identified to species level by means of morphological and molecular phylogenetic methods. The phylogenetic analysis of these fungal endophytes revealed their affinities to three classes of the phylum of Ascomycota: Eurotiomycetes, Dothideomycetes and Sordariomycetes representing nine genera: *Alternaria*, *Aspergillus*, *Chaetomium*, *Dendrothyrium*, *Diaporthe*, *Fusarium*, *Macrophomina*, *Penicillium* and *Preussia*. Among the isolated fungal endophytes, eight were selected for small scale fermentation in three different liquid media. Their extracts showed prominent antimicrobial activity in a screening for novel antibiotics by the serial dilution assay. A scale-up of fermentation of selected five fungi including three strains of *Chaetomium madrasense*, *Dendrothyrium variisporum* and *Preussia similis*, yielded twenty eight secondary metabolites, twelve of which turned out to be novel natural products. The structures of the isolated metabolites were elucidated using a combination of spectral methods, including 1D and 2D NMR spectroscopy, high-resolution mass spectrometry, and CD spectroscopy. The biological activities of both, the known and new compounds were extensively studied. Thirteen metabolites were isolated from the *Preussia similis* complex including six new bicyclic polyketides (for which the trivial names preussilides A–F are proposed) and one new dimer of 2 amino benzoid acid moieties, along with several known cytochalasins and xanthones derivatives. The preussilides were tested for antimicrobial and antiproliferative effects, and, in particular, preussilides A and C showed selective activities against eukaryotes. Subsequent studies on their influence on the morphology of human osteosarcoma cells (U2OS) suggest that these polyketides might target an enzyme involved in coordination of the cell division cycle. Hence, they might, for instance, affect timing or spindle assembly mechanisms, leading to defects in chromosome segregation and/or spindle geometry. Studies on the secondary metabolite production of *Dendrothyrium variisporum* in various culture media led to the isolation of twelve compounds. Massarilactones D and H were isolated as the major components as well as two new furanone derivatives for which we propose the trivial names (5S)-cis-gregatin B and graminin D, three new anthranilic acid derivatives, two known anthranilic acid analogues and three cyclopeptides. The new anthranilic acid derivatives, 2-phenylethyl-3-hydroxyanthranilate and 2-phenylethyl anthranilate exhibited antimicrobial activity while 2-phenylethyl anthranilate showed cytotoxicity against HeLa cells. Finally, from cultures of *Chaetomium madrasense*, three known compounds, xanthoquinodins A1, A3 and N-acetytryptamin were isolated.

Keywords: Fungal endophytes, biodiversity, *Globularia alypum*, secondary metabolites, *Preussia similis*, *Dendrothyrium variisporum*, *Chaetomium madrasense*, structure elucidation.

Résumé

Le mycobiote endophyte constitue une source riche de produits naturels bioactifs qui ont été développé au cours de la relation symbiotique endophyte-plante. La diversité des endophytes fongiques isolés à partir des racines de la plante *Globularia alypum* (Plantaginaceae, Scrophulariales), collectée à Batna, (Algérie), a été étudiée dans le présent travail. Au total, dix-sept souches fongiques ont été identifiées jusqu'au rang de l'espèce à l'aide de méthodes morphologiques et phylogénétiques. L'analyse phylogénétique de ces endophytes fongiques a révélé leurs affinités à trois classes du phylum d'Ascomycota: Eurotiomycètes, Dothideomycètes et, Sordariomycètes représentées par neuf genres: *Alternaria*, *Aspergillus*, *Chaetomium*, *Dendrothyrium*, *Diaporthe*, *Fusarium*, *Macrophomina*, *Penicillium* et *Preussia*. Parmi les endophytes fongiques isolés, huit ont été sélectionnés pour une fermentation à petite échelle dans trois milieux liquides différents. Leurs extraits ont montré une activité antimicrobienne importante au cours du screening pour de nouveaux antibiotiques par le test de dilution en série. La fermentation à grande échelle de cinq champignons sélectionnés, y compris trois souches de *Preussia similis*, *Dendrothyrium variisporum* et *Chaetomium madrasense*, a donné vingt-huit métabolites secondaires, dont douze ont été identifiés comme nouveaux produits naturels. Les structures des métabolites isolés ont été élucidées en utilisant une combinaison de méthodes spectrales, y compris la spectroscopie RMN 1D et 2D, la spectrométrie de masse à haute résolution et la spectroscopie CD. Les activités biologiques des composés connus et nouveaux ont été largement étudiées. Treize métabolites ont été isolés du complexe *Preussia similis*, y compris six nouveaux polycétides bicycliques (pour lesquels les noms triviaux preussilides A-F ont été proposés) et un nouveau dimère de l'acide 2-amino benzoïque, ainsi que plusieurs autres métabolites connus comme les cytochalasines et des dérivés de xanthone. Les preussilides ont été testés pour leurs effets antimicrobiens et antiprolifératifs et, en particulier, les preussilides A et C qui ont montré des activités sélectives contre les eucaryotes. Des études ultérieures sur leur influence sur la morphologie des cellules d'ostéosarcome humain (U2OS) suggèrent que ces polycétides pourraient cibler une enzyme impliquée dans la coordination du cycle de la division cellulaire. Par conséquent, ils pourraient, par exemple, affecter les mécanismes de la synchronisation ou d'assemblage des fuseaux mitotiques, conduisant à des défauts de ségrégation des chromosomes et / ou de la géométrie du fuseau mitotique. Des études portées sur la production de métabolites secondaires de *Dendrothyrium variisporum* ont conduit à l'isolement de douze composés. Les massarilactones D et H ont été isolés comme principaux composants ainsi que deux nouveaux dérivés de furanone pour lesquels les noms triviaux (5S) -cis-grégatine B et graminine D ont été proposés, trois nouveaux dérivés d'acide anthranilique, deux analogues connus de l'acide anthranilique et trois cyclopeptides. Les nouveaux dérivés de l'acide anthranilique, le 2-phényléthyl-3-hydroxyanthranilate et le 2-phényléthyl anthranilate, ont présenté une activité antimicrobienne tandis que le 2-phényléthyl anthranilate présentait une cytotoxicité contre les cellules HeLa. Enfin, à partir des cultures de *Chaetomium madrasense*, trois composés connus à savoir xanthoquinodines A1, A3 et N-acétyltryptamine ont été isolés.

Mots-clés: Endophytes fongiques, biodiversité, *Globularia alypum*, métabolites secondaires, *Preussia similis*, *Dendrothyrium variisporum*, *Chaetomium madrasense*, caractérisation structurale.

Dedications

My dedications go with love and affection to my mother. Thank you for being the embodiment of sacrifice to ensure a better life for me. Without your enormous effort and unconditional love and care, I would not have never become the individual that I am today. You have been a source of motivation and strength during moments of despair and discouragement. There are not enough words I can describe how important my mother was to me and what a powerful influence she continues to be.

I also dedicate this work to my husband Bilal, whose patience, constant encouragement, limitless giving and understanding, helped me to accomplish my degree. You were always beside me during the challenges of my PhD research and life. I truly thank God for having you in my life.

I dedicate this work to my lovely daughter Olina, the major source of my joy and strength.

My dedications go to my beloved sister Rima and brother Abdelmoutaleb. Thank you for the love, encouragement and support you have given me in numerous ways.

To the memory of my beloved father

I love you all

Sara

Acknowledgments

First and foremost, I would like to thank Allah Almighty for giving me the strength, knowledge, ability and opportunity to undertake this research study. Without his blessings and guidance, this achievement would have never become true.

I am *deeply* grateful to my supervisor Prof. Daoud Harzallah (University of Ferhat Abbas, Sétif 1) for his patience and for the many times he supplied me with advice and suggestions. Thank you for being always generous during all phases of the research.

I am greatly indebted to my co-supervisor Prof. Dr. Marc Stadler, head of Department of Microbial Drugs at Helmholtz Center for Infection Research, Braunschweig (Germany) for giving me the opportunity to work in his department and let me dive into the world of fungi and natural products. I would like to thank you explicitly for your expert advice, your excellent work facilities, steadfast support and encouragements that have been great contributors in the completion of the thesis. Thank you Marc not only for your tremendous academic support, but also for giving me so many wonderful opportunities which have a positive influence in growing my career.

My acknowledgements are also expressed to Prof. Mohamed Mihoub Zerroug (University of Ferhat Abbas, Sétif 1) for having honored me by being the chair of the jury, to Prof. Ammar Ayachi (University of Batna 1), Prof. Idoui Tayeb (University of Jijel) and Dr. Samia Mezaache-Aichour (University of Ferhat Abbas, Sétif 1) for showing their willingness to examine this work and to be members of the jury.

I highly appreciate the valuable time and the efforts expended by Dr. Soleiman Essayed Helaly, without his tireless devotion and chemical skills, this work would not have seen the light. *Thank you* for being kind and patient for teaching me chemistry. Your assistance proved to be a milestone in the accomplishment of my end goal.

I also would like to express my wholehearted thanks to Prof. Dr. Theresia Stradal, head of Department of Cell Biology at Helmholtz Center for Infection Research, Braunschweig (Germany) for allowing me to use her laboratory facilities and for the generous support she provided me during time pressure and challenges throughout my cell biology experiments. I also extend my thanks to her lab team: Anika, Annette, Markus, Jana, Stephanie, Marco and Jessica for the excellent technical assistance in cell biology experiments. You were all wonderful.

I offer my thanks to Dr. Rémy Bertrand Teponno for our pleasant and fruitful collaboration.

I want to express my deep thanks to Simone Heitkämper for her kind and excellent assistance. Further, I would like to thank Wera Collisi for her patience and her excellent technical assistance in conducting the bioassays. I am very grateful to Cécilia Schwager for conducting HPLC-MS data, you were really kind and generous. Also, many thanks go to Silke Reinecke, for her generous help.

I would like to take this opportunity to say warm thanks to all my beloved friends Wilawan, Sandra, Sara, Lucile.

Many thanks to the amazing team of microbial drugs: Christiane, Rolf, Kathrin, Frank, Christian, Clara, Zeldjka, Stephan, Birthe, Lucky, Eric, Enge, Kerstin, Anke and to all the international students I have met during my internship, I have learnt a lot from you.

I owe my profound gratitude to Dr. Manfred Rohde, head of the Research Group of Molecular mechanisms of *streptococci* at Helmholtz Center for Infection Research, Braunschweig (Germany) for his support with electron microscopy.

I gratefully thank Dr. Carlos Plaza for kindly providing fluorescent substrate Cell Event Caspase 3/7 and staurosporine and also for his support with flow cytometry.

I acknowledge the Ministry of Higher Education and Scientific Research of Algeria for the financial support.

Last but not least, deepest thanks go to all people who took part in making this thesis real.

To all of you, thank you very much

Sara

List of abbreviations

BLAST	Basic Local Alignment Search Tool
CBS	Centraalbureau Voor Schimmelcultures, Utrecht, The Netherlands
CD	Circular Dichroism
COSY	Correlation Spectroscopy (NMR)
DAD	Diode Array Detection
DAPI	4',6-Diamidino-2-Phenylindole
DCM	Dichloromethane
DMEM	Dulbecco's modified eagle medium
DSMZ	German Collection of Microorganisms and Cell Cultures
EDTA	Ethylene Diamine Tetraacetic acid
EF1-α	Elongation Factor 1- α
EtOAc	Ethyl Acetate
FACS	Fluorescence-activated cell sorting.
GC –MS	Gas Chromatography - Mass Spectrometry
GMAK	Genomanalytik (Genome Analytics Group)
GTR	Generalised time reversible
HA	Habitat-adapted
HPLC	High Performance Liquid Chromatography
HRESIMS	High resolution electrospray ionization mass spectrometry.
ITS	Internal Transcribed Spacer Region Of The Ribosomal DNA
LSU	Large Subunit
MAFFT	Multiple alignment using fast Fourier transform
MEA	Malt Extract Agar
MeOH	Methanol
MIC	Minimum Inhibitory Concentration
MS	Mass Spectrometer
MTT	3-(4, 5-dimethylthiazol-2-yl)-2, 5-diphenyltetrazolium bromide
MUCL	Mycothèque De L'université Catholique De Louvain, Louvain-La-Neuve, Belgium
NA	Nutrient Agar
NHA	Nonhabitat-adapted
NMR	Nuclear Magnetic Resonance
OMA	Oat Meal Agar
PBS	Phosphate-buffered saline
PCR	Polymerase Chain Reaction.
PDA	Potato Dextrose Agar
PFA	Paraformaldehyde
PhyML	Phylogenetic Estimation By Maximum Likelihood
PI	Propidium iodide
RAxML	Randomized A(x)ccelerated Maximum Likelihood
ROESY	Rotating Frame Nuclear Overhauser Effect Spectroscopy
RP	Reversed Phase
SEM	Scanning Eletron Microscopy
TAE	Tris-Acetate-EDTA
TFA	Trifluoroacetic Acid
t_R	Retention time
STMA	Stadler Marc private culture collection
YEA	Yeast Extract Agar
YMG	Yeast Malt Glucose

List of figures

Figure N°	Title	Page
Figure 1	Different localization patterns of fungal endophytes within plant tissues	3
Figure 2	Location of the different classes of endophytes (according to Rodriguez et al., 2009)	6
Figure 3	Paradigm of balanced antagonism as suggested by Schulz et al. (2015)	9
Figure 4	Schematic representation of endophyte-endophyte interspecies crosstalk	12
Figure 5	Chemical structures of secondary metabolites isolated from the conglomerate <i>Preussia/Sporormiella</i> as indicated in Table 2	15
Figure 6	Chemical structures of selected secondary metabolites isolated from <i>Chaetomium</i> spp. as indicated in Table 3.	18
Figure 7	<i>Globularia alypum</i>	19
Figure 8	<i>Globularia alypum</i> used in this study	21
Figure 9	Root fragments on agar plates	22
Figure 10	Schematic diagram showing purification steps of metabolites isolated from mycelial and supernatant crude extracts of derived from fermentation culture of the fungal isolate DSM 10466 in 8L of ZM/2 liquid medium.	31
Figure 11	Schematic diagram showing purification steps of metabolites isolated from mycelial and supernatant crude extracts derived from fermentation culture of fungal isolate STMA 16219 in 8L of Q6/2 liquid medium	32
Figure 12	Schematic diagram showing purification steps of metabolites isolated from mycelial and supernatant crude extracts derived from fermentation culture of fungal isolate DSM 32328 in 5L of Q6/2 liquid medium.	33
Figure 13	Schematic diagram showing purification steps of metabolites isolated from flasks culture in 8L of YMG medium of the fungal isolate STMA 16226.	34
Figure 14	Schematic diagram showing purification steps of metabolites isolated from mycelial and supernatant crude extracts derived from bioreactor culture of the fungal isolate STMA 16226 in 10 L of YMG medium	35
Figure 15	Schematic diagram showing purification steps of metabolites isolated from the supernatant crude extract derived from fermentation culture of the fungal isolate STMA 16225 in 3L YMG medium	36

Figure 16	Macroscopic morphology of fungal endophytes on YMG agar medium on 9 cm dish.	44
Figure 17	Phylogenetic relationship of fungal endophytes harbored in the roots of <i>G. alypum</i> based on ITS sequences with <i>Paludomyces mangrovei</i> as out group.	46
Figure 18	Phylogenetic tree of <i>Preussia</i> spp. based on combined data set of four markers. Multigenes alignment, PhyML (ITS, LSU, EF1- α).	48
Figure 19	Sterile mycelia of <i>P. similis</i> DSM32328	49
Figure 20	Teleomorph features of <i>Preussia similis</i> DSM 104666	50
Figure 21	Teleomorph characters of <i>P. similis</i> STMA 16219	51
Figure 22	Phylogenetic tree of <i>Dendrothyrium</i> spp. and the closely related genera based on combined data set of four markers. Multigenes alignment, RxML (ITS, LSU, Tub and Actin)	53
Figure 23	Anamorph characteristics of <i>Dendrothyrium variisporum</i>	54
Figure 24	Teleomorph features of <i>Chaetomium madrasense</i>	56
Figure 25	Results of MIC assays of the most potent extracts	59
Figure 26	HPLC chromatogram of crude extracts from ZM/2 liquid culture of <i>P. similis</i> DSM 104666	60
Figure 27	Chemical structures of preussilides A-F (1-6)	61
Figure 28	Antifungal activity of preussilides A (1) and C (3) against phytopathogen <i>S. sclerotiorum</i> determined by Agar diffusion at 100 μ g/disk	63
Figure 29	Results of bioassay-guided fractionation by RP-HPLC using <i>B. subtilis</i> as indicator organism.	64
Figure 30	Microscopic view of fragmented nuclei of preussilide C-treated L929 in MTT assay	66
Figure 31	Mono and co-cultures on YMG agar medium of <i>P. similis</i> and <i>S. sclerotiorum</i>	66
Figure 32	HPLC chromatograms of individual axenic and co-culture of <i>P. similis</i> DSM 104666	67
Figure 33	Effects of preussilides A and C (1 and 3) on the Morphology of Human Osteosarcoma Cells (U2OS)	69-70
Figure 34	Preussilides treatment induces generation of small cells with reduced nuclear size in the human Osteosarcoma Cell Line U2OS.	72

Figure 35	Chemical structures of the compounds (7-8) obtained from <i>P. similis</i> STMA 16219	73
Figure 36	HPLC chromatograms of crude extracts from Q6/2 liquid culture of <i>P. similis</i> 16219	74
Figure 37	Mono and co-cultures of <i>P. similis</i> and <i>S. sclerotiorum</i> on YMG agar medium	76
Figure 38	HPLC chromatograms of individual axenic and co-culture of <i>Preussia similis</i> STMA 16219	76
Figure 39	Chemical structures of the compounds (10-13) isolated from <i>Preussia similis</i> DSM 32328	77
Figure 40	HPLC chromatograms of both mycelial and supernatant crude extracts derived from liquid culture in Q6/2 medium of <i>Preussia similis</i> DSM 32328	78
Figure 41	Microscopic view of fragmented nuclei of cytochalasin B-treated L929 in MTT assay	80
Figure 42	Effect of cytochalasin B on actin cytoskeleton of U2OS cells at concentrations of 1 µg/mL and 5 µg/mL for 24 hours	81
Figure 43	Phytotoxic test results of cytochalasin B on seedling growth.	82
Figure 44	Mono and co-cultures of <i>Preussia similis</i> DSM 32328 and <i>S. sclerotiorum</i> on YMG agar medium	83
Figure 45	HPLC chromatograms of individual axenic and co-culture of <i>P. similis</i> DSM 32328	83
Figure 46	Chemical structures of compounds (14-25) isolated from <i>Dendrothyrium variisporum</i>	85
Figure 47	HPLC chromatograms of mycelial and supernatant crude extracts derived from YMG liquid culture of <i>Dendrothyrium variisporum</i> in shake flasks and bioreactor	86
Figure 48	HPLC profile of mycelial crude extract derived from YMG liquid culture of <i>Chaetomium madrasense</i>	90
Figure 49	Chemical structure of compounds (26-28) isolated from <i>Chaetomium madrasense</i>	90

List of tables

Table N°	Title	Page
Table 1	Symbiotic criteria used to characterize fungal endophytic classes criteria	8
Table 2	Compounds isolated from the conglomerate <i>Preussia/Sporormiella</i>	14
Table 3	Selected compounds isolated from <i>Chaetomium</i> spp.	17
Table 4	Botanical classification of <i>Globularia alypum</i>	19
Table 5	Detailed PCR programs for the used marker genes amplification (ITS, LSU, EF-1 α , Tub and Actin)	25
Table 6	Media used for large scale fermentation and cultivation period	30
Table 7	Fungal endophytes isolated from <i>G. alypum</i> and their closest hits from BLAST research	43
Table 8	MIC values [$\mu\text{g/mL}$] of the crude extracts from small scale fermentations of the screened fungi in various media	58-59
Table 9	LC-MS data of preussilides 1-6 and their physical properties	61
Table 10	MIC [$\mu\text{g/mL}$] values of the six preussilides against the tested organisms.	62
Table 11	Cytotoxic effect (IC ₅₀) of preussilides A-F (1 - 6) against different normal and cancer cell lines	65
Table 12	LC-MS data of three compounds of <i>P. similis</i> STMA 16219 and their physical properties	73
Table 13	MIC [$\mu\text{g/mL}$] values of <i>P. similis</i> STMA 16219 compounds	75
Table 14	LC-MS data of the four cytochalasins and their physical properties	78
Table 15	MIC [$\mu\text{g/mL}$] values of cytochalasin B and deoxaphomin against the tested microorganisms	79
Table 16	Cytotoxic effect (IC ₅₀) of cytochalasin B and deoxaphomin against different normal and cancer cell lines	79
Table 17	Suggested chemotypes for <i>P. similis</i> based on compounds isolated from four strains in the current study	84
Table 18	LC-MS data of the twelve compounds and their physical properties	87
Table 19	MIC [$\mu\text{g/mL}$] values of compounds 14, 15, 17-25 against the tested microorganisms	89
Table 20	Cytotoxic effect (IC ₅₀) of compounds 14, 15, 17-25 against two cancer cell lines	89

Table 21	LC-MS data of the three known compounds and their physical properties	91
Table 22	MIC [$\mu\text{g/mL}$] values of compounds 26-28	92
Table 23	Cytotoxic effect (IC_{50}) of compounds 26-28 against two cancer cell lines	93

List of Publications

1. **Noumeur S.R.**, Helaly S. E, Jansen R, Gereke M., Stradal T. E. B., Harzallah D., Stadler M. 2017. Preussilides A–F, bicyclic polyketides from the endophytic fungus *Preussia similis* with antiproliferative activity. *Journal of natural products* **80** (5). 1531-1540.
2. Teponno R. B., **Noumeur S. R.**, Helaly S. E, Hüttel S., Harzallah D., Stadler M. 2017. Furanones and anthranilic acid derivatives from the endophytic fungus *Dendrothyrium variisporum*. *Molecules* **22** (10). 1-10.

Table of Contents

Introduction	1
---------------------------	---

Literature Review

I. Endophytes

I.1. Definition.....	3
I.2. Fungal endophytes.....	4
I.3. Transmission.....	4
I.3.1. Vertical transmission.....	4
I.3.2. Horizontal transmission.....	4
I.4. Colonisation of host plant by fungal endophytes.....	5
I.5. Adaptation.....	5
I.6. Classes of fungal endophytes.....	6
I.6.1. Clavicipitaceous fungal endophytes (Class 1).....	6
I.6.2. Non-Clavicipitaceous fungal endophytes.....	7
I.7. Balanced antagonism.....	9
I.7.1. Plant- endophyte interactions.....	10
I.7.2. Endophyte- competitors (endophytes, pathogens).....	10
I.8. Secondary metabolites production by endophytes.....	12
I.8.1. Genus <i>Preussia</i>	13
I.8.2. Genus <i>Dendrothyrium</i>	15
I.8.3. Genus <i>Chaetomium</i>	16

II. <i>Globularia alypum</i>	18
---	----

II.1. Taxonomy and botanical aspect of <i>Globularia alypum</i>	18
II.2. Chemical constituents of <i>G. alypum</i> and their biological activities.....	20

Experimental Section

Chapter I: Material and methods

1. Plant material	21
2. Isolation of the endophytic fungi.....	21
3. Identification of fungal isolates	22
3.1.Morphological studies.....	22
3.1.1. Macroscopic features.....	22
3.1.2. Microscopic features	23
3.1.3. Ultrastructure of ascospores by electron microscopy.....	23
3.2. Molecular studies.....	23
3.2.1. DNA extraction.....	23
3.2.2. Amplified regions used for the identification.....	24
3.2.3. Gel electrophoresis.....	25
3.2.4. Purification of the PCR products and sequencing.....	25
3.3.5. Phylogenetic analysis.....	26
4. Small scale fermentation and preparation of extracts from cultures.....	27
4.1. Small scale fermentation.....	27
4.2. Extraction	27
5. Generation of secondary Metabolite profiles of crude extracts.....	28
6. Serial dilution assay.....	28
7. Bioactive-guided fractionation of crude extracts.....	29
8. Scale-up fermentation.....	29
9. Isolation and purification of secondary metabolites.....	30
10. Dual culture.....	36
11. Structure elucidation	37
11.1. HRESIMS	37
11.2.NMR	37
11.3. Optical rotation and UV-spectra and CD spectroscopy.....	38
12. Biological assays of pure compounds.....	38
12.1. Antimicrobial activity	38
12.2. Standard disk assay	38

12.3. Cytotoxicity assay.....	39
12.4. Phytotoxicity test	39
12.5. Nematicidal Activity Assay.....	40
13. Cell biology experiments.....	40
13.1. Effect on cells morphology.....	40
13.1.1. Immunofluorescence.	41
13.1.2. Flow cytometry	42

Chapter II: Results and discussion

1. Isolation and identification of fungal isolates.....	43
2. Small scale fermentation and screening for antimicrobial activity.....	57
3. Large scale fermentation, isolation and purification of bioactive metabolites.....	59
3.1. Compounds isolated from <i>Preussia similis</i> strains.....	59
3.1.1. Compounds isolated from <i>Preussia similis</i> DSM 10466.....	59
3.1.1.1. Fermentation and metabolites isolation.....	59
3.1.1.2. Biological activity of preussilides.....	61
3.1.1.3. Co-culture of <i>P. similis</i> with phytopathogen <i>S. sclerotiorum</i>	66
3.1.1.4. Effects of preussilides on cell morphology.....	68
3.1.2. Compounds isolated from <i>Preussia similis</i> STMA 16219.....	73
3.1.2.1. Fermentation and metabolites isolation.....	73
3.1.2.2. Biological activity.....	74
3.1.2.3. Dual culture.....	75
3.1.3. Compounds isolated from <i>Preussia similis</i> DSM 32328.....	77
3.1.3.1. Fermentation and metabolites isolation.....	77
3.1.3.1. Biological activity.....	78
3.1.3.2. Dual culture.....	82
3.1.4. Chemotaxonomy of <i>Preussia similis</i>	83
3.2. Compounds isolated from <i>Dendrothyrium variisporum</i>	85
3.2.1. Fermentation and metabolites isolation.....	85
3.2.2. Biological activity.....	88

3.3. Compounds isolated from <i>Chaetomium madrasense</i>	90
3.3.1. Fermentation and metabolites isolation.....	90
3.3.2. Biological activity	91
Conclusion and perspectives	94
References	97
Appendices	

Introduction

The need for new and beneficial therapeutic agents to cope with the health and environmental problems faced by society today is never ending (Li *et al.*, 2015). The rising tide of bacteria resistance to antibiotic is one of the biggest issues to global health, due to the wide uses of antibiotics not only in human medicine but also in livestock and poultry farming in order to promote growth and prevent infection. The threat posed by the spread of antibiotic resistance is enhanced by an alarming decline in the discovery and development of new classes of antibiotic with new biologically active pharmacophores. In addition, the apparent increase in viral and fungal infections, the lack of anticancer agents and the search for alternatives to harmful synthetic pesticides are also among the problems that underscore the need of new effective drugs (Richter *et al.*, 2016).

Fungi are a prolific source of secondary metabolites that may serve as leads for the development of novel badly needed new agents. In particular, certain ecological groups of fungi like the endophytic mycobiota have recently been proved to yield a plethora of novel metabolites exhibiting a variety of biological activities (Kusari *et al.*, 2008). Endophytic fungi, which colonize their host plants without causing visible disease symptoms, can grow inter- or intracellularly, systemically or locally within their hosts. Up to date, no endophyte-free plant species has been reported (Arora and Ramawat, 2017). In fact, the endophytes are involved in multipartite interactions to maintain a balanced antagonism *in planta*, not only with their host plant, but also with other microbial competitors sharing the same habitat, both bacteria and fungi. Secondary metabolites are important factors for maintaining these equilibria. Through a long time communication, evolutionary adaptation of endophytes in plants to the complex environment enabled them to have a tremendous biosynthetic capability. The repertoire of their biosynthetic capacities over the co-evolutionary process as well as microbial biodiversity encompassing an arsenal and unique of chemical scaffolds, once isolated and characterized, may increase the chances to develop new pharmaceutical agents to prevent and cure human ailments (Aly *et al.*, 2013; Schulz *et al.*, 2015).

So far, many natural product researchers are attracted by the ubiquitous presence of this intriguing plant mycobiota and their ability in promoting plant growth as well as in improving plant defence systems in order to strive against abiotic and biotic stresses (Kusari *et al.*, 2012; Schulz *et al.*, 2015; Netzker *et al.*, 2015; Deka *et al.*, 2017).

This thesis reports for the first time the diversity of fungal endophytes of the medicinal plant *Globularia alypum* (Plantaginaceae, Scrophulariales), used in the Algerian traditional medicine as a healing agent, such as hypoglycaemic agent, laxative, cholagogue, stomachic, purgative and sudorific (Boutiti *et al.*, 2008). Furthermore, the isolated fungal endophytes were screened for their secondary metabolites production.

Aims of the thesis

The aims of the thesis can be divided into a taxonomic and a chemical part, and are as follows:

- Isolation of several endophytic fungi inhabiting the Algerian plant *Globularia alypum* collected from Ain Touta Batna (Algeria).
- Identification of the fungal isolates by morphological description and by ITS sequencing. For some fungi, the phylogenetic position was further illustrated and discussed by using protein coding genes.
- From our collection of endophytic fungi, some fungal strains were selected for further study (small-scale fermentations), based on a phylogenetic preselection in order to select the most promising fungal strains and search for novel and biologically active secondary metabolites.
- HPLC/DAD/MS profiling and antimicrobial screening of extracts derived from small-scale fermentations.
- Large-scale fermentations of the interesting strains were performed.
- Isolation and structure elucidation of pure compounds.
- Extensive biological screening of the identified compounds to explore their potential biological importance.

Literature review

I. Endophytes

I.1. Definition

The term “endophyte” is derived from the Greek words “endon” meaning within, and “phyton” meaning plant, and originally introduced by de Bary in 1866 referred to any organism occurring within plant tissues, distinct from the epiphytes that live on plant surfaces (Schulz and Boyle, 2006). So far, the most accepted definition of endophyte is that of Petrini (1991) “*all organisms inhabiting plant organs that at some time in their life, can colonize internal plant tissues without causing apparent harm to the host*” (Hyde and Soyong, 2008). They spend the whole or part of its life cycle colonizing inter- and/or intracellularly (Figure 1), systemically or locally inside the healthy leaves, petioles, stems, twigs, bark, root, fruit, flower and seeds (Schroeckh *et al.*, 2014). However, some endophytes remain as latent pathogens. This lifestyle as parasitism may occur either during host senescence or when the plant is under stress (Hyde and Soyong, 2008). The endophytes include both prokaryotic and eukaryotic microorganisms. The prokaryotic endophytes which are represented by bacteria and actinomycetes are often colonisers of vascular tissues of host plants. They play very important roles in the plant fitness such as nitrogen fixation. The eukaryotic endophytes are represented by fungi (Schulz and Boyle, 2006).

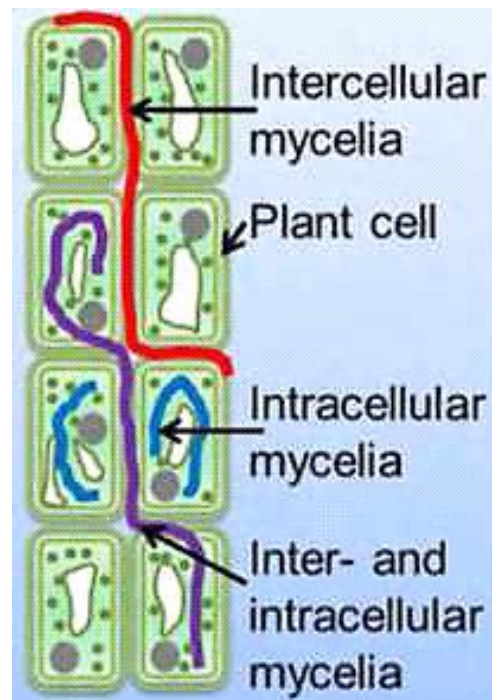


Figure 1: Different localization patterns of fungal endophytes within plant tissues (Kusari and Spiteller, 2012)

I.2. Fungal endophytes

Endophytic fungi are a polyphyletic group of microorganisms that may present in almost all plants (Hodgson *et al.*, 2014). Nowadays, it is a well-established fact that plants are hosts for many types of microbial endophytes residing in different tissues, no endophyte-free plant species has been reported (Sandhu *et al.*, 2017). Also, many species of plants can harbour the same species of endophytes (Zabalgogea, 2008). The majority of endophytic fungi are members of Ascomycota and their anamorphs, only a small community of the total number of fungal endophytes is represented by Basidiomycota (Hyde and Soyong, 2008; Martin *et al.*, 2015; Das *et al.*, 2017).

I.3. Transmission

The endophytes may originate from the outside environment; rhizosphere and phyllosphere. So far, there are two known transmission routes for fungal endophytes: vertical and horizontal transmission (Tintjer *et al.*, 2008). In some cases the transmission takes place by mixed modes (Foster and Wenseleers, 2006).

I.3.1. Vertical transmission

The vertical transmission occurs from the parent to the offspring *via* fungal hyphae invading the host's seeds. The fungal endophytes being transmitted vertically are often mutualistic and referred to as “true” endophytes, since their reproductive success is completely dependent on host reproductivity. Such a way of transmission keeps the continuity of partnerships between plant and endophytes by ensuring accurate transmission of the beneficial symbionts through generations (Tadych *et al.*, 2014). This mode of transmission seems to be restricted to some asexual fungi in the family Clavicipitaceae which inhabit grasses. The vertical transmission is limited only to asexual reproduction.

I.3.2. Horizontal transmission

Horizontally transmitted fungal endophytes are sexual and are transmitted by means of spores (mitotic asexual or meiotic sexual spores) or possibly hyphae. The spores can be disseminated by water or air movement and/or insect vectors. The sexual reproduction requires production of meiotic sexual spores and is therefore always horizontal (Kandel *et al.*, 2017). Horizontal transmission is predicted to enhance virulence whereas vertical transmission evolves beneficial partners. The species of

the genus *Epichloe* are the most studied fungi on this phenomenon. However, not all mutualists are mandatorily transmitted vertically, and there are many examples of mutualistic horizontally transmitted symbioses (Schulz and Boyle, 2005; Foster and Wenseleers, 2006).

I.4. Colonisation of host plant by fungal endophytes

The fungal endophytes often originate from the soil. The roots are frequently the primary site for endophytic infection as the root exudates facilitate their attachment and consequently their entry into plant tissues. Eventually, other portal entries beyond roots are possible, such as, the stems, leaves, flowers and seeds, however the endophytic growth has been found to be narrow (Schulz and Boyle, 2006; Andrade-Linares and Franken, 2013). In case of flowers and seeds colonisation, the endophytes are thereby transmitted vertically from the maternal endophyte community into the offspring (Arora and Ramawat, 2017). Up to now, it is not clear if fungal endophytes sense root exudates for colonization (Rodriguez *et al.*, 2009). The endophytic Ascomycota penetrate the roots by different mechanisms. In addition to the adhesion tips, it was found that fungal endophytes grow around roots by forming a network and produce appressoria like-structure as well as swollen cells on hyphal tips. Afterwards, the runner hyphae penetrate through between the intercellular spaces. Later, each single hyphae grows along the longitudinal axis of the organ between epidermal and cortical cells, and intracellular colonization is visualized as formation of microsclerotia. Root colonisation can be both inter- and intra-cellular, the hyphae often forming intracellular coils. The fungal hyphae cross the cell wall to reach the intracellular space leaving a constriction at entry sites (Arora and Ramawat, 2017).

I.5. Adaptation

Endophytic communities inhabiting a particular plant host are frequently referred to host specificity (some authors use the terms host preference or host exclusivity). The latter is the result of adaptation success between the endophyte and the host. However, some fungi can be found as endophytes, but in reality, they are specific to another substrate, normally found growing on it. An example of these accidental opportunists might be coprophilous species, which are a type of saprobic fungi that grow on animal dung, are sometimes detected as endophytes (Schroeckh and Brakhage, 2014). Also, the insect associated fungus *Daldinia hawksworthii*, which is normally a symbiont with the willow woodwasp *Xiphydria prolongata*, was found as endophyte of *Salix* (Pažoutová *et al.*, 2013).

I.6. Classes of fungal endophytes

Endophytic fungi have been classified into two broad groups based on their phylogeny and life history traits, the clavicipitaceous and the non-clavicipitaceous fungal endophytes. Now, the fungal endophytes are classified as class 1 (clavicipitaceous endophytes), and three other classes (class 2, class 3 and class 4) representing the group of non-clavicipitaceous endophytes (Figure 2) (Table1) (Rodriguez *et al.*, 2009).

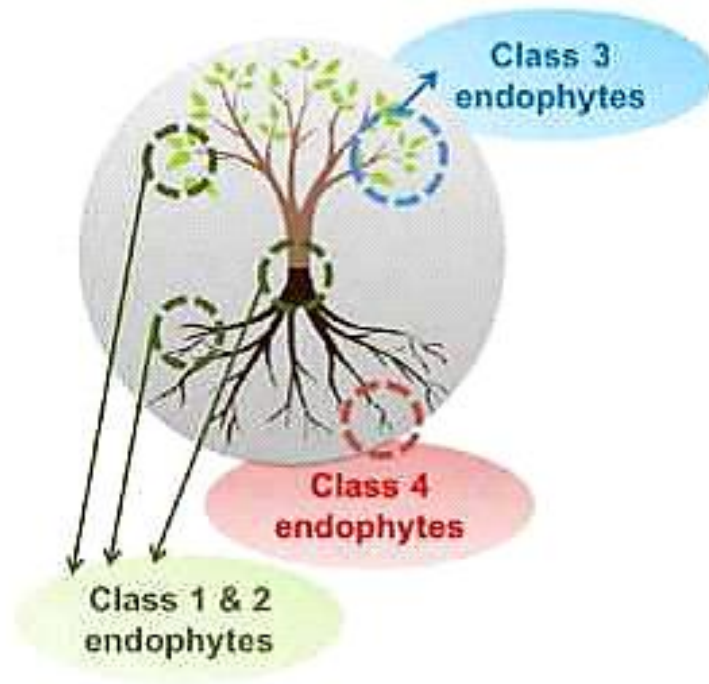


Figure 2: Location of the different classes of endophytes (according to Rodriguez *et al.*, 2009) (Kusari and Spittler, 2012)

I.6.1. Clavicipitaceous fungal endophytes (Class 1)

The group of clavicipitaceous endophytes represents the class 1 of fungal endophytes that form a symbiotic relationship with a broad spectrum of grasses (especially the family of Poaceae). They are mostly obligate biotrophic ascomycetes of the family Clavicipitaceae that perennially and systemically colonise the intercellular spaces of leaf primordia, leaf sheaths and culms of vegetative tissue (Scott, 2001; Sánchez Márquez *et al.*, 2012). Due to their lack of the biosynthetic capacity for the production of secondary metabolites, grasses cohabit these fungi which are known as a good producers of a set of secondary metabolites. The advantages of this grasses-endophytes association appear practically in the higher performance of bioprotection by inducing eco-physiological changes that make plants more tolerant to different biotic and abiotic stresses (Kuldau and Bacon, 2008).

Therefore, the infected grasses have been found to be very vigorous especially in enhancing plant biomass, drought tolerance, protection against herbivore and insects. Such a defensive mutualistic association is very important to the ecological fitness and species diversity of grasses (Sánchez Márquez *et al.*, 2012; Kusari and Spiteller, 2012). On the other hand, mutualistic benefits for endophytes may involve access to nutrients from the host apoplast, abiotic and biotic stress avoidance and dissemination by seed (Scott, 2001). The genus *Epichloë* is the most studied group of these associated grasses endophytes. These grass-fungal endophyte symbioses have been showed a range from pathogenic to mutualistic. The species from the genus *Epichloë* are often considered to be pathogenic to host grasses as they may induce abortion of plant reproductive structures when reaching sexual reproduction state and horizontal spreading may cause partial or complete sterilization of the hosts due to the production of a fungal stroma on the flowering culms (choke disease) (Gundel *et al.*, 2012). In mutualistic relationships, the *Epichloë* endophyte grows systematically within its host including the developing seeds, and it is completely dependent of the survival and growth of the grass host plant for its own growth (Scott, 2001; Schaechter, 2012).

I.6.2. Non-Clavicipitaceous fungal endophytes

The non-clavicipitaceous endophytes are polyphyletic fungi, often poorly defined or with unknown ecological roles. They traditionally have been treated as a single functional group forming the class 2 of fungal endophytes until Rodriguez *et al.* (2009), have differentiated them into three functional classes (class 2, class 3 and class 4) based on host colonization patterns, mechanism of transmission between host generations, *in planta* biodiversity levels, and ecological function (Table 1).

a. Class 2

The fungal endophytes belonging to the class 2 may grow in the aerial and ground parts of the plant host. Most of their species are members of Ascomycota (Pezizomycotina) with minority being Basidiomycota (Agaricomycotina and Pucciniomycotina). Transmission of fungal endophytes of class 2 can be vertical or horizontal.

b. Class 3

The occurrence of Class 3 fungal endophytes is strongly related to aerial tissues and they are transmitted horizontally. Thus, their entry portal to the host plant is always the aerial part, where their

growth will be limited or they spread to the lower part. Due to the above-tissues dependence, these fungi induce the formation of highly localized infections.

These fungi are found within photosynthetic and herbaceous tissues in addition to flowers and fruits, as well as in asymptomatic wood and inner bark. The biodiversity of class 3 endophytes is extremely high *in planta*. They include the endophytic fungi associated with leaves of tropical trees, the highly diverse associates of above-ground tissues of nonvascular plants, seedless vascular plants, conifers, and woody and herbaceous angiosperms in biomes ranging from tropical forests to boreal and Arctic/Antarctic communities.

c. Class 4

The class 4 endophytes are distinguished from the other two classes of non clavicipitaceous fungi based on their exceptional nature of hyphae. The latter are septate and dark in color due to the presence of melanin. They are known as dark septate endophytes (DSE), which colonize only the roots of the plant, extensively. Their mode of transmission is exclusively horizontal. In general, Class 4 endophytes are primarily ascomycetous fungi that are conidial or sterile and that form melanized structures such as inter- and intracellular hyphae and microsclerotia in the roots (Rodriguez *et al.*, 2009).

Table 1: Symbiotic criteria used to characterize fungal endophytic classes criteria (Rodriguez *et al.*, 2009)

Criteria	Clavicipitaceous		Non Clavicipitaceous		
	Class 1	Class 2	Class 3	Class 4	
Host range	Narrow	Broad	Broad	Broad	
Tissue(s) colonized	Shoot and rhizome	Shoot, root and rhizome	Shoot	Root	
<i>In planta</i> colonization	Extensive	Extensive	Limited	Extensive	
<i>In planta</i> biodiversity	Low	Low	High	Unknown	
Transmission	Vertical and horizontal	Vertical and horizontal	horizontal	horizontal	
Fitness benefits*	NHA	NHA and HA	NHA	NHA	

*Nonhabitat-adapted (NHA) benefits such as drought tolerance and growth enhancement are common among endophytes regardless of the habitat of origin. Habitat-adapted (HA) benefits result from habitat-specific selective pressures such as pH, temperature and salinity.

I.7. Balanced antagonism

The theory predicts that endophytes produce phytotoxic metabolites toward their host plant and the latter can react by inducing its defence responses. Questions have been raised about the asymptomatic growth and survival of endophytes inside the living tissues of the host plant and how can these two partners succeed in the establishment and maintenance of this symbiosis relationship. Some authors have mainly been interested in questions concerning the mysterious endophytes-plant interactions, Schulz *et al.* (1999, 2015) have hypothesized that the asymptomatic relationship endophyte-plant is a result of a balanced antagonism in which virulence factors and defence response are balanced. However, the balanced antagonism is a transitory period and it can be destabilized. In the unbalanced antagonism, either the fungus is pruned or the plant becomes diseased. Even so, the switch between a balanced and unbalanced interaction depends of the status of two partners. In fact, the plant defense and endophyte virulence can be modified by environmental factors as well as senescence stressors. In addition to their escape to host defences systems, fungal endophytes must in the same time avoid the toxins of other microbial inhabitants, including pathogens and other endophytes competitors. Therefore, they must be engaged in multipartite interactions (Schulz *et al.*, 1999; Kusari *et al.*, 2012; Schulz *et al.*, 2015). The equilibrium established between fungal endophytes and their host as well as other competitors is shown in figure 3.

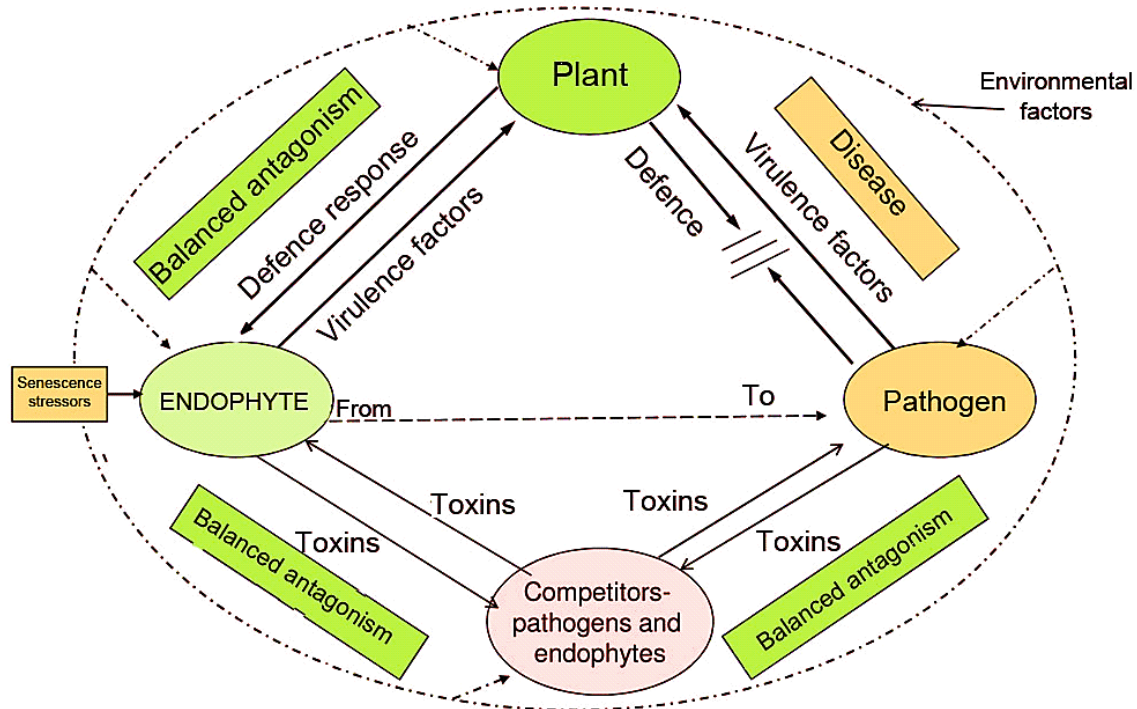


Figure 3: Paradigm of balanced antagonism as suggested by Schulz *et al.* (2015)

The interactions of endophytes with their host plants and with other endophytes and pathogens microorganisms (both fungi and bacteria) are summarized as follows:

I. 7.1. Plant- endophyte interactions

Mutualistic interactions involving fungi and bacteria that endophytically colonise plant roots, benefit the microbial partner with a reliable supply of nutrients as well as protection from environmental stresses. The plant, in turn, reaps the benefit of nutrient uptake and protection against biotic (e.g. pathogens, herbivores) and abiotic (e.g. drought tolerance) stress factors. In fact, the fungal endophytes could confer deterrence to their host plants in different ways. Many endophytes due their ability to produce antibacterial and antimycotic metabolites, can suppress or reduce severity of plant invasion by pathogens sharing the same habitat (Arora and Ramawat, 2017). Very likely, the synergetic effect of the total of antimicrobial compounds secreted by endophytic microbiota could enhance the plant protection (Kusari *et al.*, 2012).

Even through, the intimate and prolong relationship between plant and microbe observed as a genetic exchange among plant and microbes to transfer information inherent among both organisms. This co-evolution of endophytes and their host plants is believed to shape natural product patterns of endophytic fungi, which often contribute in multiple ways to endophyte- host communication as well as host fitness and adaptation to environmental challenges. However, little is known about this relationship (Sandhu *et al.*, 2017).

I.7.2. Endophyte- competitors (endophytes, pathogens)

One living tissue of a host plant harboring a single type of endophytes is an exotic exception. Usually, the plant is inhabited by diverse taxa of endophytic microorganisms including bacteria and fungi. Thus, the endophytes must interact with their neighbours sharing the same habitat. The diverse intra- and interspecies cross-talk is accomplished by a huge number of metabolites, most of them belong to the group of secondary metabolites. This cross-talk often involve secretion of antibacterial and antifungal metabolites against competitors in order to maintain balanced antagonisms. It is mostly like chemical warfare in which each endophytes secrete toxic metabolite to the respective partner leading to a reciprocal antagonisms to ensure their maintenance in the plant host. Also, the interaction between the inhabitants of the same plant does not occur only metabolically by production of inhibitory metabolites, but also occurs in a chemical communication between symbionts partners by

secreting signal molecules which might have a crucial role in environmental recognition (Kusari *et al.*, 2012). This view is supported by Schulz *et al.* (2015), who found that in co-culture experiments, the microorganisms secrete metabolites even before they make intimate physical contact, suggesting that a number of signal molecules might be involved in order to inform the partners of the presence of each other before they engage in the transfer of molecular and genetic information that include many mechanisms and classes of molecules. On the other hand, these interactions could trigger silent biosynthetic pathways. Each compound released by microorganism could have an impact on the metabolic profiles of other microorganisms sharing the same ecological niche. Therefore, their mutual interplay could lead to a significant and chemical diversity in the natural compounds released (Figure 4). Such a chemical diversity is a result of the expression of genes clusters previously unexpressed in individual axenic culture under standard laboratory growth conditions. In this respect, many authors have mainly highlighted the importance of the co-cultivation to induce silent genes clusters under standard laboratory conditions or can allow also a tremendously enhanced production of already known natural compounds (Scherlach and Hertweck, 2009; Schroeckh and Brakhage, 2014; Ola *et al.*, 2013; Netzker *et al.*, 2015; Wakefield *et al.*, 2017). Also, another example of fungus-bacterial endosymbiont crosstalk was found by Partida-Martinez and Hertweck (2005) reporting that the phytopathogenic fungus *Rhizopus microsporus* as causing rice seedling blight was found to not be responsible for the production of rhizoxin as thought previously, but rather an endosymbiotic bacterium belonging to the genus *Burkholderia*, occupying the intracellular space of *Rhizopus* (Partida-Martinez and Hertweck, 2005). Interestingly, the endosymbiont not only produces the phytotoxin but also controls the differentiation and sporulation of the fungal host (Partida-Martinez *et al.*, 2007). This unexpected tripartite plant–symbionts revealed that there are many complex networks of chemical communications between plant and endophytes, mediating by a diversity of chemical molecules. However, little is known about these hidden intriguing mechanisms.

There is evidence now, that using the traditional approach by using individual culture to discover natural products is often frustrating and usually the producer organism is qualified as incompetent. Now, with the co-cultivation approach a valuable insight is provided and the respective microorganisms could become competent just their silent biosynthetic metabolisms need to be encrypted by exposing them to the appropriate conditions (Kusari *et al.*, 2012; Wakefield *et al.*, 2017).

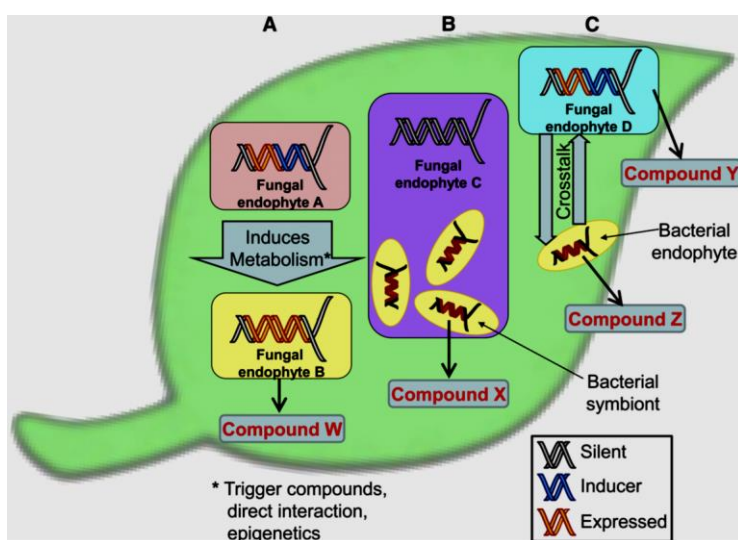


Figure 4: Schematic representation of endophyte-endophyte interspecies crosstalk (Kusari *et al.*, 2012)
 (A) Fungus-fungus crosstalk is illustrated, (B) Fungus-bacterial endosymbiont crosstalk is demonstrated,
 (C) Fungus-bacteria crosstalk is presented.

I.8. Secondary metabolites production by endophytes

Fungi can produce a large array of low-molecular-mass organic compounds called secondary metabolites. In contrast to primary metabolites, secondary metabolites are usually regarded as non-essential for the survival of living organisms, while their role is quiet versatile. They often confer competitive outcomes to their producing organisms usually as mediators in interactions with others organisms including plants, animals and microorganisms that may indirectly influenced their growth and development by increasing their fitness (Bills *et al.*, 2013; Netzker *et al.*, 2015). Up to date, many classes of secondary metabolism biosynthesis pathways have been characterized in fungi, especially filamentous Ascomycota which their genomes encode a broad spectrum of enzymes that synthesize secondary metabolites, including nonribosomal peptide synthetases, polyketide synthases and terpene synthases (Bills *et al.*, 2013). Endophytic fungi are of biotechnological interest due to their potential as an excellent source of various bioactive compounds (chemically and in terms of their biological activities) that have evolved during their symbiotic plant relationship with plants. The quality and quantity of secondary metabolite produced is related to each fungal species. This specificity, which imparts a species-specific chemical marker, can be used as additional characters to distinguish closely related fungal species (chemotaxonomy).

I.8.1. Genus *Preussia*

The genus *Preussia* is a member of the family of Sporormiaceae in the order Pleosporales, subclass Pleosporomycetidae, class Dothideomycetes, subphylum Pezizomycotina, and phylum Ascomycota. Its species are most commonly found on various types of animal dung, but they can also be isolated from plant debris, soil and wood (Arenal *et al.*, 2005; Porrás-alfaro and Sinsabaugh, 2011), or as endophytes in plants (Arenal *et al.*, 2007; Herrera *et al.*, 2010; Mapperson *et al.*, 2014). This genus was proposed by Fuckel (1866) with *Preussia funiculata* (Preuss) Fuckel as type species (Abdullah *et al.*, 1999). The genus morphologically most closely related to *Preussia* is *Sporormiella* Ellis & Everh. The two genera have been mostly treated as congeneric because their salient discriminatory morphological features are known to depend on culture conditions (Kruys and Wedin, 2009). Moreover, recent molecular phylogenetic studies have revealed that *Preussia* and *Sporormiella* do not form monophyletic clades, but rather their DNA sequences become intermingled in phylogenetic trees (Arenal *et al.*, 2005; Kruys and Wedin 2009; Kruys, 2015; Mapperson *et al.*, 2014). In the current taxonomy, the genus *Preussia* includes *Sporormiella* and contains more than 100 species (Index fungorum, 2018). The species are morphologically characterized by brown to black pseudothecia, bitunicate asci, and dark brown, septate ascospores. A gelatinous sheath covers each ascospore and in general, each cell has a germ slit (Khan and Cain, 1979; Arenal *et al.*, 2007). Even though, *Preussia* species are common coprophilous fungi, many authors have isolated them from different plant species. The spores of coprophilous species stick easily to the plant surface because they are often surrounded by gelatinous sheath. When a plant is foraged by an herbivore, the spores pass in the herbivore gastrointestinal tract and they are ending up in the new dung pile, the spores germinate and produce new fruit bodies. Again the spores attach to the surface plant and the cycle restarts. However, much uncertainty still exists about the life cycle of coprophilous fungi. One hypothesis to explain their endophytic state, might be that the spores remain on the surface of plant as epiphytes and due to their resistance to surface-sterilants, they could escape to the surface sterilization of plant tissues and are actually isolation artefacts, rather than the endophytes (Newcombe *et al.*, 2016).

The conglomerate *Preussia/Sporormiella* has been known as potent producers of bioactive compounds, in particular polyketides (Du *et al.*, 2012, 2014; Rangel-Grimaldo *et al.*, 2016). Among them, *Preussia similis* (*Sporormiella similis*) (Khan & Cain) Arenal (Khan and Cain, 1979; Arenal *et*

al., 2004) was found to be a rich source of antifungal compounds, e.g. preussomerin A (Weber and Gloer, 1991), or similin A and B (Weber *et al.*, 1992) (Table 2 and Figure 5).

More recently, Gonzalez-Menendez *et al.* (2017), have reviewed the diversity of *Preussia* species and characterized for the first time the occurring chemotypes. In fact, thirty-one species have been divided into eleven chemotypes based on a combined data of morphological and phylogenetic analysis together with the chemical profile of the corresponding strains. The latter chemotaxonomic work did not attributed *Preussia similis* to any of these chemotypes.

Table 2. Compounds isolated from the conglomerate *Preussia/Sporormiella*

Species	Isolation source	Compound	Compound family	Biological activity
<i>Preussia aurantiaca</i>	Mangrove	Auranticins (Poch and Gloer, 1991)	Depsidone	Antibacterial
<i>Preussia fleischhakii</i>	Rabbit dung	Diphenyl esters (Weber and Gloer, 1988)	Diphenyl esters	Antifungal.
<i>Preussia isomera</i>	Cattle dung	Preussomerins (Weber <i>et al.</i> , 1990; Weber and Gloer, 1991)	Polyketides	Antifungal, Ras-farnesyl- protein transferase inhibitors, and cytotoxic
<i>Preussia minimoides</i>	Leaves of <i>Hintonia latiflora</i>	Minimoidiones A and B (Rangel-Grimaldo <i>et al.</i> , 2016)	Polyketides	α - Glucosidase inhibitor
<i>Preussia typharum</i>	Degraded organic matter	- Preussiadins A and B (Du <i>et al.</i> , 2014) - Preussidone (Du <i>et al.</i> , 2012)	-Epipolythio- Diketopiperazine alkaloids - 2,5- diarylcyclopentene	- P- glycoprotein- mediated drug resistance. - Antioxydant
<i>Sporormiella minimoides</i>	Basidioma of <i>Trametes hirsutum</i>	Sporminarins A and B (Mudur <i>et al.</i> , 2006)	Polyketides	Antifungal
<i>Sporormiella similis</i>	Marmot dung	Similins A and B (Weber <i>et al.</i> , 1992)	Polyketides	Antifungal
<i>Sporormiella intermedia</i>	Cotton tail rabbit dung	Zaragozic acids (Bergstrom <i>et al.</i> , 1995)	4,6,7-trihydroxy- 2,8- dioxobicyclo[3.2.1] octane-3,4,5- tricarboxylic acid core	Antifungal and inhibitors of squalene synthase

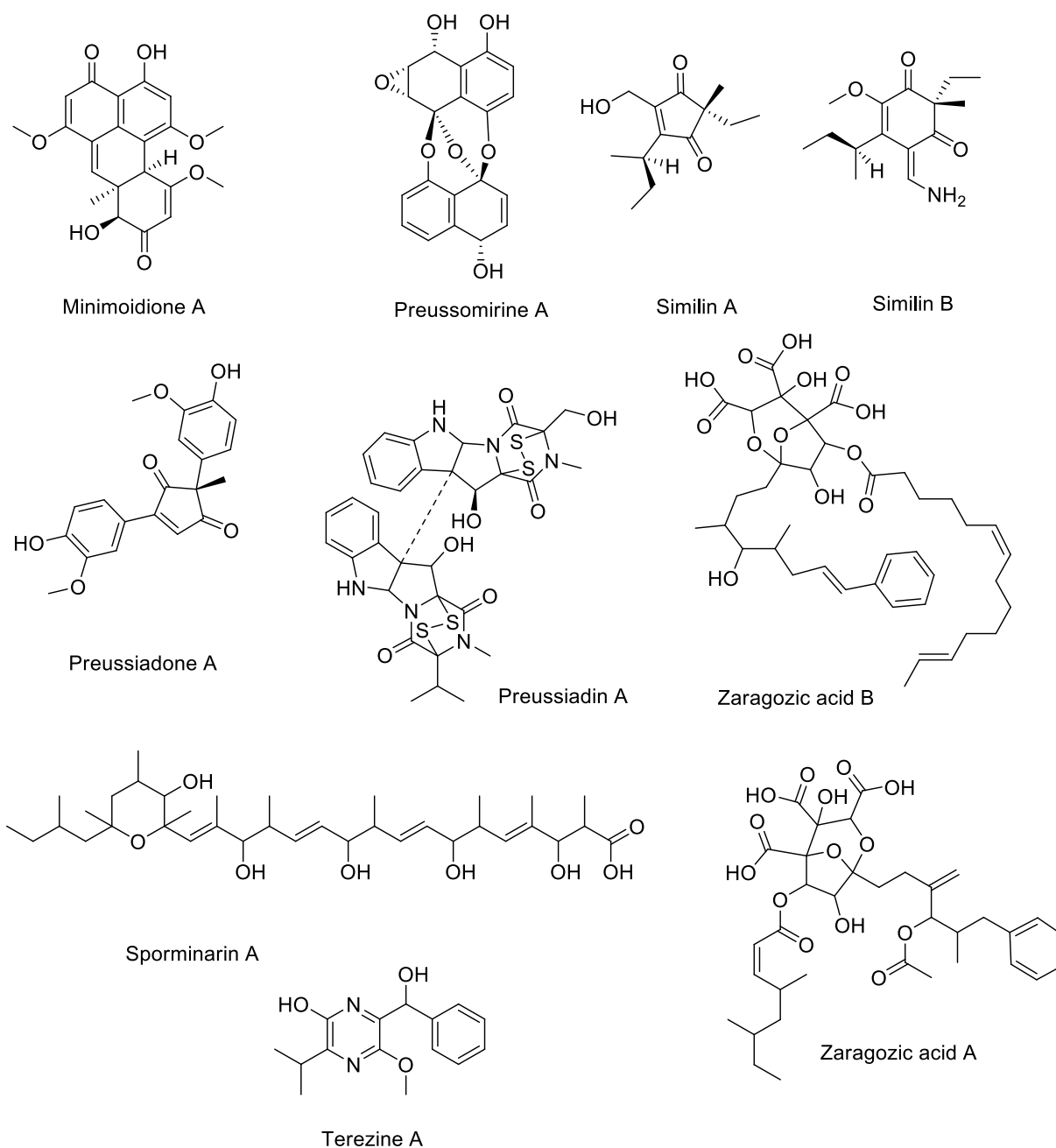


Figure 5: Chemical structures of secondary metabolites isolated from the conglomerate *Preussia/Sporormiella* as indicated in Table 2

I.8.2. Genus *Dendrothyrium*

Dendrothyrium Verkley, Göker & Stielow, has been described recently as a new coelomycete genus belonging to the family Montagnulaceae (Pleosporales, Pleosporomycetidae, Dothideomycetes, Pezizomycotina and Ascomycota). *Dendrothyrium* species were previously named as *Coniothyrium* spp. and their taxonomy was re-assessed based on analyses of concatenated ITS of the nrDNA operon,

LSU, γ -actin and β -tubulin gene sequences. The genus name refers to the branched, tree (= dendron)-like conidiophores.

The genus *Dendrothyrium* includes two species: *Dendrothyrium longisporum* and *Dendrothyrium variisporum*. The latter is the type species of this genus. They are coelomycetous asexual morphs of Pleosporales (Ascomycota), characterised by pycnidial or stromatic conidiomata producing mostly relatively small, subhyaline to pigmented, 1-celled conidia. The sexual morph is unknown. The two species of this genus are distinguished according to the shape of their conidia. In fact, the species *Dendrothyrium variisporum* is characterized by conidia different in their shape comparatively to the long conidia characteristic of *Dendrothyrium longisporum*. The genus *Dendrothyrium* includes mostly fungi found as endophytes or plant pathogens associated with a wide range of hosts (Verkley *et al.*, 2014). To the best of our knowledge, no study has been made regarding the production of secondary metabolites by the genus *Dendrothyrium*.

I.8.3. Genus *Chaetomium*

The genus *Chaetomium* (Chaetomiaceae, Sordariales, Sordariomycetidae, Sordariomycetes, Pezizomycotina, and Ascomycota) comprises more than 400 of marine and terrestrial species. The genus *Chaetomium* was established by Kunze and Schmidt (1817), based on *Chaetomium globosum* as its type species (Wang *et al.*, 2016). This genus is characterized by superficial ascomata usually covered with hairs, membranaceous peridium, consisting of several pseudoparenchymatous layers; asci that are clavate or fusiform (with biserially arranged ascospores) or sometimes cylindrical (with uniseriately arranged ascospores), thin-walled, evanescent and without apical structures; scarce paraphyses that disappear before ascomata mature; ascospores that are brown or gray-brown (never opaque or black), one-celled, with one or sometimes two germ pores, and exuding as a dark, black, sticky mass (Asgari and Zare, 2011).

Members of the genus *Chaetomium* are known to use a variety of substrates, especially cellulose. More than 200 compounds have been isolated from *Chaetomium* species including: chaetoglobosins, epipolythiodioxopiperazines, azaphilones, depsidones, xanthonones, anthraquinones, chromones and steroids (Zhang *et al.*, 2012) (Table 3 and Figure 6). The presence of the fungal genus *Chaetomium* and its secondary metabolites in building material is suspected to be harmful to the human health. In fact, the most common species in indoor environments are *Chaetomium globosum* and *Chaetomium elatum*, which can contaminate even new gypsum wallboards. In addition to the dissemination of their

ascospores and hyphae in the environment, the production of toxic metabolites including chaetoglobosins, chaetoviridins and cochliodone were detected in building materials (Došen *et al.*, 2017). These compounds are likely to contribute to the development of the symptoms of both rhinitis and asthma (Wang *et al.*, 2016).

Table 3: Selected compounds isolated from *Chaetomium* spp.

Species	Isolation source	Compound	Compound family	Biological activity
<i>Chaetomium elatum</i> (<i>C. elatum</i>)	Endolichenic (<i>Everniastrum cirrhatum</i>)	Xanthoquinodins A1-A6 (Chen <i>et al.</i> , 2013)	Xanthone- anthraquinone	Antibacterial, antifungal, anticoccidial, antiplasmodial, and cytotoxic
<i>C. globosum</i>	Marine fish (<i>Mugil cephalus</i>)	Chaetomugilins A-F (Yasuhide <i>et al.</i> , 2008)	Chlorinated azaphilones	Cytotoxic
<i>C. globosum</i>	Unknown	Chaetoglobosins (Sekita <i>et al.</i> , 1973)	Macrocyclic polyketide alkaloids	Cytoskeleton inhibitors
<i>C. cochliodes</i>	Soil	Cochliodinol (Brewer <i>et al.</i> , 1968)	Bis (3- indolyl)- benzoquinones	Antimicrobial
<i>Chaetomium sp.</i>	Algicolous marine fungus	Chaetominedione (Abdel-Lateff, 2008)	Benzonaph- thyridinedione derivative	Tyrosine kinase inhibitor
<i>C. brasiliense</i>	Colonist of sclerotia of <i>Aspergillus flavus</i>	Chaetochalasin (Oh <i>et al.</i> , 1998)	Decalin derivative	Cytotoxic and Antimicrobial
<i>C. globosum</i>	Leaves of <i>Ginkgo biloba</i>	Gliotoxin (Qin <i>et al.</i> , 2009)	Epipolythiodio xopiperazine	Antifungal

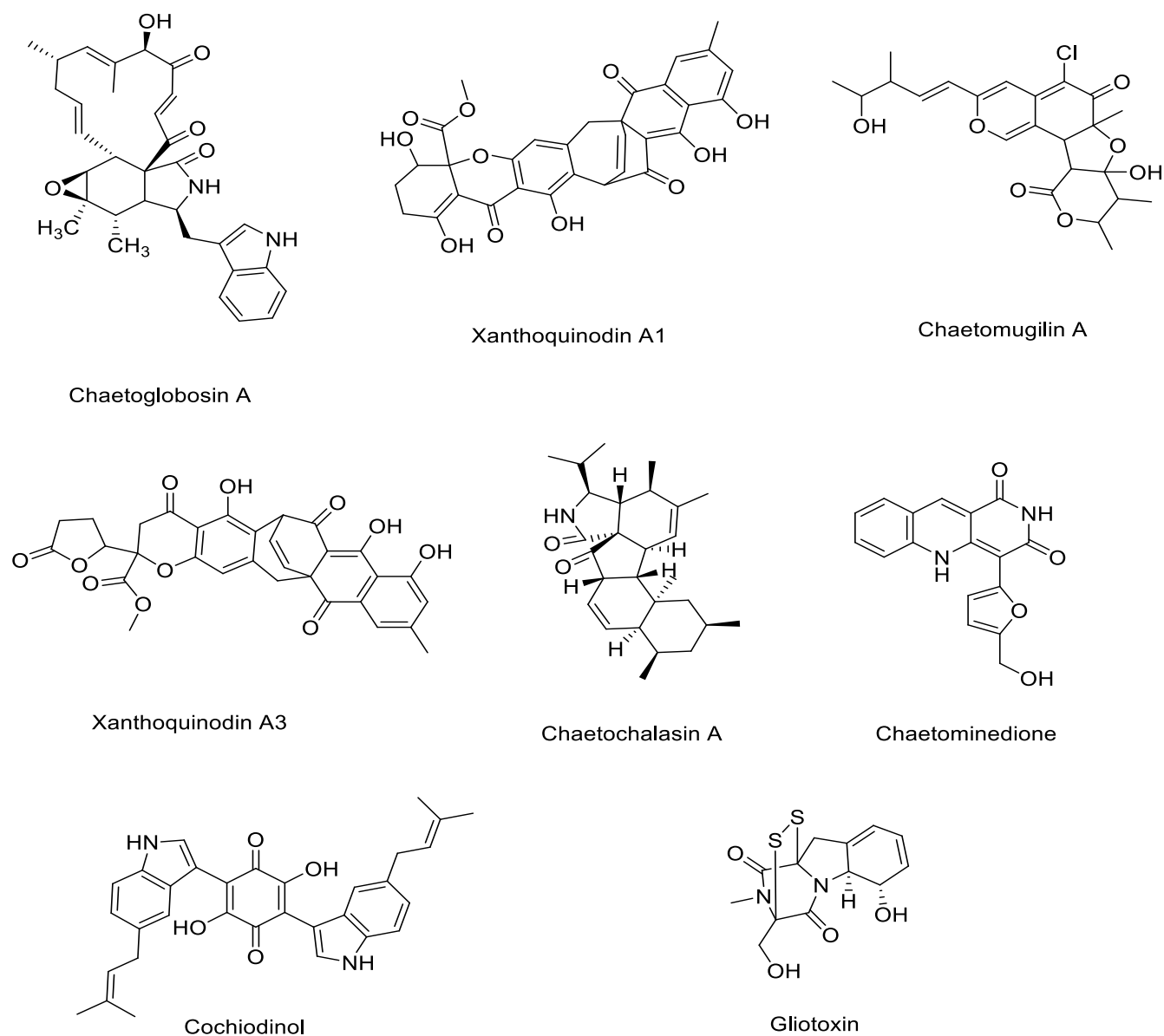


Figure 6: Chemical structures of selected secondary metabolites isolated from *Chaetomium* spp. as indicated in Table 3.

II. *Globularia alypum*

II.1. Taxonomy and botanical aspect of *Globularia alypum*

The genus *Globularia* was recently included in the family Plantaginaceae (Albach *et al.*, 2005). It contains about 22 species (Chaudhari and Badole, 2014) of evergreen perennials and small shrubs, recognizable by blue flowers assembled in globular capitula, after which it was named (Touaibia and Zohra, 2016). *Globularia* is native to central and southern Europe, Macaronesia, northwestern Africa and southwestern Asia (Djellouli *et al.*, 2014).

The Mediterranean region is viewed as their primary center of diversification (Touaibia and Zohra, 2016). In Algeria, two species were reported, one of them is endemic, *Globularia eriocephala* (Pomel); the other is *Globularia alypum* L. (*G. alypum*) (Khelifi *et al.*, 2011). The latter, locally named Tasselgha (Djellouli *et al.*, 2014; Boutemak *et al.*, 2015), Ain Larnab and Zriga (Khelifi *et al.*, 2011) is a nanophanerophyte reaching 0.3–1 m height (Estiarte *et al.*, 2011) characterized by erect and ligneous stems with lanceolate leaves. Flowers in globose heads (Figure 7) are lilac-blue tilling 2.5 in diameter. Bracts are very perceptible and imbricate (Chograni *et al.*, 2013). *G. alypum*, called shrubby globularia, lives in calcareous soils and is typical of the termophyllous shrublands (Estiarte *et al.*, 2011). Table 4 presents the taxonomy of *G. alypum*.



Figure 7: *Globularia alypum* (IUCN, 2005)

Table 4: Botanical classification of *Globularia alypum* (Albach *et al.*, 2005; Boutiti *et al.*, 2008)

Kingdom	<i>Plantae</i>
Division	Magnoliophytes
Class	Magnoliopsida
Sub classe	Asteridae
Order	Scrophulariales
Family	Plantaginaceae
Genus	<i>Globularia</i>
Species	<i>Globularia alypum</i> L.

II.2. Chemical constituents of *G. alypum* and their biological activities

G. alypum is a rich source of bioactive substances such as iridoid glycosides (catapol), aromatic/phenolic acids, flavonoid glycosides and aglycons, phenylethanoids (Djeridane *et al.*, 2007) and tanins (Leporatti and Ghedira, 2009; BenMansour *et al.*, 2011). It is reputed to exhibit several potent pharmacological activities specially their leaves which are recognized as a good source of antioxidants (Harzallah *et al.*, 2010; Khlifi *et al.*, 2011; Chograni *et al.*, 2013). This could explain why they are frequently used in folk medicine. *G. alypum* is commonly used in Algerian traditional medicine as a healing agent, such as hypoglycaemic agent, laxative, cholagogue, stomachic, purgative, sudorific (Boutiti *et al.*, 2008), antimicrobial and also in the treatment of cardiovascular, antitumorous and renal diseases (Harzallah *et al.*, 2010). Their leaves are reported to be used in the treatment of skin diseases (notably eczema), diabetes (BenMansour *et al.*, 2011) and antimalarial (Leporatti and Ghedira, 2009).

Experimental section

Chapter I

Material and methods

1. Plant material

The plant *G. alypum* (Figure 8) was selected to study its endophytic fungal content. Sampling site of this study was the region of Al chihat, Ouled Aouf, Ain Touta (Batna, Algeria). The plant samples were collected by the author in June 2015 and identified by Mr. Hamchi Abdelhafid from National Park of Belezma (Batna, Algeria) and stored in sterile bags. Processing of samples occurred within three hours from collection.



Figure 8: *Globularia alypum* used in this study
(A) Natural growing plant, (B) Collected plant specimen used for endophytes isolation.

2. Isolation of the endophytic fungi

The endophytic fungi were isolated from the healthy roots of *G. alypum*. The tissue samples were washed exhaustively in running tap water followed by distilled water to remove any soil and dirt and then were cutted into several 1 cm section pieces. In order to eliminate the epiphytic microorganisms, the surface of the root fragments were sterilized by step-wise washing in 70 % ethanol for 1 minute, immersed in sodium hypochlorite for 3 minutes, then soaked in 70 % ethanol for 30 seconds and followed by three rinses in sterile distilled water for 1 minute each to remove surface sterilization agents and dried in a sterile filter (Kusari *et al.*, 2008). Thereafter, the surface-sterilized root fragments were aseptically transferred to Petri dishes containing MEA, NA, PDA and YEA (Figure 9). The efficiency of surface sterilization procedure was ascertained by plating aliquots of the last rinsate on the same media to verify sterility. The success of surface sterilization method was confirmed by the absence of microbial growth on the cultural media. Afterwards, all Petri dishes were sealed with parafilm and incubated at $28 \pm 2^{\circ}\text{C}$. Cultures were examined regularly for emerging

fungal colonies. The growing edges of any fungal hyphae developing from tissue fragments were then transferred aseptically to YMG agar. After purification, all isolates were routinely maintained in 10% glycerol at -80°C for long-term storage and on YMG agar slant tubes in active form and for further identification (Stadler *et al.*, 2001).



Figure 9: Root fragments on agar plates.

3. Identification of fungal isolates

The fungal strains were characterized by both morphological and molecular phylogenetic methods as described in Ahmed and Cain (1972), Arenal *et al.* (2005, 2007) and Verkley *et al.* (2014).

3.1. Morphological studies

Fungal cultures were examined for macro- and micromorphological characters. Therefore, the cultures were grown at 23°C on YMG and OMA agar media.

3.1.1. Macroscopic features

Colony diameter was recorded on YMG and OMA after 7 to 21 days in three replicates. Macroscopic characteristics such as colony appearances, mycelial textures and pigmentations on both obverse and reverse plates were assessed. All macroscopic features on YMA and OMA in 9 cm Petri dishes were observed using a stereomicroscope. A number of endophytic fungi consist of sterile mycelia or non-sporulating fungi and are consequently cannot be identified by morphological methods, therefore molecular strategy are required. In parallel, these fungi that did not produce any reproductive structure were cultivated on OMA and kept under alternating cycles of 12 hours near blue light (wavelengths from about 470 to 495 nm)/day light during one month in order to induce teleomorphic state. The cultures were checked for eventual mycelia differentiation. In case of teleomorphic structures, shape and size of ascomata, size and form of the perithecia were also examined.

3.1.2. Microscopic features

For microscopic characters, observations and measurements were made with optical microscope and photos were taken through a brightfield microscope at 400–1,000 × magnification. Microscopic mounts were made in sterile distilled water from YMG and OMA colonies:

a. Teleomorphic state: the descriptions were made according to those used by Ahmed and Cain 1972: shape and size of the asci and ascospores, examination of ascospores for presence of gelatinous sheath, septa, germ slit and its position.

b. Anamorphic state: taxonomic identification keys for conidiogeneous structures were recorded using standard protocols: colour, size, and morphology of hyphae, conidiophores, conidiogenous cells and conidia.

3.1.3. Ultrastructure of ascospores by electron microscopy

To further investigate the ultrastructure of asci and ascospores, micrographs with a field-emission scanning electron microscope (FE-SEM Merlin, Zeiss, Germany) were kindly taken by Prof. Dr. Manfred Rohde, Head of the Research Group Molecular mechanisms of streptococci (Helmholtz Centre for Infection Research, Braunschweig, Germany). For this propose, pseudothecia were transferred from OMA plates into sterile filter paper. At the moment of microscopic observation, the material was softly pressed in order to release the asci and their ascospores contents.

All fungi of interest were preserved in the private culture collection of Prof. Dr. Marc Stadler (STMA, Helmholtz Centre for Infection Research, Braunschweig, Germany), some of them were deposited at DSMZ Braunschweig (Germany).

3.2. Molecular studies

In this study, molecular strategy specifically utilizing of ITS rDNA gene sequence and phylogenetic analysis were achieved.

3.2.1. DNA extraction

DNA extraction was performed with the EZ-10 Spin Column Genomic DNA Miniprep kit (Bio Basic Canada Inc., Markham, Ontario, Canada) following the manufacturer's protocol. The genomic DNA was isolated from pure cultures. In a first step, up to 1 cm² (depending on the density) of young mycelia were removed and put into 1.5 mL screw cap tubes containing 6-10 Precellys (1.4

mm) ceramic beads (Peqlab, Germany) and 150 μ L PCL buffer (Lysis buffer). A Precellys 24 homogenizer (Bertin Technologies, France) was used for cell disruption at a speed of 6000 rpm for 2 \times 40s. To lyse the cells, the samples were incubated for 20 minutes at 65°C. Subsequently, 25 μ L PP solution was added and the samples were thoroughly mixed, incubated for 15 minutes on ice and subsequently centrifuged for 2 minutes at 4°C and a speed of 10000 rpm. In the following, the supernatant of the lysed samples was applied on a silica column (EZ-10 Spin Column) containing 300 mL PB buffer to adjust the binding conditions of the DNA to the silica membrane. The samples were incubated for 3 minutes and mixed by inverting occasionally. Subsequently, the samples were centrifuged for 30 seconds at a speed of 10000 rpm and the flow-through was discarded. To clean the DNA sample 500 μ L washing buffer was added to the DNA samples and the samples were centrifuged at 14000 rpm for 30 seconds. The follow-through was discarded and the washing step was repeated. Afterwards, the samples were centrifuged for an additional minute at 10000 rpm without any ingredients in order to remove all solvents from the membrane. The collection tube was discarded and replaced with a clean 1.5 mL reaction tube (Eppendorf, Germany). To elute the DNA, 50 μ L of 65°C warm elution buffer was applied to the center of the silica membrane, incubated for 3 minutes and subsequently centrifuged at 10000 rpm for 2 minutes. The silica column was discarded and the eluted DNA was stored at -20°C until further use.

3.2.2. Amplified regions used for the identification

The ITS region is regarded as a DNA barcode marker for the identification of fungi (Schoch *et al.*, 2012). Therefore, the ITS region (5.8S gene region, the internal transcribed spacer 1 and spacer 2) of all extracted DNA, was amplified using primers ITS1F and ITS4 (White and Bruns, 1990). The sequencing results were compared with sequences in the BLAST GenBank: <https://blast.ncbi.nlm.nih.gov/Blast.cgi>. Reference sequences with high homology were collected from the BLAST GenBank and used to assign identity. Additionally, for some strains, further molecular markers were used to achieve higher support values for taxon separation and shed a better light on the phylogeny of our fungi.

The partial large subunit (LSU) and the ribosomal RNA genes: elongation factor gene that includes one intron (EF-1 α), β -tubulin gene (Tub) and partial γ actin (Act) were amplified using the following primer set: LR0R/LR7 (Vilgalys and Hester, 1990), EF1-728F/ EF-986R, (Carbone, 1999) T1/T22 (O'Donnell and Cigelnik, 1997), ACT 512F/ACT783R (Verkley *et al.*, 2014) respectively. The PCR programs setup for the used marker genes are displayed in Table 5. The PCR was performed using the

Mastercycler nexus Gradient (Eppendorf, Germany). The PCR's were carried out in 25 μ L assays containing 1x JumpStart™ Taq ReadyMix™ (containing 2.5 U JumpStart Taq DNA polymerase, 10 mM Tris-HCl, 50 mM KCl, 1.5 mM MgCl₂, 0.001% gelatine, 0.2 mM dNTP) and 0.2 μ M of the respective forward and reverse primer.

Table 5: Detailed PCR programs for the used marker genes amplification (ITS, LSU, EF-1 α , Tub and Actin).

Step	Gene markers					
	ITS	LSU	EF-1 α	BTub	γ Actin	
Primer set	ITS1F/ITS4	LROR/LR7	EF1 728F/ 986R	T1/T22	ACT 512F/783R	
Denaturation	94°C/5min	94°C/5min	95°C/8min	94°C/35 s	94°C/5min	
Denaturation	94°C/30s	94°C/1min	95°C/15s	94°C/35 s	94°C/1min	x34, x34,
Annealing	52°C/30s	52°C/1min	53°C/20s	52°C/55 s	61°C/1min 30s	x35, x32,
Elongation	72°C/1min	72°C/1min	72°C/60s	72°C/2 min	72°C/2min	x35, cycles respectively
Elongation	72°C/10min	72°C/10min	72°C/5min	72°C/10min	72°C/10min	

3.2.3. Gel electrophoresis

The success of the PCR was verified *via* gel electrophoresis in a 0.8 % agarose gel (in 1x TAE buffer). The basic principle of gel electrophoresis is, that due to its negative loading, the DNA shifts to the cathode in an electrical field. For the monitoring of the amplification, 3 μ L of each PCR product was mixed with 2 μ L Loading dye made of TAE, Midori Green Direct DNA stain and gel loading buffer (0.25 % vol. bromophenol blue, 0.25 % vol. xylene cyanol, 0.8 % vol. FICOLL 400 and 1.20 mM EDTA) at a ratio of 1:1:1. To control the size of the PCR fragments 3 μ L of a 1kb Ladder was mixed with 2 μ L of Loading dye and used as standard. The PCR products were separated electrophoretic at 100 V for 30 minutes in the Mupid®-One electrophoresis chamber and documented with the FastGene® gelPic LED Box (NIPPON Genetics Europe GmbH, Germany).

3.2.4. Purification of the PCR products and sequencing

The samples with the desired PCR products were purified with the EZ-10 Spin Column PCR Purification Kit (Bio Basic Inc., Canada) in order to get rid of remaining molecules, such as remaining (oligo-) nucleotides from the PCR to prevent interferences in the successional sequencing.

Like the DNA extraction kit, the basic principle of this kit is the binding of the DNA molecules to a silica membrane and the removal of unwanted substances through particular washing steps. Oligonucleotides of a size of 40 bases or smaller, cannot bind to the membrane and were removed, too. The remaining PCR product was mixed with the B3 Buffer in a ratio of 1:4 to adjust the binding conditions and the samples were applied to the silica membrane of the EZ-10 Spin Columns. After 2 minutes of incubation, the columns were centrifuged at 100000 rpm for 30 seconds and the flow-through was discarded. Subsequently, 500 μ L washing buffer was added to the spin column and the columns were centrifuged for another 30 seconds at 100000 rpm. The washing step was repeated and the spin columns were centrifuged at 100000 rpm for 1 minute in order to remove remaining washing buffer from the membrane. The collection tube was replaced by a clean 1.5 mL reaction tube and 15 μ L of 65°C elution buffer was applied to the center of the silica membrane. After an incubation period of 2 minutes, the Spin columns were centrifuged at 100000 rpm for 1 minute in order to elute the DNA from the membrane. The purified PCR products were stored at -20°C until further use.

The purified PCR products and the desired primers (2 μ M of each primer) were send to the in-house sequencing service of the Genome Analytics Group (GMAK), Helmholtz Centre for Infection Research, Braunschweig, Germany. The amplified products were sequenced using an ABI 3730xl, capillary sequencer machine.

3.2.5. Phylogenetic analysis

For the phylogenetic reconstruction, the sequences of each gene marker derived from authentic strains were automatically aligned with sets of previously published sequences originating from reliable sources. Multiple alignment of sequences of each gene marker was performed by E-INS-i algorithm of MAFFT v7.017 (Fast Fourier Transformation) (Kato *et al.*, 2002; Kato and Toh, 2008). The alignments were cured with low stringency using Gblocks v0.91b (http://molvol.cmima.csic.es/castresana/Gblocks_server.html). The aligned sequences were then concatenated to generate multigenes alignment (MGA). Phylogenetic tree construction was carried out using PhyML (Guindon and Gascuel, 2003) and RxML to infer the tree topology in Geneious® software tool version 7.1.5 (Kearse *et al.*, 2012), using a substitution model: GTR G+I, GTR+G. Outgroup taxa were used to root trees. The reliability of the trees was tested by bootstrapping 1000 replicates. Morphological observation, analysis of ITS sequence and multigenes alignment to identify the fungal strains.

4. Small scale fermentation and preparation of extracts from cultures

4.1. Small scale fermentation

For screening, small scale fermentation was carried out primarily to perform, preliminary biological assays and HPLC-MS based dereplication. The cultivation of fungal strains was done in three different liquid media, differed in their carbon and nitrogen source, to evaluate the production of the bioactive secondary metabolites (**YMG medium**: 1% malt extract, 0.4% glucose, 0.4% yeast extract, pH 6.3; **Q6/2 medium**: 1% glycerol, 0.25% glucose, 0.5% cotton seed flour, pH 7.2; **ZM/2 medium**: 0.5% molasses, 0.5% oatmeal, 0.15% glucose, 0.4% sucrose, 0.4% mannitol, 0.05% edamine, 0.05% ammonium sulphate, 0.15% calcium carbonate, pH 7.2). One 500 mL Erlenmeyer flask for each medium was used to afford enough extract for preliminary bioactivity screening and metabolite profile analysis. Five mycelial plugs were cut from mature YMG agar plates and placed in Erlenmeyer flasks (500 mL) filled each with 200 mL of each medium. These media were chosen according to previous studies (Stadler *et al.*, 2003; Bitzer *et al.*, 2008) which revealed that they are optimal for attaining complementary secondary metabolite profiles of filamentous ascomycetes (Halecker *et al.*, 2014). The submerged cultures were incubated at 23 °C in the dark on a rotary shaker at 140 rpm. Fermentations were aborted after two days of carbon source depletion. In this respect, the amount of free glucose was measured during fermentation by using commercial glucose test strips.

4.2. Extraction

After the end of the fermentation, the mycelium was separated from the fermentation broth by vacuum filtration and extracted with acetone in an ultrasonic bath at 40 °C for 30 minutes. The solvent was evaporated *in vacuo* under reduced pressure until some aqueous phase remained, followed by three times extractions in a separation funnel with equal amounts of EtOAc and water. The extract was dried over anhydrous sodium sulfate (Na_2SO_4), filtered and concentrated in vacuum to yield the mycelial crude extract.

To prepare the crude extract from the supernatant, EtOAc was added to culture filtrate (1:1). The organic solvent was evaporated *in vacuo* under reduced pressure at 40 °C using a rotary evaporator to give the organic phase. The concentrated organic phase was dissolved in MeOH and put in vial, then under nitrogen evaporator, to give supernatant crude extract.

5. Generation of secondary metabolite profiles of crude extracts

The secondary metabolite profiles of the crude extracts were measured using an analytical HPLC instrument (Agilent 1260 Infinity Series, Santa Clara, USA) equipped with a DAD and an ESI-iontrap mass spectrometer (amazon speed, Bruker; Bremen, Germany). An ACQUITY UPLC BEH C18 column (50 × 2.1 mm, particle size 1.7 μm; from Waters) was used as stationary phase. The mobile phase was composed of solvent A (water + 0.1 % formic acid) and solvent B (acetonitrile + 0.1 % formic acid). The gradient started with 0.5 minute isocratic conditions at 5 % solvent B which increased in 19.5 minutes to 100% solvent B followed by 5 minutes isocratic conditions. A flow rate of 600 μL/min was applied and compounds were detected with the DAD in a range between 200 – 600 nm. The HPLC profiles were evaluated with the Bruker DataAnalysis software (version 4.1). DAD absorption spectra and mass spectra of the corresponding peaks were compared to those of known compounds in internal databases which summarized the MS data for many secondary metabolites from different organisms.

6. Serial dilution assay

Screening for antimicrobial activity of crude extracts was carried out by determination of MIC against the following microorganisms: *Bacillus subtilis* DSM 10, *Escherichia coli* DSM 498, *Candida tenuis* MUCL 29892 and *Mucor plumbeus* MUCL 49355. Firstly, inoculum suspension was prepared by transferring stock suspension of each bacterium and yeast (100 μL) to 100 mL of EBS (0.5 % casein peptone, 0.5 % glucose, 0.1 % meat extract, 0.1 % yeast extract, 50mM HEPES [11.9 g/L], pH 7.0) (Halecker *et al.*, 2014) and YMG medium, respectively. They were incubated on a rotary shaker at 30°C for 16-20 h. After incubation, the suspension was adjusted to a concentration of 6.7×10^5 cells/mL using a hemacytometer. The spore suspension of *Mucor plumbeus* was prepared at a concentration of 2.7×10^7 conidia/mL and stored at -20°C. This was further diluted to 6.7×10^5 conidia/mL using YMG medium. The serial dilution assays were performed in 96-well microtiter plates. Fungal crude extracts were dissolved in MeOH at a concentration of 4.5 mg/mL. Firstly, 20 μL aliquots of crude extract or pure compounds were pipetted on the first well of each column (1-10). Standard antibiotics and MeOH were added into the first well of column 11 and 12 as positive and negative controls, respectively. Using a multichannel pipet, 150 μL of a mixture of the test pathogen and the culture medium was aliquoted in all the rows. To the first row, an additional 130 μL of the pathogen-medium mixture was added and mixed by repeated pipetting, before transferring the same

amount to the second row. The solutions were then serially 2-fold diluted in the subsequent rows, 150 μL discarded after the last row (H). Eight concentrations ranging from 2.34-300 $\mu\text{g}/\text{mL}$ for the crude extracts. Plates were incubated on a microplate-vibrating shaker (Heidolph Titramax 1000) at 600 rpm at 30°C for 24 to 48 h. After incubation, the lowest concentration of the drug preventing visible growth of the pathogen was taken as MIC (Okanya *et al.*, 2011). Ciproloxacin (1 mg/mL) was used as positive control in case of both Gram positive and Gram negative bacteria. Nystatin (1 mg/mL) was used as positive control against yeasts and filamentous fungi.

7. Bioactive-guided fractionation of crude extracts

The extracts showing high antimicrobial activity in the serial dilution assay (MIC value of 2.34 $\mu\text{g}/\text{mL}$) were fractionated to localize the activity. A bioactivity guided fractionation of the extracts was performed with an Agilent 1260 HPLC (high performance liquid chromatography) system equipped with an UV (ultraviolet) DAD and a fraction collection unit for 96-well plates using an XBridge™ C18 column (100 \times 2.1 mm; particle size 3.5 μm) from Waters. The mobile phase was composed of 95% deionised water/ 5% acetonitrile (solvent A) and 95% acetonitrile/5% deionised water (solvent B) and both contained 5mM ammonium acetate and 40 $\mu\text{L}/\text{mL}$ acetic acid. The gradient was set from 10% to 100% B in 30 minutes and maintained at 100% B for 10 minutes with a flow rate of 0.3 mL/min. The run was conducted with an injection volume of 5 μL . The molecules in the extract will pass the detector (chromatogram) and the extract will be fractionated. Every 30 seconds a new fraction will be collected in a well of a 96 well plate. After fractionation the solvent was removed by nitrogen-aeration and filled with EBS medium with a cell suspension of 6.7×10^5 cell/mL for later observation for antibiotic activity against *B. subtilis*. After over-night incubation on a microplate-vibrating shaker (Heidolph Titramax 1000) at 600 rpm at 30°C, the inhibited well can be correlated to the retention time and the corresponding peak. Using this methodology, the retention time and UV of the bioactive compound were determined and compared with HPLC-MS chromatogram.

8. Scale-up of fermentation

The large-scale culture was done based on the biological activity screening and the metabolite profiles analysis of the extract that had previously shown the most promising activities. Batches of flask fermentations of up to 8 L were fermented using the original protocols, in order to provide sufficient quantities for preparative work. The volume of culture as well as the cultivation period are indicated in table 6.

Table 6: Media used for large scale fermentation and cultivation period

Fungal strain	Medium	Volume	Fermentation period
Strain DSM 104666	ZM/2	8 L	34 days
Strain STMA 16219	Q6/2	8 L	7 days
Strain DSM 32328	Q6/2	5 L	7 days
Strain STMA 16226	YMG	8 L	12 days
Strain STMA 16225	YMG	3 L	9 days

For extraction, instead of using EtOAc for the supernatant as explained in small scale fermentation, the broth was treated with 2% of adsorber resin Amberlite XAD™-16N and incubated for two hours. After filtration, acetone was added to the XAD and extracted by sonication at 40°C for 30 minutes. The eluate was then treated as described above for mycelial extract. For both mycelium and culture filtrate, the extraction procedure was repeated 3 times with fresh organic solvent.

9. Isolation of secondary metabolites

All crude extracts were dissolved in the appropriate organic solvent and centrifuge 4000 rpm for 10 minutes prior to preparative HPLC to eliminate any undesired particles. Preparative HPLC was performed at room temperature on an Agilent 1100 series preparative HPLC system (Agilent Technologies), ChemStation software (Rev. B.04.03 SP1); binary pump system; column: Kromasil RP C18, particle size 7 µm, dimensions 250 x 25 mm; mobile phase: acetonitrile (ACN) and water; flow rate 20 mL/min; diode-array UV detector; 226 fraction collector.

For the separation of large amounts of crude extracts, the samples were subjected to flash chromatography (GRACE Reveleris X2 flash system). The details of the isolation of the metabolites from different crude extracts obtained from large scale fermentation of the selected five fungal endophytes as well as the gradients used are illustrated by schematic diagrams in figures 10, 11, 12, 13, 14 and 15.

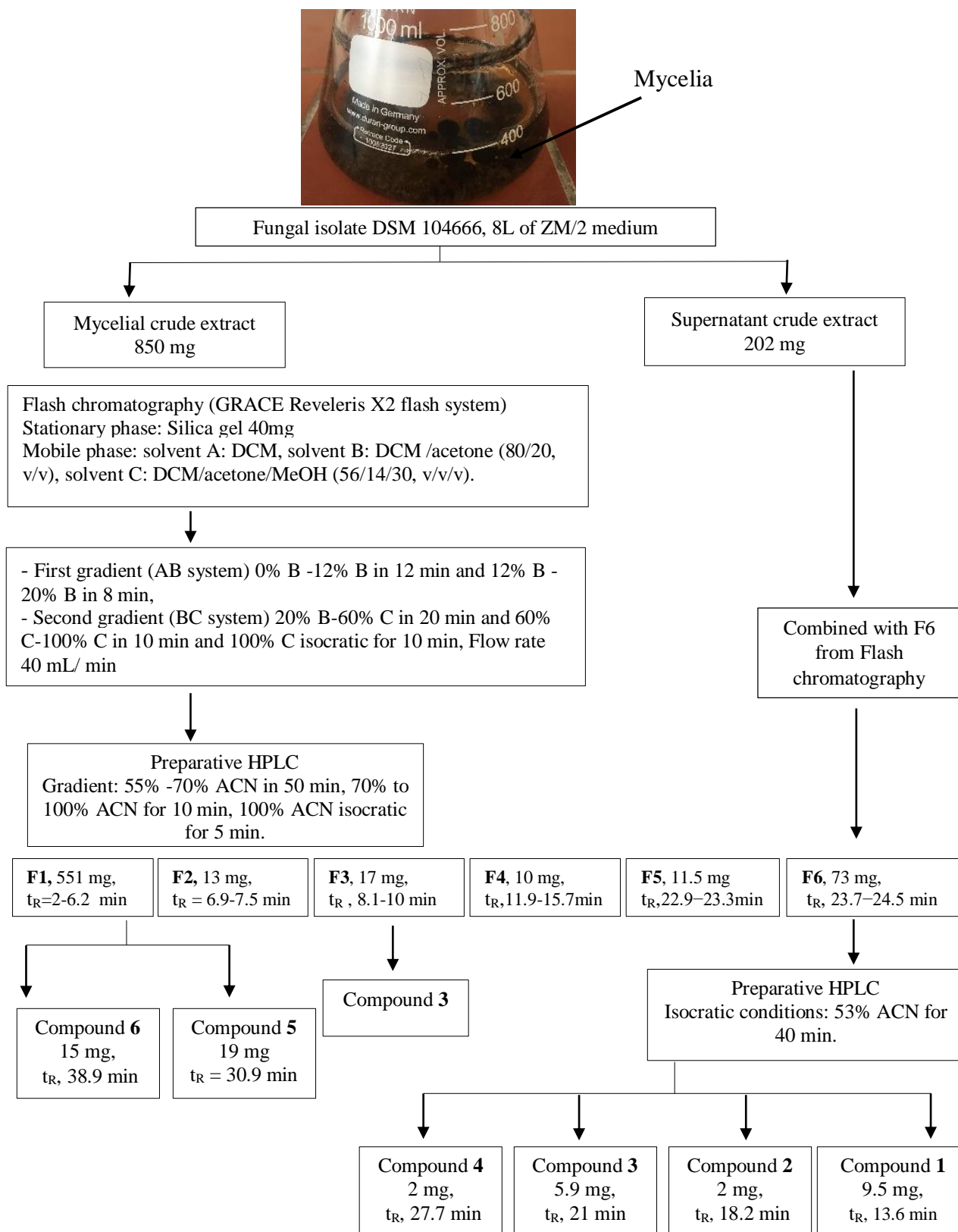


Figure 10: Schematic diagram showing purification steps of metabolites isolated from mycelial and supernatant crude extracts derived from fermentation culture of the fungal isolate DSM 104666 in 8L of ZM/2 liquid medium.

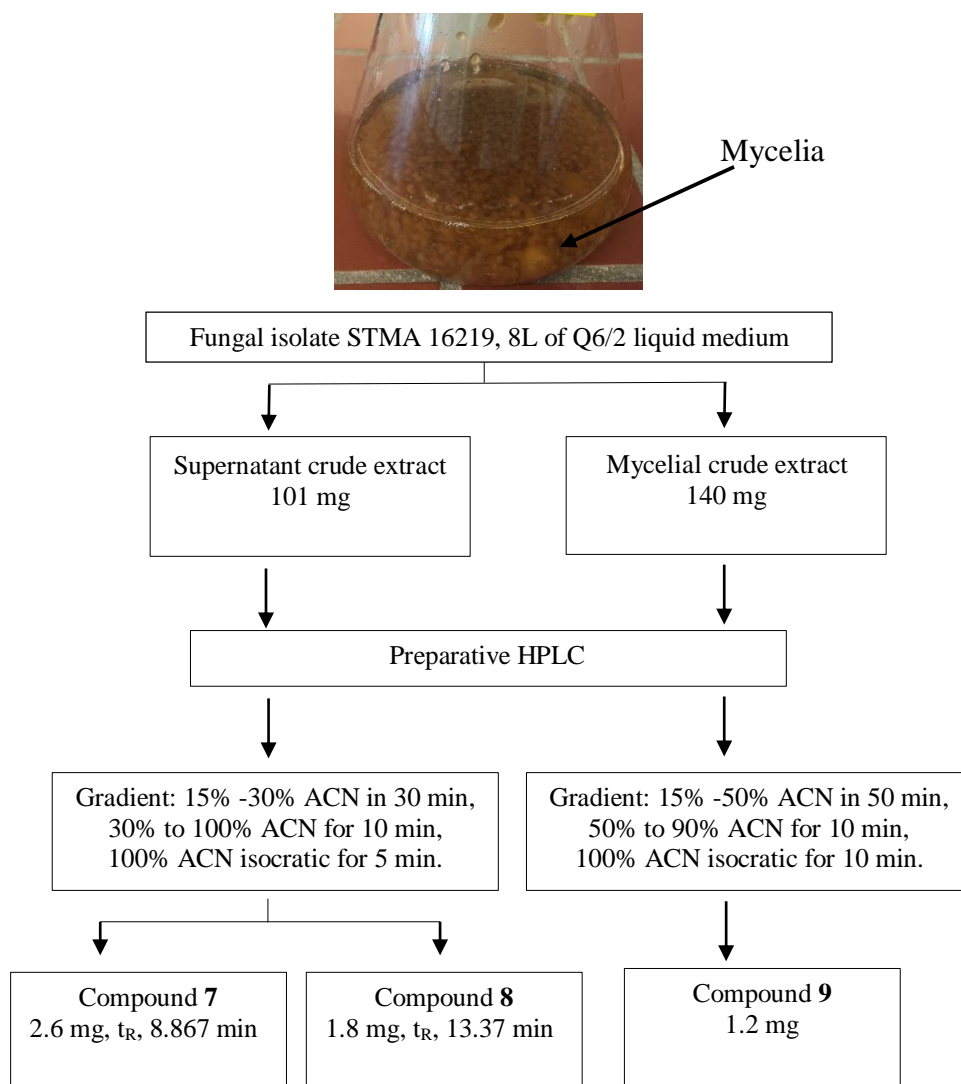


Figure 11: Schematic diagram showing purification steps of metabolites isolated from mycelial and supernatant crude extracts derived from fermentation culture of fungal isolate STMA 16219 in 8L of Q6/2 liquid medium.

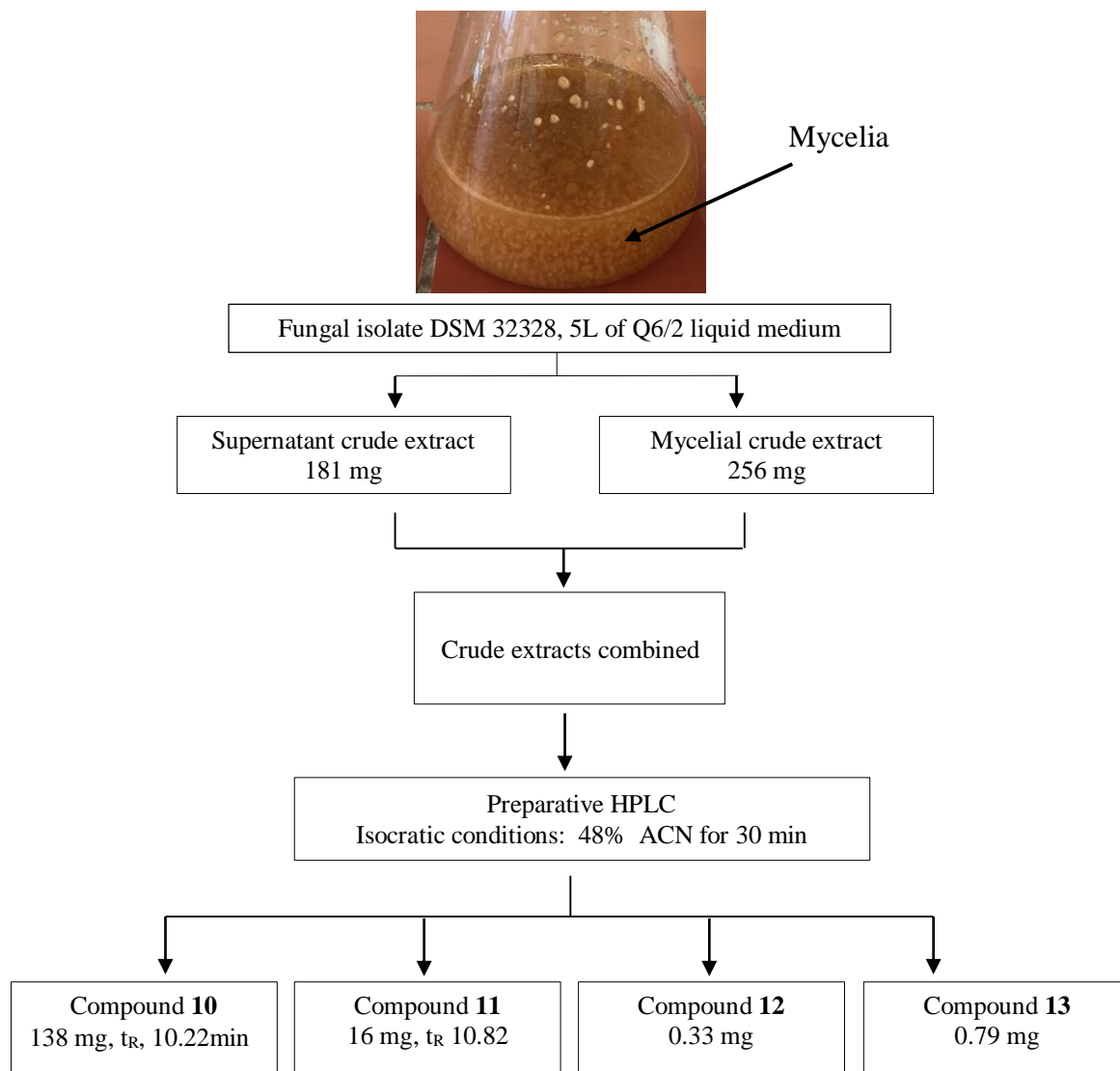


Figure 12: Schematic diagram showing purification steps of metabolites isolated from mycelial and supernatant crude extracts derived from fermentation culture of fungal isolate DSM 32328 in 5L of Q6/2 liquid medium.

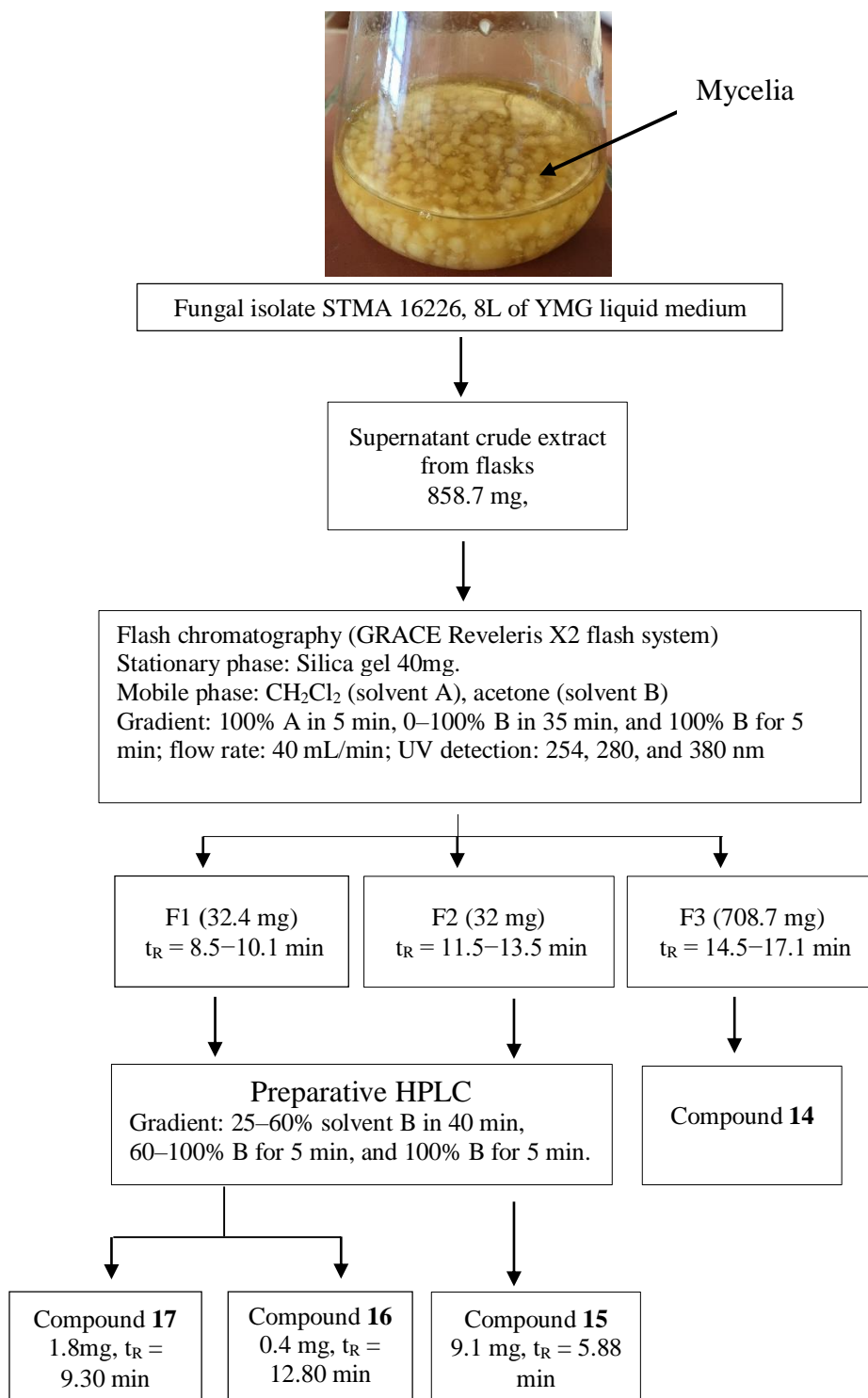


Figure 13: Schematic diagram showing purification steps of metabolites isolated from flasks culture in 8L of YMG medium of the fungal isolate STMA 16226.

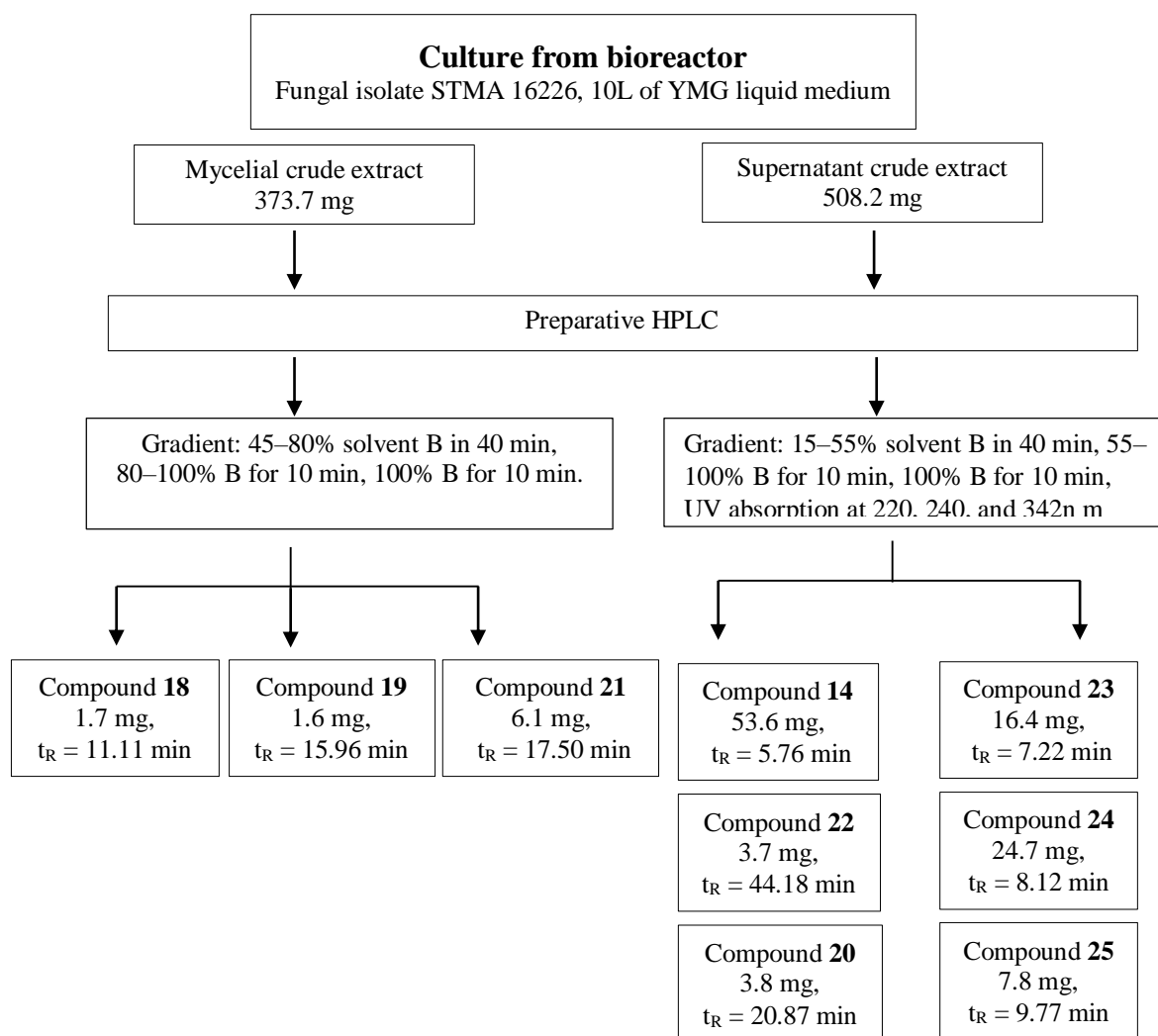


Figure 14: Schematic diagram showing purification steps of metabolites isolated from mycelial and supernatant crude extracts derived from bioreactor culture of the fungal isolate STMA 16226 in 10 L of YMG medium

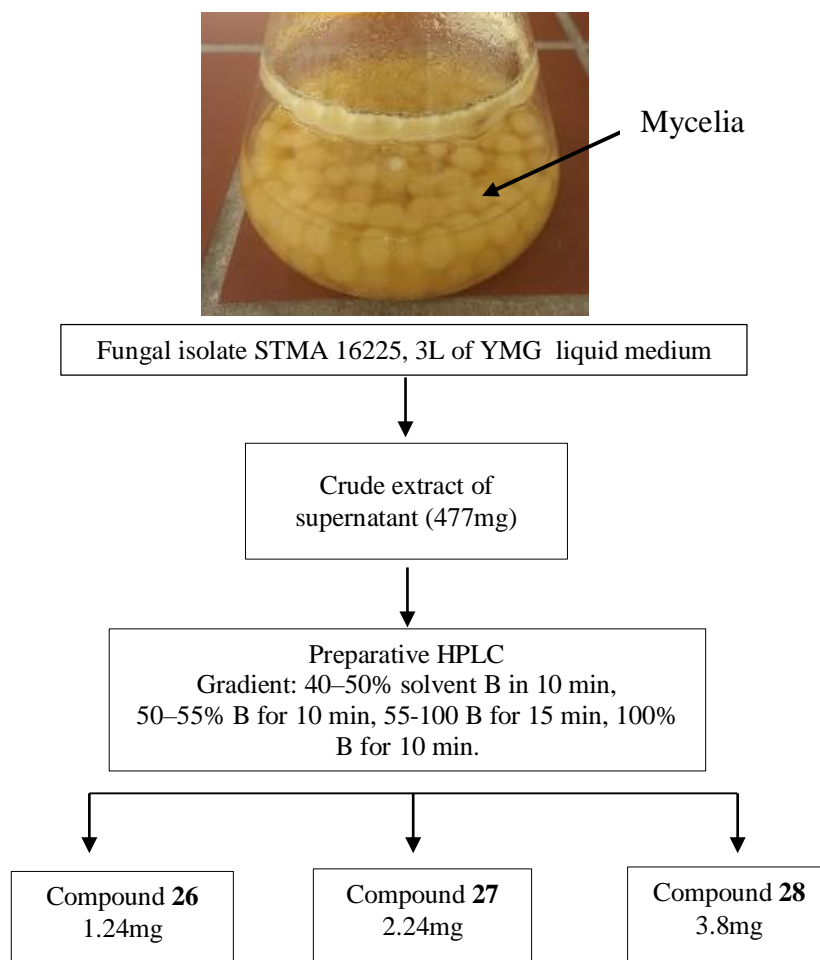


Figure 15: Schematic diagram showing purification steps of metabolites isolated from the supernatant crude extract derived from fermentation culture of the fungal isolate STMA 16225 in 3L YMG medium.

10. Dual culture

For further investigation of the nature of compounds involved in interaction between the endophytic fungi and phytopathogen *S. sclerotiorum* DSM 1946, a co-culture has been done. *S. sclerotiorum* is a necrotrophic, phytopathogenic ascomycete with worldwide distribution, which attacks more than 400 species of plants (Xiao et al., 2014). The two fungi were simultaneously inoculated at a distance of 4.5 cm from each on YMG agar medium and incubated for 2 weeks at 23°C. Additionally, both plant pathogen and endophytic fungi were mono-cultured. The readings obtained were then transformed into percentage to indicate the ability of the bacteria to inhibit the radial growth of the pathogen.

The percent of radial growth inhibition was calculated as the following formula:

$$\frac{R1 - R2}{R1} \times 100$$

R1= Radial growth of *S. sclerotiorum* in the absence of the antagonist (control).

R2= Radial growth of *S. sclerotiorum* in the presence of the antagonist (treatment)

Furthermore, the agar of inhibition zone and the mycelial agar of the fungal partners in both mono and co-cultures were minced with a spatula and put into flasks. Afterwards, 100 μ L of EtOAc were added to each flask (the cultures were extracted three times). After evaporation of solvents, all dried extracts were dissolved in the same amounts of MeOH and subjected to LC-MS analysis in order to verify the chemical profiles of metabolites in mono and co-cultures.

11. Structure elucidation

All obtained fractions were checked for their purity using LC-MS and H NMR analysis. The structure elucidation of the pure compounds was performed by Dr. Soleiman Helaly and Dr. Rémy Bertrand Tepono by means of HRESIMS and NMR.

11.1. HRESIMS

HRESIMS spectra were recorded on a maXis ESI TOF mass spectrometer (Bruker Daltonics) [scan range m/z 100–2500, rate 2 Hz, capillary voltage 4500 V, dry temperature 200 °C], coupled to an Agilent 1200 series HPLC-UV system (Agilent Technologies) [column 2.1 \times 50 mm, 1.7 μ m, C₁₈ Acquity uPLC BEH (Waters), solvent A: H₂O + 0.1 % formic acid; solvent B: ACN + 0.1 % formic acid, gradient: 5 % B for 0.5 min increasing to 100 % B in 19.5 min, maintaining 100 % B for 5 min, FR = 0.6 mL/min, UV-Vis detection 200-600 nm]. The molecular formulas were calculated including the isotopic pattern (Smart Formula algorithm).

11.2. NMR

NMR spectra were recorded on Bruker 500 MHz Avance III spectrometer with a BBFO (plus) SmartProbe (¹H 500 MHz, ¹³C 125 MHz) and a Bruker 700 MHz Avance III spectrometer with a 5 mm TCI cryoprobe (¹H 700 MHz, ¹³C 175 MHz), locked to the deuterium signal of the solvent. Data acquisition, processing, and spectral analysis were performed with standard Bruker software and

ACD/NMR Spectrus. Chemical shifts are given in parts per million (ppm), and coupling constants in Hertz (Hz). All spectra were measured in deuterated methanol (methanol-d₄), deuterated chloroform (CDCl₃), deuterated acetone (acetone-d₆) and deuterated dimethyl Sulfoxide-d₆ (DMSO-d₆). Chemical shifts were referenced to the solvent signals.

11.3. Optical rotation, UV-spectra and CD spectroscopy

Optical rotation, UV and CD spectra were determined for new compounds. Optical rotations were determined with a PerkinElmer 241 MC polarimeter (using the sodium D line and a quartz cuvette with 10 cm path length and 1 mL volume). UV/Vis spectra were recorded on a Shimadzu UV/vis-2450 spectrophotometer using ethanol (UVASOL, Merck). CD spectra were recorded on JASCO spectropolarimeter, model J-815.

12. Biological assays of pure compounds

12.1. Antimicrobial activity

To investigate the antimicrobial activity of pure compounds, the test was implemented by determination of MIC as described above in screening of crude extracts for antimicrobial activity. The stock solutions were prepared at 1mg/mL in MeOH. Each compound was tested in two columns, 20 μ L and 2 μ L were added to the first well of each column and serially diluted two-fold to their final concentrations ranging from 0.52-66.66 μ g/mL and 0.052-6.66 μ g/mL respectively. In addition, other organisms test were used including: Gram-positive bacteria- *Micrococcus luteus* DSM 1790, *Staphylococcus aureus* DSM 346, *Mycobacterium smegmatis* ATCC 700084, Gram-negative bacteria- *Escherichia coli* DSM 1116, *Pseudomonas aeruginosa* PA14, *Chromobacterium violaceum* DSM 30191, yeasts- *Candida albicans* DSM 1665, *Rhodotorula glutinis* DSM 10134, *Pichia anomala* DSM 676, *Schizosaccharomyces pombe* DSM 70572, and against filamentous fungus *Mucor hiemalis* DSM 2656 MUCL 49355.

12.2. Standard disk assay

Compounds with selective antifungal activity were tested against the plant pathogen *S. sclerotiorum* DSM 1946, which did not produce spores. In this instance, a standard disk diffusion assay was performed. Firstly, A liquid culture of *S. sclerotiorum* was prepared by adding 5 mycelial plugs to 200 mL of YMG medium in 500 mL flasks and incubated for four days. Later, the mycelial with medium were homogenized with a Heidolph Silent Crusher and serve to prepare mycelial

suspension by adding 70 mL of mycelial suspension in 1 L of sterile melted YMG medium and pouring it in Petri dishes. After solidification, filter disks of 6 mm diameter were placed on YMG agar medium supplemented with mycelial suspension of test fungus. 10 μ L of pure compounds and controls were pipetted onto filter disks. The concentrations of pure compounds and nystatin (positive control) were adjusted to 100 μ g /paper disk and 20 μ g/ paper disk respectively. MeOH was used as negative control. The plates were incubated for seven days at 23 °C (Anke and Zähler, 1978). Each experiment was performed in triplicate.

12.3. Cytotoxicity assay

In vitro, the cytotoxicity of pure compounds was determined in most of the cases against two mammalian cell lines including the murine fibroblast cell line L929 and the cervix carcinoma cell line KB-3-1. Additional cancer cell lines were tested depending on the screened compound class including: squamous carcinoma A431, Human lung carcinoma A549, Ovarian carcinoma SKOV-3, Human prostate cancer PC-3, Human breast adenocarcinoma MCF-7, Human osteosarcoma U2OS. All cell lines were cultured in DMEM supplemented with 10% of foetal bovine serum (Gibco) and incubated at 37°C under 10% CO₂. The cytotoxicity activity was determined by the MTT colorimetric assay in 96-well microplates (Mosmann, 1983). First, 60 μ L aliquots of serial dilutions from an initial stock solution (1 mg/mL in MeOH) were added to 120 μ L aliquots of a cell suspension (5×10^4 cells/mL) in 96-well microplates. After 5 days incubation, Cells were then treated with MTT reagent (20 μ L in each well) and were further incubated for 1-3 h (depending on the cell type) at 37°C. The optical density was recorded at 595 nm in a microplate reader (Infinite M200 PRO). The half maximal inhibitory concentration IC₅₀ represents the concentration at which the growth of cells was inhibited to 50% of the control was obtained by sigmoidal curve fitting (Wittstein et al., 2016). Negative and positive controls were MeOH and epothilone B.

12.4. Phytotoxicity test

To investigate the phytotoxicity of the pure compounds, a seedling bioassay was carried out toward seeds of two plants: *Lepidium sativum* (dicotyledon) and *Setaria italica* (monocotyledon). 5 mL of sterile 0.5% agarose gel were loaded in the lit of closed plastic chamber with 40 mm diameter. Eight seeds of each plant were assorted in a circle on the gel. Afterwards, a filter disk of 6 mm diameter was placed in the middle of the vial and loaded directly with 10 μ L of each compound (dissolved in Methanol) to yield a final concentration of 100 μ g/filter disk. A negative control without compounds,

solvent control with 10 μ L of MeOH and a positive control with 50 μ g/filter disk of herbicide methyl viologen dichloride hydrate (MeViDiHydr) (98% Sigma Aldrich) were used. The seeds were incubated in the dark at 20 °C for 72 h and subsequently for 48h at daylight and room temperature. Each experiment was performed in triplicate (Anke *et al.*, 1989; Helaly *et al.*, 2016).

12.5. Nematicidal Activity Assay

The determination of nematicidal activity against *Caenorhabditis elegans* (*C. elegans*) was performed in a 24-microwell plate using a microwell plate assay (Stadler *et al.*, 1993; Kuephadungphan *et al.*, 2017). The free-living nematode, *C. elegans* was monoxenically cultured on nematodes agar [soy peptone 2 g, NaCl 1 g, Agar 20 g, 1000 mL of distilled water; after autoclaving, the following ingredients were added: cholesterol (1 mg/mL ethanol) 0.5 mL, CaCl₂ (1M) 1 mL, MgSO₄ (1M) 1 mL, potassium phosphate buffer (40 mM) 12.5 mL, the pH was adjusted to 6.8] with living *E. coli* DSM 498, at 20 °C in the dark for a week. After incubation, adult nematodes were suspended in sterile distilled water and the nematode suspension was then adjusted to give a concentration of 500 nematodes/mL. Four concentrations of 100, 50, 20 and 10 g/mL of each compound were tested (total volume 1 mL/well). Standard nematicide, ivermectin and 1% MeOH were used as the positive inhibitory control and solvent control, respectively. The plate was incubated at 20°C in the dark and nematicidal activity was recorded after 18 h of incubation.

13. Cell biology experiments

The compounds which exhibited low IC₅₀ values in the cytotoxic assay were further subjected to additional testing to investigate their impacts on actin filaments, microtubules, nuclear envelop and nucleus. The most potent compounds were subsequently selected to a detailed cell cycle analysis using flow cytometry. These experiments were conducted in the department of Cell Biology under the supervision of Prof. Dr. Theresia Stradal.

13.1. Effect on cells morphology

The effects on cell morphology were carried out on U2OS (ACC785-DSMZ, Braunschweig, Germany). U2OS cells were grown in DMEM (4.5g/L glucose “Ivitrogen, Germany” with 10% fetal bovine serum (Sigma) and 1 % glutamate, 1% sodium pyruvate and 1% nonessential amino acids) at 37°C and 7% CO₂. Cells started to grow and became confluent in about 3 days. Confluent cells were washed with 8 mL of a PBS and subsequently harvested by trypsinization by adding 2 mL of solution

of trypsin/EDTA and incubated for 2 minutes at 37°C. The resulting suspension of cells was transferred to a centrifuge tube and centrifuged at room temperature for 5 minutes at 1200 rpm. The supernatant fluid was discarded and the cells were resuspended in culture medium and dilute them in fresh medium (split ratio 1:5). For cell counting, the cells were trypsinized as described in the preceding section, using 2 mL of trypsin solution, centrifuged, and resuspended in fresh medium. Cells suspension was counted in Neubauer improved counting chamber using Trypan blue (ratio 1:1) to distinguish between dead and live cells (the live cells exclude Trypan Blue and appear white, whereas the dead cells pick up the dye and appear blue in color). 12 mm diameter glass coverslips were put in 24 well plates and coated with 100 μ L of fibronectin (25 μ g/mL in PBS prepared from stock solution 1mg/mL in 2M urea). After 1 hour, U2OS cells were seeded with 3×10^4 cells/well on coated glass coverslips and allowed to adhere and spread for 16 h. Varying concentrations (0.25, 0.5, 2.5, 5 and 10 μ g/mL in DMEM) of the tested compounds were prepared from stock solutions (1mg/mL in DMSO). Adhered cells were treated with the different prepared concentrations and incubated for 24 hours. DMSO-treated (mock) cells were prepared as negative control. The trials were prepared in duplicate.

13.1.1. Immunofluorescence

Subsequent staining of DNA, actin filaments and microtubules was carried out. For actin and tubulin labelling, the treated cells were fixed with prewarmed 4% PFA in PBS for 20 minutes at room temperature and washed three times with PBS. The cells were permeabilized by adding 300 μ L of Triton X100 (0.1% in 4% PFA/PBS) to each well and incubated exactly for 1 minute. Upon three times washing in PBS, cells were blocked with 300 μ L of 5% horse serum in 1% BSA/PBS for 30 minutes at room temperature. Immunofluorescence staining was performed by using standard procedure. The coverslips were washed three times in PBS and incubated with 20 μ L of primary antibody dilution in 4% BSA/PBS. The cells were kept in a humidified chamber and dark 2 hours at room temperature. After incubation, the cells were washed three times with PBS and incubated with 20 μ L of secondary antibody. For microtubules (MTs) staining, a mouse monoclonal anti- α -tubulin antibody (Sigma-Aldrich, clone DM1A) was used and Phalloïdin Alexa Fluor 488 (ThermoFisher, A123799) for F-actin. Secondary reagents were goat anti-mouse Alexa 594 (ThermoFisher, A32723). Finally, after washing with PBS, coverslips were mounted on glass microscope slides in ProLong Diamond antifade mountant with DAPI (ThermoFisher, P36971).

The compounds were also probed for potential effects on the nuclear lamina during cell cycle phases. The cells were treated with 0.5 $\mu\text{g}/\text{mL}$ and 5 $\mu\text{g}/\text{mL}$ for 24 hours and then fixed with ice-cold methanol for 15 minutes and stepwise re-hydrated using PBS. Afterwards, cells were blocked and then co-stained with antibodies against nuclear envelop and MTs by using anti-pan Lamin antibody (abcam, ab20740) and a rat monoclonal antibody to tyrosinated alpha-tubulin overnight. Goat anti-mouse Alexa fluor 594 (A110329) and goat anti-rat Alexa fluor 488 (A11006) were used as secondary reagents. The coverslips were mounted on glass microscope slides in ProLong Diamond antifade mountant with DAPI (ThermoFisher, P36971).

Images were acquired on a Zeiss Axiovert 135TV microscope, equipped with a Coolsnap 4k cooled CCD device driven by VisiView software (Vistron Inc. Munich). Images were processed using Fiji (ImageJ)(Schindelin et al., 2012) and Photoshop CS6 (Adobe) software.

13.1.2. Flow cytometry

6-well plates were seeded with 7×10^5 /well U2OS cells and treated with 5 and 10 $\mu\text{g}/\text{mL}$ of compounds for 18 hours upon spreading. The cells were then harvested by trypsination and fixed with 2% PFA/PBS. After rehydration with PBS, cell pellets were collected by centrifugation at $500 \times g$, resuspended in ice cold methanol, and kept on ice for 30 minutes. Afterwards, the cells were centrifuged and resuspended in FACS-Buffer and stained with a mixture of anti-tubulin/anti-lamin antibodies as above in combination with RNase A and propidium iodide (PI) to stain DNA. As secondary antibodies, antibody goat-anti-rat Alexa488 and goat-anti mouse Alexa 647 (A-21235) were used. For detection of apoptosis, cells were incubated with the fluorescent substrate Cell Event Caspase-3/7 Green Detection Reagent C10723 (ThermoFisher) for 10 minutes prior to fixation. Staurosporine was used to induce apoptosis in U2OS as a positive control (250 nM for 16 hours). Cells were analyzed using a (FACS Canto/BD Biosciences). Data were analyzed using DIVA 6.1 Software.

Chapter II

Results and discussion

1. Isolation and identification of fungal isolates

A total of seventeen endophytic fungi were isolated from healthy root tissues. Absence of any growth on agar media used, plated with water obtained from last rinse of tissues suggests that efficient surface sterilization has been performed. The growth medium of each fungus was noted (Table 7). For preliminary characterisation, the fungal isolates were subjected to sequencing of their rDNA ITS, which could give hints as to their taxonomic position at the genus or family rank. Concurrent morphological studies were conducted, but as is often the case with endophytic fungi, those did not always reveal conclusive results. Other protein coding genes needed to be used to narrow down the genus and species and, in particular, to investigate the phylogenetic relationship of some species. The results from macroscopic and microscopic characteristics of endophytic colonies for taxonomic evaluation purpose, were congruent with results of ITS DNA sequence BLAST analysis of these isolates. The macroscopic morphology of all isolated fungal endophytes are shown in figure 16.

Table 7: Fungal endophytes isolated from *G. alypum* and their closest hits from BLAST research

N°	Code	Medium of isolation	Closest hits	Query cover	Identity	Accession number
1	S1	NA	<i>Penicillium chrysogenum</i> PO14	100%	100 %	KR233454
2	S2	YEA	<i>Chaetomium truncatulum</i> C77	96%	99 %	HM365263
3	S3	PDA	<i>Penicillium canescens</i>	97%	99 %	KX359603
4	S4	PDA	<i>Alternaria sorghi</i> AY918	100%	100 %	MG250470
5	S5	PDA	<i>Fusarium solani</i> isolate 62 FS	100%	99 %	KX9293306
6	S9	NA	<i>Penicillium chrysogenum</i> PO14	100%	100 %	KR233454
7	S18	PDA	<i>Fusarium falciforme</i>	99%	100 %	AB779669
8	S22	MEA	<i>Fusarium solani</i> isolate 62 FS	100%	99 %	KX9293306
9	S32	YEA	<i>Macrophomina phaseolina</i> MPKS307	100%	100%	FJ395243
10	S42	NA	<i>Aspergillus terreus</i> KAML04	100%	100 %	KC119206
			<i>Aspergillus terreus</i> KARVS02	100%	100 %	KC119198
11	S50	MEA	<i>Diaporthe ambigua</i> 6KF	100%	99%	KJ210025
12	S59	PDA	<i>Fusarium acuminatum</i> Fus1/17-011/1	100%	100%	MF509746
13	STMA 16219	YEA	<i>Preussia similis</i> S19	84 %	100%	AY510419
14	DSM 32328	MEA	<i>Preussia similis</i> CBS 80473	97%	100%	DQ468028
15	DSM 104666	MEA	<i>Preussia similis</i> S19	96%	100%	AY510419
16	STMA 16225	NA	<i>Chaetomium madrasense</i> CBS 315.74	100%	100%	KC109751
17	STMA 16226	MEA	<i>Dendrothyrium variisporum</i> CBS 121517	100%	100%	JX496030

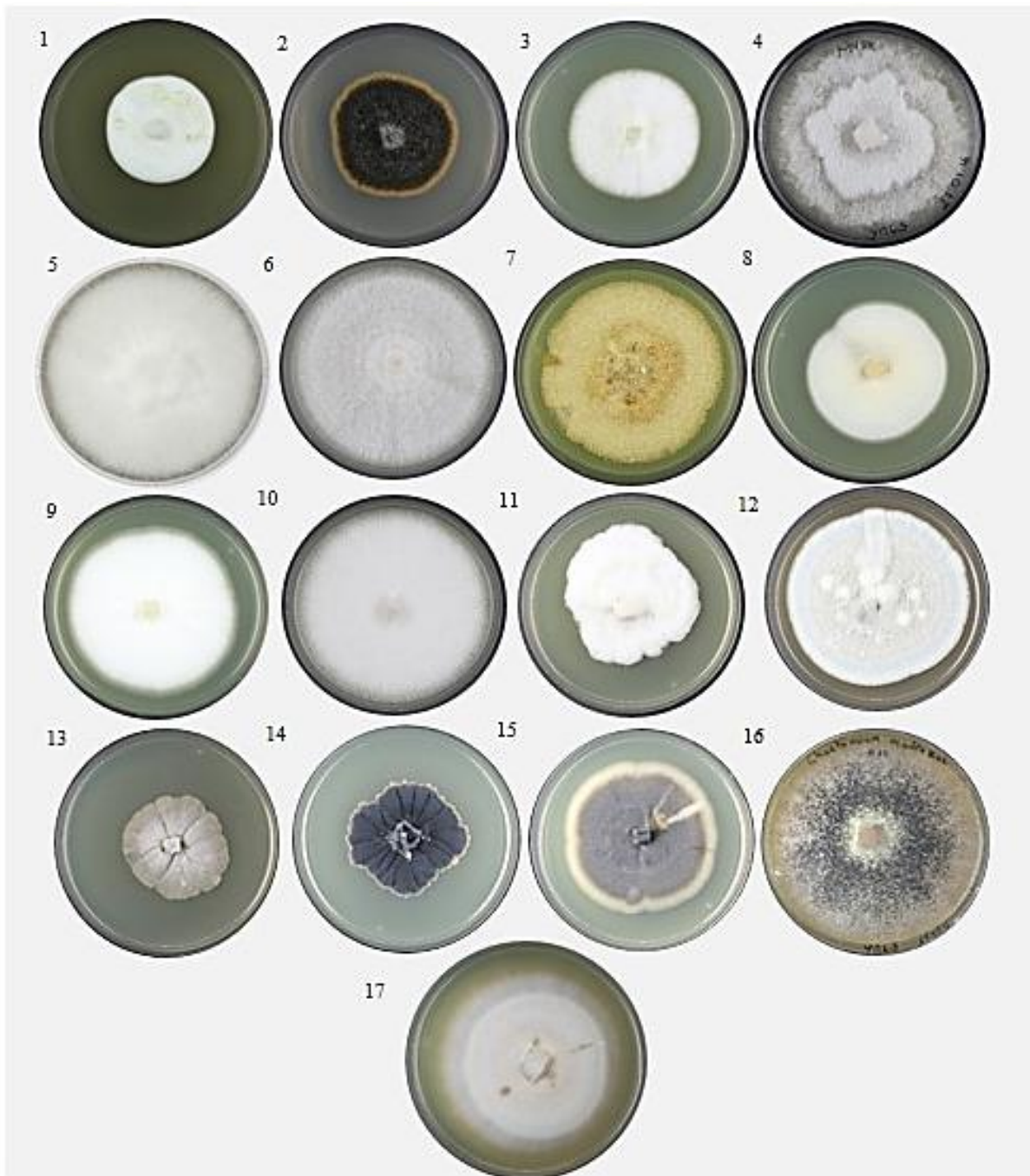


Figure 16: Macroscopic morphology of fungal endophytes on YMG agar medium on 9 cm Petri dish.

1. Isolate S2 after 8 days, 2. Isolate S4 after 15 days, 3. Isolate S5 after 15 days, 4. Isolate S50 after 15 days, 5. Isolate S32 after 15 days, 6. Isolate S22 after 21 days, 7. Isolate S42 after 21 days, 8. Isolate S9 after 15 days, 9. Isolate S58 after 21 days, 10. Isolate S18 after 15 days, 11. Isolate S59 after 15 days, 12. Isolate S3 after 15 days, 13. Isolate DSM 32328 after 15 days, 14. Isolate DSM 104666 after 15 days, 15. Isolate STMA 16219 after 15 days, 16. Isolate STMA 16225 after 21 days, 17. Isolate 16226 after 21 days.

To confirm the identification and clustering results, the closest hits with high similarity given after BLAST search from NCBI database of the nrITS nucleotide sequences were aligned. The phylogenetic tree inferred from the nuclear ITS region was calculated with PhyML by using GTR+G as substitution model. The fungus *Paludomyces mangrovei*, belonging to the phylum

Chytridiomycota, was used as out-group as all fungal endophyte isolates obtained from *G. alypum* belonged to the Ascomycota, a finding that was in agreement with that of previous reports (Hyde and Soyong, 2008; Rodriguez *et al.*, 2009).

The phylogenetic tree derived from ITS data (Figure 17) showed that all fungal endophytes isolated in the present study are members of the sub phylum Pezizomycotina of Ascomycota. The phylogenetic analysis has placed the fungal endophytes in three major clades representing one group of Sordariomycetes (clade 1), one group of Eurotiomycetes (clade 2) and third group of Dothideomycetes (clade 3). The dominant group of endophytic fungi is the Sordariomycetes represented by three orders: Diaporthales (1 species), Sordariales (2 species) and Hypocreales (3 species), followed by Dothideomycetes which contains two orders: Pleosporales (three species) and Botryosphaerales (1 species). The endophytic fungi categorized in the Eurotiomycetes include on order of Eurotiales (three species). These characteristics match those in the class 2 of non-clavicipitaceous fungal endophytes indicated by Rodriguez *et al.* (2009), and therefore our fungal isolates can be classified within this class. The results indicate that the healthy roots of *G. alypum* accommodate a diversity of fungal endophytes. Nevertheless, this study does not recover the total endophytic fungi and therefore it may not be a good representation of the whole endophytic diversity of the plant *G. alypum*, because in one hand, we have targeted only the root mycobiota and during our manipulation many fungal isolates were lost. On the other hand, the quality and the quantity of the endophytic mycotaxa isolated are usually influenced by many factors. The antagonisms between endophytes species plays the major role in the dominance of some fungal species that eliminate or reduce other fungi. Similarly, sampling, culture media and methods as well as laboratory conditions are probably implicated (Kusari *et al.*, 2012; Schulz *et al.*, 2015)

The group of Dothideomycetes forms a monophyletic clade including five isolates belonging to Pleosporales. Yet, the Botryosphaerales taxa (*Macrophomina phaseolina*) is left out of this clade and thus, an additional gene may be helpful for ultimate characterization of phylogenetic position of this isolate. The class of Dothideomycetes is the largest class of Ascomycota with highly ecological diversity (Hyde *et al.* 2013).

The sequence of the isolate S32 is clustered along with the reference strain *Macrophomina phaseolina* MPKS307 in a well-supported clade (100% bootstraps).

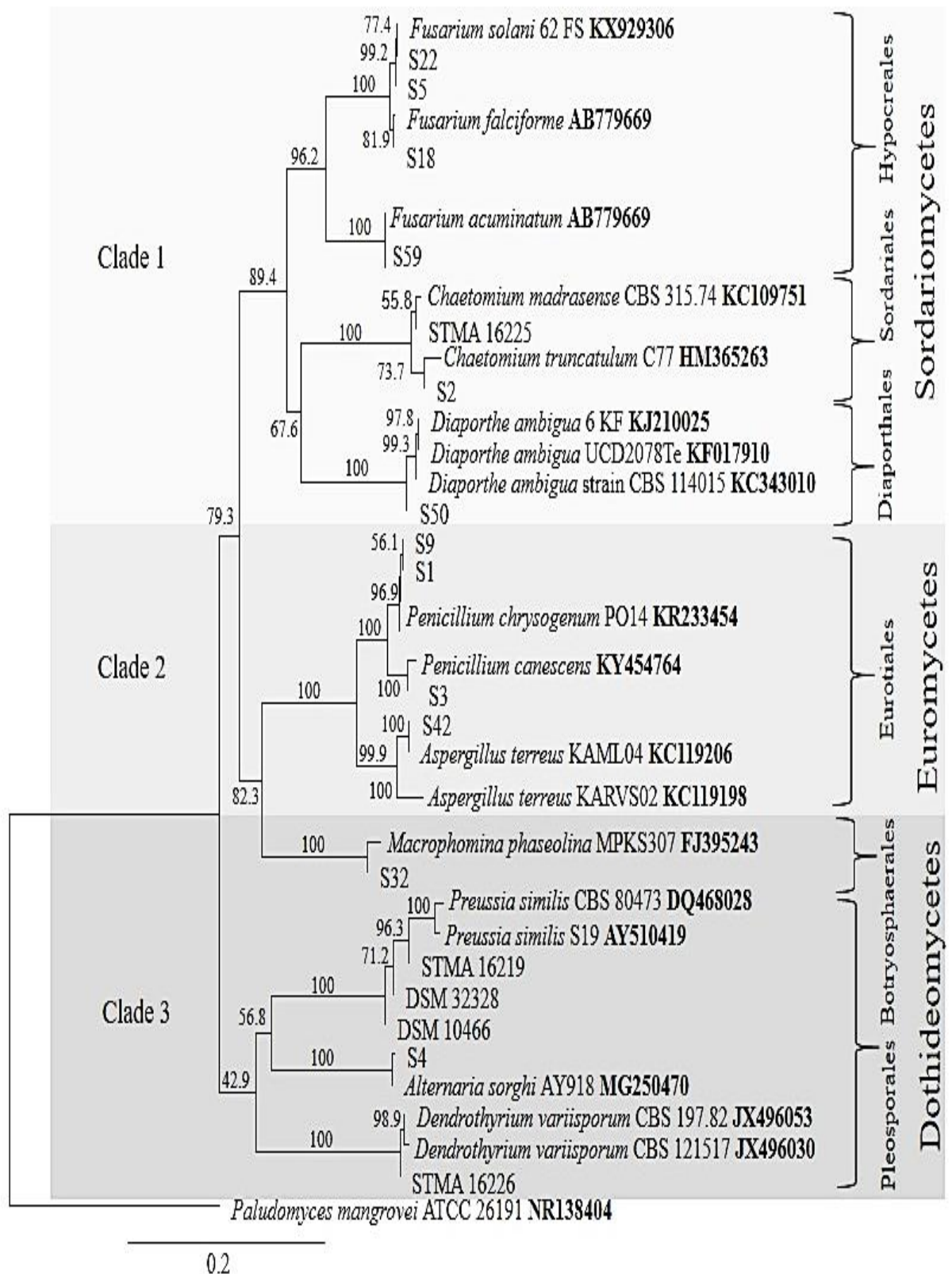


Figure 17: Phylogenetic relationship of fungal endophytes harbored in the roots of *G. alypum* based on ITS sequences with *Paludomyces mangrovei* as out group. The phylogenetic tree was calculated with PhyML by using GTR+G as substitution model and 1000 bootstraps.

Macrophomina phaseolina (*M. phaseolina*) (Botryosphaeriaceae, Botryosphaeriales) is recognized as an opportunistic fungus that may transform from a saprophyte to a pathogen particularly in high temperature or water stress and causes charcoal rot in different crop and non-crop species (Sarr, 2014). However, it has been often isolated as endophyte. It is worth to notice that no blackish appearance in root tissues due to fungal microsclerotia was detected. Although, fungal endophytes are known to adopt a variety of symbiotic lifestyles such as mutualism, and parasitism and their lifestyle transitions are dependent on plant state (senescence, biotic or abiotic stresses) (Hyde and Soyong, 2008; Schulz *et al.*, 2015). Colonies of *M. phaseolina* each appeared as a ring, with fluffy white mycelium surrounding a central area with black microsclerotia (Figure 16).

The sequences of the isolates DSM 104666, DSM 32328 and STMA 16219 are clustered in the clade of *Preussia similis* (sporormiaceae, Pleosporales) (100% bootstrap support). *Preussia* species are coprophilous fungi which grow on animal dung but they were also recovered as endophytes in plant hosts (Arenal *et al.*, 2005; Herrera *et al.*, 2010; Mapperson *et al.*, 2014; Cosoveanu *et al.*, 2018). Their endophytic state can be considered as accidental opportunism and it might be an alternate step of their life cycle. Accordingly, they are not specifically adapted to their host plant (Schulz and Boyle, 2005) but an eventual coevolution with animal grazing and plant might takes place during their life cycle (Porrás-Alfaro *et al.*, 2008). The spores are covered by a mucilaginous sheaths or have gelatinous appendages, helping them to attach to the surface of the plants and remain as epiphytes, where they will be fed by herbivores on along with plant materials and pass through an animal digestive. Finally, they end in a new dung pile to repeat the cycle. The dark pigmentation and the mucilage coverage of these ascospores let them resistant to sun UV light and aggressive agents such as gastric juice. Likewise, it seems possible that ascospore resistance of these fungi, might help them to survive during surface sterilization and are actually isolation artefacts, rather than the endophytes (Newcombe *et al.*, 2016).

Additionally, the phylogenetic position of the three fungal strains of the taxon *Preussia similis* was further characterized by a multigenes alignment analysis together with the closely related GenBank reference sequences of *Preussia* species, mainly submitted by Arenal *et al.* (2005, 2007) (Table S1, appendix A). Multiple alignment of sequences of each gene marker (ITS, LSU, EF1- α) was performed by E-INS-i algorithm of MAFFT v7.017 (Fast Fourier Transformation) (Kato *et al.*, 2002; Kato and Toh, 2008).

The aligned ITS, LSU and EF1- α sequences were then concatenated to generate MGA. Phylogenetic tree construction was carried out using PhyML and GTR+G+I as substitution model. *Pleospora herbarum* (Pleosporaceae, Pleosporales) was used as the outgroup taxon to root the phylogenetic tree. Phylogenetic tree inferred from the multigenes analysis (Figure 18) revealed that the three strains fell together within a strongly supported monophyletic clade (100 % bootstraps) of *P. similis* complex. The latter included one sub-clade that nested the isolate DSM 104666 together with the reference strains (*P. similis* S19) supported with 74% bootstrap value. The seconde well supported sub-clade (78% bootstraps) clustered the fungal strain DSM 32328. Finally the third sub-clade nested both the reference strain *Preussia similis* 80473 together with the strain STMA 16219 supported with a 100 % bootstrap value.

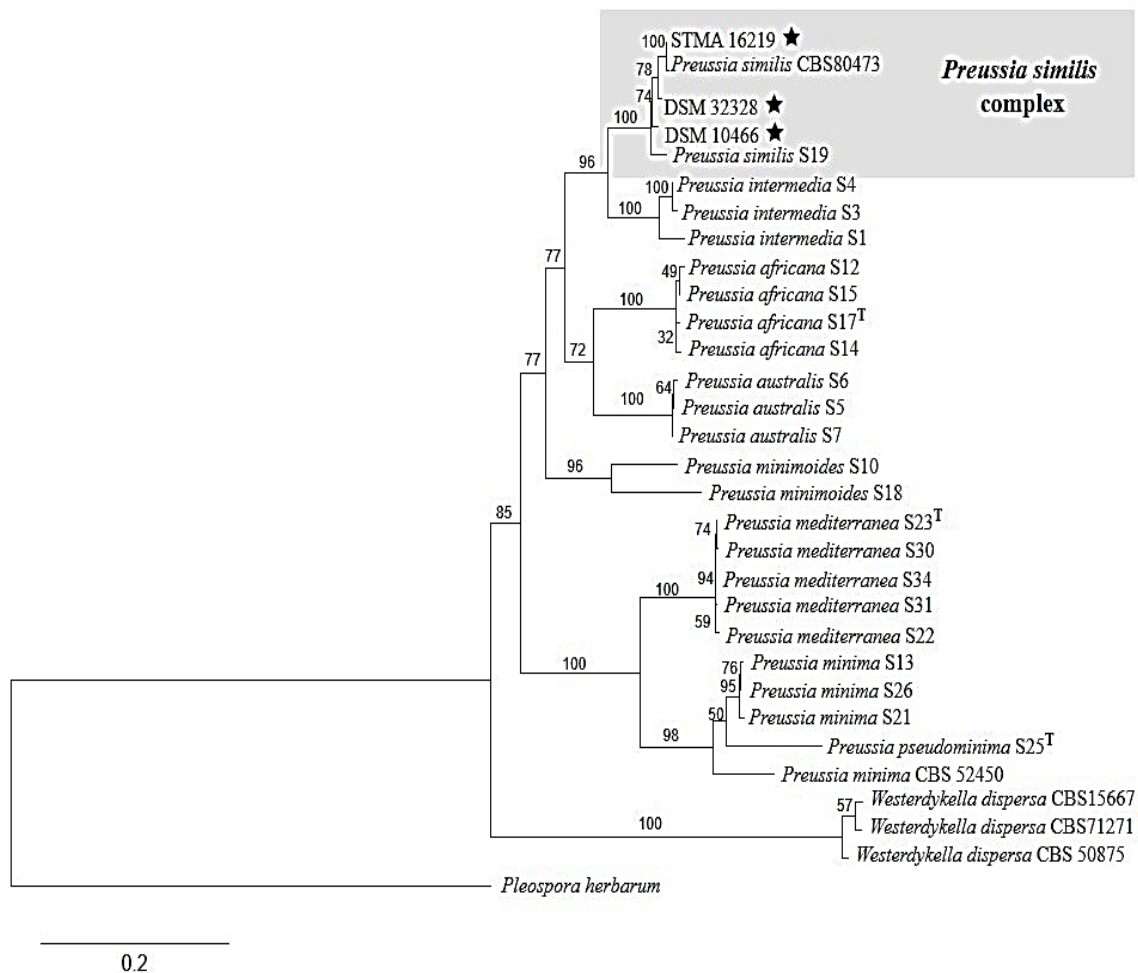


Figure 18: Phylogenetic tree of *Preussia* spp. based on combined data set of four markers. Multigenes alignment, PhyML (ITS, LSU, EF1- α). Our fungal strains are marked with star (GTR G+I model, E-INS-i algorithm of MAFFT v7.017 and 1,000 replicate bootstrap). *Pleospora herbarum* (Pleosporaceae, Pleosporales) was used as the outgroup taxon. Type strains are marked by a superscript capital T.

All three strains of *P. similis* were isolated as sterile mycelia. Firstly, morphology and size of macroscopic features of the culture on the plate were determined. All three strains show often a tendency to sectoring and no further mycelial differentiation and sporulation were observed on YMG (Figure 16) and OMA. For *P. similis* DSM 104666, the colonies attaining a diameter of 30 mm and 37 mm in three weeks at 23°C YMG (Figure 16) and OMA respectively. At the beginning dark brown then becoming black when old. Colonies of *P. similis* DSM 32328 on YMG and OMA media reach a diameter of 47 mm (Figure 16) and 66 mm in 21 days at 23°C respectively. It appears pale white when young and become grey with age.

The fungal strain *P. similis* STMA 16219 is the fastest growing isolate, in three weeks, the plate of 9 cm being covered on OMA and reached diameter of 76 mm on YMG (Figure 16). Due to the fact that these three strains were isolated without any reproductive structures, their identification by phenotypic characters was impossible by conventional methods. Hence, in order to induce sporulation, the three isolates were cultivated on OMA and exposed to 12-hours blue light/dark schedule during one month. The attempts to induce the sexual stages of the three strains was successful for both DSM 104666 and STMA 16219, while no mycelial differentiation were observed for DSM 32328 (Figure 19). The teleomorph characters of DSM 104666 and STMA 16219 are represented in figure 20 and figure 21 respectively.

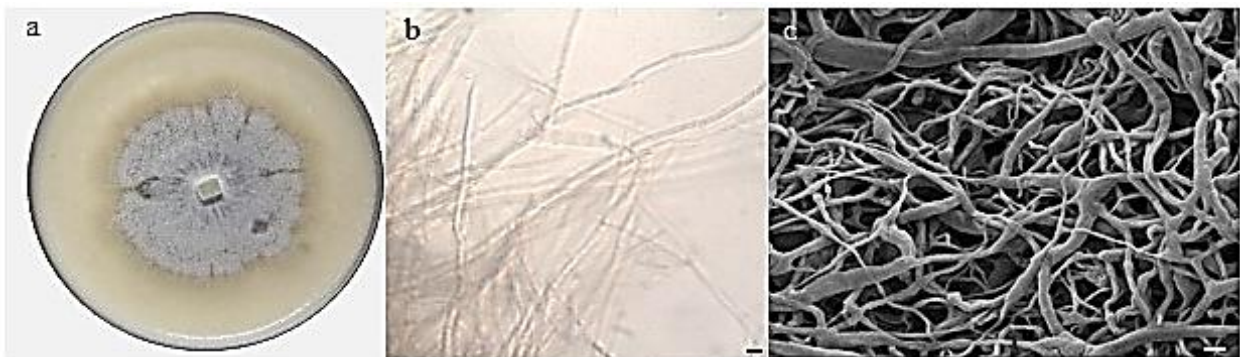


Figure 19: Sterile mycelia of *P. similis* DSM 32328

- a. Aspect of culture on OMA after 1 month on 9 cm Petri dish showing no mycelial differentiation.
- b. Sterile mycelia observed in optical microscope, c. Hyphae in SEM microphotography. b, c=2 μ m.

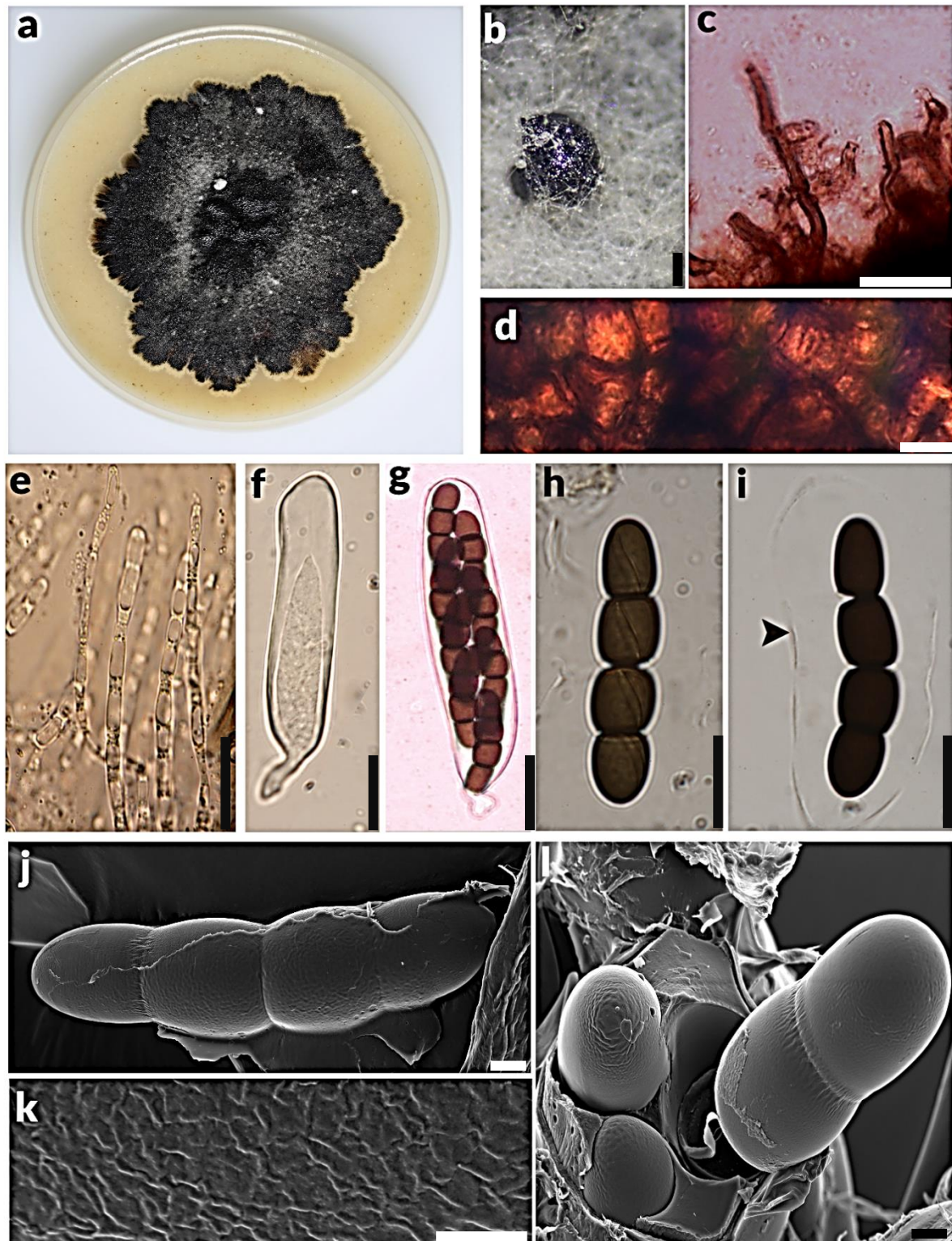


Figure 20: Teleomorph features of *Preussia similis* DSM 104666. **a** Culture on OMA after 4 weeks on 9 cm Petri dish with sporulating regions as black spots in the centre and periphery, **b** Pseudoperithecium without ostiole, **c** Ascomata hyphae ornamentations, **d** Details of exoperidium, **e** Pseudoparaphyses, **f** Immature ascus, **g** Mature ascus, **h** Ascospore showing germ slit, **i** Ascospore surrounded by hyaline gelatinous sheath indicated by arrow, **j** Gelatinous sheath showed in SEM microphotography, **k** SEM microphotography showing perispore details, **l** SEM microphotography showing ascospores arrangements within bitunicate ascus, apical view, part of ascospore cleaved out of ascus, Scale bars: **b**=100 μ m, **c**, **h**, **i**, **e** = 20 μ m, **j**, **l**=2 μ m, **k** = 1 μ m, **f**, **g** = 50 μ m, **d** = 10 μ m.

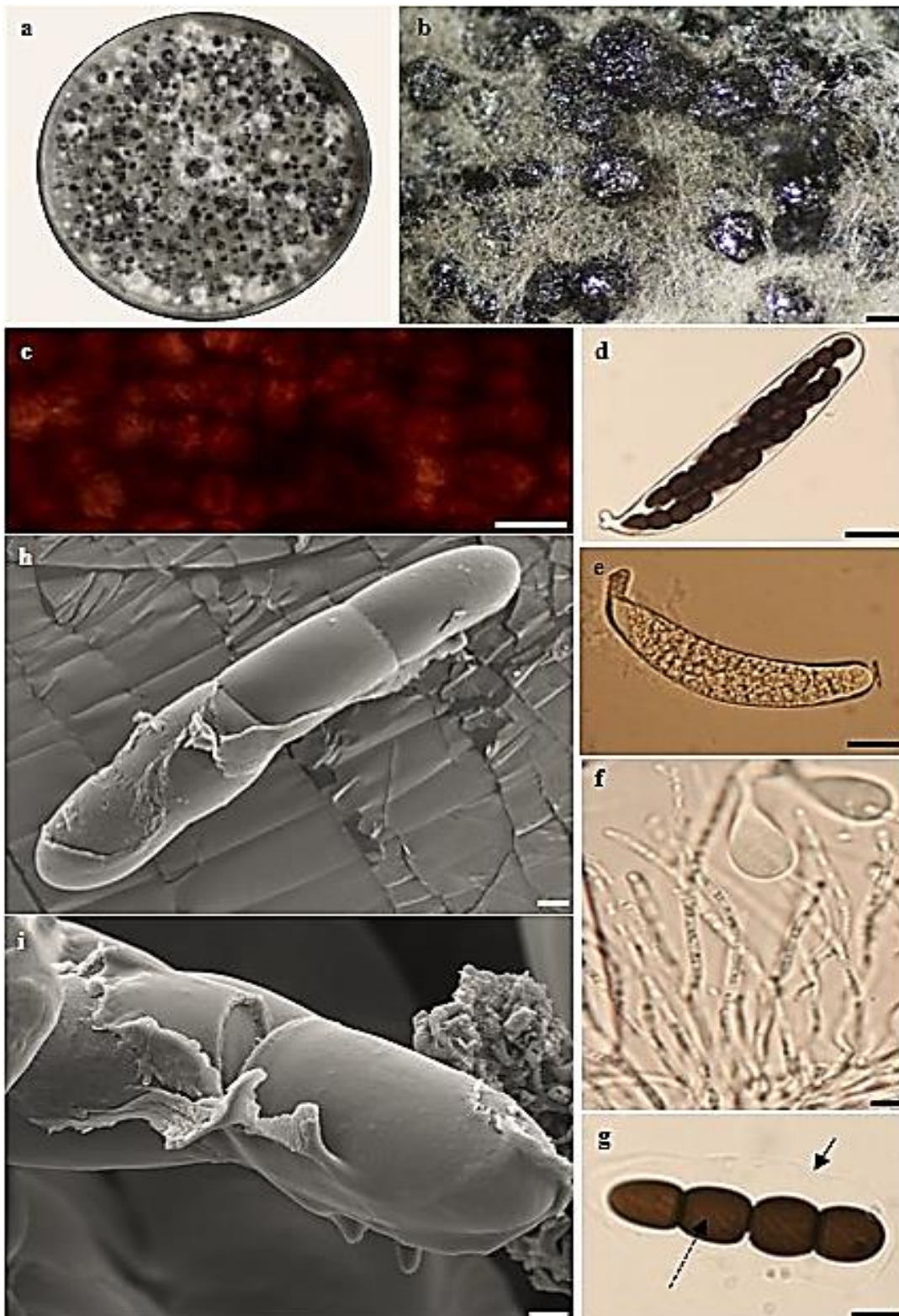


Figure 21: Teleomorph characters of *P. similis* STMA 16219

a. Culture on OMA after 1 month, b. Perithecia on OMA, c. Outer surface of perithetium, d. Mature ascus
 e. Immature ascus, f. Pseudoparaphyses, g. Mature ascospore, the gelatinous sheath is showed by continuous arrow, germ slit is indicated by dotted arrow, h. SEM microphotography showing 4-celled ascospore with gelatinous sheath. i. SEM microphotography showing ascospore broken in septum and surrounded with gelatinous sheath. Scale bars: **b**=100 μ m, **c**, **d**, **e**, **f** = 20 μ m, **g** = 10 μ m, **h**, **i**=2 μ m.

The two *P. similis* isolates DSM 104666 and STMA 16219 are characterized by ascomata scattered or in small groups, immersed, or partially immersed in culture media when young. Pseudothecia 200-240 μm in diameter, dark, globose, not ostiolates. Asci, 150-165 (158) \times 28-30 (29) μm , eight spored, bitunicate with short stipe. Pseudoparaphyses 3-4 μm in wide, filamentous, septate, branched, exceeding the asci. The ascospores 42-57 (52) \times 10-12 (11) μm , four celled, cylindrical with rounded ends, arranged biserially, brown when young often-becoming dark brown with age, surrounded by hyaline gelatinous sheath. The ascospore is constricted at the septa, which divides the ascospore to four cell compartments, each cell has oblique germ slit (Figures 20 and 21).

For the first time, the ultrastructure of ascospores was further investigated by Scanning Electron Microscopy (SEM). The SEM microphotography (Figure 20 j, k, l and figure 21 h, i) showed that the ascosporic ultrastructure is composed of irregular wrinkled and shrunken surface. The wrinkles are irregular on surface and horizontal on septa.

The isolate STMA 16226 falls in a sister clade (100 % bootstrap) with the clade grouped the reference strains *Dendrothyrium variisporum* CBS 19782 and *Dendrothyrium variisporum* CBS 121517. The genus *Dendrothyrium* (Montagnulaceae, Pleosporales), has genus by Verkley et al. (2014). Furthermore, the inclusion of the additional DNA loci, LSU, β -tubulin and actin, molecular markers resulted in a multigene alignment and their alignment with the closely related genus mainly submitted by Verkley et al. (2014), showed a high supported clustering (73% bootstrap value) of the isolate STMA 16226 with *Dendrothyrium variisporum* CBS 121517. The corresponding phylogenetic tree (Figure 22) confirmed the taxonomic affiliation to *Dendrothyrium variisporum*.

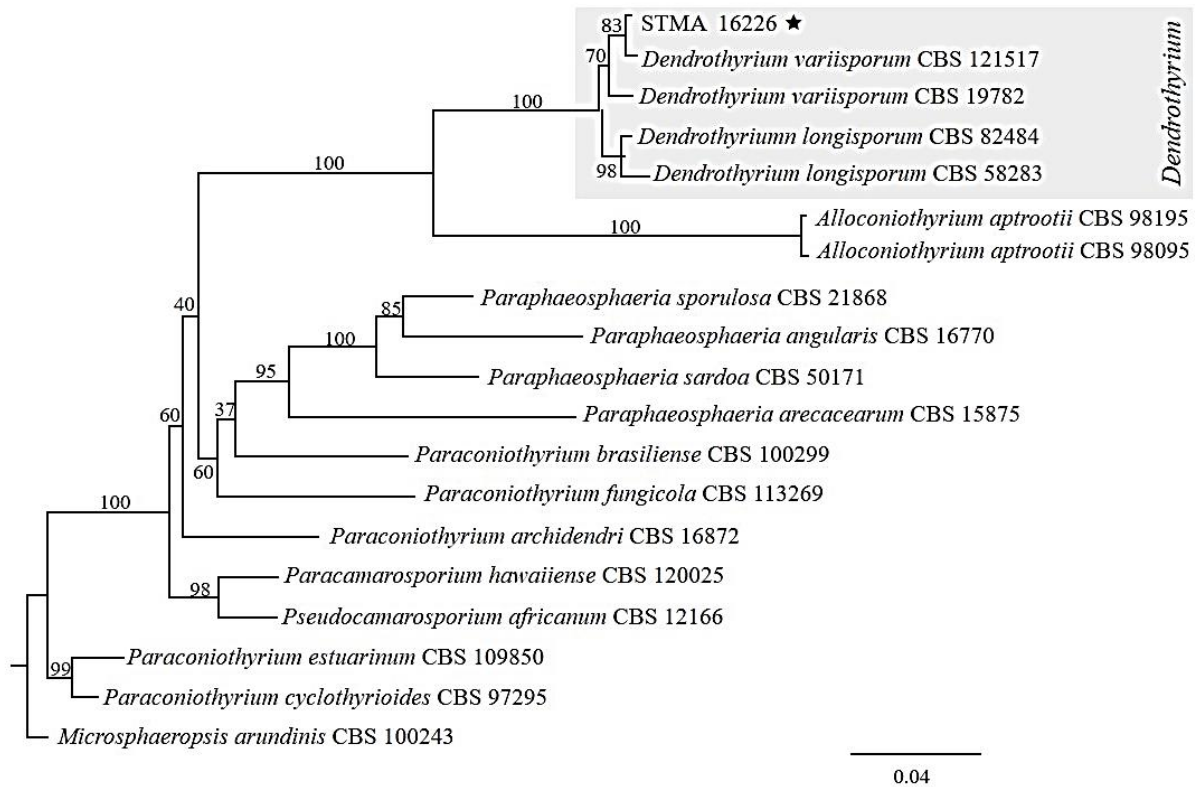


Figure 22. Phylogenetic tree of *Dendrothyrium* spp. and the closely related genera based on combined data set of four markers. Multigenes alignment, RxML (ITS, LSU, Tub and Actin), GTR+G, calculated with, 1000 bootstraps.

Thereby, the anamorphic features of the fungal isolate STMA 16226 were described (Figure 23). Morphology and size of macroscopic features of the culture on the plate were determined. Colonies on YMG and OMA spread over the whole 9 cm Petri dish after 21 days. Colonies on YMG appear white in the center with an even buff margin. On OMA, colonies with even colourless margin and white aerial mycelium in the center are observed while conidiomata are formed on the edge of culture. Conidiomata eustromatic, formed on the edge of culture, often merged to complexes, dark brown to dark, reaching 300-500 μm of diameter. The outer surface covered by glabrous hyphae. Conidia (1-2 μm) \times (3-4 μm), aseptate, variable in shape: subglobose, ellipsoid or obovoid, oliveous-brown. Conideogeous cells (12-20 μm) \times (2-3 μm) integrated in 1-4-septate acropleurogenous conidiophore.

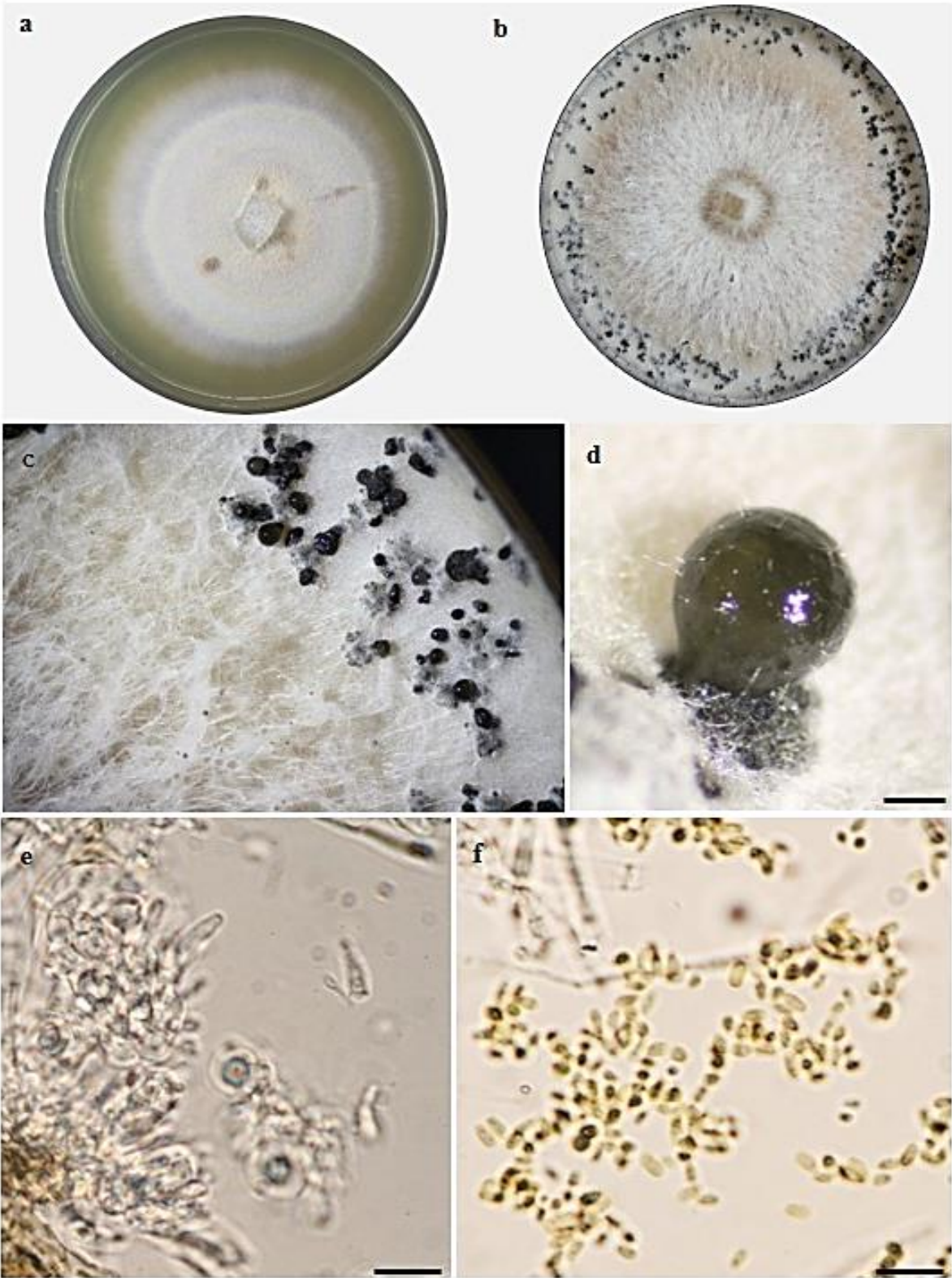


Figure 23: Anamorph characteristics of *Dendrothyrium variisporum*
a. Culture on YMG after 21 days on 9 cm Petri dish, b. Culture on OMA after 21 days on 9 cm Petri dish, c. Conidiomata forming on the edge of culture on OMA medium, d. Conidiomata, e. Conidiogenous cells, f. Conidia, Scale bar: e, f =10 μ m, d=100 μ m.

The class of Eurotiomycetes (clade 2) is represented by the sole Order Eurotiales. Three isolates are clustered within this group. Strain S42 showed similarity with *Aspergillus terreus* KAML04 (100% bootstrap), while strain S3 was related to *Penicillium canescens* (100% BLAST similarity and 100 % bootstrap). The strain S9 and S1 are clustered together (56.1 % bootstrap) and both showed similarity to *Penicillium chrysogenum* with 96.9 % bootstrap value. *Penicillium* were identified as being members of commonly observed genera of soil fungi. Representatives of these genera have been identified as endophytes in cultivated rice roots. The members of the two genera: *Penicillium* and *Aspergillus* (Trichocomaceae, Eurotiales) are characteristically free-living saprophytes that can also be opportunistic root symbionts.

Seven strains are clustered in the class of Sordariomycetes (clade 3). The ITS-PhyML resulted in a monophyletic clade, which accommodates three order; Diaporthales, Sordariales and Hypocreales. Within the clade of Diaporthales is clustered the isolate S50 along with reference strains *Diaporthe ambigua*. This isolate was recovered from the plant roots as sterile mycelia. The genus *Diaporthe* (Diaporthaceae, Diaporthales) and its anamorph *Phomopsis* have often been isolated as endophytic fungi from wide range of host plants (Gomes *et al.*, 2013; Cosoveanu *et al.*, 2018). They are recognized as a rich source of secondary metabolites and enzymes with large spectra of biological activities such as antibiotic, anticancer, herbicides (Gomes *et al.*, 2013).

The order Sordariales (100% bootstraps), is represented here by the genus *Chaetomium*. The isolate STMA 16225 showed affinity to *Chaetomium madrasense* CBS 31574 while the isolate S2 is clustered with *Chaetomium truncatulum* C77 HM365263. The teleomorphic features of the fungus *Chaetomium madrasense* STMA 16225 are showed in figure 24. The plate of 9 cm Petri dish is covered by *Chaetomium madrasense* colonies on YMG and OMA agar media after 21 days. It is characterized by superficial and olivaceous ascomata (260-300 µm of diameter) with spirally coiled ascomatal hairs. The ascomata appear after 15 days. Colonies on OMA lacking aerial hyphae, producing pale orange exudates diffusing into the medium. The ascospores (11.5–13 × 8–10 µm) are subglobose and brown, become dark brown when mature, usually irregular with two apical, subapical or lateral germ pores (Wang *et al.*, 2016). The anamorphic state is absent.

Finally, the order Hypocreales is represented by three *Fusarium* species: *Fusarium acuminatum*, *Fusarium solani* and *Fusarium falciforme*.

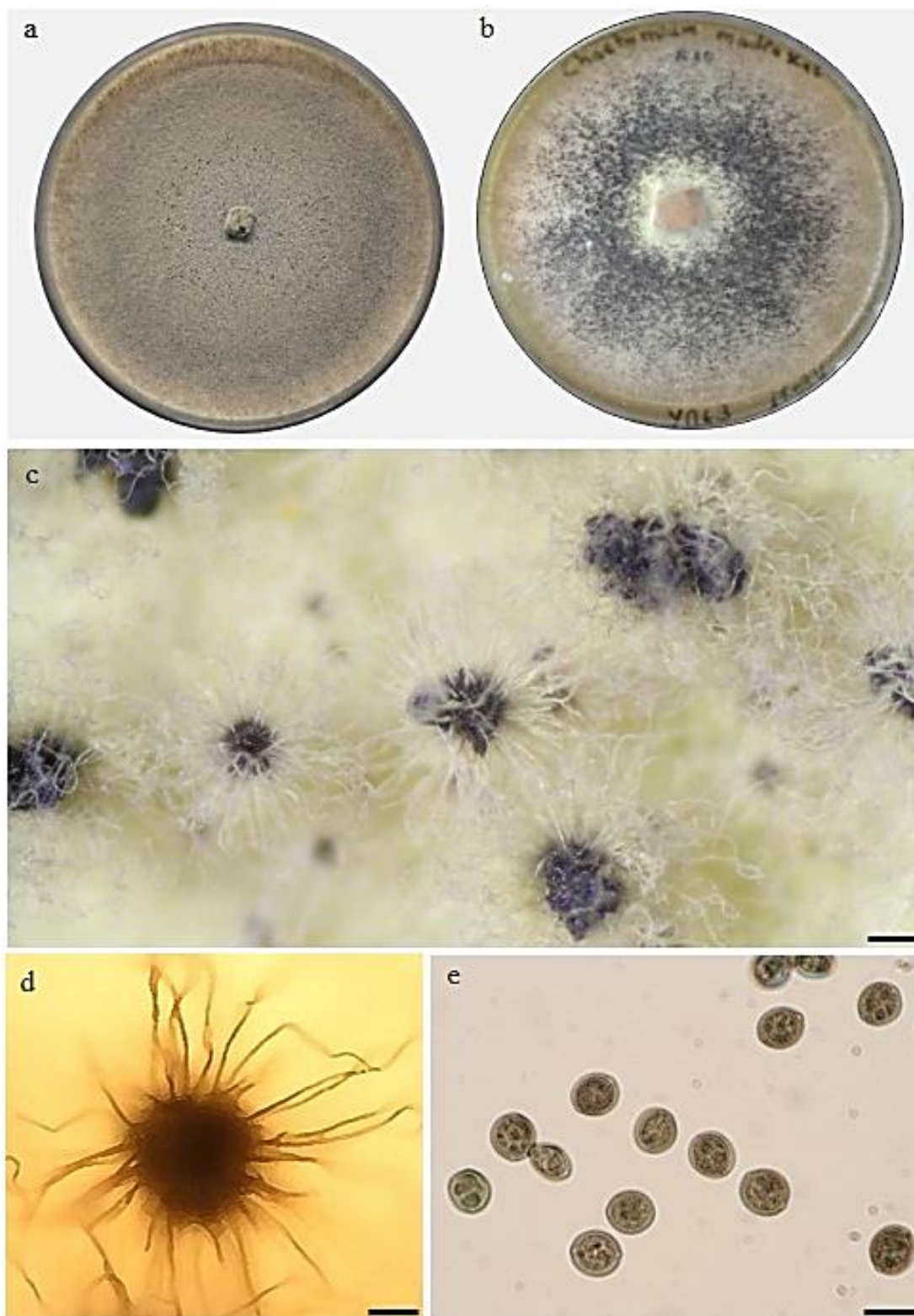


Figure 24: Teleomorphic features of *Chaetomium madrasense*.

a. Culture on OMA after 21 days on 9 cm Petri dish, b. Culture on YMG after 21 days on 9 cm Petri dish, c. Ascomata with spirally coiled ascomatal hairs on YMG agar, d. Ascomata on slide, e. Ascospores. Scale bar: c=200 μ m, c=100 μ m, e=10 μ m.

2. Small scale fermentation and screening for antimicrobial activity

Among seventeen fungal isolates, eight were selected for small scale fermentation in three different liquid media. From each culture medium, two crude extracts are obtained. In total, 48 extracts have subsequently submitted to a preliminary antimicrobial screening. The MIC values of the tested crude extracts are shown in table 8. The results showed that all crude extracts from mycelia and supernatant inhibit the growth of at least one test microorganism. In case of Gram positive bacteria, extracts of all isolates screened have shown MIC ranged from 300 to 2.34 $\mu\text{g}/\text{mL}$ for *B. subtilis*. The most potent extracts were from the mycelial and supernatant of *C. madrasense* cultures in both media Q6/2 and ZM/2 with MIC value 2.34 $\mu\text{g}/\text{mL}$ and with the mycelial extract of *P. similis* DSM 104666 (Figure 25). The antibacterial activity was very high comparable to ciprofloxacin.

Most of the isolated fungi had antibacterial activity only against the Gram positive bacteria. The antibacterial activity against Gram negative bacteria was obtained only in case of broth extracts from *M. phaseolina* culture in ZM/2 and from *P. similis* 104666 culture in YM which they have exhibited inhibition activity against *E. coli* with MIC values of 150 and 300 $\mu\text{g} / \text{mL}$ respectively.

The anti-yeast activity was recorded only in case of both mycelial and supernatant extracts from *P. similis* DSM 32328 cultivated in both YM and Q6/2 media with MIC values 150 and 75 $\mu\text{g}/\text{mL}$ respectively.

From overall results, it was found that the best antibacterial and antifungal activity was obtained from mycelial and supernatant crude extract from *C. madrasense* and the mycelial crude extract from *P. similis* DSM 104666 cultivated both in ZM/2.

The most effective extracts in inhibiting *M. plumbeus*, were crude extracts from ZM/2 culture of *C. madrasense* and supernatant crude extract from ZM/2 culture of *P. similis* DSM 104666 with MIC value recorded at 18.75 $\mu\text{g}/\text{mL}$.

Accordingly, it seems that ZM/2, is the best medium for the production of antimicrobial compounds of the eight actually screened fungal strains.

Table 8: MIC values [$\mu\text{g/mL}$] of the crude extracts from small scale fermentations of the screened fungi in various media.

Code	Fungus	Medium	C.E	MIC($\mu\text{g/mL}$)			
				<i>B. subtilis</i>	<i>E. coli</i>	<i>C. tenius</i>	<i>M. plumbeus</i>
STMA 16225	<i>Chaetomium madrasense</i>	YM	M	4,7	n.a	n.a	n.a
			S	18.75	n.a	n.a	n.a
		Q6/2	M	2.34	n.a	n.a	n.a
			S	2.34	n.a	n.a	n.a
		ZM	M	2.34	n.a	n.a	18.75
			S	2.34	n.a	n.a	18.75
DSM 104666	<i>Preussia similis</i>	YM	M	n.a	n.a	300	n.a
			S	150	300	150	150
		Q6/2	M	n.a	n.a	n.a	150
			S	n.a	n.a	n.a	75
		ZM/2	M	2.34	n.a	n.a	n.a
			S	37.5	n.a	n.a	18.75
DSM 32328	<i>Preussia similis</i>	YM	M	n.a	n.a	150	150
			S	n.a	n.a	150	150
			M	300	n.a	n.a	n.a
			S	n.a	n.a	n.a	n.a
		ZM/2	M	n.a	n.a	75	75
			S	150	n.a	75	75
STMA 16219	<i>Preussia similis</i>	YM	M	n.a	n.a	n.a	300
			S	n.a	n.a	n.a	n.a
		Q6/2	M	n.a	n.a	n.a	300
			S	n.a	n.a	n.a	n.a
		ZM/2	M	n.a	n.a	n.a	75
			S	n.a	n.a	n.a	75
STMA 16226	<i>Dendrothyrium variisporum</i>	YM	M	n.a	n.a	n.a	37.5
			S	150	n.a	n.a	37.5
		Q6/2	M	n.a	n.a	n.a	n.a
			S	n.a	n.a	n.a	150
		ZM/2	M	n.a	n.a	n.a	n.a
			S	n.a	n.a	n.a	150
S32	<i>Macrophomina phaseolina</i>	YM/2	M	300	n.a	n.a	n.a
			S	n.a	n.a	n.a	75
		Q6/2	M	n.a	n.a	n.a	150
			S	n.a	n.a	n.a	150
		ZM/2	M	18.75	n.a	n.a	300
			S	37.5	150	n.a	150
S50	<i>Diaporthe ambigua</i>	YM	M	n.a	n.a	n.a	37.5
			S	n.a	n.a	n.a	37.5
		ZM/2	M	n.a	n.a	n.a	n.a
			S	n.a	n.a	n.a	n.a
		Q6/2	M	n.a	n.a	n.a	150
			S	n.a	n.a	n.a	75

Table 8 (continued)

S2	<i>Chaetomium truncatulum</i>	YM	M	n.a	n.a	n.a	n.a
			S	n.a	n.a	n.a	300
		ZM/2	M	18.75	n.a	n.a	300
			S	37.5	n.a	n.a	300
		Q6/2	M	n.a	n.a	n.a	300
			S	n.a	n.a	n.a	n.a
ATB	Ciprofloxacin			0.52	0.52		
ATF	Nystatin					0.52	4.16

ATB: antibiotic, ATF: antifungal, *B. subtilis*: *Bacillus subtilis*, C.E: crude extract, *C. tenius*: *Candida tenius*, *E. coli*: *Escherichia coli*, *M. plumbeus*: *Mucor plumbeus*.

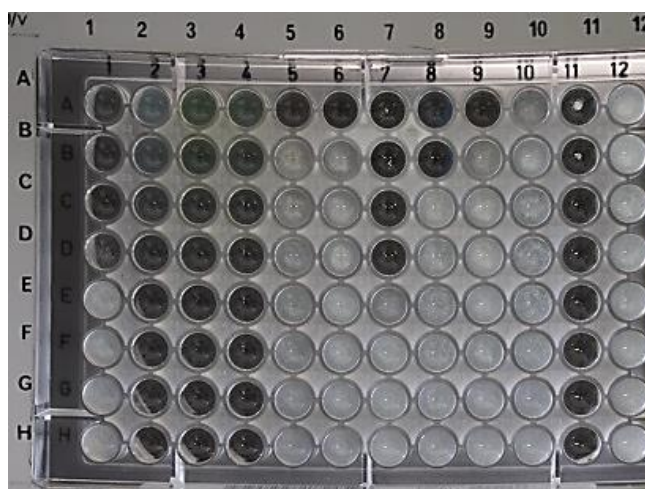


Figure 25: Results of MIC assays of the most potent extracts.

Columns 1, 2, 3, 4, 11, 12 show MIC results of supernatant crude extracts from ZM/2 culture of *P. similis* DSM 104666, mycelial crude extracts from ZM/2 culture of *P. similis* DSM 104666, mycelial crude extract from ZM/2 culture of *C. madrasense*, supernatant crude extract from ZM/2 culture of *C. madrasense*, Ciprofloxacin and MeOH respectively.

3. Large scale fermentation, and purification of bioactive metabolites

In total twenty-eight (1-28) metabolites were isolated from five selected fungal endophytes.

3.1. Compounds isolated from *Preussia similis* strains

Thirteen (1-13) compounds have been isolated from the three strains of *Preussia similis*, in which seven were new.

3.1.1. Compounds isolated from *Preussia similis* DSM 104666

3.1.1.1. Fermentation and metabolites isolation

The metabolic profiles and antimicrobial screening of *Preussia similis* DSM 104666 in different media were performed. The crude extracts derived from the prolonged fermentation in ZM/2 medium (34 days) showed a high antibacterial (2.34 $\mu\text{g/mL}$) and antifungal (18.75 $\mu\text{g/mL}$) activities

as mentioned earlier on screening for antimicrobial activity. Moreover, the metabolomics profiling by LC-MS analyses of both supernatant and mycelial extract, indicated a high production of many metabolites. Evaluation of the secondary revealed the presence of metabolites whose UV-Vis spectra and mass spectra differed from those of all known compounds (Figure 26). Based on results of antimicrobial activity and LC-MS data, ZM/2 medium was chosen as production medium and selected for scale-up fermentation (8L) of *P. similis* DSM 104666, for metabolites isolation and characterization. Six novel bicyclic polyketides (**1–6**) were isolated from cultures of *Preussia similis* DSM 104666. The chemical structures of the six new metabolites **1–6**, for which the trivial names preussilides A–F are proposed, are shown in figure 27. The details of structure elucidation and absolute configuration are illustrated and discussed in Noumeur *et al.* (2017) (paper I). Preussilides A, B, C and D (**1**, **2**, **3** and **4**) were detected and isolated from both supernatant and mycelial crude extract (extracellular metabolites), where preussilide C was the major metabolite yielded followed by preussilide A, while preussilides B and D were minor (Figure 27 A). Only preussilides E and F (**5** and **6**) were intracellular polyketides produced in high amount, their isolation was restricted to mycelial extracts (Figure 27 B). The LC-MS data of preussilides **1–6** and their physical properties are shown in table 9.

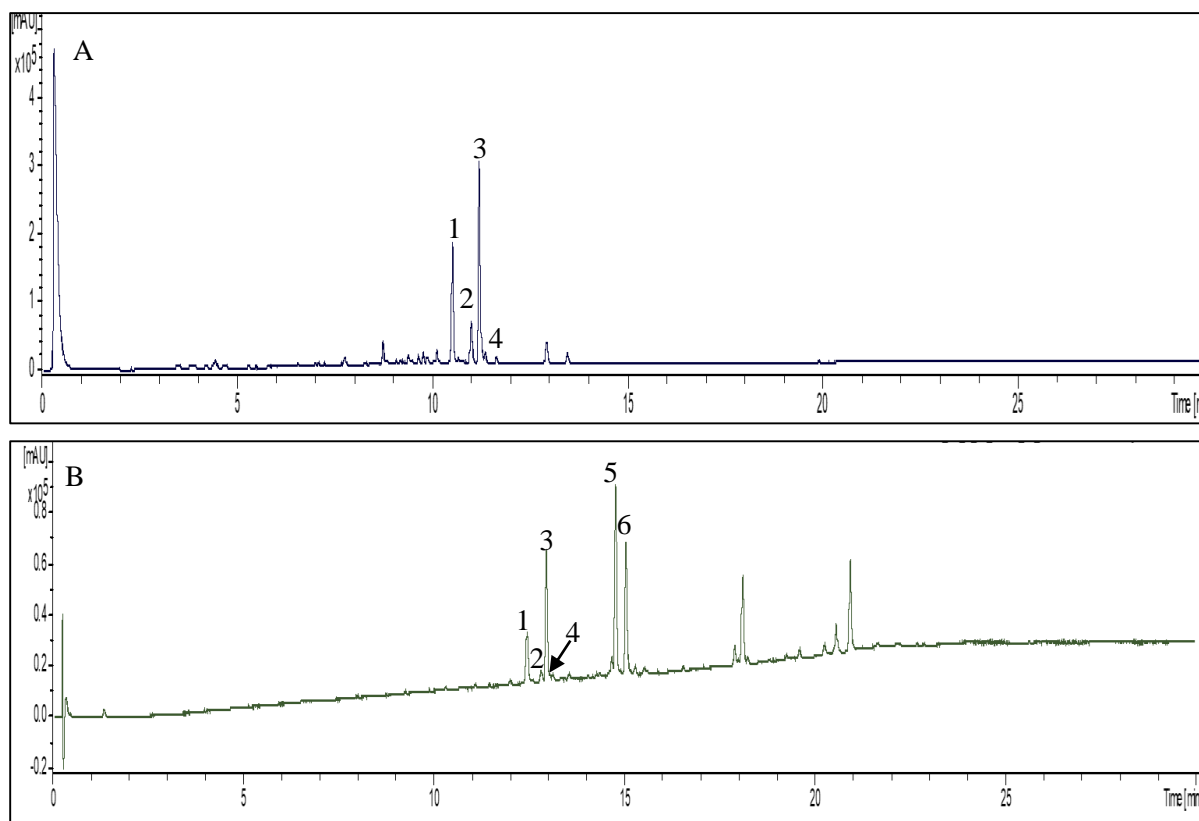
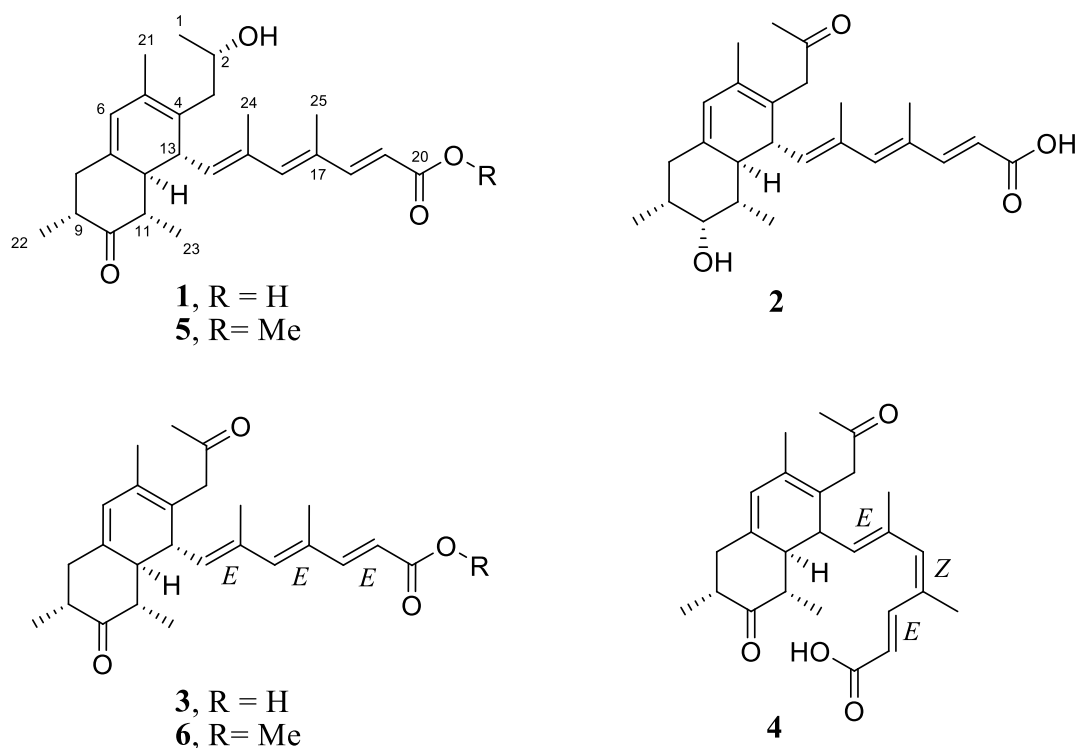


Figure 26: HPLC chromatograms of crude extracts from ZM/2 liquid culture of *P. similis* DSM 104666
A. Supernatant crude extract chromatogram, B. Mycelial crude extract chromatogram.

Table 9: LC-MS data of preussilides **1-6** and their physical properties.

Compounds	Molecular formula	LC-MS(m/z)	Physical properties
Preussilide A	C ₂₅ H ₃₄ O ₄	398.31	Pale yellow gum
Preussilide B	C ₂₅ H ₃₄ O ₄	398.30	Pale yellow gum
Preussilide C	C ₂₅ H ₃₂ O ₄	396.30	Yellow gum
Preussilide D	C ₂₅ H ₃₂ O ₄	396.30	Pale yellow gum
Preussilide E	C ₂₆ H ₃₆ O ₄	412.31	Pale yellow gum
Preussilide F	C ₂₆ H ₃₄ O ₄	410.38	Yellow gum

**Figure 27:** Chemical structures of preussilides A-F (**1-6**)

3.1.1.2. Biological activity of preussilides

The antimicrobial and cytotoxic activity of preussilides A-F were extensively evaluated. The antimicrobial activity profile of preussilides A - F (**1-6**) was determined. The MIC values against filamentous fungi showed that only compounds **1** and **3** exhibited mild antifungal activity, whereas remaining compounds **2**, **4**, **5** and **6** were inactive against the organisms tested. The MIC values of compounds **1** and **3** were determined against *Mucor plumbeus* as 150 µg/mL and 37.5 µg/mL, respectively. Interestingly, the triene acid preussilide C (**3**) showed the strongest activity against

Aspergillus fumigatus with MIC value of 8.33 $\mu\text{g/mL}$, and was thus more potent than the positive control cycloheximide (MIC 33.33 $\mu\text{g/mL}$), followed by preussilide A (**1**) with MIC value of 35.5 $\mu\text{g/mL}$. No antibacterial nor anti-yeast activity was observed with preussilides (table 10). Furthermore, in a standard disk assay, preussilide A (**1**) and C (**3**) inhibited the growth of the plant pathogen *S. sclerotiorum*, affording inhibition zones of *ca.* 28 and 29 mm, respectively, at 100 $\mu\text{g/paper disk}$, as compared to the positive control nystatin (32 mm at 20 $\mu\text{g/paper disk}$) after five days (Figure 28).

Table 10: MIC [$\mu\text{g/mL}$] values of the six preussilides against the tested organisms.

Test organism	MIC [$\mu\text{g/mL}$]						References
	1	2	3	4	5	6	
Gram positive bacteria							
<i>Micrococcus luteus</i> DSM 1790	n.a	n.a	n.a	n.a	n.a	n.a	2.08 ^a
<i>Bacillus subtilis</i> DSM 10	n.a	n.a	n.a	n.a	n.a	n.a	1.04 ^a
<i>Staphylococcus aureus</i> DSM 346	n.a	n.a	n.a	n.a	n.a	n.a	0.42 ^a
<i>Mycobacterium smegmatis</i> ATCC 700084	n.a	n.a	n.a	n.a	n.a	n.a	0.52 ^b
Gram negative bacteria							
<i>Escherichia coli</i> DSM 498	n.a	n.a	n.a	n.a	n.a	n.a	3.33 ^a
<i>Pseudomonas aeruginosa</i> PA 14	n.a	n.a	n.a	n.a	n.a	n.a	0.52 ^c
<i>Chromobacterium violaceum</i> DSM 30191	n.a	n.a	n.a	n.a	n.a	n.a	1.67 ^a
Yeasts							
<i>Candida albicans</i> DSM 1665	n.a	n.a	n.a	n.a	n.a	n.a	33.33 ^d
<i>Rhodotorula glutinis</i> DSM 10134	n.a	n.a	n.a	n.a	n.a	n.a	2.08 ^d
<i>Pichia anomala</i> DSM 6766	n.a	n.a	n.a	n.a	n.a	n.a	8.33 ^d
<i>Schizosaccharomyces pombe</i> DSM 70572	n.a	n.a	n.a	n.a	n.a	n.a	8.33 ^d
<i>Candida tenuis</i> MUCL 29892	n.a	n.a	n.a	n.a	n.a	n.a	0.78 ^d
Filamentous fungi							
<i>Aspergillus fumigatus</i> DSM 819	66.67	n.a.	8.33	n.a	n.a	n.a	33.33 ^e
<i>Mucor hiemalis</i> DSM 2656	n.a	n.a	n.a	n.a	n.a	n.a	16.67 ^d
<i>Mucor plumbeus</i> MUCL 49355	150	n.a	37.5	n.a	n.a	n.a	3.12 ^d

^a Oxytetracycline hydrochloride (1 mg/mL), ^b Kanamycin (10 mg/mL), ^c Gentamycin (10 mg/mL), ^d Nystatin (1 mg/mL), ^e Cycloheximide (10mg/mL), n.a : no activity.

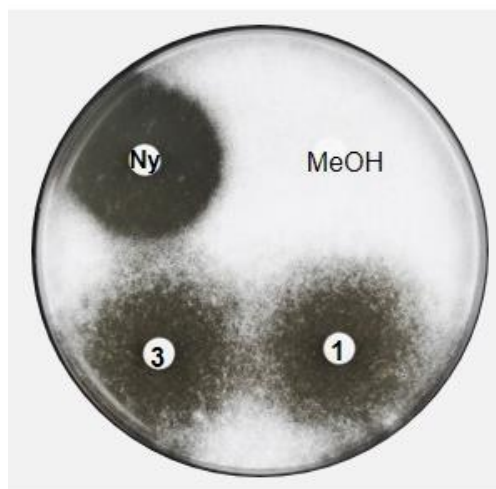


Figure 28: Antifungal activity of preussilides A (1) and C (3) against phytopathogen *S. sclerotiorum* determined by Agar diffusion at 100 μ g/disk. Ny: nystatin as positive control and MeOH as negative control.

Moreover, no nematicidal activity at up to 100 μ g/mL against *Caenorhabditis elegans* and no phytotoxic effects in plant germination assays with *Setaria italica* and *Lepidium sativum* at 100 μ g/paper disk were observed.

In spite of the fact that the mycelial crude extract showed a very high antibiotic activity against *B. subtilis*, all preussilides were inactive in tests for antibacterial activity. This suggests that either the antibacterial metabolite is produced in very minor amount, or that the antibacterial activity observed was due to a combined effect of multiple metabolites acting together. This astounding result let us to conduct a bioactivity-guided fractionation by RP-HPLC using *B. subtilis* as indicator organism to look for the pic responsible of the antibacterial activity. As result of this fractionation, it appears that the metabolite pic conferring the interest antibacterial effect of the mycelial crude extract (2.34 μ g/mL) is, a tiny pic which presented a retention time of 23.334 min and one UV maxima at 310 nm (Figure 29 A, B and C). The LC-MS analysis of the mycelial crude extract revealed that this pic, with a mass of 572 (Figure 29 D), was yielded in small amounts, that is why it was difficult, if not impossible to have it in pure fraction. Therefore, the scaled-up fermentation and/or optimization of growing conditions could lead to significantly increased production of this antibacterial compound.

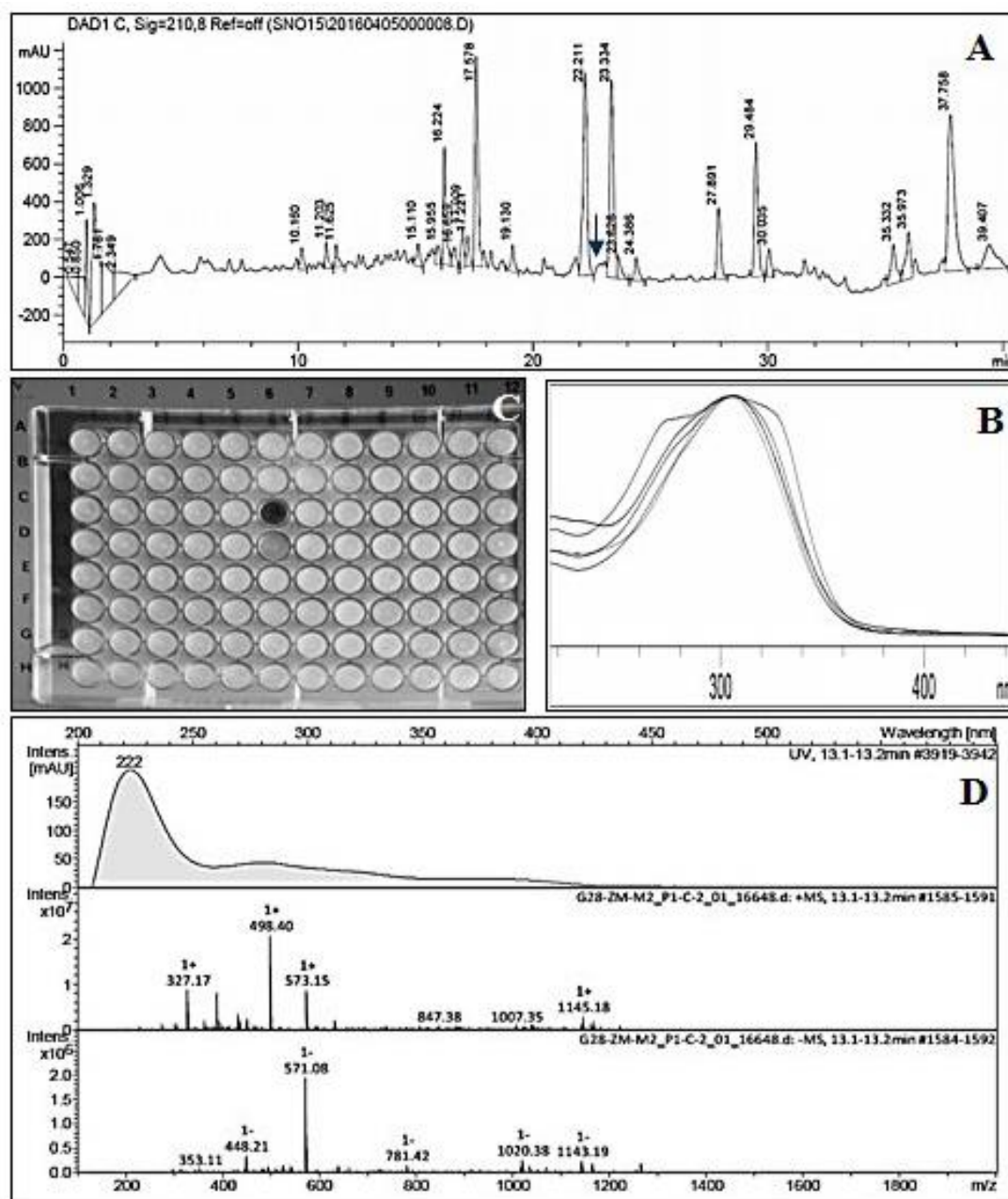


Figure 29: Results of bioassay-guided fractionation by RP-HPLC using *B. subtilis* as indicator organism. A. HPLC chromatogram obtained after fractionation, tiny pic of metabolite of interest is indicated by arrow B. UV of bioactive metabolite of interest, C. Fractionation plate with inhibited well, D. Mass of the metabolite of interest from LC-MS.

Furthermore, to evaluate cytotoxicity of the six polyketides on viability of different mammalian cell lines, MTT assays were performed. The results in table 11 showed that all compounds exhibit modest cytotoxicity (Table 4) with IC_{50} values ranging from 1 to 28 $\mu\text{g}/\text{mL}$. Preussilides A (**1**) and C (**3**) showed the highest antiproliferative effect against HeLa KB.3.1 cells with 2.4 $\mu\text{g}/\text{mL}$ and 1 $\mu\text{g}/\text{mL}$ values, respectively.

Preussilide F exerts moderate cytotoxicity toward L929 and KB3.1 but does not exhibit cytotoxic effects in all other cell lines tested. Moreover, all compounds cause nucleic fragmentation in the range of IC₅₀ values in L929 cells (Figure 30).

Table 11: Cytotoxic effect (IC₅₀) of preussilides A-F (1 - 6) against different normal and cancer cell lines

Cell line	IC ₅₀ [μg/mL]						Reference
	1	2	3	4	5	6	
Mouse fibroblasts L929	2.6	6.9	3.6	9.8	33	22	9 × 10 ⁻⁴
HELA cells KB3.1	2.4	4.5	1	6.9	9.5	21	3.1 × 10 ⁻⁵
Squamous carcinoma A431	8.1	14	4	7.1	23	>10 ³	3.7 × 10 ⁻⁵
Human lung carcinoma A549	24	28	9.1	19	17	>10 ³	8 × 10 ⁻⁵
Ovarian carcinoma SKOV-3	9	13	6.2	8	12	>10 ³	1.2 × 10 ⁻⁵
Human prostate cancer PC-3	19	24	7.3	18	17	>10 ³	1.2 × 10 ⁻⁴
Human breast adenocarcinoma MCF-7	9.7	8.8	2.9	6.1	23	>10 ³	8 × 10 ⁻⁵
Human osteosarcoma U2OS	2.8	>10 ³	2.7	>10 ³	>10 ³	9.1	5.3 × 10 ⁻⁵

Reference: Epothilone B

The structurally closest related metabolites to preussilides are hamigerone, dihydrohamigerone (Breinholt *et al.*, 1997), antarones (Shiono *et al.*, 2008) and unnamed “highly methylated polyketides”(Stierle *et al.*, 1999). The Hamigerones were isolated from *Hamigera avellanea*, and antarones were obtained from *Penicillium antarcticum*, while the unnamed “highly methylated polyketides” were isolated from a yew-associated *Penicillium* species. Hamigerones were reported to have antifungal activity against the plant pathogens *Pyricularia oryzae* and *Venturia inaequalis*, while the “highly methylated polyketides” were active against *Sclerotinia sclerotiorum*. The antarones, however, were reported to be devoid of antimicrobial and cytotoxic effects.

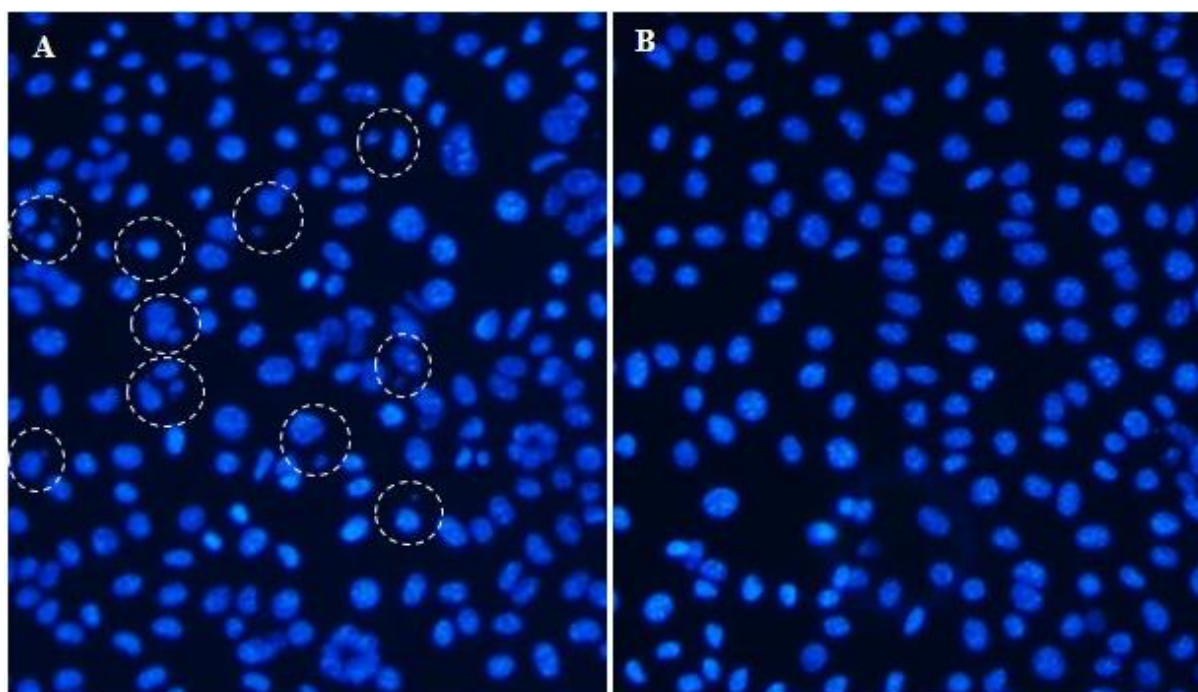


Figure 30: Microscopic view of fragmented nuclei of preussilide C-treated L929 in MTT assay.
 (A) DAPI staining of preussilide C-treated L929 cells, showing fragmented nuclei in MTT assay in the range of IC_{50} value. The areas encircled by dotted circles show inaccurate DNA division.
 (B) DAPI staining of MeOH-treated L929 cells in MTT assay.

3.1.1.3. Co-culture of *P. similis* with phytopathogen *S. sclerotiorum*

In order to search for the chemical nature of the metabolites of *P. similis* DSM 104666 produced in the presence of an antagonist, a co-culture was carried out with the phytopathogen *S. sclerotiorum*. As first observation of dual culture assay with phytopathogen *S. sclerotiorum*, *Preussia similis* DSM 104666 was found to subdue *S. sclerotiorum* growth, (Figure 31) up to 43 %, based on the percentage of growth analysis; thus indicating that *S. sclerotiorum* was sensitive towards the endophytic fungus secretions.

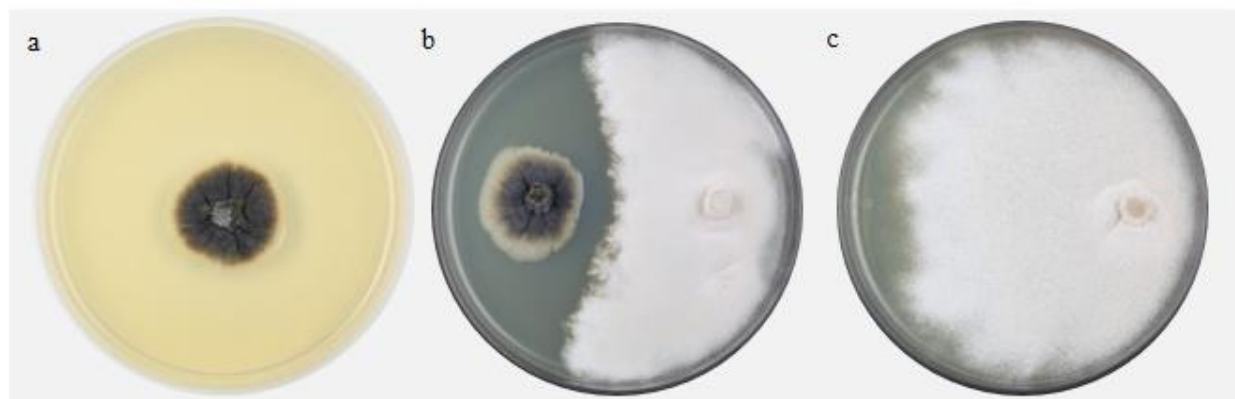


Figure 31: Mono and co-cultures on YMG agar medium of *P. similis* and *S. sclerotiorum*.
 a. monoculture of *P. similis* DSM104666, b. Co-culture of *P. similis* DSM 104666 with *S. sclerotiorum* results in inhibition of the phytopathogen, c. monoculture of *S. sclerotiorum*.

Furthermore, in order to examine the antifungal compounds involved in growth inhibition of the pathogen, the agar of the inhibition zone was cut and subsequently extracted with EtOAc. Interestingly, the HPLC chromatogram of the EtOAc extract of the inhibition zone agar revealed that preussilide C is the most abundant metabolite produced by the strain followed by preussilide A in co-culture with the phytopathogen (Figure 32 A).

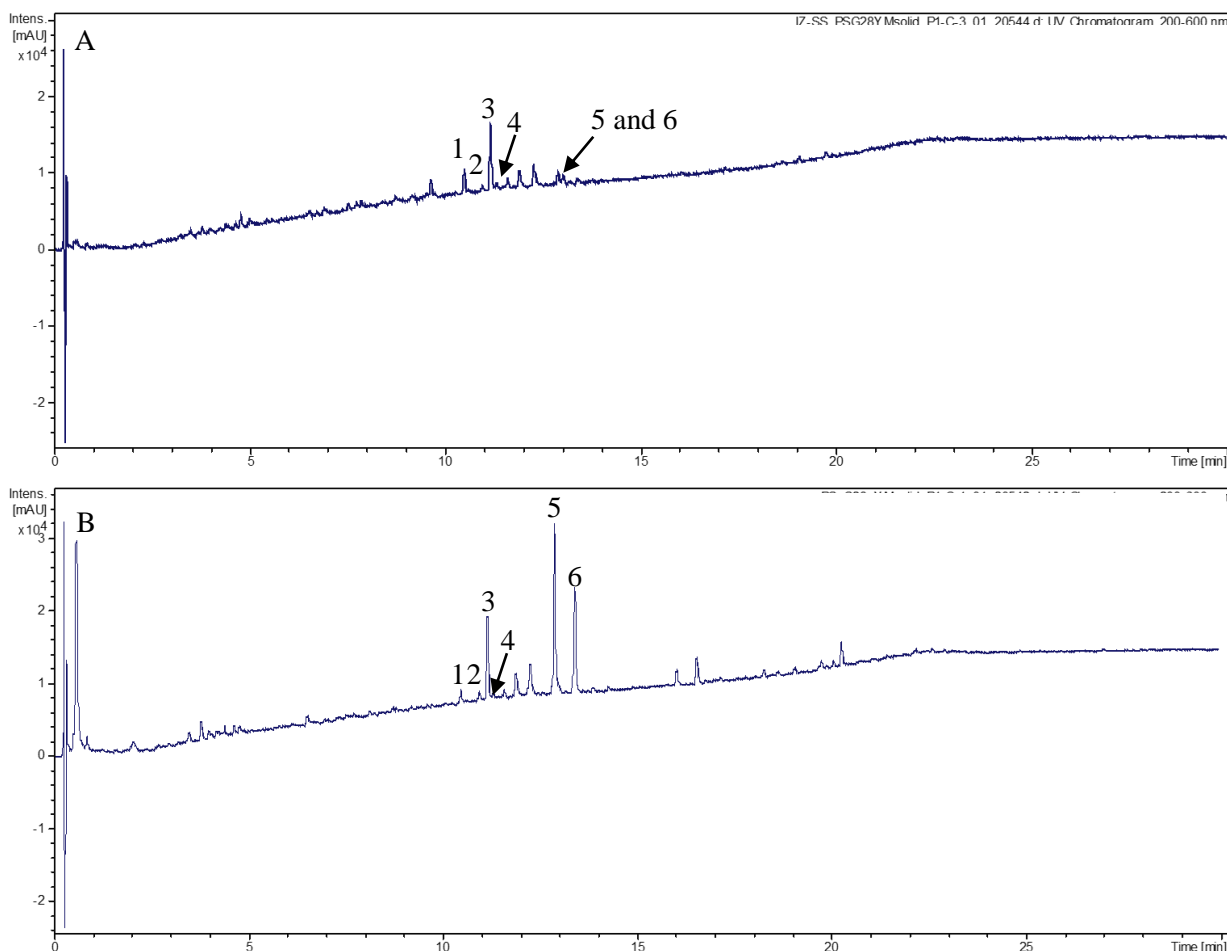


Figure 32: HPLC chromatograms of individual axenic and co-culture of *P. similis* DSM 104666
A. Co-culture of *P. similis* DSM 104666 and *S. sclerotiorum*, B. Axenic culture of *P. similis* DSM 104666.

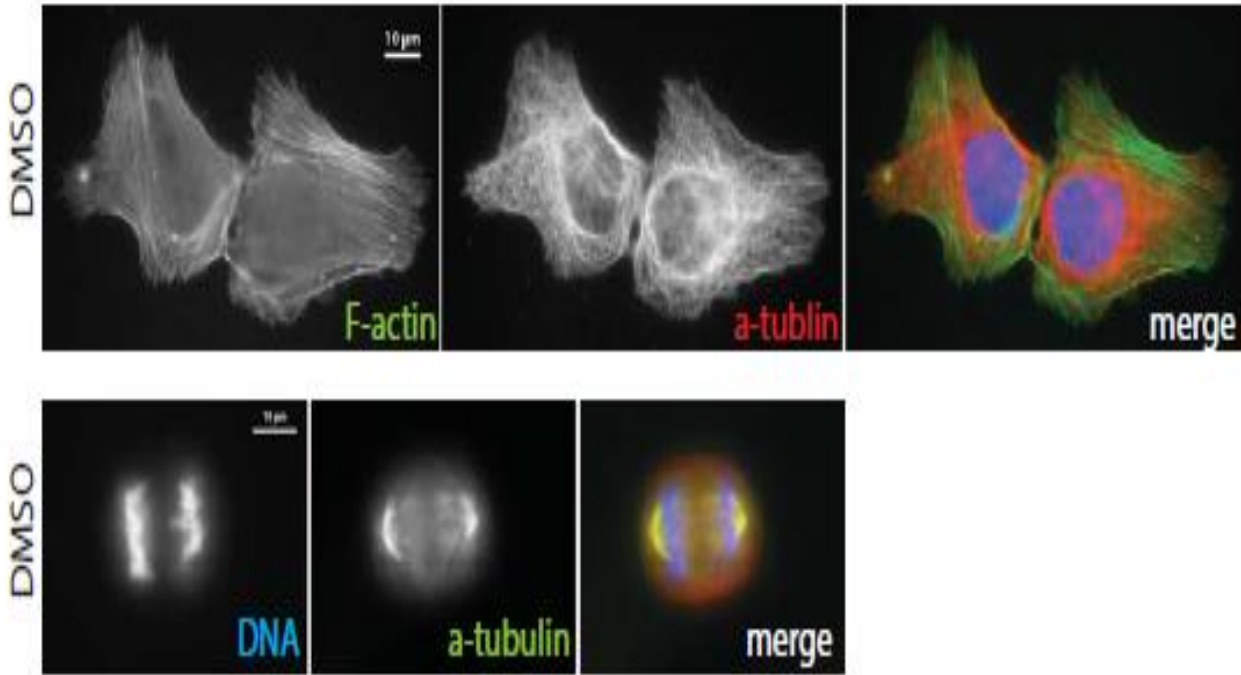
Moreover, the pics of preussilides E and F were very minor (Figure 32 A) in comparison to the chromatograms of the mono-culture control in which they were produced in a largest amounts (Figure 32 B). The detection of preussilide C as the major antifungal compound in the confrontation assay could be reasonably related to its potent antifungal activity (as showed in MIC testing and agar diffusion assay) and therefore the strain involves this compound in the inhibition of the pathogen. However, the concentration reduction of preussilides E and F in co-cultures can be explained by the fact that these two compounds are devoided of any antifungal activity and thus they will not be sufficient to inhibit competitor, so the fungus reduce their biosynthesis and keep the biosynthesis of

preussilides C and A. In the same vein, Schulz et al. (2015), have reported that fungi would not expend energy to produce such metabolites, if they did not have a function *in situ*. Likewise, mixed cultivation has been proved by many authors to be a powerful trigger of secondary metabolites production. This co-cultivation can help either to encrypt silent fungal secondary metabolites gene clusters under standard laboratory growth conditions or can allow a tremendously enhanced production of already known natural compounds (Scherlach and Hertweck, 2009; Schroeckh and Brakhage, 2014; Netzker et al., 2015; Wakefield et al., 2017). In the same respect, Ola et al. (2013) have shown that *Bacillus subtilis*, most commonly Gram positive organism found in the rhizosphere, is an important fungal partner that led to the activation the gene clusters during its mutual interplay with *Fusarium tricinctum*. Such an interaction leads to the production of new compounds such as: macrocarpon C, 2(carboxymethylamino) benzoic acid and citreoisocoumarinol. In addition, a remarkable increase production of the constitutively present compounds including lateropyrone, cyclic depsipeptides of the ennatin type and fusaristatin A, which was 78-fold higher than in fungal monoculture. This situation might suggest that the less concentration of the antibacterial compound aforementioned detected in the chemical profile of the mycelial crude extract of *P. similis* DSM 104666 could be widely synthesized in the presence of a potential bacterial antagonist.

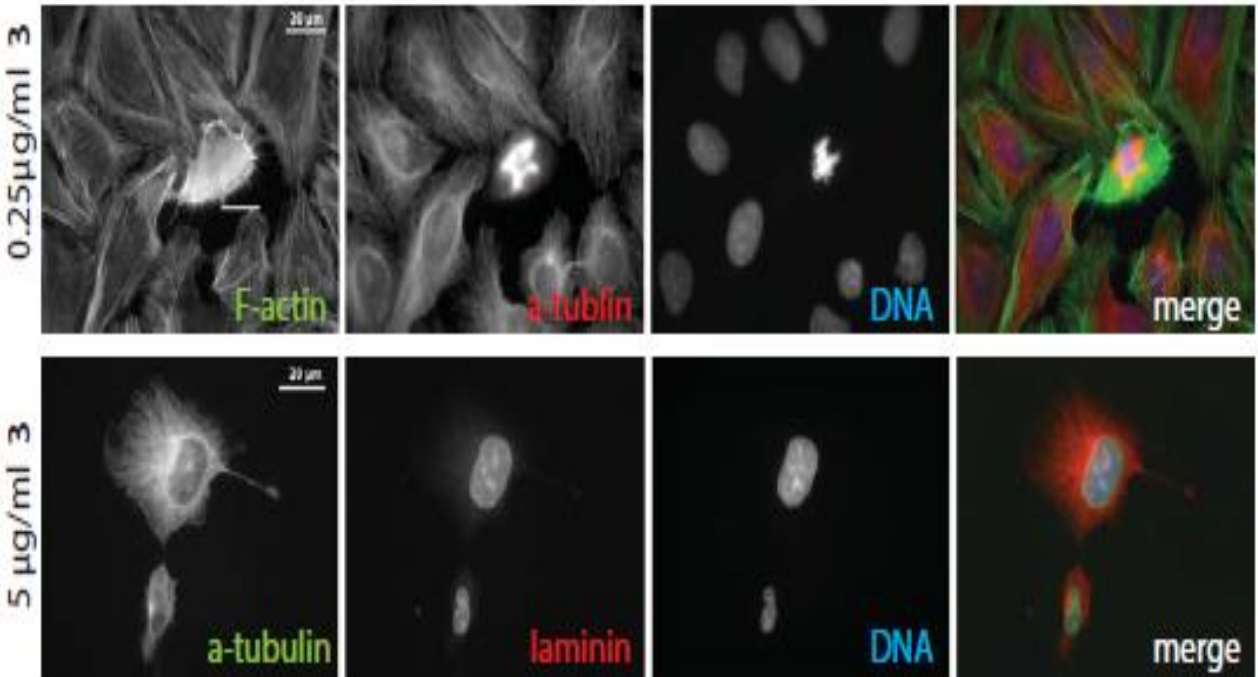
3.1.1.4. Effects of preussilides on cell morphology

To further analyze alterations observed in standard-screening assays, the actin and microtubule cytoskeleton, as well as the nuclear lamina and DNA of treated cells were stained. Effects were most pronounced when using preussilides A (**1**) and C (**3**), and a more detailed analysis of their biological effects was conducted. Complementary results from the other compounds can be viewed in figure 33. Immunofluorescence experiments revealed that the actin cytoskeleton was not affected by any of the tested compounds. In contrast to actin, the microtubule cytoskeleton showed significant alterations during mitosis with multipolar spindles (Figure 33 B, C) in a significant amount of dividing cells. Whereas this can in principle occur in cancer cells such as U2OS, multipolar spindles were rare in control-treated U2OS, which mainly displayed normal bipolar mitotic spindles, and properly divided cells (Figure 33 A). Moreover, in treated populations we observed numerous ‘inaccurate’ cell divisions, giving birth to daughter cells with unequal cell and nuclear sizes (Figure 33 B lower panel). Hence, this phenotype leads to unequal DNA distribution between the two new cells, while both daughter cells form a complete nucleus with intact nuclear lamina despite the uneven size. The most significant effects were again observed in cells treated with preussilide C (**3**).

A



B



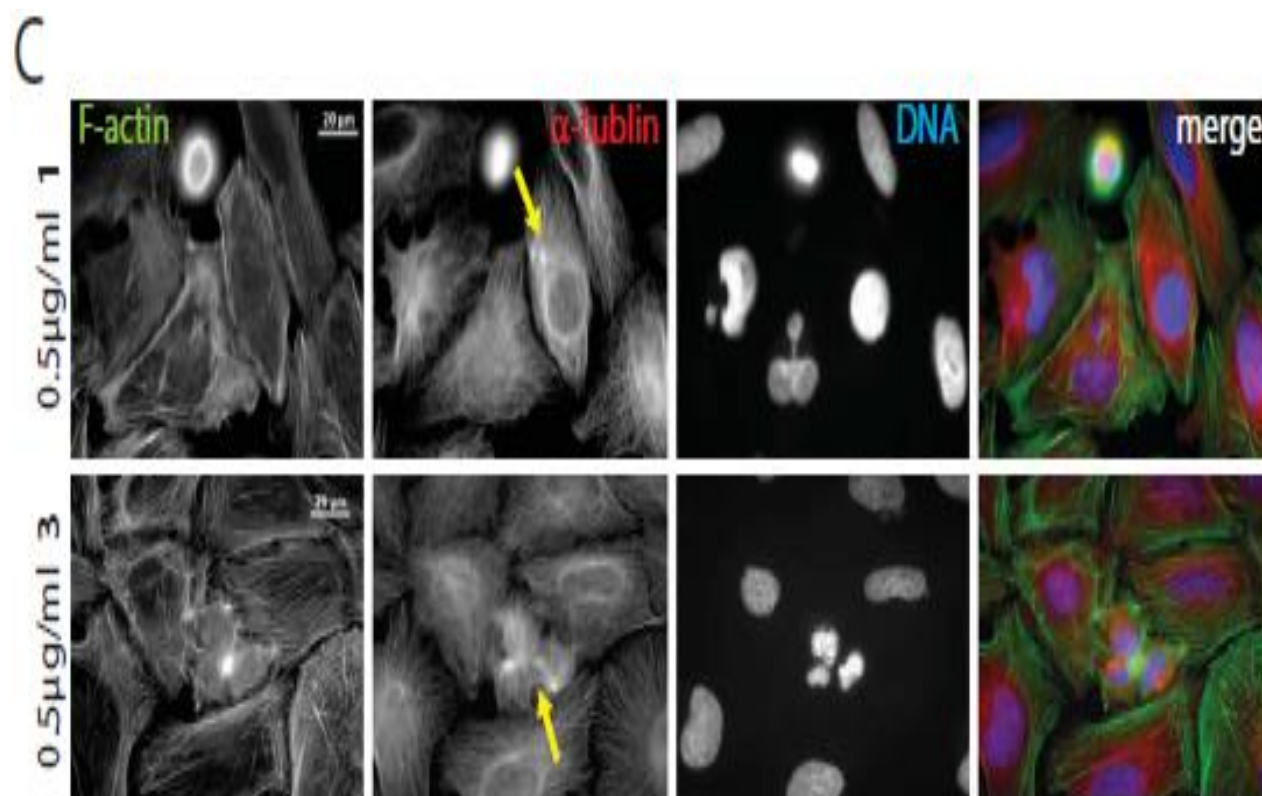


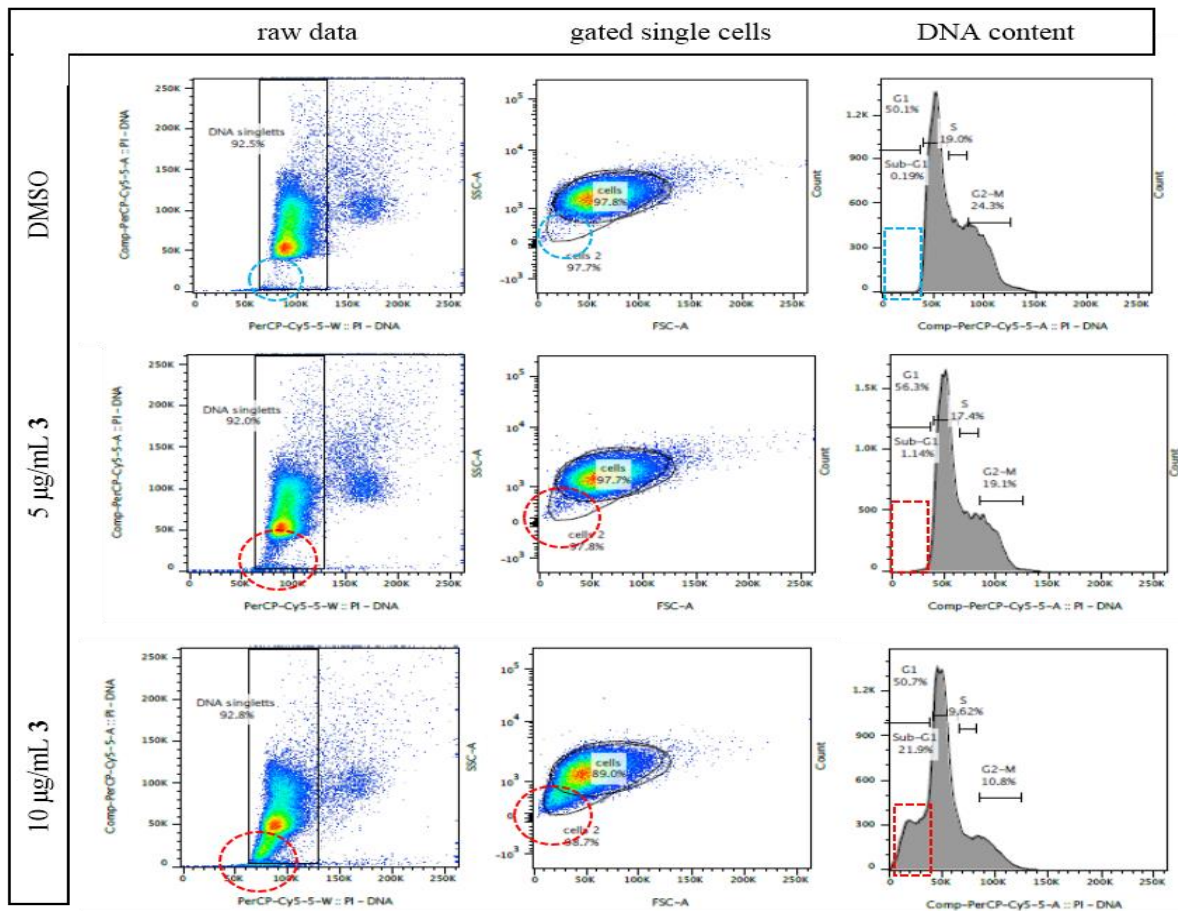
Figure 33: Effects of preussilides A and C (**1** and **3**) on the Morphology of Human Osteosarcoma Cells (U2OS). The actin cytoskeleton is not altered upon treatment (B and C) as compared to controls (A). Antibody staining of microtubules (as indicated in panels) uncovers multipolar and duplicated spindles in treated cell populations as compared to predominantly canonical bipolar spindles in mock treated cells. Aberrantly sized cells with abnormal small nuclei, are observed in treated cells (B, bottom panel). Note that small cells may originate from inaccurate cell division, e.g., due to spindle multiplication. Pseudo-colored merge is shown in the very right of every panel. Scale bar is 20 μm .

Also, cells with fragmented nuclei were observed more frequently than in control populations, reminiscent of the screening result in L929 cells.

In complementary experiments, preussilide-treated cells were subjected to FACS. To do so, cells were either left untreated, mock treated or treated with 5 and 10 $\mu\text{g/mL}$ of each compound, and prepared for flow cytometric analysis upon staining of DNA, tubulin and lamin. DNA-staining was used to classify cells according to cell cycle phases (G1, G2-M, S and sub-G1). Strikingly, flow cytometry of cells treated with 5-10 $\mu\text{g/mL}$ of preussilides A (**1**) and C (**3**) revealed the appearance of a significant population of sub-G1 cells/particles (Figure 34 A; figures S1 and S2 appendix B). While this population in most cases indicated programmed cell death/apoptosis, we conclude that this sub-G1 population represents those smaller cells observed before eventually deriving from inaccurate cell divisions (Figure 33).

This conclusion is supported by the fact that no apoptotic figures were observed in fluorescence microscopy experiments that could explain this population. To verify that we here induce a specific phenotype other than apoptosis, we repeated treatments leading to most significant sub-G1 populations and specifically stained for caspase activation, a hallmark of apoptosis. As a positive control, cells were treated with staurosporine to induce apoptosis. The result clearly showed the small cells represented in the sub-G1 population in FACS experiments were not apoptotic, i.e., do not show caspase 3/7 activation, whereas staurosporine clearly induced apoptosis in U2OS cells (Figure 34 B). Noteworthy, preussilide C-treated cells in general, and preussilide C-treated sub-G1 cells in particular, displayed increased amounts of tubulin and lamin staining (Figure S2, appendix B), which also speaks against apoptosis that would otherwise lead to declining signals due to protein degradation. Together, these data suggested that preussilides A (**1**) and C (**3**) treatment had a profound effect on the cell cycle with multipolar spindles and inaccurate/unequal cell divisions resulting in cells that cannot multiply further and die, explaining the loss of biomass observed in the cytotoxic screening. Some of these cells were abnormally small as seen in immunofluorescence and as detected as sub-G1-population in FACS. Apoptotic cell death appears not to be the predominant reason, as canonical apoptotic figures were rarely observed in immunofluorescence, and moreover, caspase 3/7 activation was at the detection level even after prolonged incubation with high concentrations of the most active preussilide C. Nonetheless, multipolar spindles were observed more frequently at concentrations as low as 0.25 $\mu\text{g/mL}$, which is 10 to 20-fold below concentrations showing significant cytotoxicity. Thus, our data indicate that the mechanism of cell manipulation by preussilides might target an enzyme involved in coordination of the cell division cycle by affecting, for instance, timing or spindle assembly mechanisms, leading to defects in chromosome segregation and/or spindle geometry.

A



B

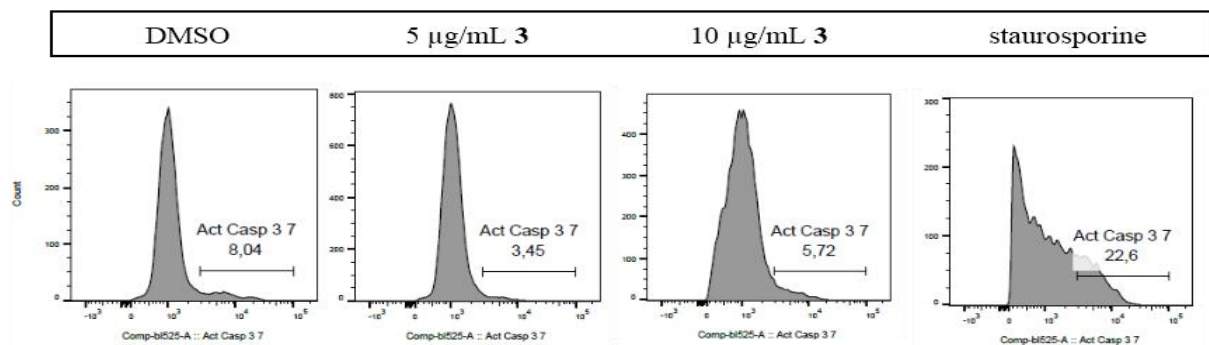


Figure 34: Preussilides treatment induces generation of small cells with reduced nuclear size in the human Osteosarcoma Cell Line U2OS. (A) FACS data of PI-stained preussilides and control treated cells. Note the occurrence of small cells/particles with low DNA content in the treated populations (middle panel, 5 µg/mL, 1,96% of cells; bottom panel, 10 µg/mL, 25,5% of cells) as compared to mock treated (top panel, DMSO treated, 0,19% of cells). When classifying cell cycle phases by analyzing the DNA content per cell/particle (right panel) then this population fell into the sub-G1-window (outlined in red as compared to blue in control). (B) Cells treated with DMSO, 5 or 10 µg/mL of preussilide C or treated with 250 nM staurosporine and stained with fluorescent caspase 3/7 Green substrate were analysed by FACS. Note that there is no increase in apoptosis as compared to DMSO control (8%) upon preussilides treatment (5 µg/mL 3.5% and 10 µg/mL 5.7%). In contrast, staurosporine induced significant programmed cell death (22.6%).

3.1.2. Compounds isolated from *Preussia similis* STMA 16219

3.1.2.1. Fermentation and metabolites isolation

The mycelial and supernatant crude extracts from culture of *Preussia similis* STMA 16219 grown in Q6/2 liquid medium (8L) were purified by using preparative HPLC. Three pure compounds were obtained: one new dimer of 2-aminobenzoic acid moities (dibenzo [c, h] [1,6,2,7] dioxadiazecine-7,14 (5H, 12H)-dione) (**7**) along with two known xanthenes derivatives: secosterigmatocystin (**8**) and sterigmatocystin (**9**). The chemical structures of three metabolites are shown in figure 35. The new compound and secosterigmatocystin were purified from the supernatant crude extract while sterigmatocystin was isolated from the mycelial crude extract (Figure 36). The LC-MS data of three compounds and their physical properties are shown in table 12

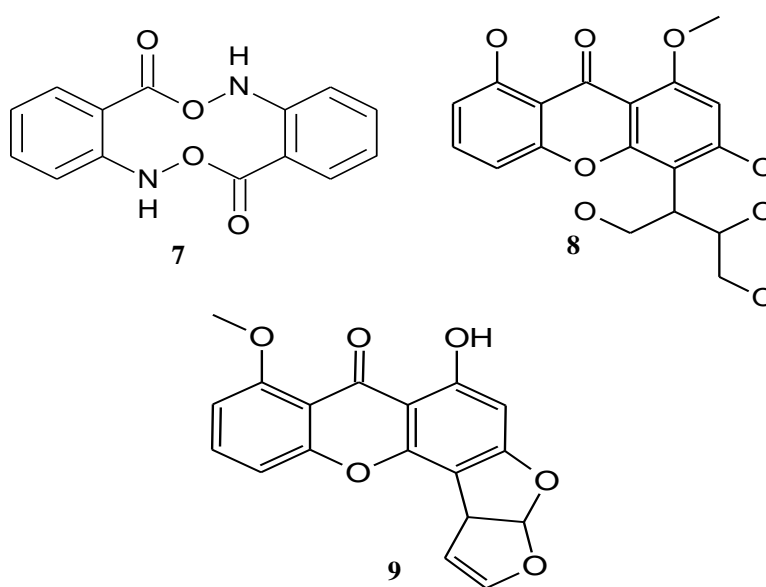


Figure 35: Chemical structures of the compounds (**7-8**) obtained from *P. similis* STMA 16219

Table 12: LC-MS data of three compounds of *P. similis* STMA 16219 and their physical properties.

N°	Compound	Molecular formula	LC-MS (m/z)	Physical properties
7	Dimer of 2-aminobenzoic acid moities	C ₁₄ H ₁₀ N ₂ O ₄	270,08	Red gum
8	Secosterigmatocystin	C ₁₈ H ₁₈ O ₈	362,14	White crystals
9	Sterigmatocystin	C ₁₈ H ₁₂ O ₆	342,07	White crystals

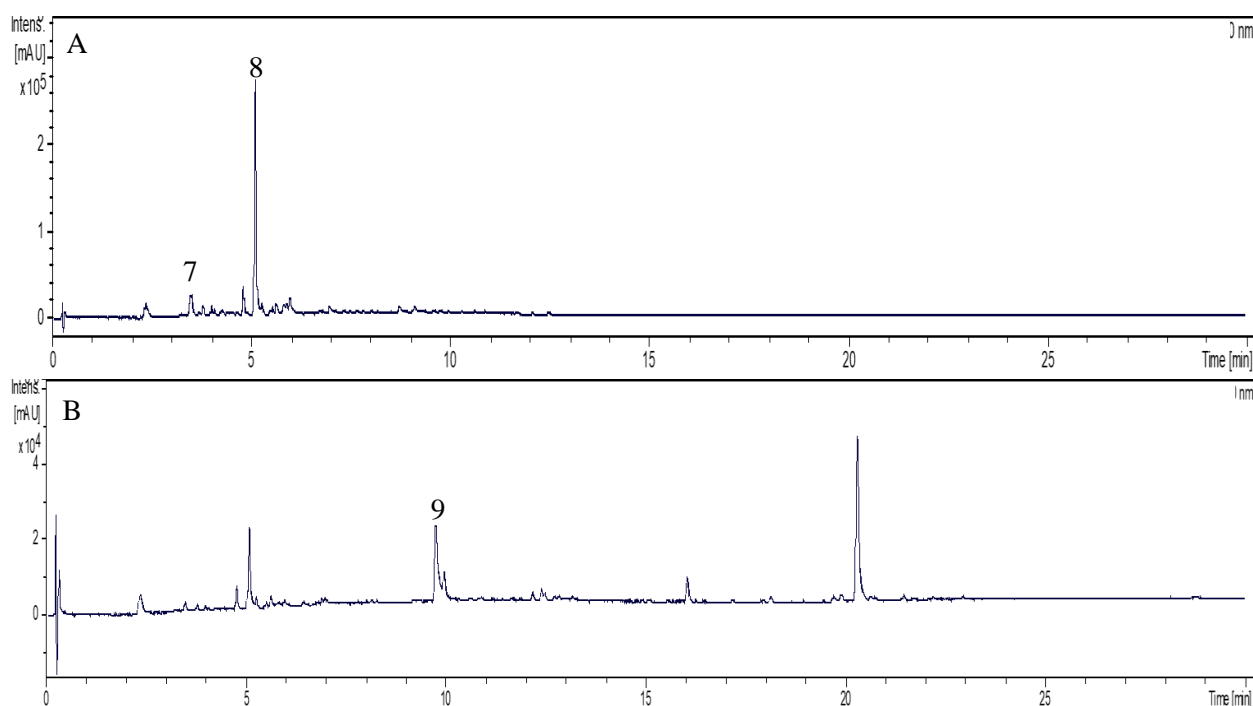


Figure 36: HPLC chromatograms of crude extracts from Q6/2 liquid culture of *P. similis* 16219
A. Supernatant crude extract chromatogram, B. Mycelial crude extract chromatogram.

3.1.2.2. Biological activity

Neither antibacterial nor antifungal activity was observed for secosterigmatocystin and sterigmatocystin, while the dimer of 2-aminobenzoid acid moieties exhibited a selective antifungal activity against *Mucor hiemalis* with MIC value 33.33 $\mu\text{g}/\text{mL}$. Quantities available of three compounds were not sufficient for testing cytotoxicity activity. Sterigmatocystin (STC) is a product of other distantly related taxa, it is known mainly as a typical metabolite of *Aspergillus* species mainly *Aspergillus versicolor* (Veršilovskis and De Saeger, 2010; Rank *et al.*, 2011; Despot *et al.*, 2016; Nomura, 2017). Other genera were also found to be producers of STC such as *Aschersonia*, *Aspergillus*, *Bipolaris*, *Botryotrichum*, *Chaetomium*, *Emericella*, *Eurotium*, *Farrowia*, *Fusarium*, *Humicola*, *Moelleriella*, *Monocillium* and *Podospora* (Rank *et al.*, 2011). So far, no previous studies have reported the production of STC from *Preussia* spp., this is the report on the STC isolation from the respective organisms. STC is a toxic metabolite chemically closed to the aflatoxins and known to be its biosynthesis intermediate (Bhatnagar *et al.*, 1987). Recently, STC has attracted increasing research attention because it poses a risk to human and animal health specially after its detection in different food stuffs (Nomura, 2017) and indoor air (Jak *et al.*, 2016). The cytotoxicity of STC is well studied, it is recognized as a potential carcinogen, mutagen and teratogen in animals while the

importance of STC as a human health hazard is unknown (Veršilovskis and De Saeger, 2010). The phytotoxic and nematicidal activity of the three compounds were not tested.

Table 13: MIC [$\mu\text{g}/\text{mL}$] values of *P. similis* STMA 16219 compounds.

Test organism	MIC [$\mu\text{g}/\text{mL}$]			
	7	8	9	Reference
Gram positive bacteria				
<i>Micrococcus luteus</i> DSM 1790	n.a	n.a	n.a	2.08 ^a
<i>Bacillus subtilis</i> DSM 10	n.a	n.a	n.a	1.04 ^a
<i>Staphylococcus aureus</i> DSM 346	n.a	n.a	n.a	0.42 ^a
<i>Mycobacterium smegmatis</i> ATCC 700084	n.a	n.a	n.a	0.52 ^b
Gram negative bacteria				
<i>Escherichia coli</i> DSM 498	n.a	n.a	n.a	3.33 ^a
<i>Pseudomonas aeruginosa</i> PA 14	n.a	n.a	n.a	0.52 ^c
<i>Chromobacterium violaceum</i> DSM 30191	n.a	n.a	n.a	1.67 ^a
Yeasts				
<i>Candida albicans</i> DSM 1665	n.a	n.a	n.a	33.33 ^d
<i>Rhodotorula glutinis</i> DSM 10134	n.a	n.a	n.a	2.08 ^d
<i>Pichia anomala</i> DSM 6766	n.a	n.a	n.a	8.33 ^d
<i>Schizosaccharomyces pombe</i> DSM 70572	n.a	n.a	n.a	8.33 ^d
<i>Candida tenuis</i> MUCL 29892	n.a	n.a	n.a	0.78 ^d
Filamentous fungi				
<i>Mucor hiemalis</i> DSM 2656	33.33	n.a	n.a	16.67 ^d
<i>Mucor plumbeus</i> MUCL 49355	n.a	n.a	n.a	3.12 ^d

^a Oxytetracycline hydrochloride (1 mg/mL), ^b Kanamycin (10mg/mL), ^c Gentamycin (10 mg/mL), ^d Nystatin (1 mg/mL), n.a: no activity.

3.1.2.3. Dual culture

The evaluation of antagonistic effect between fungal endophyte and the selected phytopathogen demonstrated the potential ability of the candidate fungus to inhibit the radial growth on YMG agar cultures of *S. sclerotiorum* (30%) (Figure 37).



Figure 37: Mono and co-cultures of *P. similis* and *S. sclerotiorum* on YMG agar medium
 a. Monoculture of *Preussia similis* STMA 16219, b. Co-culture of *Preussia similis* STMA 16219 with *S. sclerotiorum* results in inhibition of the phytopathogen, c. Monoculture of *S. sclerotiorum*.

The comparison between the HPLC chromatograms derived from both individual axenic and co-culture of *P. similis* STMA 16219 (Figure 38) showed an apparent increase in sterigmatocystin (**9**) and decrease in secoterigmatocystin (**8**), while, no new metabolites are detected in HPLC profile of the co-culture with the phytopathogen.

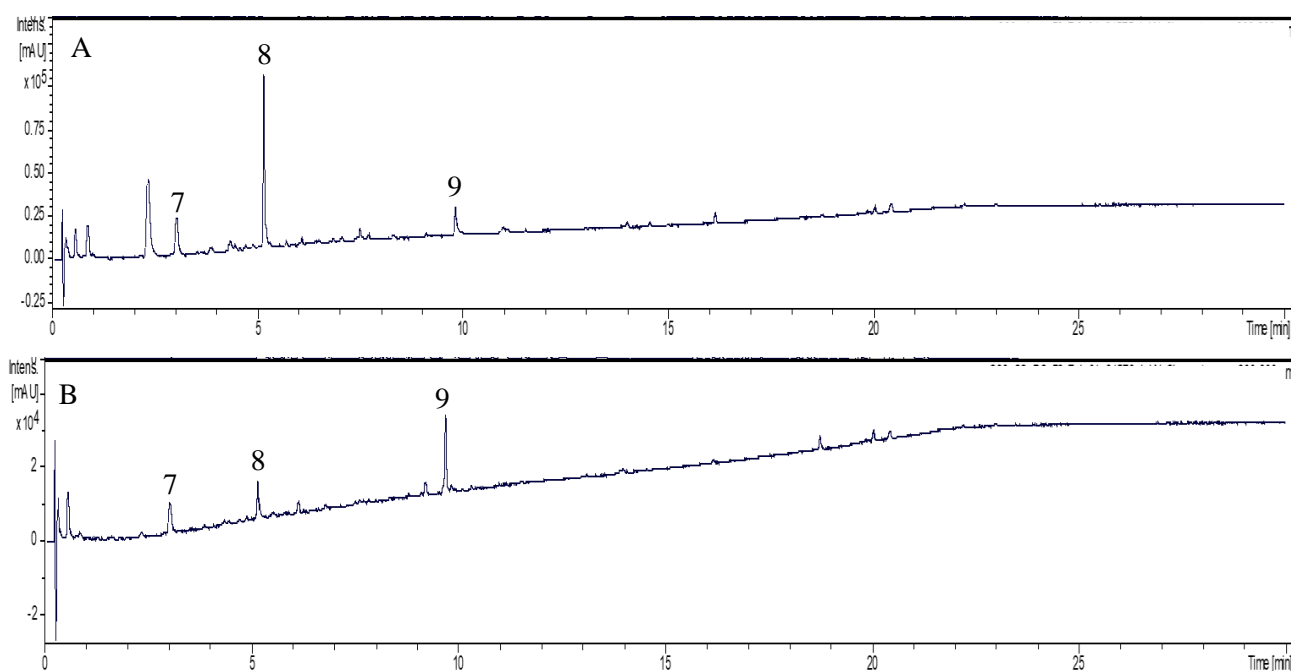


Figure 38: HPLC chromatograms of individual axenic and co-culture of *Preussia similis* STMA 16219
 A. Axenic culture of *Preussia similis* STMA 16219, B. Co-culture of *Preussia similis* STMA 16219 and *S. sclerotiorum*

3.1.3. Compounds isolated from *Preussia similis* DSM 32328

3.1.3.1. Fermentation and metabolites isolation

In both YM and Q6/2 liquid media, *Preussia similis* DSM 32328 consistently produced identical secondary metabolites. The compounds are present in the mycelium as well as in the culture filtrate of the fermentation broth. They can be extracted either from the mycelia or from the supernatant. Consequently, four known cytochalasins were isolated from the culture of *P. similis* DSM 32328: cytochalasin B (**10**), deoxaphomin (**11**), cytochalasin Z2 (**12**) and cytochalasin F (**13**). The chemical structures of cytochalasins are shown in figure 39. Cytochalasin B is the main compound, followed by deoxaphomin, while cytochalasins F and Z2 were minor metabolites of *P. similis* DSM 32328 as shown in the same HPLC profile of both mycelial and supernatant crude extracts (Figure 40). Recently, Cytochalasins B and F were reported to be produced by some strains of *P. intermedia*, *P. minima* and *P. australis* (Gonzalez-Menendez *et al.*, 2017). Our study reports for the first time the isolation of cytochalasins from *P. similis*. The LC-MS data of the four known cytochalasins and their physical properties are shown in table 14.

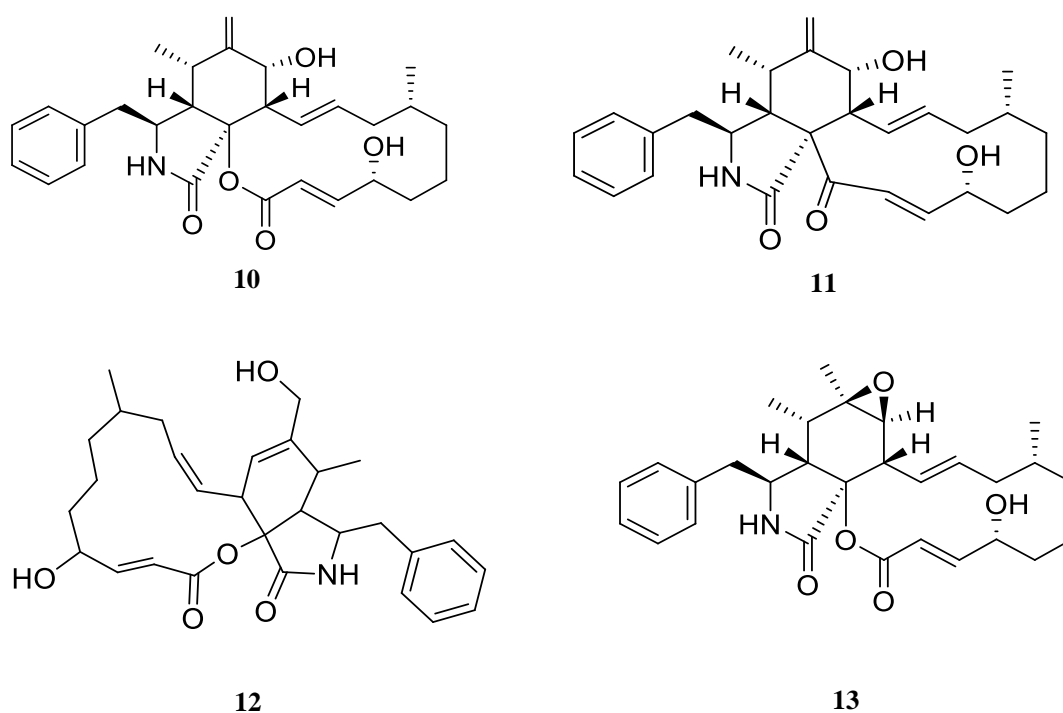
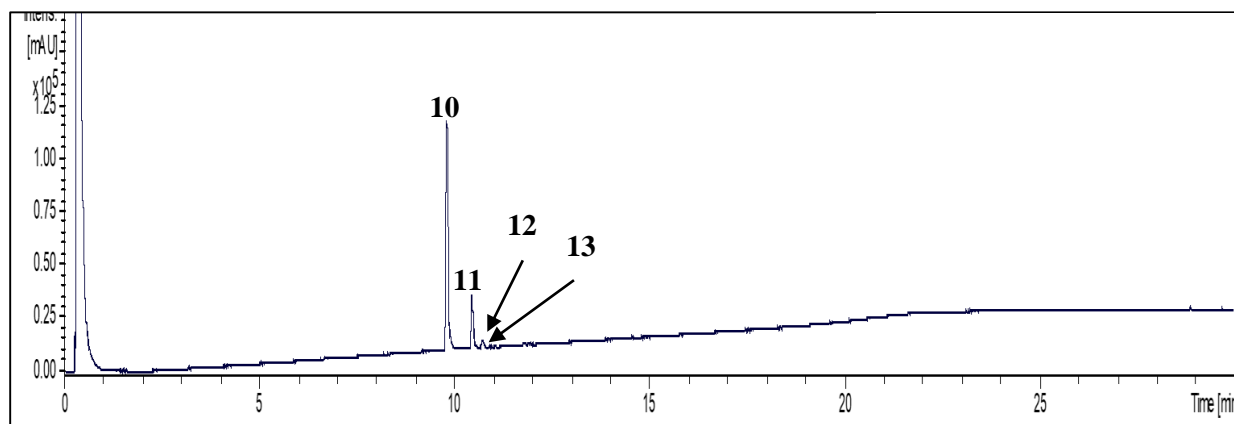


Figure 39: Chemical structures of the four cytochalasins (**10-13**) isolated from *Preussia similis* DSM 32328

Table 14: LC-MS data of the four cytochalasins and their physical properties

N°	Compounds	Molecular formula	LC-MS (m/z)	Physical properties
10	Cytochalasin B	C ₂₉ H ₃₇ NO ₅	479	White crystals
11	Deoxaphomin	C ₂₉ H ₃₇ NO ₄	463	White crystals
12	Cytochalasin Z2	C ₂₉ H ₃₇ NO ₅	479	White crystals
13	Cytochalasin F	C ₂₉ H ₃₇ NO ₅	479	White crystals

**Figure 40:** HPLC chromatogram of both mycelial and supernatant crude extracts derived from liquid culture in Q6/2 medium of *Preussia similis* DSM 32328.

3.1.3.1. Biological activity

Cytochalasin B and deoxaphomin were tested for their biological activity while cytochalasins Z2 and F were not tested due to limited quantities. Thus, cytochalasin B shows only weak inhibition of the bacterium *Micrococcus luteus*, whereas the other test bacteria were not affected. Furthermore, Cytochalasin B showed no antifungal activity, neither against yeasts nor against filamentous fungi. Deoxaphomin was devoided of any antimicrobial activity (Table 15). Furthermore, *in vitro*, cytotoxicity assays of metabolites extracted from *P. similis* DSM 32328 against the cell lines revealed that cytochalasin B and deoxaphomin exhibited cytotoxic activities on cancer cell lines and normal cell lines (Table 16). Both compounds cause nucleus fragmentation in the range of 0.45 – 1.37 µg/mL (Figure 41). It is obvious that deoxaphomin is more cytotoxic than cytochalasin B.

Table 15: MIC [$\mu\text{g/mL}$] values of cytochalasin B and deoxaphomin against the tested microorganisms.

Test organism	MIC [$\mu\text{g/mL}$]		
	10	11	Reference
Gram positive bacteria			
<i>Micrococcus luteus</i> DSM 1790	200	n.a	0.83 ^a
<i>Bacillus subtilis</i> DSM 10	n.a	n.a	16.67 ^a
<i>Staphylococcus aureus</i> DSM 346	n.a	n.a	0.42 ^a
<i>Mycobacterium smegmatis</i> ATCC 700084	n.a	n.a	4.17 ^a
Gram negative bacteria			
<i>Escherichia coli</i> DSM 498	n.a	n.a	3.33 ^b
<i>Pseudomonas aeruginosa</i> PA 14	n.a	n.a	2.08 ^c
<i>Chromobacterium violaceum</i> DSM 30191	n.a	n.a	8.33 ^a
Yeasts			
<i>Candida albicans</i> DSM 1665	n.a	n.a	8.33 ^d
<i>Rhodotorula glutinis</i> DSM 10134	n.a	n.a	2.08 ^d
<i>Pichia anomala</i> DSM 6766	n.a	n.a	8.33 ^d
<i>Schizosaccharomyces pombe</i> DSM 70572	n.a	n.a	4.17 ^d
<i>Candida tenuis</i> MUCL 29892	n.a	n.a	0.52 ^d
Filamentous fungi			
<i>Mucor hiemalis</i> DSM 2656	n.a	n.a	16.67 ^d
<i>Mucor plumbeus</i> MUCL 49355	n.a	n.a	2.08 ^d

^a Oxytetracycline hydrochloride (1 mg/mL), ^b Kanamycin (10mg/mL), ^c Gentamycin (10 mg/mL), ^d Nystatin (1 mg/mL), n.a: no activity

Table 16: Cytotoxic effect (IC₅₀) of cytochalasin B and deoxaphomin against different normal and cancer cell lines.

Cell line	IC ₅₀ [$\mu\text{g/mL}$]		
	10	11	Reference
Mouse fibroblasts L929	0.6	0.28	9×10^{-4}
HeLa cells KB3.1	0.6	0.081	3.1×10^{-5}
Squamous carcinoma A431	2.2	0.22	3.7×10^{-5}
Human lung carcinoma A549	1	0.23	8×10^{-5}
Ovarian carcinoma SKOV-3	n.t.	0.26	1.2×10^{-5}
Human prostate cancer PC-3	0.29	0.38	1.2×10^{-4}
Human breast adenocarcinoma MCF-7	0.59	0.32	8×10^{-5}
Human osteosarcoma U2OS	0.27	0.095	5.3×10^{-5}

Reference: Epothilone B.

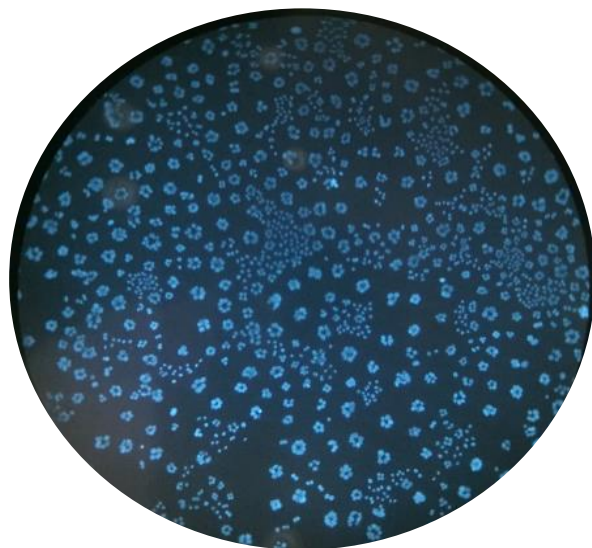


Figure 41: Microscopic view of fragmented nuclei of cytochalasin B-treated L929 in MTT assay

Cytochalasin B is known to have negative effect on cytoskeleton networks. It has the ability to diffuse through the cell membranes and bind to the barbed ends of actin filaments. The association of the molecules of cytochalasin B to the actin filaments inhibit both their polymerization and depolymerisation, which have a main affect as disrupter of cytoplasm cleavage and consequently cell division blockage (MacLean-Fletcher and Pollard, 1980). Cytochalasins have contributed to better understanding of actin polymerization mechanism. In order to confirm this effect, U2OS cells were treated with cytochalasin B with $1\mu\text{g/mL}$ and $5\mu\text{g/mL}$ and incubated for 24 hours. Substantially, phalloïdin and DAPI staining were performed to visualized F actin and DNA respectively. The results shown in figure 42 indicated that the substance is clearly affecting actin dynamics. This starts already at low concentration ($1\mu\text{g/mL}$) where all dynamic elements (lamellipodia/filopodia) are lost and only stress fibers are left over in addition to these newly occurring dots. Moreover, at the same concentration, all cells are binucleate indicating that also cytokinesis (cell division) but not nuclear division is affected. Indeed, the cytokinesis is abolished because it requires actin dynamics.

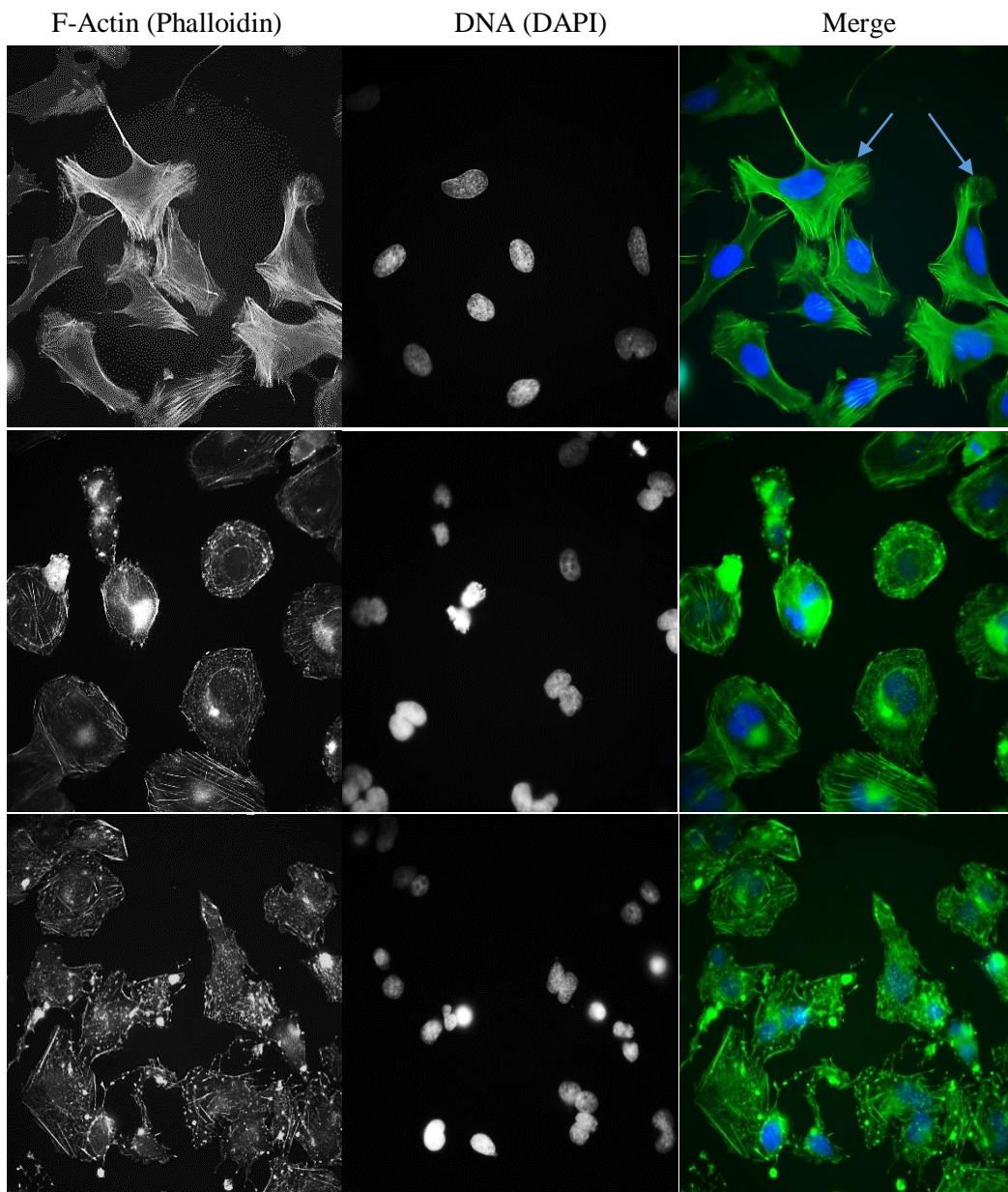


Figure 42: Effect of cytochalasin B on actin cytoskeleton of U2OS cells at concentrations of 1 µg/mL and 5 µg/mL for 24 hours. A. DMSO treated U2OS cells (negative control), the white arrows indicated lamellipodia. B. U2OS cells treated with 1 µg/mL of cytochalasin B for 24 hours, C. U2OS cells treated with 5 µg/mL of cytochalasin B for 24 hours

In order to determine the effect of cytochalasins on seedling growth, phytotoxic activity were tested toward *L. sativum* and *S. italica* at 100 µg paper disk. At this concentration, seeds of *L. sativum* can germinate in medium containing cytochalasin B compared to positive control sample. However, stem elongation was markedly affected compared to the negative control and MeOH (Figure 43 A). In contrast, *S. italica* germination and growth were not inhibited by cytochalasin B at 100 µg/filter disk (Figure 43 B). Cytochalasin B was not toxic compared to results reported earlier on monocotyledon

seeds, in which a 10^{-4} M solution decreased root length of wheat seedlings of the control (Evidente *et al.*, 2002) and 5 days coleoptile and radicle length at 10^{-3} and 10^{-4} M relative to the control (Masi *et al.*, 2014).

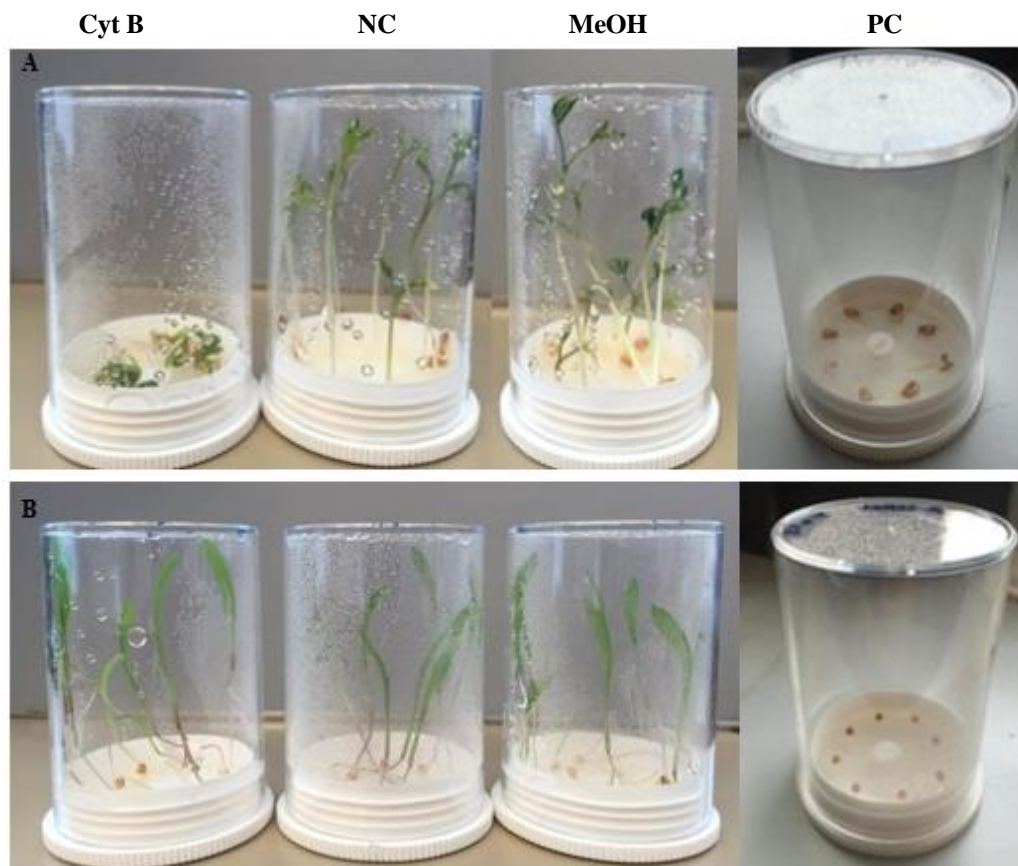


Figure 43: Phytotoxic test results of cytochalasin B on seedling growth.

A. Effect of cytochalasin B on stem elongation of *L. sativum* at 100 μ g/filter disk. B. No phytotoxic activity of cytochalasin B toward *S. italica* at 100 μ g/filter disk. Cyt B: Cytochalasin B, NC: negative control, MeOH: Methanol, PC: positive control.

In contrast, deoxaphomin showed no effect on both seedlings at a concentration of 100 μ g/filter disk. Furthermore, both cytochalasin B and deoxaphomin were deprived of any nematicidal activity against *C. elegans*.

3.1.3.2. Dual culture

The radial growth of *S. sclerotiorum* was inhibited by *P. similis* DSM 32328 at 41.33% (Figure 44). In the comparative analysis between EtOAc extracts of the axenic monoculture for *P. similis* DSM 32328 and its co-cultivation with *S. sclerotiorum*, the HPLC profiling of both cultures was

exactly the same and no stimulatory molecules has been detected in presence of the antagonist (Figure 45).



Figure 44: Mono and co-cultures of *Preussia similis* DSM 32328 and *S. sclerotiorum* on YMG agar medium
 a. Monoculture of *P. similis* DSM 32328, b. Co-culture of *P. similis* DSM 32328 with *S. sclerotiorum* results in inhibition of the phytopathogen, c. Monoculture of *S. sclerotiorum*.

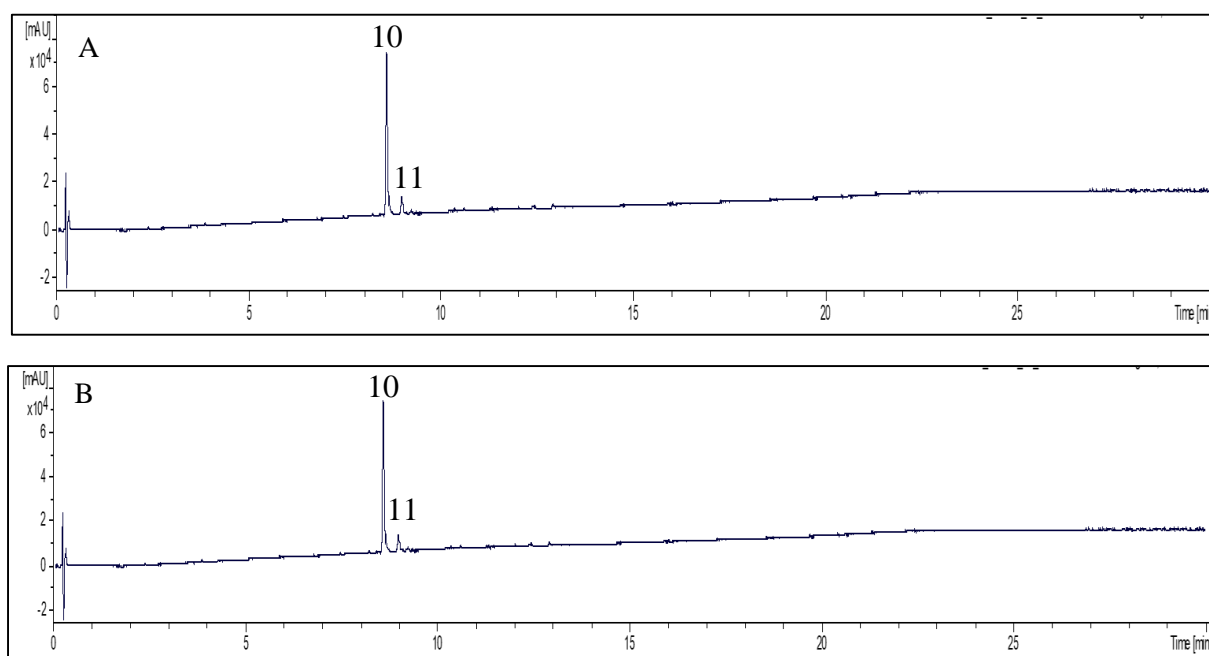


Figure 45: HPLC chromatograms of individual axenic and co-culture of *P. similis* DSM 32328
 A. Axenic culture of *P. similis* DSM 32328, B. Co-culture of *P. similis* DSM 32328 and *S. sclerotiorum*.

3.1.4. Chemotaxonomy of *Preussia similis*

In the recent study published by Gonzalez-Menendez et al., 2017, eleven chemotypes have been identified based on the combined data of morphological and phylogenetical study and analysis of liquid chromatography/high resolution mass spectrometry spectra recorded from thirty-two isolates of *Preussia* and their sixteen secondary metabolites. The latter, were not found to be produced by

Preussia similis and therefore, this species was not attributed to any of the 16 inferred chemotypes. Additionally, the thirty two isolates of *Preussia* were shown to have variable HPLC profiles, but never contained the compounds isolated in our study. In order to study the HPLC profiling of the available reference strain of *P. similis*, the isolate CBC 80473 was obtained from public collections CBS and was subcultured in three screening media following the same protocol as described above. Surprisingly, the isolate *P. similis* CBS 80473 was found to produce cytochalasins with identical HPLC profiles to *Preussia similis* DSM 32328. Taken together, the thirteen compounds reported in our study in which seven are new, and HPLC profile of the reference strain ordered *P. similis* CBS 80473 can help in the update of the chemotaxonomy of *Preussia* species. These chemical features might be considered as good chemotaxonomic markers of the genus *Preussia*. Meanwhile, we suggest that *Preussia similis* strains could be clustered at least in 4 chemotypes (Table 17).

Table 17: Suggested chemotypes for *P. similis* based on compounds isolated from four strains in the current study

Isolate	Molecular formula	Name		Chemotype
- <i>Preussia similis</i> DSM 32328	C ₂₉ H ₃₇ NO ₅	Cytochalasin B	Known	1
- <i>Preussia similis</i> CBS 80773	C ₂₉ H ₃₇ NO ₄	Deoxaphomin	Known	
	C ₂₉ H ₃₇ NO ₅	Cytochalasin Z2	Known	
	C ₂₉ H ₃₇ NO ₅	Cytochalasin F	Known	
<i>Preussia similis</i> DSM 104666	C ₂₅ H ₃₄ O ₄	Preussilide A	New	2
	C ₂₅ H ₃₄ O ₄	Preussilide B	New	
	C ₂₅ H ₃₂ O ₄	Preussilide C	New	
	C ₂₅ H ₃₂ O ₄	Preussilide D	New	
	C ₂₆ H ₃₆ O ₄	Preussilide E	New	
	C ₂₆ H ₃₄ O ₄	Preussilide F	New	
<i>Preussia similis</i> STMA 16219	C ₁₈ H ₁₂ O ₆	Sterigmatocystin	Known	3
	C ₁₈ H ₁₈ O ₈	Secosterigmatocystin	Known	
	C ₁₄ H ₁₀ N ₂ O ₄	Dimer of 2-aminobenzoic acid moities	New	4

3.2. Compounds isolated from *Dendrothyrium variisporum*

3.2.1. Fermentation and metabolites isolation

Since *Dendrothyrium* is a newly described species, the fungal strain *Dendrothyrium variisporum* seemed worth considering for closer inspection, because up to now, the *Dendrothyrium* species have never been tapped by secondary metabolite screenings. Indeed, this is the first report describing the secondary metabolite profiles of this genus. Twelve secondary metabolites (**14-25**) were isolated from the respective fungus in which five are new. *Dendrothyrium variisporum* was shown to produce in flasks mainly two known polyketides: massarilactone D (**14**) and as well as massarilactone H (**15**), and two new minor furanone derivatives, for which the corresponding trivial names are proposed: (5*S*)-cis-gregatin: (5*S*) cis-gregatin B (**16**) and graminin D (**17**). However, HPLC-MS analysis of the crude extracts revealed the presence of numerous minor constituents that could not be isolated in sufficient quantities to allow for their complete structure elucidation. A scale-up of production in a 10 L bioreactor for maximum production of bioactive secondary metabolites was performed. The separation of the resulted extracts (from supernatant and mycelia) yielded massarilactone D and eight further metabolites. Among those were three new anthranilic acid derivatives (**18-20**) [2-phenylethyl-3-hydroxyanthranilate (**18**), phenylmethyl anthranilate (**19**) and 3-hydroxy-3-methylbutyl anthranilate (**20**)], two known anthranilic acid analogues (**21** and **22**): [ethyl anthranilate (**21**) and 2-phenylethyl anthranilate (**22**)] and and three cyclopeptides (**23-25**) [cyclo-(L-pro-L-isoleu) (**23**), cyclo-(L-pro-L-leu) (**24**) and cyclo-(L-pro-L-phe) (**25**)].

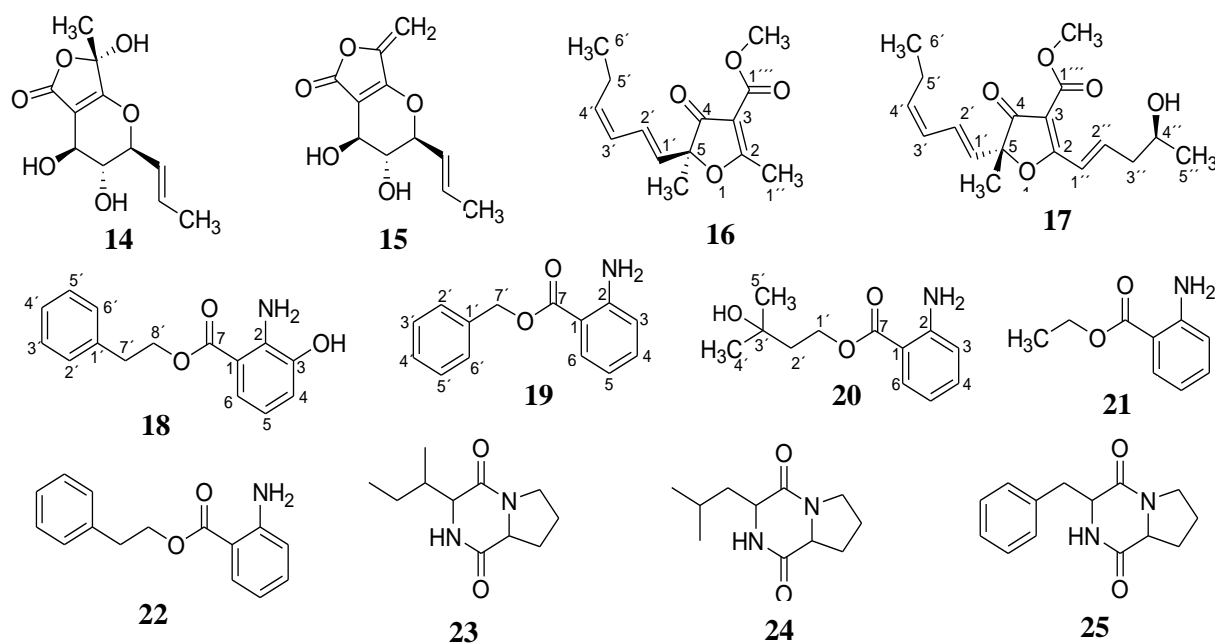


Figure 46: Chemical structures of compounds (**14-25**) isolated from *Dendrothyrium variisporum*.

The chemical structures of the twelve isolated metabolites are shown in figure 46. The metabolite profiles of the obtained crude extracts are shown in figure 47. The details of structure elucidation are illustrated in Teponno *et al.* (2017) (paper II). Also, the LC-MS data of these compounds and their physical properties are indicated in table 18.

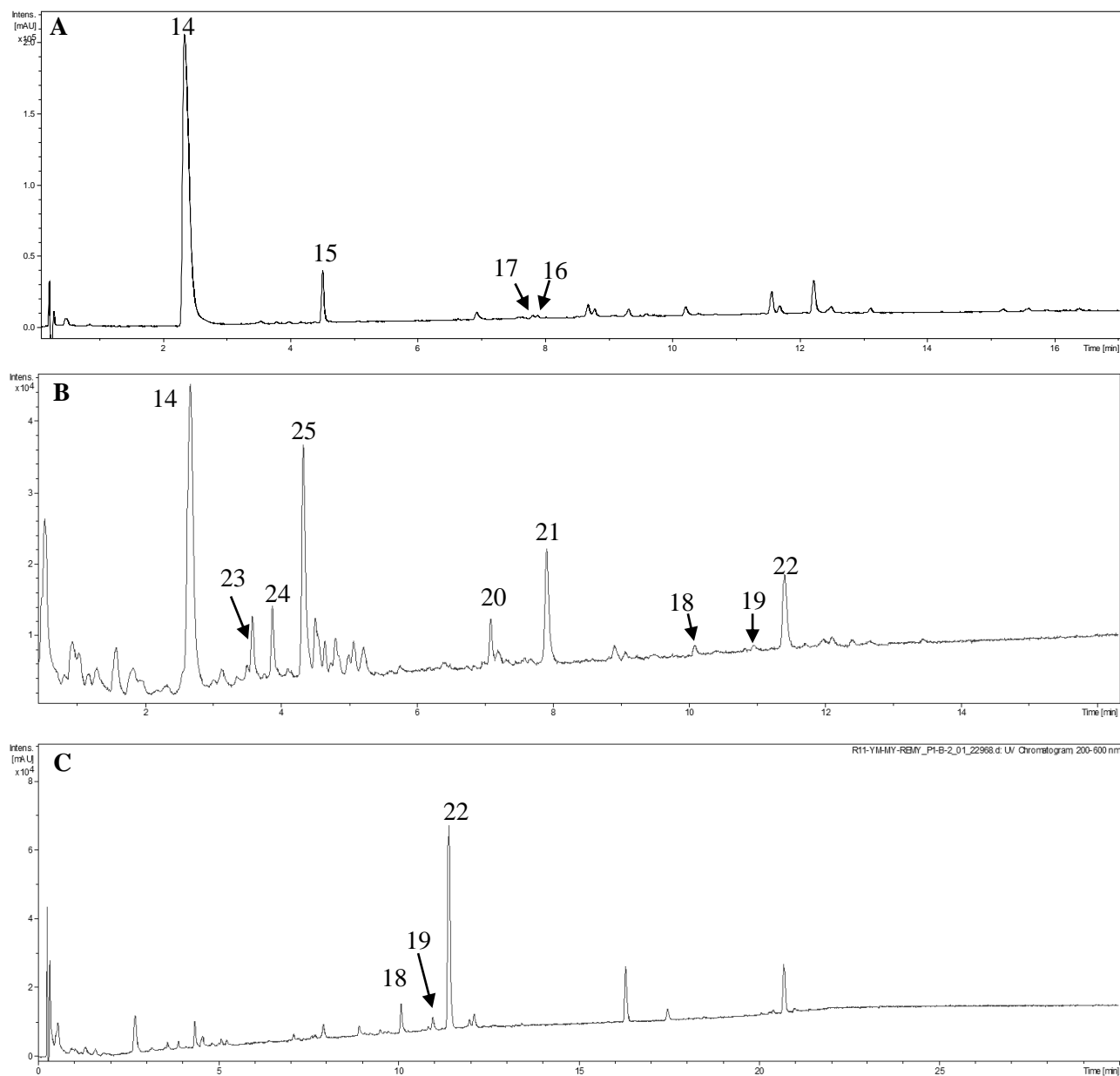


Figure 47. HPLC chromatograms of mycelial and supernatant crude extracts derived from YMG liquid culture of *Dendrothyrium variisporum* in shake flasks and bioreactor.
A. HPLC chromatogram of supernatant extract from YMG liquid culture in shake flasks.
B. HPLC chromatogram of supernatant extract from YMG liquid culture from bioreactor.
C. HPLC chromatogram of mycelial extract from YMG liquid culture from bioreactor.

Table 18: LC-MS data of the twelve compounds and their physical properties

N°	Compound	Molecular formula	LC-MS (m/z)	Physical properties
14	Massarilactone D	C ₁₁ H ₁₄ O ₆	242.04	Yellow solid
15	Massarilactone H	C ₁₁ H ₁₂ O ₅	224	Brown gum
16	(5S) cis-gregatin B	C ₁₄ H ₁₈ O ₄	250	Colorless oil
17	Graminin D	C ₁₈ H ₂₄ O ₅	320	Colorless oil
18	2-phenylethyl 3-hydroxyanthranilate	C ₁₅ H ₁₅ NO ₃	257	Brown gum
19	Phenylmethyl anthranilate	C ₁₄ H ₁₃ NO ₂	227	Brown gum
20	3-hydroxy-3-methylbutyl anthranilate	C ₁₂ H ₁₇ NO ₃	223	Brown gum
21	Ethyl anthranilate	C ₉ H ₁₁ NO ₂	165	Colorless oil
22	2-phenylethyl anthranilate	C ₁₅ H ₁₅ NO ₂	241	Colorless oil
23	Cyclo (L-pro-L-isoleu)	C ₁₁ H ₁₈ N ₂ O ₂	210	Colorless oil
24	Cyclo-(L-pro-L-leu)	C ₁₁ H ₁₈ N ₂ O ₂	210	Colorless oil
25	Cyclo-(L-pro-L-phe)	C ₁₄ H ₁₆ N ₂ O ₂	244	Colorless oil

Massarilactone D (**14**) and massarilactone H (**15**) are known compounds isolated from an endophytic *Coniothyrium* sp., which was isolated from the halotolerant plant *Carpobrotus edulis* (Kock *et al.*, 2007) and from the culture broth of the marine-derived fungus *Phoma herbarum* (Zhang *et al.*, 2012) respectively. Massarilactones are known secondary metabolites from *Coniothyrium* spp. (Coniothyriaceae, Pleosporales) and their production by *Dendrothyrium* confirms that the respective fungus is a *Coniothyrium*-like fungus, and massarilactones could be a good chemotaxonomic markers for these two aforementioned closely related genera.

The (5S) cis-gregatin B (**16**) and graminin D (**17**) are new furancarboxylic acid derivatives, a structural class of natural oxygenated heterocycles that have been reported only from fungi of the genera *Aspergillus*, *Cephalosporium* (*Acremonium*), *Paraconiothyrium*, *Penicillium*, and *Pulvinula* (Almeida *et al.*, 2014; Wijeratna *et al.*, 2015).

The isolation of phenylmethyl anthranilate (**19**) was previously reported as a synthetic compound with a fish anesthetic effect (Hirata *et al.*, 1970), this is the first report on its isolation from the natural source to the best of our knowledge.

The metabolite ethyl anthranilate (**21**) was previously detected by gas chromatograph-mass spectrometry (GC-MS) as one of the aroma-active compounds in Pinot Noir wines (Fang and Qian,

2006) , while 2-phenylethyl anthranilate (**22**) is a fragrance ingredient present in the essential oils from the leaves of *Cinnamomum zeylanicum* blume collected in India (Raina *et al.*, 2001). As far as we know, the ^1H -and ^{13}C -NMR data of ethyl anthranilate (**21**) and 2-phenylethyl anthranilate (**22**) are herein reported for the first time and their corresponding spectra are shown in appendix F.

The compounds (**23-25**) were known cyclopeptides: cyclo (L-pro-L-isoleu) (**23**) (Ren *et al.*, 2010), cyclo-(L-pro-L-leu) (**24**) (Ren *et al.*, 2010; Sansinenea *et al.*, 2016) and cyclo-(L-pro-L-phe) (**25**) (Sansinenea *et al.*, 2016). Cyclo-(L-pro-L-isoleu) (**23**) was isolated from the marine sponge *Dysidea* sp., cyclo-(L-pro-L-leu) (**24**) was isolated from the marine sponge *Dysidea* sp. as well as from the endophytic bacterium *Bacillus thuringiensis* isolated the inner tissues of cotton plants. From the latter bacterium, cyclo-(L-pro-L-phe) (**25**) was also isolated.

3.2.2. Biological activity

Since the crude extracts showed prominent antimicrobial activity (150 $\mu\text{g}/\text{mL}$ against *B. subtilis* and 37.5 $\mu\text{g}/\text{mL}$ against *M. plumbeus*), the isolated metabolites were screened against various bacteria and fungi. The cis-gregatin B (**16**) was not test due to limited amount. The MIC values showed that only the new 2-phenylethyl-3-hydroxyanthranilate (**18**) and 2-phenylethyl anthranilate **22** were active whereas the remaining compounds were inactive against the organisms tested (Table 19). 2-phenylethyl-3-hydroxyanthranilate (**18**) showed the strongest antibacterial activity against *Bacillus subtilis* and *Micrococcus luteus* with MIC values of 8.33 and 16.66 $\mu\text{g}/\text{mL}$, respectively and anti-yeast activity against *Rhodotorula glutinis* with MIC value 66.67 $\mu\text{g}/\text{mL}$, while the MIC value of 2-phenylethyl anthranilate (**22**) against *Mucor hiemalis* (16.66 $\mu\text{g}/\text{mL}$) was the same as that of nystatin used as positive control. The two active metabolites are anthranilic acid derivatives with a phenylethyl core. Since phenylmethyl anthranilate **19** which contains a phenylmethyl group instead of a phenylethyl residue was not active, it could be concluded that the phenylethyl moiety in compounds **18** and **22** is essential for their antimicrobial activity. The biological activities of ethyl anthranilate (**21**) and 2-phenylethyl anthranilate **22** were not tested previously. Massarilactone H displayed moderate neuraminidase inhibitory activity (Zhang *et al.*, 2012). As shown in the table 18, massarilactone D is devoided of any antimicrobial activity. This result is in the lines of earlier literature (Kock *et al.*, 2007) that found that massarilactone D was inactive in tests for biological activity against the Gram positive bacterium *Bacillus megaterium*, the fungus *Microbotryum violaceum* and the green alga *Chlorella fusca*. Moreover, the two known diketopiperazines Cyclo-(L-pro-L-isoleu) and cyclo-(L-pro-L-leu) were inactive against both bacteria and fungi as reported

previously (Ren *et al.*, 2010; Sansinenea *et al.*, 2016). Sansinenea *et al.* (2016) have reported that cyclo-(L-pro-L-phe) showed a slight inhibition in disk diffusion assay against *Fusarium oxysporum* and *Penicillium* sp.

Table 19: MIC [$\mu\text{g/mL}$] values of compounds **14**, **15**, **17-25** against the tested microorganisms

Test organism	MIC [$\mu\text{g/mL}$]											Ref.
	14	15	17	18	19	20	21	22	23	24	25	
Gram positive bacteria												
<i>Micrococcus luteus</i> DSM 1790	n.a	n.a	n.a.	16.66	n.a.	n.a	n.a	n.a	n.a	n.a	n.a	0.4 ^a
<i>Bacillus subtilis</i> DSM 10	n.a	n.a	n.a	8.33	n.a	n.a	n.a	66.67	n.a	n.a	n.a	4.16 ^a
<i>Staphylococcus aureus</i> DSM 346	n.a	n.a	n.a.	66.67	n.a	n.a	n.a	66.67	n.a	n.a	n.a	0.1 ^a
<i>Mycobacterium smegmatis</i> ATCC 700084	n.a	n.a	n.a	n.a	n.a	n.a	n.a	n.a	n.a	n.a	n.a	2.08 ^b
Gram negative bacteria												
<i>Escherichia coli</i> DSM 498	n.a	n.a	n.a	n.a	n.a.	n.a	n.a	n.a	n.a.	n.a	n.a	3.33 ^a
<i>Pseudomonas aeruginosa</i> PA 14	n.a	n.a	n.a	n.a	n.a	n.a	n.a	n.a	n.a	n.a	n.a	0.52 ^c
<i>Chromobacterium violaceum</i> DSM 30191	n.a	n.a	n.a	n.a	n.a	n.a	n.a	n.a	n.a	n.a	n.a	0.4 ^a
Yeasts												
<i>Candida albicans</i> DSM 1665	n.a	n.a	n.a	n.a	n.a	n.a	n.a	n.a	n.a	n.a	n.a	16.66 ^d
<i>Rhodotorula glutinis</i> DSM 10134	n.a	n.a	n.a	66.67	n.a	n.a	n.a	n.a	n.a	n.a	n.a	2.08 ^d
<i>Pichia anomala</i> DSM 6766	n.a	n.a	n.a	n.a	n.a	n.a	n.a	n.a	n.a	n.a	n.a	8.33 ^d
<i>Schizosaccharomyces pombe</i> DSM 70572	n.a	n.a	n.a	n.a	n.a	n.a	n.a	n.a	n.a	n.a	n.a	8.33 ^d
Filamentous fungi												
<i>Mucor hiemalis</i> DSM 2656	n.a	n.a	n.a	33.33	n.a	n.a	n.a	n.a	16.66	n.a	n.a	16.66

Ref: references: ^a Oxytetracyclin (1 mg/mL), ^b Kanamycin (10 mg/mL), ^c Gentamycin (1 mg/mL), ^d Nystatin (1 mg/mL). n.a.: no activity.

Furthermore, the ability of the isolated compounds to inhibit the proliferation of two mammalian cell lines including HeLa cells KB3.1 and mouse fibroblasts L929 was examined. Only 2-phenylethyl anthranilate (**22**) showed moderate cytotoxic activity against HeLa cells KB3.1 with IC₅₀ value of 8.8 $\mu\text{g/mL}$ (Table 20). The cis-gregatin B (**16**) was not test due to limited amount.

Table 20: Cytotoxic effect (IC₅₀) of compounds **14**, **15**, **17-25** against two cancer cell lines.

Cell line	IC ₅₀ [$\mu\text{g/mL}$]											Ref
	14	15	17	18	19	20	21	22	23	24	25	
L929	>10 ³	>10 ³	19	n.t	>10 ³	>10 ³	>10 ³	n.t	>10 ³	>10 ³	>10 ³	1.4
KB3.1	>10 ³	>10 ³	18	18	>10 ³	>10 ³	>10 ³	8.8	>10 ³	>10 ³	>10 ³	0.052

Ref: reference (Epothilone B), n.t.: not tested.

3.3. Compounds isolated from *Chaetomium madrasense*

3.3.1. Fermentation and metabolites isolation

The fungus *Chaetomium madrasense* (*C. madrasense*) was cultured in liquid YM medium (3L). The purification of the mycelial extract yielded three known fungal metabolites: N-acetyltryptamin (**26**), xanthoquinodin A3 (**27**) and xanthoquinodin A1 (**28**). Xanthoquinodin A1 (**28**) was the main metabolite produced by *C. madrasense* as shown in LC-MS chromatogram of the mycelial crude extract (Figure 48), while xanthoquinodin A3 and N-acetyltryptamine were minor. The chemical structures of the three compounds are shown in figure 49. Also, the table 21 reports the LC-MS data of the purified compounds and their physical properties

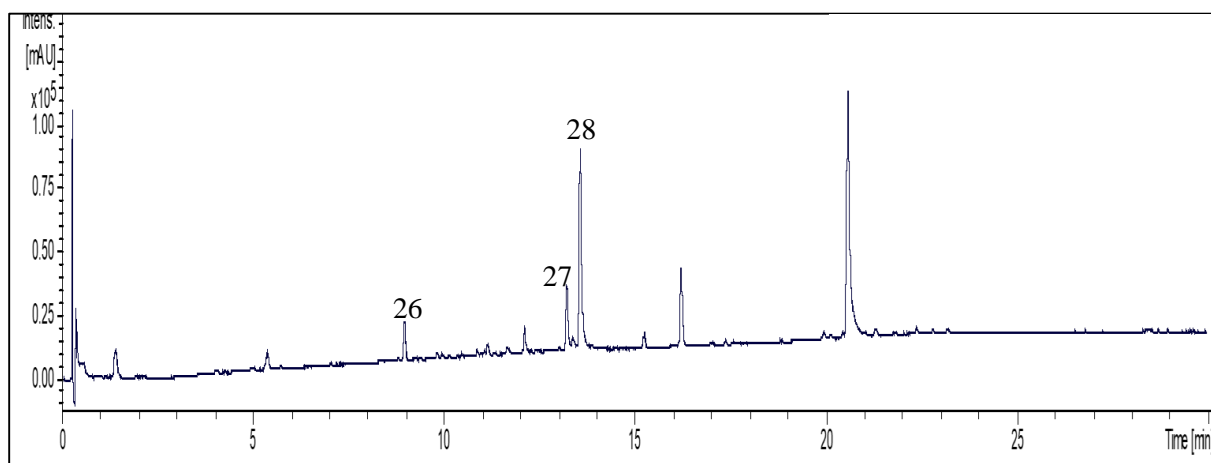


Figure 48: HPLC chromatogram of mycelial crude extract derived from YMG liquid culture of *Chaetomium madrasense*.

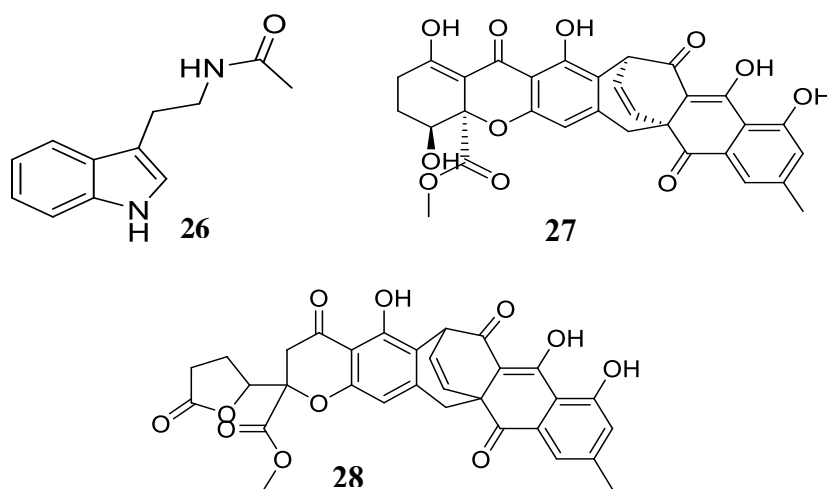


Figure 49: Chemical structures of the three known compounds (**26-28**) isolated from *C. madrasense*.

Table 21: LC-MS data of the three known compounds and their physical properties

N°	Compound	Molecular formula	LC-MS (m/z)	Physical properties
26	N-Acetyltryptamin	C ₁₂ H ₁₄ ON ₂	202.25	Yellow solid
27	Xanthoquinodin A3	C ₃₁ H ₂₄ O ₁₁	572.17	Yellow powder
28	Xanthoquinodin A1	C ₃₁ H ₂₄ O ₁₁	572.17	Yellow powder

3.3.2. Biological activity

Xanthoquinodin A1 (**28**) and A3 (**27**) were isolated for the first time from the cultured broth of the soil isolate *Humicola* sp. They were originally identified as anticoccidial compounds by Tabata *et al.* (1992) as well as having similar range of antibacterial activity at 1 mg/mL against Gram positive, Gram negative bacteria and Mycoplasma by using the paper disk method. Xanthoquinodins A1(**28**) and A3 (**27**), exhibited inhibition zone diameter of 12 and 11 mm against *Bacillus subtilis*, 8 and 9 mm against *Micrococcus luteus*, 9 and 9mm against *Staphylococcus aureus*, 8 and 8 mm against *Bacteroides fragilis* and 10 and 7 mm against the Mycoplasma *Acholeplasma laidlawli* respectively. However, in the current study, xanthoquinodin A1(**28**) and A3 (**27**) exhibited antibacterial activity against Gram positive bacteria in which xanthoquinodin A1 was more active than Xanthoquinodin A3 (Table 22) where the highest antibacterial activity was found against *B. subtilis* with MIC value 0.83 µg/mL, while MIC value of 8.33 µg/mL was recorded for A3.

In addition, xanthoquinodin A1 (**28**) was shown to have anti-yeast effect against *Pichia anomala* (66.67 µg/mL), while xanthoquinodin A3 (**27**) did not display any anti-yeast activity. The antifungal activity was recorded only against *Mucor hiemalis* for both xanthoquinodins with MIC value 66.67µg/mL.

Cytotoxicity of metabolites **26-28** against the murine mouse fibroblasts and HeLa cells were evaluated by the MTT method. The results (table 23) showed that the three compounds exhibited moderate to high cytotoxicity. In fact, xanthoquinodin A1 displayed significant cytotoxic activity with IC₅₀ of 2 and 0.2 µg/mL against mouse fibroblast and HeLa cells respectively. Both Xanthoquinodins did not show selective activity, this may explain their therapeutic use exemption until now.

N-acetyltryptamin (**26**) is a known indole alkaloid, which is widely distributed in terrestrial and marine organisms. It has been isolated from different species of plants, e.g. the leaves of *Prosopis nigra* (Liguminosae), from myxobacteria (Bettina *et al.*, 1996) as well as from fungi, e.g. *Penicillium chrysogenum* and *Penicillium expansum* (BenAmeur *et al.*, 2009), *Fusarium incarnatum* (Zafar Alam

et al., 2010) and *Aspergillus fumigatus* (Shi *et al.*, 2015). The current study reports for the first time the isolation of N-acetyltryptamin from the genus *Chaetomium*. This metabolite often carries biological and pharmacological activities. However, as shown in table 22, the N-acetyltryptamin (**26**) did not exhibit any antimicrobial activity while its cytotoxic effect was high against HeLa cells with IC₅₀ of 1 µg/mL (table 23).

Furthermore, the phytotoxic and anti nematocidal activity of the three compounds (**26-28**) were also tested. No activity of both assays was recorded for the three compounds.

Table 22: MIC [µg/mL] values of compounds **26-28**.

Test organism	MIC [µg/mL]			
	26	27	28	Reference
Gram positive bacteria				
<i>Micrococcus luteus</i> DSM 1790	n.a	8.33	n.a	0.83 ^a
<i>Bacillus subtilis</i> DSM 10	n.a	0.83	8.33	16.67 ^a
<i>Staphylococcus aureus</i> DSM 346	n.a	4.16	16.66	0.42 ^a
<i>Mycobacterium smegmatis</i> ATCC 700084	n.a	n.a	n.a	4.17 ^a
Gram negative bacteria				
<i>Escherichia coli</i> DSM 498	n.a	n.a	n.a	3.33 ^b
<i>Pseudomonas aeruginosa</i> PA 14	n.a	n.a	n.a	2.08 ^c
<i>Chromobacterium violaceum</i> DSM 30191	n.a	n.a	n.a	8.33 ^a
Yeasts				
<i>Candida albicans</i> DSM 1665	n.a.	n.a	n.a	8.33 ^d
<i>Rhodotorula glutinis</i> DSM 10134	n.a	n.a	n.a	2.08 ^d
<i>Pichia anomala</i> DSM 6766	n.a	66.67	n.a	8.33 ^d
<i>Schizosaccharomyces pombe</i> DSM 70572	n.a	n.a	n.a	4.17 ^d
<i>Candida tenuis</i> MUCL 29892	n.a	n.a	n.a	0.52 ^d
Filamentous fungi				
<i>Mucor hiemalis</i> DSM 2656	n.a	66.67	66.67	16.67 ^d
<i>Mucor plumbeus</i> MUCL 49355	n.a	n.a	n.a	2.08 ^d

^a Oxytetracycline hydrochloride (1 mg/mL), ^b Kanamycine (10mg/mL), ^c Gentamycine (10 mg/mL), ^d Nystatin (1 mg/mL), n.a, no activity.

Table 23: Cytotoxic effect (IC₅₀) of compounds **26-28** against two cancer cell lines.

Cell line	IC ₅₀ [μg/mL]			
	26	27	28	Reference
L929	3.6	18	2	9×10^{-4}
KB3.1	1	15	0.2	3.1×10^{-5}

Reference: Epothilone B.

Conclusion and perspectives

The endophytic fungi are a hidden treasure house of chemically important compounds with potential biological activity. Many natural compounds have been isolated from various species of endophytes. However, the Algerian species remain untapped by chemical investigations. The present study demonstrates for the first time, the isolation of endophytic fungi from the roots of *G. alypum* collected in summer 2015. The plant inhabits a considerable diversity of fungal endophytes. A total of seventeen fungal strains were isolated. The fungal endophyte assemblage was relatively highly diverse and was distributed in three important fungal classes of Ascomycota: Eurotiomycetes, Dothideomycetes and Sordariomycetes representing nine genera: *Alternaria*, *Aspergillus*, *Chaetomium*, *Dendrothyrium*, *Diaporthe*, *Fusarium*, *Macrophomina*, *Penicillium* and *Preussia*.

A screening involved the fermentation in various culture media of eight endophytic isolates followed by extraction and test for eventual antimicrobial activity were performed. The results revealed that all crude extracts of the selected isolates showed inhibitory activity against at least one of the test strains used in the current study.

Furthermore, the endophytic fungi were studied for the discovery of new bioactive compounds. As expected, twelve new secondary metabolites among total of twenty-eight were isolated only from five isolates belonging to *Chaetomium madrasense*, *Dendrothyrium variisporum* and *Preussia similis*. The outcomes of the work confirm that fungal endophytes are a seemingly unlimited source of novel natural products that may help to achieve a better understanding to chemical diversity of an important group of non clavicipitaceous Ascomycota. Moreover, this could also give advance to the chemotaxonomy of the respective producer organisms. The three strains of the same species *Preussia similis* have been shown to generate chemical diversity and novelty in secreted secondary metabolites. In total thirteen compounds were identified in which seven were new including six new bicyclic polyketides (preusslides A-F), new dimer of 2-aminobenzoid acid moieties, four known cytochalasins and two xanthone derivatives. These chemical features might be considered as a good chemotaxonomic markers of the genus *Preussia* as its chemotaxonomy is poorly established. Also, five new compounds along with seven known were purified from cultures of *Dendrothyrium variisporum*. Since, no previous study has encrypted the chemical profile of the recently described genus *Dendrothyrium*, these compounds could give advance regarding its chemotaxonomy.

Moreover, the screening for secondary metabolites production of *Chaetomium madrasense* yielded three known compounds; xanthoquinodins A1, A3 and N-acetyl tryptamin reported for the first time as natural products of the respective fungus.

In the course of the study, all known and new compounds were tested for their biological activities. Meanwhile preussilides, in particular preussilides A and C, have shown promising antifungal and anticytostatic activities. The latter might be result of defect of an enzyme involving in cell division coordination. This prospective antiproliferative activity should be deeply studied in order to well-establish the specific targets. Also, preussilides should be subjected to *in vivo* tests to evaluate their efficacy and bioavailability by using animal models.

Interestingly, the new dimer of 2-aminobenzoid acid moieties exhibited selective antifungal activity against the filamentous fungus *Mucor hiemalis*. The promising antimycotic activity recorded by this compound as well as by preussilides A and C should be further investigated to elucidate its mode of action. These studies can reveal new targets which could lead to the development of new drugs to treat fungal infections in human, animals and plants.

Moreover, the anthranilic acid derivatives 2-phenylethyl-3-hydroxyanthranilate and 2-phenylethyl anthranilate isolated from *Dendrothyrium variisporum* exhibited antimicrobial activity. These new products could be a promising candidates for the discovery, development, and definition of the mechanisms of effective antibiotic alternatives.

The biological activities of the isolated compounds were extensively studied using different bioassay systems. Nevertheless, the bioassays accomplished are considered as preliminary screening. The compounds can show selective effects in other targets and they should be subjected to additional bioassays such as antiviral, anti-inflammatory, antibiofilm tests which could unveil a newly unexpected activities that can lead to the development of new wave of potential drugs.

During our investigation, many metabolites were in trace amounts. Optimization of growing conditions could increase the production of the desired compounds. Also, by using the co-cultivation approach with antagonists, we can enhance the yield of antimicrobial compounds that normally are not present in individual axenic culture or produced in small amounts. This may help to open doors towards the discovery of new natural antimicrobial substances derived from endophytic fungi.

Also, the whole genome of fungal isolates should be sequenced, in order to identify gene clusters associated with secondary metabolites and uncover their real genomic potential.

The finding of this study showed that endophytic fungi are talented in producing secondary metabolites and this source of interesting compounds would bring the endophytic fungi to light to be utilized in the field of medicine and agriculture.

References

- Abdel-Lateff A. 2008.** Chaetominedione, a new tyrosine kinase inhibitor isolated from the algicolous marine fungus *Chaetomium* sp. *Tetrahedron Letters* **49** (45): 6398–6400.
- Abdullah S., Al-saadoon K. J., Abdullah H. and Guarro J. 1999.** New and interesting coprophilous ascomycetes from Iraq. *Nova Hedwigia* **69** (1–2): 211–216.
- Ahmed S. I., and Cain R. F. 1972.** Revision of the Genera *Sporormia* and *Sporormiella*. *Canadian Journal of Botany* **50**: 419–477.
- Albach D. C., Meudt H. M., and Oxelman B. 2005.** Piecing together the ‘new’ Plantaginaceae. *American Journal of Botany* **92** (2): 297–315.
- Almeida C. El Aouad N., Jesús Martín, Pérez-Victoria I., González-Menéndez V., Platas G., De La Cruz M., Cândida Monteiro M., De Pedro N., Bills G. F., Vicente F., Genilloud O. and Reyes F. 2014.** Graminin B, a furanone from the fungus *Paraconiothyrium* sp. *Journal of Antibiotics* **67** (5):421–423.
- Aly, A. H., A. Debbab, and Proksch P. 2013.** Fungal endophytes - Secret producers of bioactive plant metabolites. *Pharmazie* **68** (7): 499–505.
- Andrade-Linares D. R., and Franken P. 2013.** Fungal endophytes in plant roots: taxonomy, colonization patterns, and functions.” In *Symbiotic Endophytes, Soil Biology*, edited by Aroca R. Springer, Berlin: 311–334.
- Anke H., and Zähner H. 1978.** Metabolic products of microorganisms. On the Antibiotic Activity of Cladosporin. *Archives of Microbiology* **116**: 253–257.
- Anke H. Bergendorff O. and Sterner O. 1989.** Assays of the biological activities of guaiane sesquiterpenoids isolated from the fruit bodies of edible *Lactarius* species.” *Food and Chemical Toxicology* **27** (6):393–397.
- Arenal F., Platas G. and Peláez F. 2004.** Variability of spore length in some species of the genus *Preussia*. *Mycotaxon* **89** (1): 137–151.
- Arenal F. Platas G., and Peláez F. 2005.** Two new *Preussia* species defined based on morphological and molecular evidence. *Fungal Diversity* **20**: 1–15.
- Arenal, F., G. Platas, and F. Peláez. 2007.** A New endophytic species of *Preussia* (Sporormiaceae) inferred from morphological observations and molecular phylogenetic analysis. *Fungal Diversity* **25**: 1–17.
- Arora J. and Ramawat K. G. 2017.** Chapter 1: An introduction to endophytes. In *Endophytes: Biology and Biotechnology*. Vol. 1, Springer . Switzerland: 1-23 pp.
- Asgari B., and Zare R. 2011.** The genus *Chaetomium* in Iran, a phylogenetic study including six new species. *Mycologia* **103** (4): 863–882.
- BenAmeur M., Shaaban R. K. A., Rebai I. K., Smaoui S., Bejar S. and Mellouli L. 2009.** Five naturally bioactive molecules including two rhamnopyranoside derivatives isolated from the *Streptomyces* sp. strain TN58. *Natural Product Research* **23** (12): 1095–1107.
- BenMansour R., Gargouri B., Gargouri B., Elloumi N., Ben haj Jilani I., Ghrabi-Gammar Z., and Lassoued S. 2011.** Investigation of antioxidant activity of alcoholic extract of *Globularia Alypum* L. *Journal of Medicinal Plants Research* **6** (25): 4193–4199.

- Bergstrom J. D., Dufresne C., Bills G. F, Nallin-Omstead M., and Byrne K. 1995.** Discovery, biosynthesis, and mechanism of action of the zaragozic acids: potent inhibitors of squalene synthase." *Annual review of microbiology* **49**: 607–639.
- Bohlendorf B., Forche E., Bedorf N., Gerth K., Irschik H., Rolf J., Kunze B., Trowitzsch-Kienast W., Hans R., and Hofle G. 1996.** Indole and quinoline derivatives as metabolites of tryptophan in *Myxobacteria*. *Liebigs Annalen*: 49–53.
- Bills G. F., Gloer J. B., and An Z. 2013.** Coprophilous fungi: antibiotic discovery and functions in an underexplored arena of microbial defensive mutualism. *Current Opinion in Microbiology* **16** (5): 549–565.
- Bitzer J., Læssøe T., Fournier J., Kummer V., Decock C., Tichy V. H, Piepenbring M., Peršoh D. and Stadler M. 2008.** Affinities of *Phylacia* and the *Daldinoid* Xylariaceae, inferred from chemotypes of cultures and ribosomal dna sequences. *Mycological Research* **112** (2): 251–270.
- Boutemak K., Safta B., and Ayachi N. 2015.** Study of the anti-inflammatory activity of Flavonic extract of *Globularia alypum* L. *Acta Physica Polonica A* **128** (2): 239–240.
- Boutiti A., Benguerba A., Kitouni R., Bouhroum M., Benayache S. and Benayache F. 2008.** secondary metabolites from *Globularia alypum*. *Chemistry of Natural Compounds* **44** (4): 543–544.
- Breinholt J., Kjoer A., Olsen C. E., Rassing B. R. and Rosendahl Cannie N. 1997.** Hamigerone and dihydrohamigerone: two acetate-erived, antifungal metabolites from *Hamigera avellanea*." *Acta Chemica Scandinavica* **51**: 1241–1244.
- Brewer D, W., Jerram A., and Taylor A. 1968.** The production of cochliodinol and a related metabolite by *Chaetomium* species. *Canadian Journal of Microbiology* **14** (8): 861–866.
- Carbone I. and Kohn L. M. 1999.** A method for designing primer sets for speciation studies in filamentous ascomycetes. *Mycologia* **91** (3):553–556.
- Chaudhari S. M. and Badole S. L. 2014.** Chapter 56: Polyphenols and tuberculosis. In polyphenols in human health and disease. Vol. 6, First edition.: Elsevier: 723pp
- Chen G.D., ChenY., Gao H., Shen L. Q., Wu Y., Li X. X., Li Y., Guo L. D., Cen Y. Z. and Yao X. S. 2013.** Xanthoquinodins from the endolichenic fungal strain *Chaetomium elatum*." *Journal of Natural Products* **76** (4):702–709.
- Chograni H., Riahi L., Zaouali Y. and Boussaid M. 2013.** Polyphenols, flavonoids, antioxidant activity in leaves and flowers of tunisian *Globularia Alypum* L. (*Globulariaceae*). *African Journal of Ecology* **51** (2):343–347.
- Cosoveanu, A., and Raimundo R. Sabina, Cabrera S. 2018.** Fungi as endophytes in *Artemisia thuscula*: juxtaposed elements of diversity and phylogeny. *Journal of Fungi* **4** (1): 1-21.
- Das, A., Imtiazur Rahman M., Ferdous A. S., Mohammad Mahbubur Rahman A. A., Nahar N., Mohammad Riazul Islam, M. A. U. and Khan H. 2017.** An Endophytic basidiomycete, *Grammothele lineata*, isolated from *Corchorus olitorius*, produces ppaclitaxel that shows cytotoxicity." *PLoS ONE* **12** (6): 1–17.

- Deepak B., McCormick S. P., Lee L. S. and Hillt R. A. 1987.** Identification of o-Methylsterigmatocystin as an aflatoxin B1 and G, precursor in *Aspergillus parasiticus*. *Applied and environmental microbiology* **53** (5): 1028–1033.
- Deka, D., Tayung K. and Jha D. K. 2017.** Harnessing fungal endophytes for plant and human health. In *Endophytes: Biology and Biotechnology*. Springer. Switzerland: 59pp.
- Djellouli, F., Krouf D., Bouchenak M., and Lacaille-Dubois M. A. 2014.** Favorable effects of *Globularia Alypum* L. lyophilized methanolic extract on the reverse cholesterol transport and lipoprotein peroxidation in streptozotocin-induced diabetic rats. *International journal of pharmacognosy and phytochemical research* **6** (4): 758–765.
- Djeridane A., Yousfi M., Nadjemi B., Vidal N., Lesgards J. F. and Stocker P. 2007.** Screening of some algerian medicinal plants for the phenolic compounds and their antioxidant activity. *European food research and technology* **224** (6):801–809.
- Došen, I., Nielsen K. F., Clausen G. and Andersen B. 2017.** Potentially harmful secondary metabolites produced by indoor *Chaetomium* Species on artificially and naturally contaminated building materials. *Indoor Air* **27** (1):34–46.
- Du L., Jarrod B. K., Morrow B. H., Shen J. K., Miller A. N. and Cichewicz R. H. 2012.** “Diarylcyclopentendione metabolite obtained from a *Preussia typharum* isolate procured using an unconventional cultivation approach. *Journal of Natural Products* **75** (10):1819–1823.
- Du L., Robles A. J., Jarrod B. K., Mooberry S. L., and Cichewicz R. H. 2014.** Cytotoxic dimeric epipolythiodiketopiperazines from the ascomycetous fungus *Preussia typharum*. *Journal of Natural Products* **77** (6): 1459–1466.
- Estiarte M., Puig G. and Peñuelas J. 2011.** Large delay in flowering in continental versus coastal populations of a mediterranean shrub, *Globularia Alypum*. *International Journal of Biometeorology* **55** (6): 855–865.
- Evidente A., Andolfi A., Vurro M., Chiara M. and Motta A. 2002.** Cytochalasins Z1, Z2 and Z3, three 24-oxa[14]cytochalasans produced by *Pyrenophora Semeniperda*. *Phytochemistry* **60**: 45–53.
- Fang Y. and Qian M. C. (2006).** Quantification of selected aroma-active compounds in pinot noir wines from different grape maturities. *Journal of agricultural and food chemistry* **54** (22): 8567–8573.
- Foster K. R. and Wenseleers T. 2006.** A general model for the evolution of mutualisms. *Journal of Evolutionary Biology* **19** (4): 1283–1293.
- Gomes R. R., Glienke C., Videira S. I. R., Lombard L., Groenewald J. Z. and Crous P. W. 2013.** *Diaporthe*: a genus of endophytic, saprobic and plant pathogenic fungi. *Persoonia: molecular phylogeny and evolution of fungi* **31**:1–41.
- Gonzalez-Menendez V., Martin J., Siles J. A., Gonzalez-Tejero M. R., Gonzalo Platas F. R., Jose A. S., Gonzalez-Tejero M. R., Reyes F., Platas G., Tormo J. R. and Genilloud O. 2017.** Biodiversity and chemotaxonomy of *Preussia* isolates from the iberian Peninsula. *Mycological Progress* **16** (7): 713–728.

- Guindon, S. and Gascuel O. 2003.** A simple, fast, and accurate algorithm to estimate large phylogenies by maximum likelihood. *Systematic Biology* **52** (5): 696–704.
- Gundel P. E., Martínez-Ghersa M. A., Romina Cuyeu M. O., Raúl Ríos E. P. and Ghersa. C. M. 2012.** Mutualism effectiveness and vertical transmission of symbiotic fungal endophytes in response to host genetic background. *Evolutionary Applications* **5** (8): 838–849.
- Halecker S., Surup F., Kuhnert E., Mohr K. I., Brock N. L., Dickschat J. S., Junker C., Schulz B. and Stadler M. 2014.** Hymenosetin, a 3-decalinoyltetramic acid antibiotic from cultures of the ash dieback pathogen, *Hymenoscyphus pseudoalbidus*. *Phytochemistry* **100**: 86–91.
- Harzallah H. J., Neffati A., Skandrani I., Maaloul E., Chekir L. and Mahjoub T. 2010.** Antioxidant and antigenotoxic activities of *Globularia alypum* leaves extracts. *Journal of medicinal plants* **4** (19): 48–53.
- Helaly S. E., Richter C., Thongbai B., Hyde K. D. and Stadler M. 2016.** Lentinulactam, a hirsutane sesquiterpene with an unprecedented lactam modification. *Tetrahedron Letters* **57** (52): 5911–5913.
- Herrera J., Khidir H. H., Eudy D. M., Porrás-Alfaro A., Natvig D. O. and Sinsabaugh R. L. 2010.** Shifting fungal endophyte communities colonize *bouteloua gracilis*: effect of host tissue and geographical distribution. *Mycologia* **102** (5): 1012–1026.
- Hirata M., Isoda S., Kanao M., Shimizu H. and Inoue S. I. 1970.** Studies on anesthetics for fish. *Bulletin of the Japanese Society of Scientific Fisheries* **36** (11):1127–1135.
- Hodgson, S. De Cates C., Hodgson J., Morley N. J., Sutton B. C. and Gange A. C. 2014.** Vertical transmission of fungal endophytes is widespread in forbs. *Ecology and Evolution* **4** (8):1199–1208.
- Hyde K. D. and Soyong K. 2008.** The fungal endophyte dilemma. *Fungal Diversity* **33**:163–173.
- Hyde, K. D., Jones G. E. B., Liu J. K., Ariyawansa H., Boehm E., Boonmee S., Braun U., Chomnunti P., Crous P. W., Dai D. Q., Diederich P., Dissanayake A., Doilom M., Doveri F. 2013.** Families of Dothideomycetes. *Fungal Diversity* **63** (1):1–313.
- Index fungorum, 2018.** Available from: <http://www.indexfungorum.org/names/names.asp> h (accessed: 5 February 2015).
- IUCN. 2005.** A guide to medicinal plants in north africa. International union for conservation of nature and natural resources (IUCN) for mediterranean cooperation. Malaga, Spain: 127pp.
- Kandel, S., Joubert P. and Doty S. 2017.** Bacterial endophyte colonization and distribution within plants. *Microorganisms* **5** (4): 1-26.
- Katoh K., Misawa K., Kuma K. and Miyata T. 2002.** MAFFT: A novel method for rapid multiple sequence alignment based on fast fourier transform. *Nucleic acids research* **30** (14): 59–66.
- Katoh K., and Toh H. 2008.** Recent developments in the MAFFT multiple sequence alignment program. *Briefings in bioinformatics* **9** (4): 286–298.

- Kearse, M., Moir R., Wilson, A. Stones-Havas S., Cheung M., Sturrock S., Buxton S., Cooper A., Markowitz S., Duran C., Thierer T., Ashton B., Meintjes P. and Drummond A. 2012.** Geneious basic: an integrated and extendable desktop software platform for the organization and analysis of sequence data. *Bioinformatics* **28** (12):1647–49.
- Khan R. and Cain R. F. 1979.** The genera *Sporormiella* and *Sporormia* in East Africa. *Canadian Journal of Botany* **57**: 1174–1186.
- Khlifi D., Hamdi M., El Hayouni A., Cazaux S., Souchard J. P., Couderc F. and Bouajila J. 2011.** Global chemical composition and antioxidant and anti-tuberculosis activities of various extracts of *Globularia Alypum* L. (Globulariaceae) leaves. *Molecules* **16** (12): 10592–10603.
- Kock I., Krohn K., Egold H., Draeger S., Schulz B., and Rheinheimer J. 2007.** New massarilactones, massarigenin E, and coniothyrenol, isolated from the endophytic fungus *Coniothyrium* sp. from *Carpobrotus Edulis*. *European Journal of Organic Chemistry* **13**: 2186–2190.
- Kruys Å. 2015.** New species of *Preussia* with 8-celled ascospores (Sporormiaceae, Pleosporales, Ascomycota). *Phytotaxa* **234** (2): 143–50.
- Kruys Å. and Wedin M. 2009.** Phylogenetic relationships and an assessment of traditionally used taxonomic characters in the Sporormiaceae (Pleosporales, Dothideomycetes, Ascomycota), utilising multi-gene phylogenies. *Systematics and biodiversity* **7** (4): 465–78.
- Kuephadungphan W., Helaly S., Daengrot C., Phongpaichit S., Luangsa-ard J. J., Rukachaisirikul V. and Stadler M. 2017.** Akanthopyrones A–D, α -pyrones bearing a 4-O-methyl- β -D-glucopyranose moiety from the spider-sssociated Ascomycete *Akanthomyces novoguineensis*. *Molecules* **22** (7):1-10.
- Kuldau G., and Bacon C. 2008.** Clavicipitaceous endophytes: their ability to enhance resistance of grasses to multiple stresses. *Biological Control* **46** (1): 57–71.
- Kusari, S., Lamshöft M., Zühlke S. and Spiteller M. 2008.** An endophytic fungus from *Hypericum perforatum* that produces hypericin. *Journal of Natural Products* **71** (2):26–29.
- Kusari S., Hertweck C., and Spiteller M. 2012.** Chemical ecology of endophytic Fungi: origins of secondary metabolites. *Chemistry and Biology* **19** (7): 792–98.
- Kusari, S. and Spiteller M. 2012.** Chapter 10: Metabolomics of endophytic fungi producing associated plant secondary metabolites: progress , challenges and opportunities 241 pp. In *Metabolomics*. InTech, Rijeka, Croatia
- Leporatti, M. and Ghedira K. 2009.** Comparative analysis of medicinal plants used in traditional medicine in Italy and Tunisia. *Journal of Ethnobiology and Ethnomedicine* **5** (1): 1-8
- Li G., Kusari S., Kusari P., Kayser O. and Spiteller M. 2015.** Endophytic *Diaporthe* sp. LG23 produces a potent antibacterial tetracyclic triterpenoid. *Journal of natural products* **78** (8): 2128–2132.
- MacLean-Fletcher, S. and Pollard T. D. 1980.** Mechanism of action of cytochalasin b on actin. *Cell* **20** (2): 329–341.

- Mapperson, R. R., Kotiw M., Davis R A. and Dearnaley J. D. W. 2014.** The Diversity and antimicrobial activity of *Preussia* sp. endophytes isolated from Australian dry rainforests. *Current Microbiology* **68** (1): 30–37.
- Martin, R., Gazis R.O., Skaltsas D., Chaverri P. and Hibbett D.S. 2015.** Unexpected diversity of basidiomycetous endophytes in sapwood and leaves of *Hevea*. *Mycologia* **107** (2): 284–97.
- Masi, M., Meyer S. , Cimmino A., Clement S., Black B. and Evidente A. 2014.** Pyrenophoric Acids B and C, two new phytotoxic sesquiterpenoids produced by *Pyrenophora semeniperda*.” *Journal of Agricultural and Food Chemistry* **62** (42):10304–11.
- Mol, H., Amedeo Pietri G. J, Macdonald S. J and Anagnostopoulos C. 2015.** Survey on Sterigmatocystin in Food. *European food safety authority*: 1–56.
- Mosmann T. 1983.** Rapid colorimetric assay for cellular growth and survival: application to proliferation and cytotoxicity assays. *Journal of Immunological methods* **65** (1–2): 55–63.
- Mudur, S. V., J Gloer James B. and Wicklow D. T. 2006.** Sporminarins A and B: antifungal metabolites from a fungicolous isolate of *Sporormiella minimoides*. *The journal of antibiotics* **59** (8):500–506.
- Netzker T., Fischer J., Weber J., Mattern D. J., König C. C., Valiante V., Schroeckh V. and Brakhage A. A. 2015.** Microbial communication leading to the activation of silent fungal secondary metabolite gene clusters. *Frontiers in Microbiology* **6**: 1–13.
- Newcombe G., Campbell J., Griffith D., Baynes M., Launchbaugh K. and Pendleton R. (2016).** Revisiting the life cycle of dung fungi, including *Sordaria fimicola*. *PLOS ONE* **11** (2): 1–11.
- Nomura M. 2017.** Sterigmatocystin and aflatoxin B 1 contamination of corn , soybeanmeal , and formula feed in Japan. *Mycotoxin Research* **34** (1): 21-27.
- Noumeur S. R., Helaly S. E., Jansen R., Gereke M., Stradal T. E.B., Harzallah D. and Stadler M. 2017.** Preussilides A-F, bicyclic polyketides from the endophytic fungus *Preussia similis* with antiproliferative activity. *Journal of Natural Products* **80** (5): 1531–40.
- O’Donnell K. and Cigelnik E. 1997.** Two divergent intragenomic rDNA ITS2 types within a monophyletic lineage of the fungus *Fusarium* are nonorthologous. *Molecular Phylogenetics and Evolution* **7** (1): 103–16.
- Oh H., Swenson D. C., Gloer J. B., Wicklow D. T. and Dowd P. F. 1998.** Chaetochalasin A: A new bioactive metabolite from *Chaetomium brasiliense*. *Tetrahedron Letters* **39** (42): 7633–36.
- Okanya P. W, Mohr K. I., Gerth K., Jansen R. and Rolf M. 2011.** Marinoquinolines A-F, pyrroloquinolines from *Ohtaekwangia kribbensis* (Bacteroidetes). *Journal of natural products* **74**: 603–608.
- Partida-Martinez L. P. and Hertweck C 2005.** Pathogenic fungus harbours endosymbiotic bacteria for toxin production. *Nature* **437** (6): 884–88.
- Partida-Martinez L. P., Monajembashi S., Greulich K. O. and Hertweck C. 2007.** Endosymbiont-Dependent host reproduction maintains bacterial-fungal mutualism. *Current Biology* **17** (9): 773–77.

- Pažoutová, S., Follert S., Bitzer J., Keck K., Surup F., Šrůtka P., Holuša J. and Stadler M. 2013.** “A new endophytic insect-associated *Daldinia* Species, recognised from a comparison of secondary metabolite profiles and molecular phylogeny. *Fungal Diversity* **60**: 107–123.
- Poch. G. and Gloer J. B. 1991.** Auranticins A and B : two new depsidones from a mangrove isolate of the fungus *Preussia Aurantica*. *Journal of natural products* **54** (1): 213-2017.
- Porras-Alfaro, A., Herrera J., Sinsabaugh R. L., Odenbach K. J., Lowrey T. and Natvig D. O. 2008.** Novel root fungal consortium associated with a dominant desert grass. *Applied and environmental microbiology* **74** (9): 2805–2813.
- Porras-alfaro A. and Sinsabaugh R. L. 2011.** Diversity and distribution of soil fungal communities in a semiarid grassland **103** (1): 10–21.
- Qin J. C., Zhang Y. M., Gao J. M., Bai M. S., Yang S. X., Laatsch H. and Zhang A. L. 2009.** Bioactive metabolites produced by *Chaetomium globosum*, an endophytic fungus isolated from *Ginkgo biloba*. *Bioorganic and medicinal chemistry letters* **19** (6): 1572–1574.
- Raina V. K., Srivastava S. K., Aggarwal K. K., Ramesh S. and Kumar S. 2001.** Essential oil composition of *Cinnamomum zeylanicum* blume leaves from little Andaman, India.” *Flavour and fragrance journal* **16** (5): 374–76.
- Rangel-Grimaldo M., Rivero-Cruz I., Madariaga-Mazón A., Figueroa M. and Mata R. 2016.** α -glucosidase inhibitors from *Preussia minimoides*. *Journal of Natural Products* **80** (3): 582–87.
- Rank, C., Nielsen K. F., Larsen T. O., Varga J., Samson R. A. and Frisvad J. C. 2011.** Distribution of sterigmatocystin in filamentous fungi. *Fungal Biology* **115**: 406–420.
- Ren, S, Ma W., Xu T., Lin X., Yin H., Yang B., Zhou X. F., Yang X. W., Long L., Lee K. J., Gao Q. and Liu Y. (2010).** Two novel alkaloids from the south china sea marine sponge *Dysidea* sp. *Journal of Antibiotics* **63** (12): 699–701.
- Rodriguez R. J, White J. F., Arnold A. E. and Redman R. S. 2009.** Fungal endophytes: diversity and functional roles. *New phytologist* **182**:314–30.
- Sánchez Márquez, S., Bills G. F., Herrero N. and Zabalgoageazcoa Í. 2012.** Non-systemic fungal endophytes of grasses. *Fungal Ecology* **5** (3): 289–97.
- Sandhu, S. S., Kumar S. and Aharwal R. P. 2017.** Chapter 12: Endophytic fungi: eco-friendly future resource for novel bioactive compounds. In *Endophytes: Biology and Biotechnology*. Springer International Publishing Switzerland: 303 pp
- Sansinenea E., Salazar F., Jiménez J., Mendoza Á. and Ortiz A. 2016.** Diketopiperazines derivatives isolated from *Bacillus thuringiensis* and *Bacillus endophyticus*, establishment of Their configuration by x-ray and their synthesis. *Tetrahedron Letters* **57** (24): 2604–7.
- Sarr M. P. 2014.** Genetic diversity in *Macrophomina phaseolina*, the causal agent of charcoal rot. *Phytopathologia Mediterranea* **52** (3): 478–89.
- Schaechter M. 2012.** *Eukaryotic Microbes*. First edition Academic Press: 1-496 pp.

- Scherlach K. and Hertweck C. 2009. Triggering cryptic natural product biosynthesis in microorganisms." *Organic & Biomolecular Chemistry* **7** (9): 1753.
- Schindelin, J., Arganda-Carreras I., Frise E., Kaynig V., Longair M., Pietzsch T., Preibisch S., Rueden C., Saalfeld S., Schmid B., Tinevez J.Y., White D.J., Hartenstein V., Eliceiri K., Tomancak P., Cardona A. 2012. Fiji: An open source platform for biological image analysis. *Nature Methods* **9** (7): 676–682.
- Schoch, C. L., Seifert K. A., Huhndorf S., Robert V., Spouge J. L., Levesque C. A., Chen W. and fungal barcoding consortium author list. 2012. Nuclear ribosomal internal transcribed spacer (ITS) region as a universal dna barcode marker for fungi. *Proceedings of the national academy of sciences* **109** (16): 6241–6246.
- Schroeckh V., Nützmann H. W. and Brakhage A. A. 2014. Fungal-actinomycete interactions wakening of silent fungal secondary metabolism gene clusters *via* interorganismic Interactions 147 pp. In: Natural Products: Discourse, Diversity, and Design. First edition, John Wiley & Sons,
- Schulz B. and Boyle C. 2005. The endophytic continuum. *Mycological Research* **109** (6):661–86.
- Schulz B. and Boyle C. 2006. Chapter 1: What Are Endophytes? 1pp. In: Soil Biology. Vol. 9. Springer-Verlag Berlin Heidelberg
- Schulz B., Haas S., Junker C., André N. and Schobert M. 2015. Fungal endophytes are involved in multiple balanced antagonisms. *Current Science* **109** (1): 39-45.
- Scott B. 2001. Endophytes – Fungal symbionts of grasses. *Current opinion in microbiology* **4**: 393–98.
- Sekita, S., Yoshihira K., Natori S. and Kuwano H. 1973. Structures of chaetoglobosin a and b, cytotoxic metabolites of *Chaetomium globosum*. *Tetrahedron Letters* **14** (23): 2109–2112.
- Shi Y. S., Zhang Y., Chen X. Z., Zhang N. and Liu Y. B. 2015. Metabolites produced by the endophytic fungus *Aspergillus fumigatus* from the stem of *Erythrophloeum fordii* Oliv. *Molecules* **20** (6):10793–10799.
- Shiono Y., Seino Y., Koseki T., Murayama T. and Kimura K. I. 2008. Antarones A and B, two polyketides from an endophytic *Penicillium antarcticum*. *Zeitschrift fur naturforschung - section B Journal of chemical sciences* **63** (7): 909–914.
- Stadler, M, Anke H. , Bergquist K. E and Sterner O. 1993. Lachnumon and lachnumol A, new metabolites with nematocidal and antimicrobial activities from the Ascomycete *Lachnum papyraceum* (Karst.) Karst. II. Structural Elucidation." *Journal of Antibiotics* **46** (6):968–971.
- Stadler M., Tichy H. V., Katsiou E. and Hellwig V. 2003. Chemotaxonomy of *Pochonia* and Other conidial fungi with *Verticillium*-like anamorphs. *Mycological Progress* **2** (2): 95–122.
- Stadler M., Wollweber H., Mühlbauer A., Asakawa Y., Hashimoto T., Rogers J. D., Ju Y. M., Wetzstein H. G. and Tichy H. V. 2001. Molecular chemotaxonomy of *Daldinia* and other Xylariaceae. *Mycological Research* **105** (10): 1191–1205.
- Stierle, D. B., Stierle A. A. and Ganser B. K. 1999. Isolation of two highly methylated polyketide derivatives from a yew- associated *Penicillium* species. *Journal of Natural Products* **62** (8):1147–1150.

- Tabata N., Suzumura Y., Tomoda H., Masuma R., Haneda K., Iwai Y. and Omura S. 1992.** Xanthoquinodins, new anticoccidial agents produced by *Humicola* sp. *The Journal of Antibiotics* **46** (5): 749-755.
- Tadych, M., Bergen M. S. and White J. F. 2014.** *Epichloë* spp. associated with grasses: new insights on life cycles, dissemination and evolution.” *Mycologia* **106** (2):181–201.
- Teponno, R. B., Noumeur S. R., Helaly S. E., Hüttel S., Harzallah D. and Stadler M. 2017.** Furanones and anthranilic acid derivatives from the endophytic fungus *Dendrothyrium Variisporum*. *Molecules* **22** (10): 1-12
- Tintjer T., Leuchtman A. and Clay K. 2008.** Variation in horizontal and vertical transmission of the endophyte epichloë elymi infecting the grass *Elymus hystrix*.” *New phytologist* **179** (1): 236–46.
- Touaibia M., and Chaouch F. Z. 2016.** global chemical composition and antioxidative effect of the ethanol extracts prepared from *Globularia alypum* leaves. *Nature & Technology* **14**: 2–6.
- Verkley G. J. M, Dukik K., Renfum R., Göker M. and Stielow J. B. 2014.** Novel genera and species of *Coniothyrium*-like fungi in Montagnulaceae (Ascomycota). *Persoonia: Molecular phylogeny and evolution of fungi* **32**: 25–51.
- Veršilovskis A. and De Saeger S. 2010.** Sterigmatocystin : occurrence in foodstuffs and analytical methods – An Overview. *Molecular Nutrition & Food Research* **54**: 136–47.
- Vilgalys, R. and Hester M. 1990.** Rapid genetic identification and mapping of enzymatically amplified ribosomal DNA from several *Cryptococcus* species. *Journal of Bacteriology* **172** (8):4238–46.
- Wakefield J., Hassan H. M., Jaspars M., Ebel R., and Rateb M. E. 2017.** Dual induction of new microbial secondary metabolites by fungal bacterial co-cultivation. *Frontiers in Microbiology* **8**: 1–10.
- Wang, X. W., Houbraken J., Groenewald J. Z., Meijer M., Andersen B., Nielsen K. F., Crous P. W., and Samson R. A. 2016.** diversity and taxonomy of *chaetomium* and *chaetomium*-like fungi from indoor environments. *Studies in Mycology* **84**: 145–224.
- Wang, X W, Lombard L., Groenewald J. Z., Li J., Videira S. I. R, Samson R. A, Liu X. Z. and Crous P. W. 2016.** Phylogenetic reassessment of the *Chaetomium globosum* species complex. *Persoonia* **36**: 83–133.
- Weber H. Norman A., Baenziger C., and Gloer J. B. 1990.** Structure of preussomerin A: an unusual new antifungal metabolite from the coprophilous fungus *Preussia isomera*. *Journal of the american chemical society* **112** (18): 6718–6719.
- Weber H. A. and Gloer J. B. 1988.** Interference Competition among natural fungal competitors: an antifungal metabolite from the coprophilous fungus *Preussia fleischhakkii*. *Journal of natural products* **51** (5): 879–883.
- Weber H. A. and Gloer J. B. 1991.** The preussomerins: Novel antifungal metabolites from the coprophilous fungus *Preussia isomera* Cain. *Journal of organic chemistry* **56** (14): 4355–4360.

- Weber H. A., Dale C., S., Gloer J. B. and Malloch D. 1992.** Similins A and B: new antifungal metabolites from the coprophilous fungus *Sporormiella Similis*.” *Tetrahedron letters* **33** (9):1157–1160.
- White T. J., Bruns T. D., Lee S. B. and Taylor J. W. 1990.** Chapter 38: Amplification and direct sequencing of fungal ribosomal rna genes for phylogenetics 315pp. In PCR Protocols: A Guide to Methods and Applications, Academic press, New York USA.
- Wijeratnea, E. M. K., Xu Y., Arnoldb A. E. and Gunatilaka A. L. 2015.** Pulvinulin A, Graminin C, and cis-Gregatin B, new natural furanones from *Pulvinula* sp. 11120, a fungal endophyte of *Cupressus arizonica*. *Natural product communications*. **10** (1):107–11.
- Wittstein, K., Rascher M., Rupcic Z., Löwen E., Winter B., Köster R. W. and Stadler M. 2016.** Corallocins A–C, nerve growth and brain-derived neurotrophic factor inducing metabolites from the mushroom *Hericium coralloides*. *Journal of natural products* **79** (9): 2264–2269.
- Xiao X., Xie J., Cheng J., Li G., Yi X., Jiang D., and Fu Y. 2014.** Novel Secretory Protein Ss-Caf1 of the plant-pathogenic fungus *Sclerotinia sclerotiorum* is required for host penetration and normal sclerotial development. *Molecular Plant-Microbe Interactions* **27** (1): 40–55.
- Yasuhide, M., Yamada T., Numata A., and Tanaka R. 2008.** Chaetomugilins, new selectively cytotoxic metabolites, produced by a marine fish-derived *Chaetomium* Species. *Journal of Antibiotics* **61** (10):615–622.
- Zabalgogezcoa, I. 2008.** Review. Fungal endophytes and their interaction with plant pathogens: *Spanish journal of agricultural research* **6**:138-146.
- Zafar Alam M., , Syed Waseemuddin A. Iqbal A. , Mohammad S., Mirza T. B. and SMS Z. 2010.** Bioactive alkaloids produced by fungi i. updates on alkaloids from the species of the genera *Boletus*, *Fusarium* and *Psilocybe*. *Pakistan journal of pharmaceutical sciences* **23** (3): 349–57.
- Zhang G. F., Han W. B., Cui J. T., Ng W. S., Guo Z. K., Tan R. X., and Ge H. M. 2012.** Neuraminidase inhibitory polyketides from the marine-derived fungus *Phoma herbarum*. *Planta Medica* **78** (1):76–78.
- Zhang Q., Li H. Q., Zong S. C., Gao J.M. and Zhang A. L. 2012.** Chemical and bioactive diversities of the genus *Chaetomium* secondary metabolites. *Mini Reviews in Medicinal Chemistry* **12** (2):127–48.

Appendices

Appendix A

List of used taxa for the phylogenetic reconstruction

Table S1. List of used taxa for the phylogenetic evaluation of the three fungal isolates of *Preussia similis*. GenBank accession numbers, strain number of public culture collections, origin and isolation substrate are given. ^TType strain.

Species	Strain	Substrate	Origin	GenBank Accession Number		
				ITS	LSU	EF-1 α
<i>Preussia africana</i> (<i>P. Africana</i>)	S12	Goat dung	Tanzania	AY510420	AY510384	AY510405
<i>P. africana</i>	S14	Zebra dung	South Africa	AY510417	AY510382	AY510403
<i>P. africana</i>	S15	Zebra dung	South Africa	AY510421	AY510385	AY510404
<i>P. africana</i>	S17 ^T	<i>Viburnum tinus</i> leaves	Canary Islands	AY510418	AY510383	AY510402
<i>P. australis</i>	S5	Gazelle dung	South Africa	AY510411	AY510376	AY510399
<i>P. australis</i>	S6	Gazelle dung	Namibia	AY510412	AY510377	AY510401
<i>P. australis</i>	S7	Zebra dung	South Africa	AY510413	AY510378	AY510400
<i>P. intermedia</i>	S1	Elk dung	USA	AY510415	AY510380	AY510398
<i>P. intermedia</i>	S4	Goat dung	Greece	AY510416	AY510381	AY510397
<i>P. intermedia</i>	S3	Goat dung	Greece	AY510414	AY510379	AY510396
<i>P. pseudomina</i>	S25 ^T	Leaf litter	Puerto Rico	AY510424	AY510389	AY510407
<i>P. mediterranea</i>	S31	<i>Alnus glutinosa</i> leaves	Spain	DQ468024	DQ468044	DQ468012
<i>P. mediterranea</i>	S34	<i>Daphne gnidium</i> leaves	Spain	DQ468025	DQ468045	DQ468013
<i>P. mediterranea</i>	S30	<i>Quercus suber</i> leaves	Spain	DQ468023	DQ468043	DQ468011
<i>P. mediterranea</i>	S23 ^T	<i>Cistus albidus</i> leaves	Spain	DQ468022	DQ468042	DQ468011
<i>P. mediterranea</i>	S22	<i>Quercus ilex</i> leaves	Spain	DQ468021	DQ468041	DQ468009
<i>P. minima</i>	S26	Leaf litter	USA	AY510427	AY510392	AY510409
<i>P. minima</i>	S21	Rhinoceros dung	South Africa	AY510425	AY510390	AY510408
<i>P. minima</i>	S13	Gazelle dung	Namibia	AY510426	AY510391	AY510410

Table S1 (continued)

<i>P. minima</i>	CBS2450	Goat dung	Panama	DQ468026	DQ468046	DQ468003
<i>P. minimoides</i>	S10	Pig dung	Argentina	AY510423	AY510388	AY510406
<i>P. similis</i>	S19	Dung	USA	AY510419	AY510386	AY510395
<i>P. similis</i>	CBS 80473	Saline desert soil	Kuwait	DQ468028	DQ468048	DQ468006
<i>Westerdykella dispersa</i>	CBS 15667	Soil	Nigeria	DQ468016	DQ468036	DQ468000
<i>Westerdykella dispersa</i>	CBS 71271	Greenhouse Soil	Netherlands	DQ468031	DQ468051	DQ468005
<i>Westerdykella dispersa</i>	CBS 50875	Salt-Marsh Soil	Armenia	DQ468030	DQ468050	DQ468002

Table S2. List of used taxa for the phylogenetic evaluation of the fungal isolate *Dendrothyrium variisporum*. GenBank accession numbers, strain number of public culture collections, origin and isolation substrata are given. ^T Type strain.

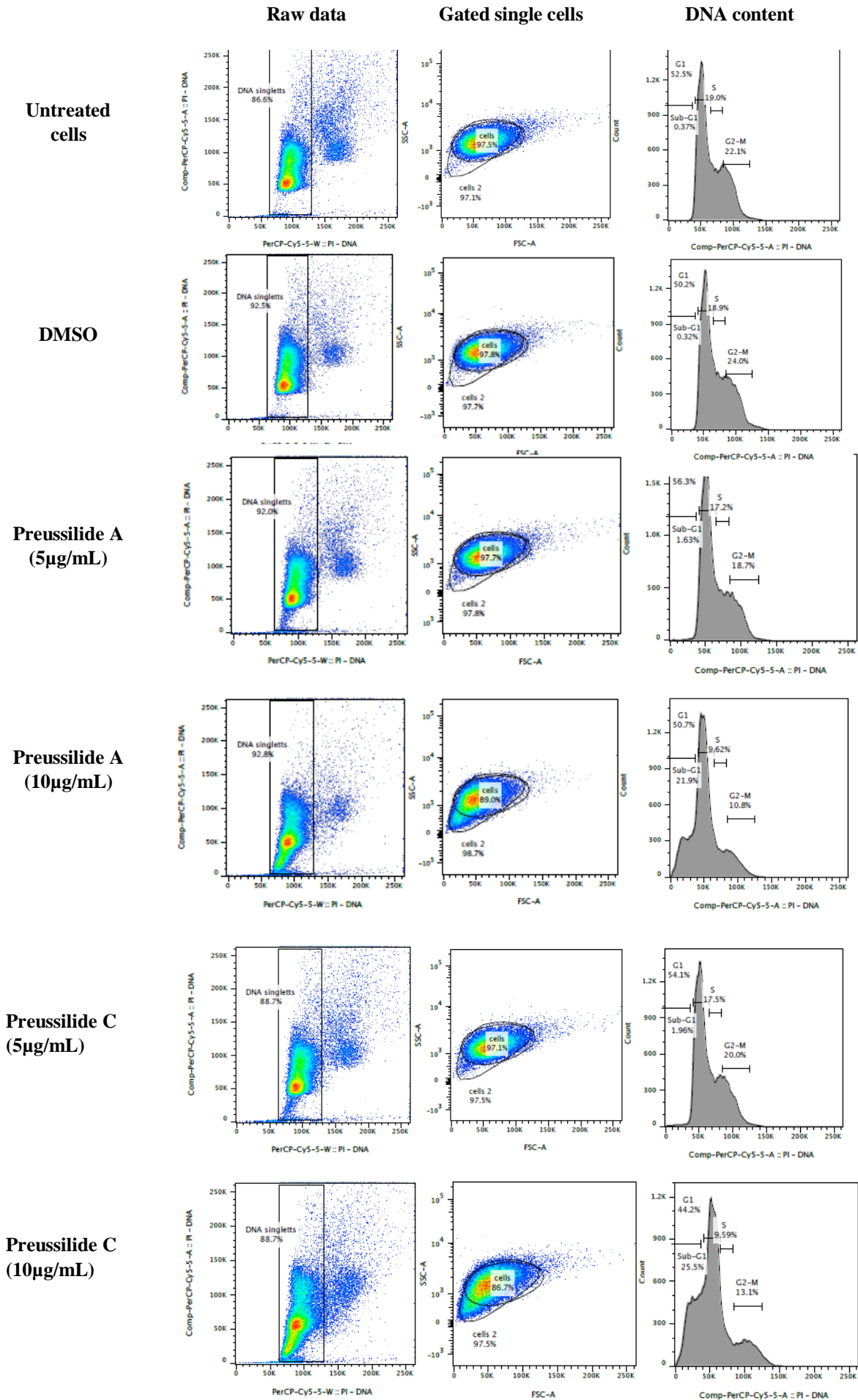
Species	Strain	Substrate	Host	Origin	GenBank Accession Number			
					ITS	LSU	Tub	Actin
<i>Dendrothyrium variisporum</i>	CBS 19782	Grapevine	-	Switzerland	JX496030	JX496143	JX496369	JX496256
<i>Dendrothyrium variisporum</i>	CBS 121217	Declined grape vine	<i>Vitis vinifera</i>	Switzerland	JX496053	JX496166	JX496392	JX496279
<i>Dendrothyrium longisporum</i>	CBS 58283	-	<i>Arceuthobium pusillum</i>	Grand Beach	JX496097	JX496210	JX496436	JX496323
<i>Dendrothyrium longisporum</i>	CBS 82484	-	<i>Triticum aestivum</i>	Germany	JX496115	JX496228	JX496454	JX496341
<i>Alloconiothyrium aptrootii</i>	CBS 98195	Soil	-	Papua New Guinea	JX496122	JX496235	JX496461	JX496348
<i>Alloconiothyrium aptrootii</i>	CBS 98095	Soil	-	Papua New Guinea	JX496121	JX496234	JX496460	JX496347
<i>Paraphaeosphaeria angularis</i>	CBS 16770 ^T	Leaf	<i>Saccharum officinarum</i>	El Salvador	JX496047	JX496160	JX496386	JX496273
<i>Paraphaeosphaeria sporulosa</i>	CBS 21868	Wheat-field soil	-	El Salvador	JX496047	JX496160	JX496386	JX496273
<i>Paraphaeosphaeria sardoa</i>	CBS 50171 ^T	Dead leaf	<i>Smilax aspera</i>	-	JX496094	JX496207	JX496433	JX496320
<i>Paraphaeosphaeria arecacearum</i>	CBS 15875 ^T	Soil	<i>Elaeis guineensis</i>	-	JX496043	JX496156	JX496382	JX496269

Table S2 (continued)

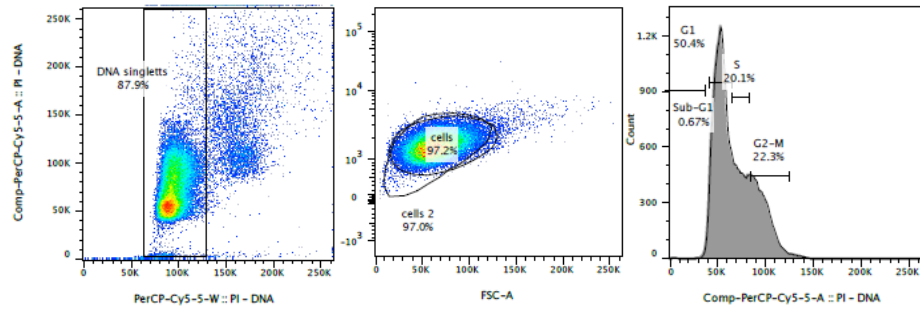
<i>Paraconiothyrium brasiliense</i>	CBS 100299	Fruit	<i>Coffea arabica</i>	-	AY642531	JX496124	JX496350	JX496237
<i>Paraconiothyrium fungicola</i>	CBS 113269	Resupinate polypore fungus	-	Albania	JX496020	JX496133	JX496359	JX496246
<i>Paraconiothyrium archidendri</i>	CBS 16877	Leaf spot	<i>Pithecelobium bigeminum</i>	Burma	JX496049	JX496162	JX496388	JX496275
<i>Paracamarosporium hawaiiense</i>	CBS 120025	Stem	<i>Sophora chrysophylla</i>	USA	JX496027	JX496140	JX496366	JX496253
<i>Paraconiothyrium cyclothyrioides</i>	CBS 97295	Soil	<i>Hevea brasiliensis</i>	-	JX496088	JX496201	JX496427	JX496314
<i>Paraconiothyrium estuarinum</i>	CBS 109850	Sediment from estuarine	-	-	JX496016	JX496129	JX496355	JX496242
<i>Pseudocamarosporium africanum</i>	CBS 121166	-	<i>Prunus persica</i>	South Africa	JX496029	JX496142	JX496368	JX496255
<i>Microsphaeropsis arundinis</i>	CBS 100243	Soil	-	-	JX496010	JX496123	JX496349	JX496236

Appendix B

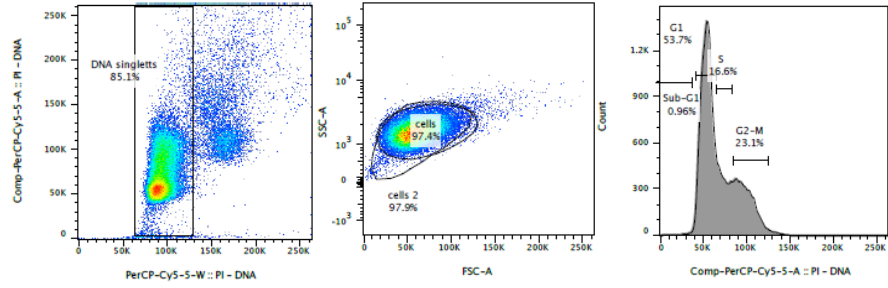
FACS data of U2OS treatment



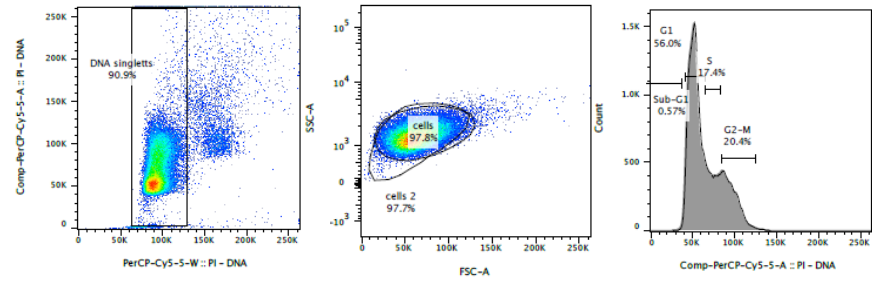
**Preussilide D
(5µg/mL)**



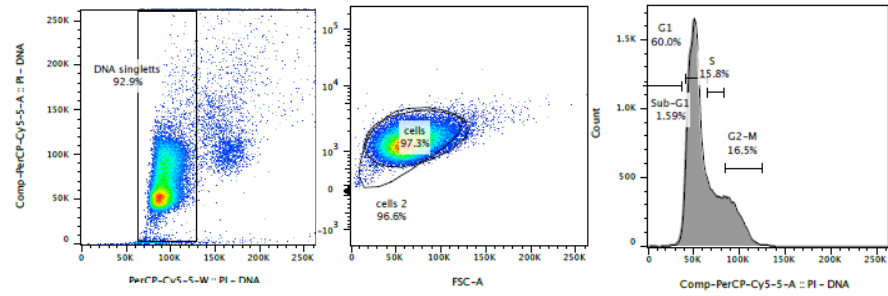
**Preussilide D
(10µg/mL)**



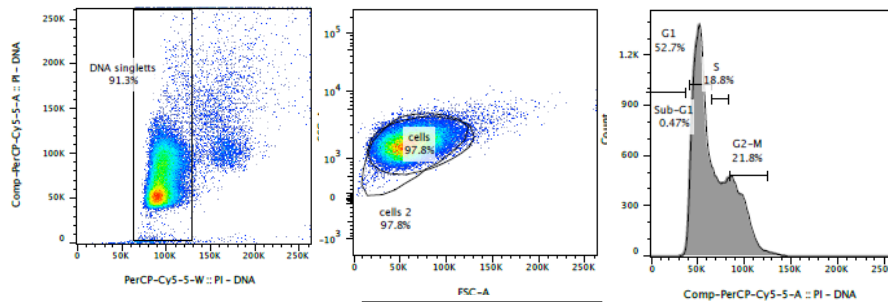
**Preussilide E
(5µg/mL)**



**Preussilide E
(10µg/mL)**



**Preussilide F
(5µg/mL)**



**Preussilide F
(10µg/mL)**

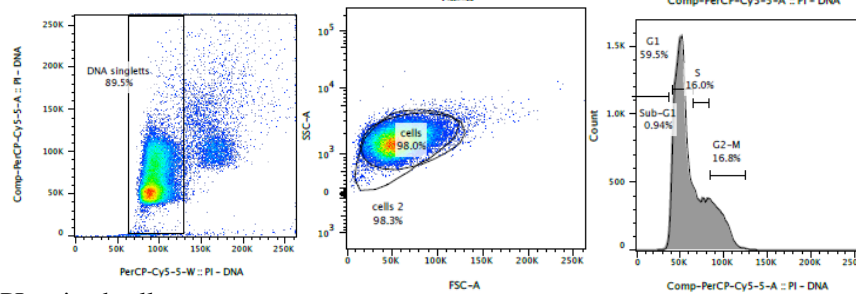


Figure S1: FACS data of PI-stained cells.

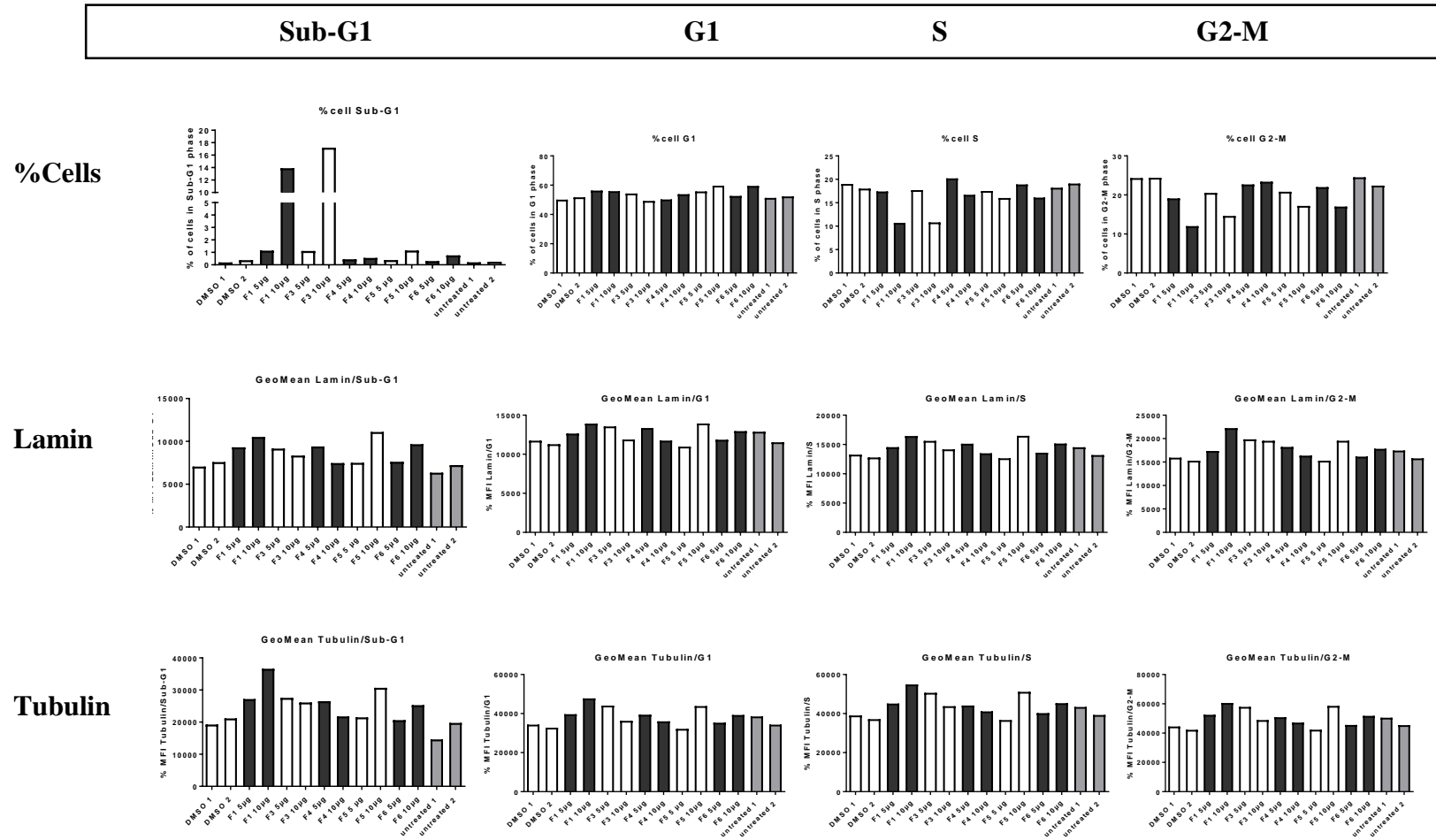


Figure S2: The Figure depicts cytofluorimetric analysis of U2OS cells treated by five of preussilides (preussilide B was not tested due to limited material) and stained for DNA, lamin and alpha - tubulin. Percentage of cells and amounts of tubulin and lamin in each cell cycle phase are shown. F1: Preussilide A, F3: preussilide C, F4: preussilide D, F5: preussilide E, F6: preussilide F.

Paper I

Preussilides A–F, Bicyclic Polyketides from the Endophytic Fungus *Preussia similis* with Antiproliferative Activity

Sara R. Noumeur,^{†,‡,§} Soleiman E. Helaly,^{†,⊥} Rolf Jansen,[†] Marcus Gereke,^{||} Theresia E. B. Stradal,^{||} Daoud Harzallah,[‡] and Marc Stadler^{*,†,§}

[†]Department of Microbial Drugs, Helmholtz Centre for Infection Research and German Centre for Infection Research (DZIF), partner site Hannover/Braunschweig, Inhoffenstrasse 7, 38124 Braunschweig, Germany

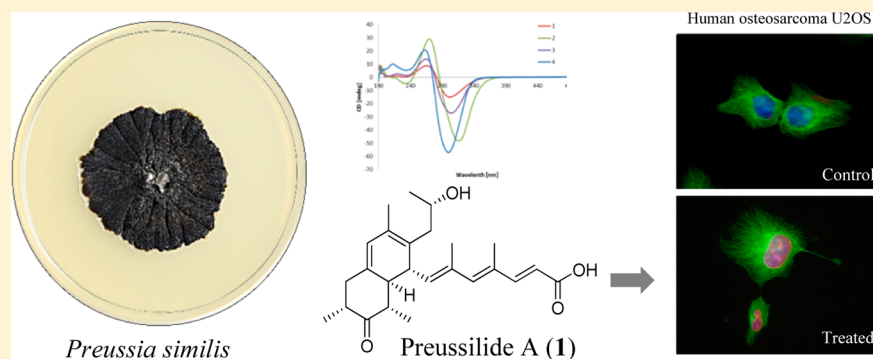
[‡]Laboratory of Applied Microbiology, Department of Microbiology, Faculty of Natural and Life Sciences, University Sétif 1 Ferhat Abbas, 19000 Sétif, Algeria

[§]Department of Microbiology-Biochemistry, Faculty of Natural and Life Sciences, University of Batna 2, 05000 Batna, Algeria

[⊥]Department of Chemistry, Faculty of Science, Aswan University, 81528 Aswan, Egypt

^{||}Department of Cell Biology, Helmholtz Centre for Infection Research, Inhoffenstrasse 7, 38124 Braunschweig, Germany

S Supporting Information



ABSTRACT: Six novel bioactive bicyclic polyketides (1–6) were isolated from cultures of an endophytic fungus of the medicinal plant *Globularia alypum* collected in Batna, Algeria. The producer organism was identified as *Preussia similis* using morphological and molecular phylogenetic methods. The structures of metabolites 1–6, for which the trivial names preussilides A–F are proposed, were elucidated using a combination of spectral methods, including extensive 2D NMR spectroscopy, high-resolution mass spectrometry, and CD spectroscopy. Preussilides were tested for antimicrobial and antiproliferative effects, and, in particular, compounds 1 and 3 showed selective activities against eukaryotes. Subsequent studies on the influence of 1 and 3 on the morphology of human osteosarcoma cells (U2OS) suggest that these two polyketides might target an enzyme involved in coordination of the cell division cycle. Hence, they might, for instance, affect timing or spindle assembly mechanisms, leading to defects in chromosome segregation and/or spindle geometry.

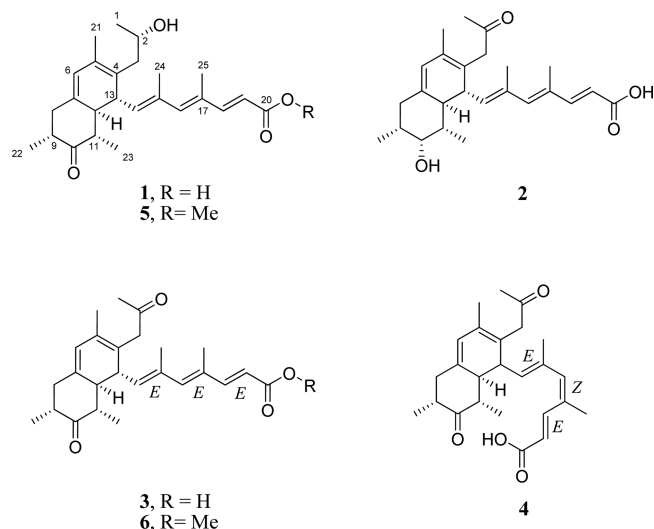
The apparent increase in human diseases such as cancer and infections calls for new and beneficial therapeutic agents. Fungi are prolific sources of bioactive natural products,¹ and in particular the endophytic mycobiota may have developed an arsenal of unique secondary metabolites that has evolved during the symbiotic endophytes–plant relationship.² The genus *Preussia* (Sporormiaceae, Pleosporales) comprises filamentous Ascomycota that live on animal dung, plant debris, soil, and wood³ or as endophytes.^{4–6} Modern taxonomic concepts of *Preussia* include the species of the genus *Sporormiella*, since the salient discriminatory morphological features by which these genera have been historically distinguished are now known to depend on culture conditions.^{6,7} Moreover, recent molecular phylogenetic studies have revealed that *Preussia* and *Sporormiella* do not form monophyletic clades, but rather their DNA sequences become intermingled in phylogenetic trees.^{6,8,9}

Both *Preussia* and *Sporormiella* are known to be prolific producers of bioactive polyketides, including depsidones.^{10–12} In particular, *Preussia similis* (Khan & Cain) Arenal^{13,14} was found to be a rich source of antifungal compounds, such as similins A and B¹⁵ and preussomerin A.¹⁶ From our collection of endophytic fungi isolated from the medicinal plant *Globularia alypum* Linn. (Plantaginaceae) collected in Batna, Algeria, *P. similis* DSM 104666 was selected for further study based on a phylogenetic preselection as outlined previously^{17,18} and screened in order to search for novel biologically active secondary metabolites. Herein we report the isolation, structure elucidation, absolute configuration, and biological activity of

Received: January 21, 2017

Published: April 11, 2017

preussilides A–F (1–6), six new bicyclic polyketides from the endophytic fungus *P. similis* DSM 104666. Furthermore, the morphological characteristics and the phylogenetic position of the producing organism are illustrated and discussed.



RESULTS AND DISCUSSION

The main component of this compound family, preussilide A (1), was obtained as a pale yellow gum with an overall yield of 13 mg/L. High-resolution electrospray ionization mass spectrometric (HRESIMS) analysis of 1 indicated the

molecular formula $C_{25}H_{34}O_4$ (calcd for $C_{25}H_{33}O_4^+$, 399.2530) with 9 degrees of unsaturation. 1H , ^{13}C , and 1H , ^{13}C HSQC NMR data indicated the presence of six methyls, two sp^3 methylenes, five sp^2 and five sp^3 methines (including an oxygenated one), and seven sp^2 nonprotonated carbons (Table 1). 1H , 1H COSY and 1H , ^{13}C HMBC NMR data established a 4,6-dimethylhepta-2,4,6-trienoic acid substructure (A, in Figure 1), as they showed a COSY correlation between H-18 and H-19 and HMBC correlations from H-18 to C-20 and C-16, from H-16 to C-14 and C-18, from H₃-25 to C-16, C-17, and C-18, and from H₃-24 to C-14, C-15, and C-16. Furthermore, three COSY correlation sequences from H₃-23 to H-12, H₃-22 to H₂-8, and H₃-1 to H₂-3, together with a network of HMBC correlations, established a decalin derivative motif (B) as shown in Figure 1. The propan-2-ol group was connected to C-4 of the decalin moiety by HMBC correlations from H-2 to C-4 and from H-13 to C-3. Finally, a COSY correlation between H-14 and H-13 and HMBC correlations from H-14 to C-12 and C-4, from H-13 to C-15, and from H-12 to C-14 interconnected structure elements “A” and “B” via methine carbon C-13 of the decalin moiety to give the new polyketide preussilide A (1). The carbon skeleton of 1 resembles those of other fungal metabolites, such as the antarones from *Penicillium antarcticum*¹⁹ and hamigerone from *Hamigera avellanea*.²⁰

The relative configuration of preussilide A (1) was determined on the basis of 1H , 1H ROESY data and vicinal coupling constants. NOE correlations (Figure 2) between the methine proton H-12 and the methyl H₃-23, H-14, and H-8b revealed they are on the same face of the decalin unit.

Table 1. 1H and ^{13}C NMR Spectroscopic Data of Preussilide A (1) (700 MHz, Methanol- d_4)^a

pos	δ_C , type	δ_H (J in Hz)	COSY	ROESY	HMBC
1	23.72, CH ₃	1.21, d (6.1)	2	2 > 3b	2, 3
2	68.08, CH	3.93, sxt (6.2)	1, 3	1 > 3a	1, 2, 3
3a	42.43, CH ₂	2.53, ⁱ dd (7.3, 14)	3b, 2	21, 3b > 2	1, 13, 2
3b		1.96, ⁱ br dd (5.8, 14)	3a, 2	3a > 13	1, 13, 2
4	127.97, C				
5	127.96, C				
6	124.53, CH	5.79, s		21 > 8a	12, 21, 8
7	137.61, C				
8b	43.78, CH ₂	2.00, ⁱ br t (12.0)	9, 8a	8a > 22, 12	22, 9, 6, 12, 10
8a		2.70, dd (11.9, 6.4)	8b, 9	8b, 6 > 9	22, 9, 6, 12, 10
9	50.04, CH	2.41, ⁱ ddquin (0.9, 12.0, 6.4)	22, 8	22, 8a > 11	7, 10, 22, 8
10	214.71, C				
11	50.02, CH	2.51, ⁱ dq (12.5, 6.4)	23, 12	23 > 9 > 13	23, 12, 13, 10
12	52.02, CH	1.74, d (12.5)	11	8b	4, 6, 8, 10, 23, 13, 14
13	41.04, CH	3.31, br d (10.3)	14	24, 23, 12 > 3b, 2, 11	12, 11, 3, 15, 5, 7
14	137.99, CH	5.38, d (10.4)	13	25	4, 12, 24, 16
15	132.77, C				
16	144.12, CH	6.23, br s		18 > 14	25, 24, 14, 18
17	133.48, C				
18	151.55, CH	7.27, d (15.6)	19	16	25, 16, 20
19	118.74, CH	5.83, br d (15.6)	18	25	17, 20
20	171.63, C				
21	18.66, CH ₃	1.84, s		6, 3a	4, 5, 6
22	15.35, CH ₃	1.06, d (6.4)	9	8b, 9 > 8a	8, 9, 10
23	12.03, CH ₃	1.12, d (6.4)	11	12, 11, 13	10, 11, 12
24	17.22, CH ₃	1.90, d (1.2)		13, 16	14, 15, 16
25	14.06, CH ₃	1.87, d (0.9)		19 > 14	16, 17, 18

^aH-13 overlapped with solvent peak, J_{H-13} value was obtained from the spectrum recorded in acetone; ⁱ overlapping signals; > stepwise decreasing intensity.

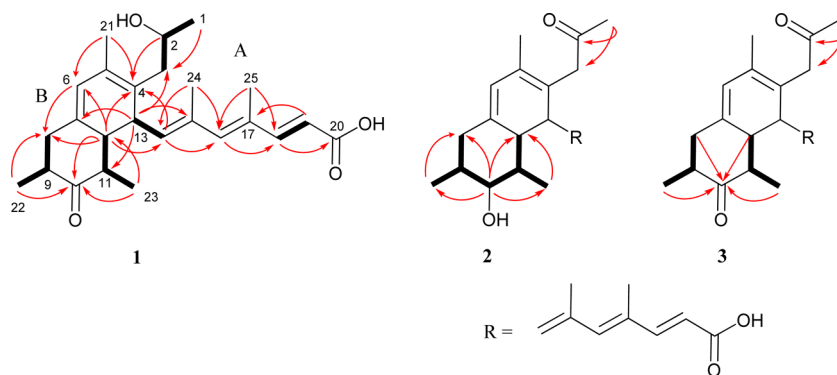


Figure 1. Selected $^1\text{H},^1\text{H}$ COSY and $^1\text{H},^{13}\text{C}$ HMBC correlations of **1**, **2**, and **3**.

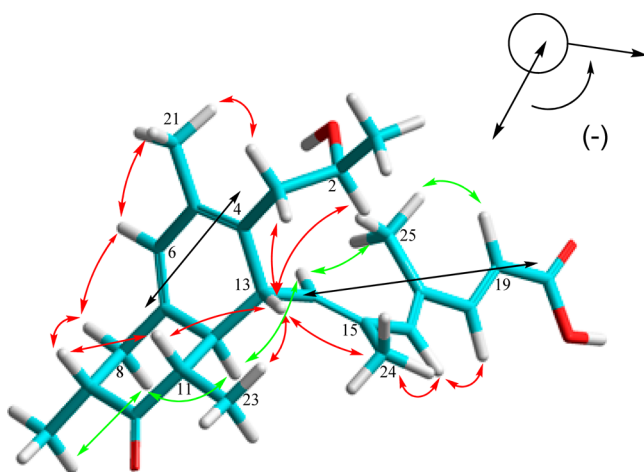


Figure 2. Energy-minimized conformation of preussilide A (**1**) in solution [selected NOEs of **1** in front (red arrows) and in the rear (green arrows); the black arrows show the negative chirality in **1** based on ECD analysis].

Furthermore, an NOE correlation between H-13 and H-11 and H₃-24 indicated that H-13 and H-11 are on the face opposite H-12. This was supported by the absence of a coupling constant between H-12 and H-13 ($J = 0$ Hz), which suggests that the dihedral angle between H-12 and H-13 is approximately 90° . A coupling constant of $J = 12.5$ Hz between H-11 and H-12 supported their *trans*-orientation. In addition, H₃-22 showed an NOE to H-8b, indicating that H₃-22 is cofacial with H-12. Thus, the relative configuration of the decalin moiety was determined as shown in Figure 2, which is consistent with the reported configuration of antarones.¹⁹ The geometry of the C18–C19 double bond of the 4,6-dimethylhepta-2,4,6-trienoic acid chain (structure element A) was determined from the coupling constant $J_{18,19} = 15.6$ Hz, indicating an *E*-configuration of this double bond. The trisubstituted double bonds $\Delta^{14,15}$ and $\Delta^{16,17}$ were assigned as *E*-configured based on NOE correlations between H₃-24 and H-13 and of H-14 and H-19 to the methyl H₃-25 as well as the NOE between H-16 and H-18. This was supported by the ^{13}C NMR shifts for H₃-24 and H₃-25, δ_{C} 17.2 and 14.1, respectively. The relatively upfield shifts confirm the *cis*-configuration of the methyl to the residue (R) at the trisubstituted double bonds and thus an *E*-configuration at $\Delta^{14,15}$ and $\Delta^{16,17}$.

To determine the absolute configuration of preussilide A (**1**), Mosher esters of **1** were prepared of the secondary alcohol C-2. Analysis of the $\Delta\delta^{\text{SR}}$ values of the MTPA esters revealed

negative values of -42 and -70 Hz of H₃-1 and H₃-21, respectively, while the $\Delta\delta^{\text{SR}}$ values of H-3a, H-3b, and H-13 were $+35$, $+42$, and $+49$ Hz, respectively. Thus, the *S*-configuration was assigned at C-2.

The absolute configurations of the remaining stereogenic centers in **1** were assigned using CD spectroscopy. With the decaline-diene and the triene side chain, compound **1** has a bichromophoric system, which, according to the exciton chirality rule, can be used to elicit the absolute configuration of **1**.^{21,22} The ECD spectrum of **1** in EtOH showed a negative Cotton effect at λ_{max} 302 nm ($\Delta\epsilon = -15.01$) and a positive Cotton effect at λ_{max} 265 nm ($\Delta\epsilon = +8.80$) (Figure 3) due to

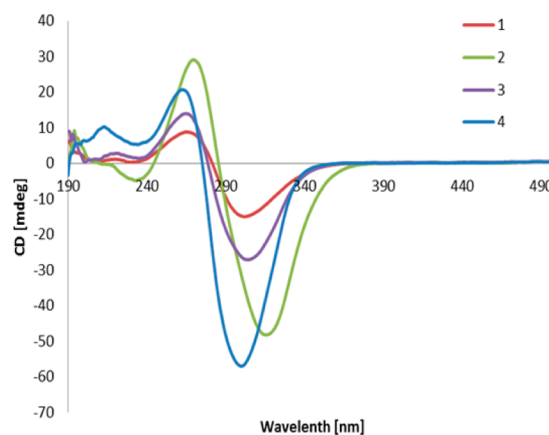


Figure 3. ECD spectra of compounds **1**–**4** in ethanol.

the transition interaction between the two different chromophores. This evidence indicated a negative chirality ($-$) for **1**. According to the exciton chirality rule, the absolute *R*-configuration of C-13 was determined as shown in Figure 2. Consequently, the 3D structure of **1** was unambiguously determined as 2*S*, 9*R*, 11*S*, 12*S*, 13*R*. A model calculated with the pm3 method using HyperChem (ver. 8.0.10) showed the energy-minimized 3D structure of preussilide A (**1**) (Figure 2). In this structure the calculated torsion angle between H-12 and H-13 was 93° and thus fully supports the absence of their vicinal coupling.

Indicated by the positive HRESIMS ion cluster $[\text{M} + \text{H}]^+$ at m/z 399.2519 (calcd 399.2530) compound **2** was an isomer of **1** sharing the elemental formula $\text{C}_{25}\text{H}_{34}\text{O}_4$. The ^1H and ^{13}C NMR spectra resembled those of **1** (Tables 2 and 3). However, the doublet signal for H₃-1 in **1** was replaced by a singlet at δ_{H} 2.13 (δ_{C} 29.4) assigned to a methyl ketone unit in **2**. This was

Table 2. ¹H NMR Spectroscopic Data of Preussilides B–F (2–6) (700 MHz, Methanol-*d*₄)

pos	2	3	4	5	6
	δ_{H} (J in Hz)	δ_{H} (J in Hz)	δ_{H} (J in Hz)	δ_{H} (J in Hz)	δ_{H} (J in Hz)
1	2.13, s	2.16, s	2.17, s	1.21, d (6.1)	2.16, s
2				3.93, m	
3b	2.89, d (14.6)	2.97, d (15.6)	3.00, d (15.9)	1.94, m	2.97, d (15.6)
3a	3.45, d (14.6)	3.56, d (15.6)	3.62, d (15.9)	2.53, m	3.55, d (15.6)
6	5.52, s	5.83, ^a s	5.77, s	5.79, s	5.82, s
8b	2.15, ^a m	2.01, t (11.6)	2.09, t (11.8)	2.00, m	2.01, br t (11.6)
8a	2.00, dd (12.0, 4.3)	2.72, dd (11.9, 6.7)	2.6 α , dd (11.8, 6.7)	2.70, dd (11.9, 6.4)	2.72, dd (11.9, 6.7)
9	1.61, ^a m	2.43, m	2.41, m	2.41, m	2.43, m
10	3.56, t (2.5)				
11	1.63, ^a m	2.49, m	2.47, m	2.50, m	2.48, m
12	2.14, d (12.5)	1.76, d (12.5)	1.83, d (12.9)	1.74, d (12.5)	1.76, d (12.8)
13	3.06, d (10.3)	3.21, d (10.4)	3.19, d (10.3)	3.32, ^b d (10.4)	3.21, d (10.4)
14	5.43, d (10.3)	5.36, d (10.4)	5.15, d (10.3)	5.39, d (10.4)	5.37, d (10.4)
16	6.21, s	6.24, s	6.08, s	6.26, s	6.26, s
18	7.24, d (15.5)	7.30, d (15.6)	7.59, d (15.9)	7.32, d (15.6)	7.32, d (15.6)
19	5.85, d (15.5)	5.82, ^a d (15.6)	5.90, d (15.9)	5.86, d (15.6)	5.86, d (15.6)
21	1.77, s	1.84, s	1.82, s	1.84, s	1.84, s
22	1.00, d (6.9)	1.07, d (6.7)	1.07, d (6.5)	1.06, d (6.7)	1.07, d (6.7)
23	1.01, d (6.9)	1.05, d (6.4)	1.06, d (6.4)	1.12, d (6.4)	1.05, d (6.4)
24	1.88, d (1.3)	1.89, d (1.9)	1.81, s	1.90, d (1.2)	1.88, d (1.2)
25	1.89, d (1.3)	1.88, d (0.9)	1.87, d (1.3)	1.87, d (1.2)	1.87, d (1.2)
OMe				3.72, s	3.72, s

^aOverlapping signals.Table 3. ¹³C NMR Spectroscopic Data of Preussilides B–F (2–6) (175 MHz, Methanol-*d*₄)

pos	2	3	4	5	6
	δ_{C} , type	δ_{C} , type	δ_{C} , type	δ_{C} , type	δ_{C} , type
1	29.4, CH ₃	29.8, CH ₃	29.8, CH ₃	23.7, CH ₃	29.8, CH ₃
2	209.9, C	209.3, C	209.7, C	68.1, CH	209.3, C
3	47.9, CH ₂	47.5, CH ₂	47.6, CH ₂	43.8, CH ₂	47.5, CH ₂
4	122.9, C	124.3, C	124.4, C	127.9, C	124.2, C
5	128.8, C	129.1, C	128.8, C	128.0, C	129.1, C
6	120.9, CH	124.1, CH	123.9, CH	124.5, CH	124.0, CH
7	143.9, C	139.0, C	139.0, C	137.6, C	139.0, C
8	39.5, CH ₂	43.6, CH ₂	43.7, CH ₂	42.4, CH ₂	43.6, CH ₂
9	43.6, CH	49.9, CH	49.9, CH	50.0, CH	49.9, CH
10	77.5, CH	214.4, C	214.7, C	214.7, C	214.4, C
11	43.3, CH	50.4, CH	50.4, CH	50.0, CH	50.4, CH
12	45.6, CH	51.7, CH	51.6, CH	52.0, CH	51.7, CH
13	39.2, CH	40.7, CH	40.8, CH	41.0, CH	40.7, CH
14	138.3, CH	136.9, CH	135.7, CH	138.3, CH	137.0, CH
15	132.2, C	133.5, C	133.2, C	132.7, C	133.5, C
16	143.7, CH	144.4, CH	140.3, CH	144.9, CH	144.7, CH
17	133.3, C	133.5, C	133.1, C	133.3, C	133.5, C
18	150.9, CH	152.1, CH	141.9, CH	152.1, CH	152.1, CH
19	119.7, ^b CH	118.0, CH	116.9, CH	117.1, CH	117.2, CH
20	172.5, ^b C	171.0, C	173.8, C	169.7, C	169.7, C
21	18.5, CH ₃	18.4, CH ₃	18.5, CH ₃	18.6, CH ₃	18.5, CH ₃
22	18.9, CH ₃	15.4, CH ₃	15.4, CH ₃	15.3, CH ₃	15.4, CH ₃
23	16.0, CH ₃	11.6, CH ₃	11.6, CH ₃	12.0, CH ₃	11.6, CH ₃
24	17.2, CH ₃	17.2, CH ₃	17.3, CH ₃	17.2, CH ₃	17.2, CH ₃
25	14.1, CH ₃	14.1, CH ₃	20.8, ^c CH ₃	14.0, CH ₃	14.0, CH ₃
OMe				52.1, CH ₃	52.1, CH ₃

^aOverlapping signals. ^bSignals were assigned from HSQC and HMBC. ^cChemical shift value supports the different double-bond geometry in 4.

supported by the downfield shift of the signals for H₂-3 in **2** at δ_{H} 2.89 and 3.45 (δ_{H} 1.96 dd and 2.53 dd in **1**). In contrast, a secondary alcohol was assigned to C-10 in **2** at δ_{H} 3.59 and δ_{C}

77.5, supported by upfield shifts of the carbon signals C-9 and C-11 at δ_{C} 43.6 and 43.3, respectively (δ_{C} 50.0 and δ_{C} 50.1 in **1**) and by relevant HMBC correlations. Thus, the planar

Table 4. Cytotoxic Effect (IC₅₀) of Preussilides A–F (1–6) against Different Normal and Cancer Cell Lines^a

cell line	IC ₅₀ [μM]						ref
	1	2	3	4	5	6	
mouse fibroblasts L929	6.5	17.3	9.1	24.7	80.0	53.6	1.7 × 10 ⁻³
HeLa cells KB3.1	6.0	11.3	2.5	17.4	23.0	51.2	6.1 × 10 ⁻⁵
squamous carcinoma A431	20.3	35.1	10.1	17.9	55.8	>2437.5	7.3 × 10 ⁻⁵
human lung carcinoma A549	60.3	70.3	22.9	47.9	41.2	>2437.5	1.5 × 10 ⁻⁴
ovarian carcinoma SKOV-3	22.6	32.4	15.6	20.19	29.1	>2437.5	2.36 × 10 ⁻⁵
human prostate cancer PC-3	47.7	60.2	18.4	45.4	41.2	>2437.5	2.5 × 10 ⁻⁴
human breast adenocarcinoma MCF-7	24.3	22.1	7.3	15.4	55.8	>2437.5	1.5 × 10 ⁻⁴
human osteosarcoma U2OS	7.03	>2511	6.8	>2523.7	>2425.6	22.2	1.04 × 10 ⁻⁴

^aReference: ephothilone B.

structure of **2** was assigned for preussilide B. Comprehensive analysis of ROESY data and coupling constant values indicated that the relative configuration of **2** is analogous to that of **1**. Furthermore, NOE correlations between H-10 and its neighbors H-9 and H-11 together with the small *J* values (2.5 Hz) showed that all three were on the same face of the decalin moiety. Preussilide B (**2**) again showed a negative Cotton effect at λ_{max} 316 nm (Δε = -48.21) and a positive Cotton effect at λ_{max} 270 nm (Δε = +29.04). Thus, the ECD data of **2** indicated an absolute configuration analogous to that of **1**, so that the absolute configuration of preussilide B (**2**) was unambiguously assigned as 9*R*, 10*R*, 11*S*, 12*S*, 13*R*.

Preussilide C (**3**) was obtained as a yellow gum. The molecular formula was determined as C₂₅H₃₂O₄ by positive HRESIMS analysis. The molecular weight of **3** showed a difference of 2 Da less than that of **1** and **2**, suggesting an additional double bond in **3**. The NMR data of **3** were very similar to those of **1** and **2**, except for the presence of two ketone carbonyl carbon signals at δ_C 209.3 and 214.4 in the ¹³C NMR spectrum (Table 3). In addition, the ¹³C NMR spectrum lacked the carbon signal for the oxygenated methines C-2 and C-10 in **1** and **2**, respectively. HMBC correlations confirmed the diketone planar structure of preussilide C (**3**) as shown in Figure 1. Compound **3** showed a similar ECD spectrum to that of **1**, with a negative Cotton effect at λ_{max} 304 nm (Δε = -27.09) and a positive Cotton effect at λ_{max} 265 nm (Δε = +13.96) (Figure 3). Thus, the absolute configuration of preussilide C (**3**) was deduced to be 9*R*, 11*S*, 12*S*, 13*R*.

Preussilide D (**4**) has the same molecular formula as preussilide C (**3**) (C₂₅H₃₂O₄) and showed nearly identical NMR spectra, except that the resonances attributed to methine C-18 shifted from δ_C 152.1, δ_H 7.30 in **3** to δ_C 141.9, δ_H 7.59 in **4**. Furthermore, the methyl group C-25 signals were shifted from δ_C 14.1, δ_H 1.89 in **3** to δ_C 20.8, δ_H 1.87, while methine C-16 was shifted from δ_C 144.4, δ_H 6.24 in **3** to δ_C 140.3, δ_H 6.08, suggesting that the unsaturated side chain of **4** incorporates a stereochemical change relative to **3**. The ROESY spectrum of **4** showed NOE correlations between H-16 and H₃-25, indicating the Δ^{16,17} *Z*-configuration. This was supported by an NOE between H-14 and H-18. Furthermore, the ¹³C NMR shift for H₃-25 (δ_C 20.8), which is downfield compared to H₃-25 in all preussilides confirms the *Z*-configuration at Δ^{16,17}. Consequently, the geometry of the double bonds in **4** was assigned as 14*E*, 16*Z*, 18*E*. The ECD data of **4** indicated the same absolute configuration of the decalin rings as for **3** (9*R*, 11*S*, 12*S*, 13*R*) (Figure 3).

Compounds **5** and **6** were identified as methylated derivatives of **1** and **3** with the molecular formulas of C₂₆H₃₆O₄ and C₂₆H₃₄O₄, respectively. The NMR spectra

showed additional methyl ester signals at δ_C 52.1, δ_H 3.72 in both compounds, indicating the esterification of the C-20 carboxylic acid in **5** and **6**. The ROESY and electronic circular dichroism (ECD) data of preussilide E (**5**) indicated the same absolute configuration as for **1** (2*S*, 9*R*, 11*S*, 12*S*, 13*R*) and the same absolute configuration for preussilide F (**6**) as that for **3** (9*R*, 11*S*, 12*S*, 13*R*). A culture broth from a small fermentation of the fungus was extracted with acetone, and contact with methanol was completely avoided in order to check the biogenetic origin of the methoxy groups in preussilides E (**5**) and F (**6**). The LCMS analysis provided an identical chromatogram showing the expected peaks for preussilides E (**5**) and F (**6**), which thus were confirmed as genuine metabolic products of the fungus.

The structurally closest related metabolites to preussilides are hamigerone, dihydrohamigerone,²⁰ antarones,¹⁹ and two unnamed “highly methylated polyketides”.²³ The hamigerones were isolated from *Hamigera avellanea*, and antarones were obtained from *Penicillium antarcticum*, while the unnamed “highly methylated polyketides” were isolated from a yeast-associated *Penicillium* species. Hamigerones were reported to have antifungal activity against the plant pathogens *Pyricularia oryzae* and *Venturia inaequalis*, while the “highly methylated polyketides” were active against *Sclerotinia sclerotiorum*. The antarones, however, were reported to be devoid of antimicrobial and cytotoxic effects.

The antimicrobial activity profile of preussilides A–F (1–6) was determined. The MIC values against filamentous fungi showed that only compounds **1** and **3** exhibited mild antifungal activity, whereas remaining compounds **2**, **4**, **5**, and **6** were inactive against the organisms tested (Supporting Information, Table S2). The MIC values of compounds **1** and **3** were determined against *Mucor plumbeus* as 150 and 37.5 μg/mL, respectively. Interestingly, the triene acid preussilide C (**3**) showed the strongest activity against *Aspergillus fumigatus*, with an MIC value of 8.3 μg/mL, and was thus more potent than the positive control cycloheximide (MIC 33.3 μg/mL), followed by preussilide A (**1**), with an MIC value of 35.5 μg/mL. Furthermore, in a standard disk assay, preussilides A (**1**) and C (**3**) inhibited the growth of the plant pathogen *S. sclerotiorum*, affording inhibition zones of ca. 28 and 29 mm, respectively, at 100 μg/paper disk, as compared to the positive control nystatin (32 mm at 20 μg/paper disk) after 5 days. No antibacterial or antiyeast activity (see Supporting Information) was observed with preussilides. No nematocidal activity at up to 100 μg/mL against *Caenorhabditis elegans* and no phytotoxic effects in plant germination assays with *Setaria italica* and *Lepidium sativum* at 100 μg/paper disk were observed.

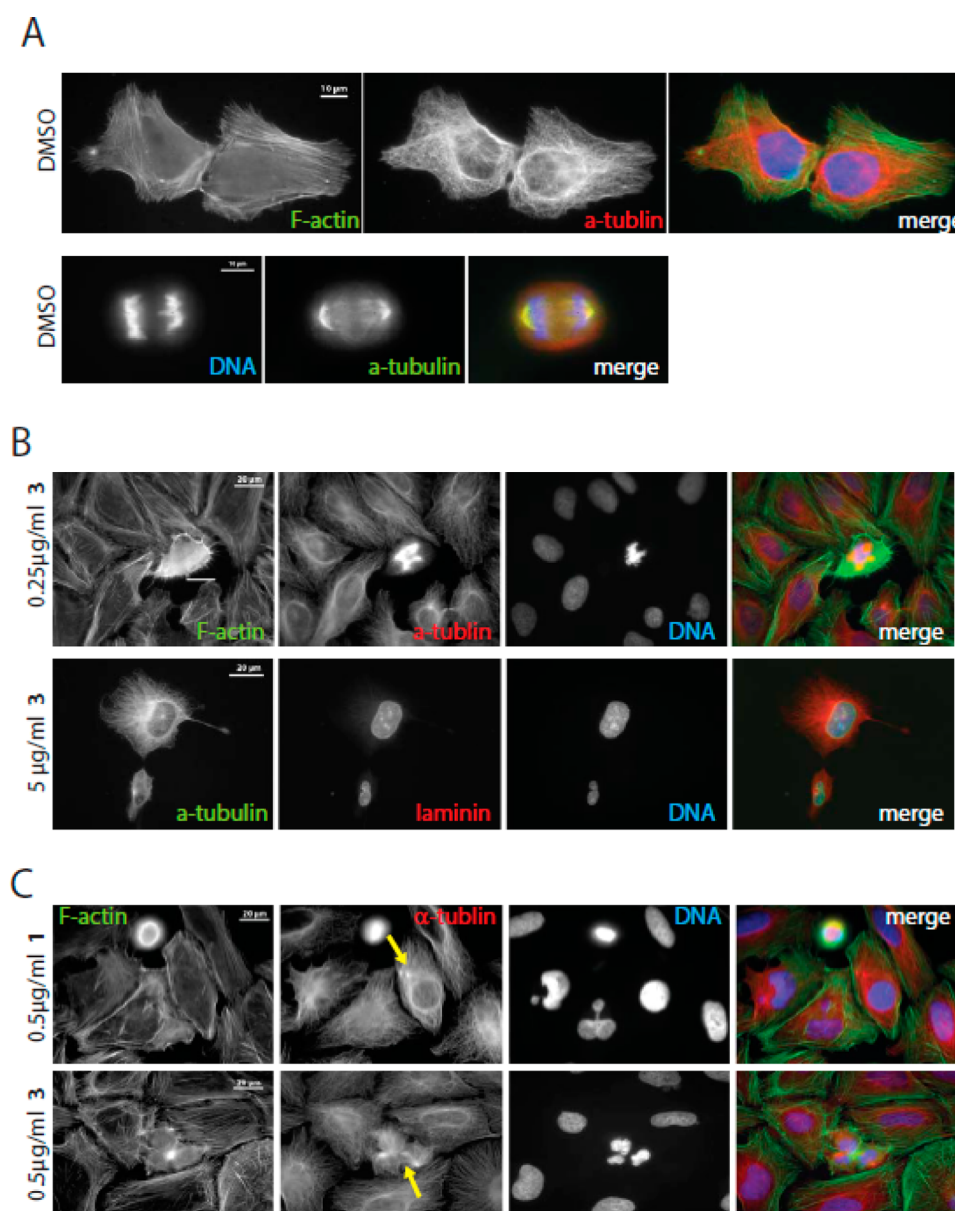


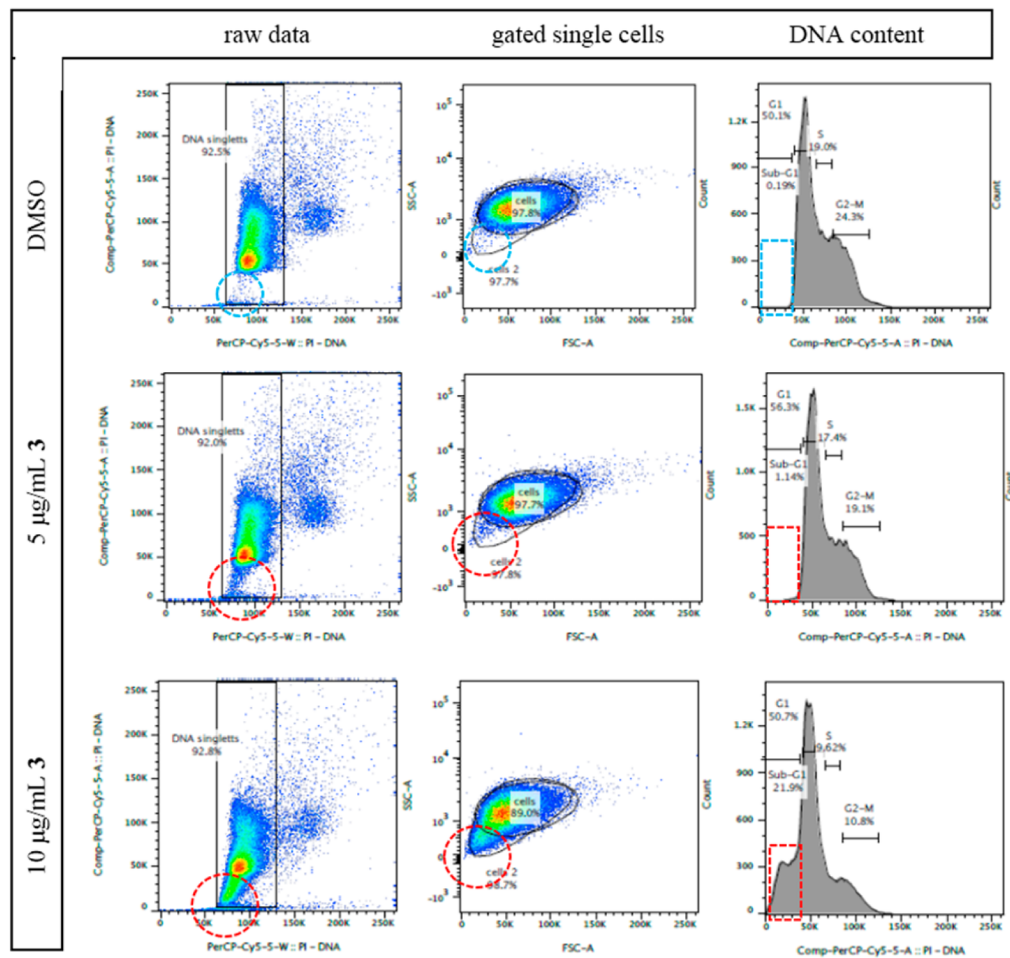
Figure 4. Effects of preussilides A and C (1 and 3) on the morphology of human osteosarcoma cells (U2OS). The actin cytoskeleton is not altered upon treatment (B and C) as compared to controls (A). Antibody staining of microtubules (as indicated in the panels) uncovers multipolar and duplicated spindles in treated cell populations as compared to predominantly canonical bipolar spindles in mock-treated cells (DMSO-treated U2OS). Aberrantly sized cells with abnormal small nuclei are observed in treated cells (B, bottom panel). Note that small cells may originate from inaccurate cell division, e.g., due to spindle multiplication. Pseudocolored merge is shown in the far right of every panel. Scale bar is 20 μm .

Cytotoxicity Screening. To evaluate cytotoxicity of the six polyketides on viability of different mammalian cell lines, we performed MTT assays. The results showed that all compounds exhibit modest to very weak cytotoxicity (Table 4) with IC_{50} values ranging from 2.5 to 80.0 μM . Only preussilides A (1) and C (3) showed IC_{50} values below 10 μM for the murine cells (L929) and cancer cell lines used (HeLa KB.3.1 and U2OS, in addition to MCF-7 for preussilide C only). However, their effect against the other cancer cell lines tended to lack activity. Moreover, all compounds caused nucleic fragmentation in the range of IC_{50} values in L929 cells (see Supporting Information).

Effects on Cell Morphology. To further analyze alterations observed in standard-screening assays, the actin and microtubule cytoskeleton, as well as the nuclear lamina and

DNA of treated cells, were stained. Effects were most pronounced when using preussilides A (1) and C (3), and a more detailed analysis of their biological effects was conducted. Complementary results from the other compounds can be viewed in the Supporting Information. Immunofluorescence experiments revealed that the actin cytoskeleton was not affected by any of the tested compounds. In contrast to actin, the microtubule cytoskeleton showed significant alterations during mitosis with multipolar spindles (Figure 4B,C) in a significant amount of dividing cells. Whereas this can in principle occur in cancer cells such as U2OS, multipolar spindles were rare in control-treated U2OS, which mainly displayed normal bipolar mitotic spindles, and properly divided cells (Figure 4A). Moreover, in treated populations we observed numerous “inaccurate” cell divisions, giving birth to

A



B

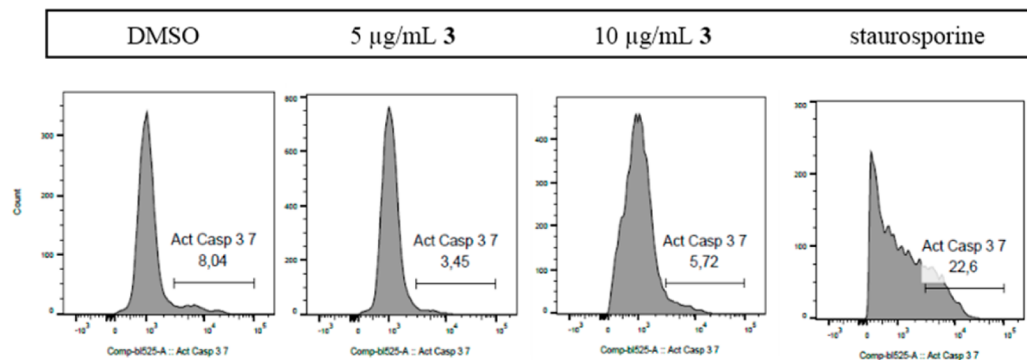


Figure 5. Preussilide treatment induces generation of small cells with reduced nuclear size in the human osteosarcoma cell line U2OS. (A) FACS data of PI-stained preussilides and control-treated cells. Note the occurrence of small cells/particles with low DNA content in the treated populations (middle panel, 5 µg/mL, 1.96% of cells; bottom panel, 10 µg/mL, 2.5% of cells) as compared to mock-treated (top panel, DMSO-treated, 0.19% of cells). When classifying cell cycle phases by analyzing the DNA content per cell/particle (right panel), this population fell into the sub-G1 window (outlined in red as compared to blue in the control). For a full panel on all compounds refer to the [Supporting Information](#)). (B) Cells treated with DMSO, 5 or 10 µg/mL of compound 3, or 250 nM staurosporine and stained with fluorescent caspase 3/7 Green substrate were analyzed by FACS. Note that there is no increase in apoptosis as compared to the DMSO control (8%) upon preussilide treatment (5 µg/mL 3.5% and 10 µg/mL 5.7%). In contrast, staurosporine induced significant programmed cell death (22.6%).

daughter cells with unequal cell and nuclear sizes (Figure 4B lower panel). Hence, this phenotype leads to unequal DNA distribution between the two new cells, while both daughter cells form a complete nucleus with intact nuclear lamina despite

the uneven size. The most significant effects were again observed in cells treated with preussilide C (3). Also, cells with fragmented nuclei were observed more frequently than in

control populations, reminiscent of the screening result in L929 cells.

In complementary experiments, preussilide-treated cells were subjected to FACS. To do so, cells were either left untreated, mock-treated, or treated with 5 and 10 $\mu\text{g}/\text{mL}$ of each compound, and prepared for flow cytometric analysis upon staining of DNA, tubulin, and lamin. DNA staining was used to classify cells according to cell cycle phases (G1, G2-M, S, and sub-G1). Strikingly, flow cytometry of cells treated with 5–10 $\mu\text{g}/\text{mL}$ of preussilides A (1) and C (3) revealed the appearance of a significant population of sub-G1 cells/particles (Figure 5A and Supporting Information, Figure S4). While this population in most cases indicated programmed cell death/apoptosis, we conclude that this sub-G1 population represents those smaller cells observed before eventually being derived from inaccurate cell divisions (Figure 4). This conclusion is supported by the fact that no apoptotic figures were observed in fluorescence microscopy experiments that could explain this population. To verify that we here induce a specific phenotype other than apoptosis, we repeated treatments leading to the most significant sub-G1 populations and specifically stained for caspase activation, a hallmark of apoptosis. As a positive control, cells were treated with staurosporine to induce apoptosis. The result clearly showed the small cells represented in the sub-G1 population in FACS experiments were not apoptotic, i.e., do not show caspase 3/7 activation, whereas staurosporine clearly induced apoptosis in U2OS cells (Figure 5B). Noteworthy, preussilide C-treated cells in general, and preussilide C-treated sub-G1 cells in particular, displayed increased amounts of tubulin and lamin staining (see Supporting Information), which also speaks against apoptosis that would otherwise lead to declining signals due to protein degradation.

Together, these data suggested that treatment with preussilides A (1) and C (3) had a profound effect on the cell cycle with multipolar spindles and inaccurate/unequal cell divisions, resulting in cells that cannot multiply further and die, explaining the loss of biomass observed in the cytotoxic screening. Some of these cells were abnormally small, as seen in immunofluorescence and as detected as a sub-G1 population in FACS. Apoptotic cell death appears not to be the predominant reason, as canonical apoptotic figures were rarely observed in immunofluorescence, and moreover, caspase 3/7 activation was at the detection level even after prolonged incubation with high concentrations of the most active preussilide C. Nonetheless, multipolar spindles were observed more frequently at concentrations as low as 0.25 $\mu\text{g}/\text{mL}$, which is 10- to 20-fold below concentrations showing significant cytotoxicity. Thus, our data indicate that the mechanism of cell manipulation by preussilides A (1) and C (3) might target an enzyme involved in coordination of the cell division cycle. Hence, they might, for instance, affect timing or spindle assembly mechanisms, leading to defects in chromosome segregation and/or spindle geometry.

EXPERIMENTAL SECTION

General Experimental Procedures. Optical rotations were determined with a PerkinElmer 241 MC polarimeter (using the sodium D line and a quartz cuvette with a 10 cm path length and 1 mL volume). UV/vis spectra were recorded on a Shimadzu UV/vis-2450 spectrophotometer using ethanol (UVASOL, Merck); CD spectra were recorded on a JASCO spectropolarimeter, model J-815. HPLC-DAD/MS analysis was performed using an amaZon speed ETD ion

trap mass spectrometer (Bruker Daltonics) in positive and negative ionization modes. The mass spectrometer was coupled to an Agilent 1260 series HPLC-UV system (Agilent Technologies) [column 2.1 \times 50 mm, 1.7 μm , C₁₈ Acquity uPLC BEH (Waters), solvent A: H₂O + 0.1% formic acid; solvent B: acetonitrile (ACN) + 0.1% formic acid, gradient: 5% B for 0.5 min, increasing to 100% B in 20 min, maintaining isocratic conditions at 100% B for 10 min, flow = 0.6 mL/min, UV-vis detection 200–600 nm]. HRESIMS spectra were recorded on a maXis ESI TOF mass spectrometer (Bruker Daltonics) [scan range m/z 100–2500, rate 2 Hz, capillary voltage 4500 V, dry temperature 200 °C], coupled to an Agilent 1200 series HPLC-UV system [column 2.1 \times 50 mm, 1.7 μm , C₁₈ Acquity uPLC BEH (Waters), solvent A: H₂O + 0.1% formic acid; solvent B: ACN + 0.1% formic acid, gradient: 5% B for 0.5 min, increasing to 100% B in 19.5 min, maintaining 100% B for 5 min, FR = 0.6 mL/min, UV-vis detection 200–600 nm]. The molecular formulas were calculated including the isotopic pattern (Smart Formula algorithm). Preparative HPLC purification was performed at room temperature on an Agilent 1100 series preparative HPLC system [ChemStation software (Rev. B.04.03 SP1); binary pump system; column: Kromasil RP C₁₈, particle size 7 μm , dimensions 250 \times 25 mm; mobile phase: ACN and water; flow rate 20 mL/min; diode-array UV detector; 226 fraction collector]. NMR spectra were recorded on a Bruker 500 MHz Avance III spectrometer with a BBFO (plus) SmartProbe (¹H 500 MHz, ¹³C 125 MHz) and a Bruker 700 MHz Avance III spectrometer with a 5 mm TCI cryoprobe (¹H 700 MHz, ¹³C 175 MHz), locked to the deuterium signal of the solvent. Data acquisition, processing, and spectral analysis were performed with standard Bruker software and ACD/NMR Spectrus. Chemical shifts are given in parts per million (ppm), and coupling constants in hertz (Hz). Spectra were measured in methanol-*d*₄ and acetone-*d*₆; chemical shifts were referenced to the solvent signals.

Strain Origin and Identification. The endophytic fungus *Preussia similis* strain DSM 104666 was isolated from healthy roots of the medicinal plant shrubby globularia (*Globularia alypum*) collected from Ain Touta, Batna 05000 (Algeria), in June 2015, according to established protocols involving surface sterilization.^{24,25} After purification, the fungus was maintained in 10% glycerol in a deep freezer at –80 °C and on YMG slant tubes.²⁶ *P. similis* strain DSM 104666 has been deposited at DSMZ (German Collection of Microorganisms and Cell Cultures, Braunschweig 38124, Germany). DNA from the fungal strain DSM 104666 was extracted using an EZ-10 Spin Column Genomic DNA Miniprep kit (Bio Basic Canada Inc., Markham, Ontario, Canada). Cell disruption and homogenization was performed using the homogenizer Precellys 24 (Bertin Technologies, France) at a speed of 6000 rpm for 40 s twice. The following primer combinations were used for amplification of three regions of the DNA template: ITS1F/ITS4 (5.8S gene region, the internal transcribed spacer 1 and 2, ITS),²⁷ LR0R and LR7 (part of large subunit, LSU),²⁸ and EF1-728F/EF-986R (elongation factor (EF)-1 α).²⁹ The fungal strain that produced the preussilides was identified as *P. similis* according to morphological and molecular phylogenetic methods (for more details, see the Supporting Information). The sequences used in this study were submitted to GenBank, and the accession numbers assigned to ITS, LSU, and EF-1 α gene sequences are KY652380, KY652379, and KY660720, respectively.

Fermentation and Extraction. Twelve 1 L Erlenmeyer flasks containing 400 mL of ZM/2 medium (0.5% molasses, 0.5% oatmeal, 0.15% glucose, 0.4% sucrose, 0.4% mannitol, 0.05% edamine, 0.05% ammonium sulfate, 0.15% calcium carbonate, pH 7.2) were inoculated with small pieces from mature yeast-malt-glucose-agar (YMG) plates and incubated on a rotary shaker at 23 °C and 140 rpm.^{17,30} After 34 days, the free glucose was completely depleted as determined by commercial glucose test strips, and the cultures were harvested.²⁶ The mycelium was separated from the fermentation broth by vacuum filtration and extracted three times with acetone in an ultrasonic bath at 40 °C for 30 min. The solvent was evaporated *in vacuo* until some aqueous phase remained, followed by three extractions with equal amounts of EtOAc and water. The solvent extract was dried over anhydrous sodium sulfate, filtered, and concentrated under vacuum to

yield the mycelial crude extract. To prepare the crude extract from the supernatant, the culture filtrate was treated with 2% adsorber resin Amberlite XAD-16N. After filtration, the XAD was extracted three times with acetone in an ultrasonic bath at 40 °C for 30 min. The eluate was then treated as described above for the mycelial extract.

Isolation. The crude mycelial extract (850 mg) was subjected to flash chromatography (GRACE Reveleris X2 flash system) with silica gel (40 g) as stationary phase. The column was eluted with mixtures of solvents [solvent A: CH₂Cl₂, solvent B: CH₂Cl₂/acetone (80/20, v/v), solvent C: CH₂Cl₂/acetone/MeOH (56/14/30, v/v/v)]. First gradient (AB system) from 0% B to 12% B in 12 min and from 12% B to 20% B in 8 min, second gradient (BC system) from 20% B to 60% C in 20 min and 60% C to 100% C in 10 min and 100% C isocratic for 10 min, flow rate 40 mL min⁻¹, UV detection 254, 280, and 380 nm. Six fractions were collected: F1 (551 mg, *t_R* = 2–6.2 min), F2 (13 mg, *t_R* = 6.9–7.5 min), F3 (17 mg, *t_R* = 8.1–10 min), F4 (10 mg, *t_R* = 11.9–15.7 min), F5 (11.5 mg, *t_R* = 22.9–23.3 min), and F6 (73 mg, *t_R* = 23.7–24.5 min). Fraction 1 was further purified by preparative HPLC using a gradient of 55% to 70% solvent B in 50 min, 70% to 100% B for 10 min, and 100% B isocratic for 5 min. The fractions were combined according to UV absorption at 220, 310, and 325 nm and concurrent HPLC-MS analyses. Compound 5 (19 mg) was obtained at *t_R* = 30.9 min, and compound 6 (15 mg) was eluted at *t_R* = 38.9 min. Fraction F6 (73 mg) and the crude extract derived from the supernatant (202 mg) were pooled based on similarity in their LC-MS data and further fractionated by the same preparative HPLC protocol using isocratic conditions: 53% solvent B for 40 min. Compounds 1 (9.5 mg), 2 (2 mg), 3 (17 mg), and 4 (2 mg) were eluted respectively at the following retention times: 13.6, 18.2, 21.0, and 27.7 min.

Preussilide A (1): pale yellow gum; [α]_D²⁵ -416 (*c* 0.1, EtOH); UV (*c* 0.05 mg/mL, EtOH) λ_{\max} (log ϵ) 282 (3.71), 206 nm (3.72); CD (*c* 1 mg/mL, EtOH) λ_{\max} ($\Delta\epsilon$) 302 (-15.01), 265 nm (+8.80); LCMS *m/z* 399 [M + H]⁺ (52), 421 [M + Na]⁺ (44), 381 [M + H - H₂O]⁺ (100), 397 [M - H]⁻ (50), 795 [2M - H]⁻ (100); HRESIMS *m/z* 399.2518 [M + H]⁺ (calcd for C₂₅H₃₅O₄⁺, 399.2530); ¹H NMR and ¹³C NMR see Table 1.

Preussilide B (2): pale yellow gum; [α]_D²⁵ -208 (*c* 0.1, EtOH); UV (*c* 0.05 mg/mL, EtOH) λ_{\max} (log ϵ) 291 nm (4.35); CD (*c* 1 mg/mL, EtOH) λ_{\max} ($\Delta\epsilon$) 316 (-48.21), 270 nm (+29.04); LCMS *m/z* 399 [M + H]⁺ (51), 421 [M + Na]⁺ (31), 381 [M + H - H₂O]⁺ (63), 397 [M - H]⁻ (100), 795 [2M - H]⁻ (53); HRESIMS *m/z* 399.2519 [M + H]⁺ (calcd for C₂₅H₃₅O₄⁺, 399.2530); ¹H NMR and ¹³C NMR see Tables 2 and 3.

Preussilide C (3): yellow gum; [α]_D²⁵ -78 (*c* 0.1, EtOH); UV (*c* 0.05 mg/mL, EtOH) λ_{\max} (log ϵ) 282 (4.50), 202 nm (4.61); CD (*c* 1 mg/mL, EtOH) λ_{\max} ($\Delta\epsilon$) 304 (-27.09), 265 nm (+13.96); LCMS *m/z* 397 [M + H]⁺ (48), 419 [M + Na]⁺ (71), 379 [M + H - H₂O]⁺ (100), 395 [M - H]⁻ (100), 791 [2M - H]⁻ (89); HRESIMS *m/z* 397.2362 [M + H]⁺ (calcd for C₂₅H₃₃O₄⁺, 397.2373); ¹H NMR and ¹³C NMR see Tables 2 and 3.

Preussilide D (4): pale yellow gum; [α]_D²⁵ -211 (*c* 0.1, EtOH); UV (*c* 0.05 mg/mL, EtOH) λ_{\max} (log ϵ) 281 (4.67), 206 nm (4.62); CD (*c* 1 mg/mL, EtOH) λ_{\max} ($\Delta\epsilon$) 300 (-57.0), 262 nm (+20.66); LCMS *m/z* 397 [M + H]⁺ (4), 419 [M + Na]⁺ (48), 816 [2M + Na]⁺ (100), 379 [M + H - H₂O]⁺ (7), 395 [M - H]⁻ (100), 792 [2M - H]⁻ (84); HRESIMS *m/z* 397.2362 [M + H]⁺ (calcd for C₂₅H₃₃O₄⁺, 397.2373); ¹H NMR and ¹³C NMR see Tables 2 and 3.

Preussilide E (5): pale yellow gum; [α]_D²⁵ -170 (*c* 0.1, EtOH); UV (*c* 0.05 mg/mL, EtOH) λ_{\max} (log ϵ) 299 (4.67), 202 nm (4.57); CD (*c* 1 mg/mL, EtOH) λ_{\max} ($\Delta\epsilon$) 310 (-56.17), 271 nm (+35.11); LCMS *m/z* 413 [M + H]⁺ (17), 435 [M + Na]⁺ (23), 395 [M + H - H₂O]⁺ (68), 411 [M - H]⁻ (4), 457 [M - H + HCOOH]⁻ (100); HRESIMS *m/z* 413.2685 [M + H]⁺ (calcd for C₂₆H₃₇O₄⁺, 413.2686); ¹H NMR and ¹³C NMR see Tables 2 and 3.

Preussilide F (6): yellow gum; [α]_D²⁵ -167 (*c* 0.1, EtOH); UV (*c* 0.05 mg/mL, EtOH) λ_{\max} (log ϵ) 261 (4.24), 206 nm (4.44); CD (*c* 1 mg/mL, EtOH) λ_{\max} ($\Delta\epsilon$) 302 (-7.05), 194 nm (+4.58); LCMS *m/z* 411 [M + H]⁺ (29), 433 [M + Na]⁺ (50), 393 [M + H - H₂O]⁺ (34),

409 [M - H]⁻ (100); HRESIMS *m/z* 411.2531 [M + H]⁺ (calcd for C₂₆H₃₅O₄⁺, 411.2530); ¹H NMR and ¹³C NMR see Tables 2 and 3.

Preparation of the S- and R-MTPA Esters of Preussilide A (1). R-(−)-MTPA-Cl (10 μ L) was added to a stirred solution of preussilide A (1) (1 mg) and dry pyridine (5 μ L) in dry CDCl₃ (100 μ L) at room temperature. After complete consumption of preussilide A (1 h), the reaction mixture was diluted by addition of 400 μ L of CDCl₃. The produced S-MTPA ester of 1 was submitted to NMR spectroscopy; for ¹H NMR data see the Supporting Information, Table S4. In an entirely analogous fashion, the R-MTPA ester of preussilide A (1) was prepared using S-(+)-MTPA-Cl; for ¹H NMR data see the Supporting Information, Table S4.

Biological Activity. The biological activities of the test compounds were evaluated in accordance with literature descriptions: the minimum inhibitory concentrations (MIC) toward bacteria, yeast, and filamentous fungi were obtained by a serial dilution technique using 96-well microtiter plates,³¹ except against the plant pathogen *S. sclerotiorum* DSM 1946, which did not produce spores. In this instance, a standard disk diffusion assay was performed on YMG medium supplemented with a mycelial suspension of test fungus (20 μ g/paper disk of nystatin was used as a positive control).³² Nematicidal activities were determined *in vitro* on the free-living nematode *C. elegans* as a model.³³ Phytotoxic activities were carried out by germination and seedling growth bioassay against *S. italic* and *L. sativum*.³⁴

Cytotoxicity Assay. The cytotoxicity effects (IC₅₀) of all compounds were determined against a panel of eight mammalian cell lines including mouse fibroblasts L929, HeLa cells KB3.1, squamous carcinoma A431, human lung carcinoma A549, ovarian carcinoma SKOV-3, human prostate cancer PC-3, human breast adenocarcinoma MCF-7, and human osteosarcoma U2OS, by using a 5-day MTT assay according to established procedures.³⁵

U2OS Treatment with the New Compounds. Human osteosarcoma cells U2OS (ACC785-DSMZ, Braunschweig, Germany) were grown in DMEM, 4.5 g/L glucose (Ivitrogen, Germany) with 10% fetal bovine serum (Sigma) and 1% glutamate, 1% sodium pyruvate, and 1% nonessential amino acids at 37 °C and 7% CO₂. U2OS cells were seeded on glass coverslips coated with fibronectin in 24-well plates (3 × 10⁴ cells/well) and allowed to adhere and spread for 16 h. Adhered cells were treated with varying concentrations (0.25, 0.5, 2.5, 5, and 10 μ g/mL in DMEM) prepared from a stock solution (1 mg/mL in DMSO) of the six compounds for 24 h. DMSO-treated cells were prepared as a negative control. Subsequent staining of DNA, actin filaments, and microtubules was carried out. For actin and tubulin labeling, the treated cells were fixed with 4% paraformaldehyde (PFA) in phosphate-buffered saline (PBS) for 20 min and washed with PBS. Immunofluorescence staining was performed according to standard procedures by using a mouse monoclonal anti- α -tubulin antibody (Sigma-Aldrich, clone DM1A) for microtubules (MTs) and Phalloidin Alexa Fluor 488 (ThermoFisher, A123799) for F-actin. Secondary reagents were goat anti-mouse Alexa 594 (ThermoFisher, A32723). Finally, after washing with PBS, coverslips were mounted on glass microscope slides in ProLong Diamond antifade mountant with DAPI (ThermoFisher, P36971).

Preussilides A–F (1–6) were probed for potential effects on the nuclear lamina during cell cycle phases. The cells were treated with 0.5 and 5 μ g/mL for 24 h, then fixed with ice-cold methanol for 15 min, and stepwise rehydrated using PBS. Cells were costained with antibodies against nuclear envelop and MTs by using anti-pan Lamin antibody (abcam, ab20740) and a rat monoclonal antibody to tyrosinated alpha-tubulin overnight. Goat anti-mouse Alexa Fluor 594 (A110329) and goat anti-rat Alexa Fluor 488 (A11006) were used as secondary reagents. Images were acquired on a Zeiss Axiovert 135TV microscope, equipped with a Coolsnap 4k cooled CCD device driven by VisiView software (Vistron Inc., Munich). Images were processed using Fiji (ImageJ)³⁶ and Photoshop CS6 (Adobe) software.

Flow Cytometry. Briefly, six-well plates were seeded with 7 × 10⁵/well U2OS cells and treated with 5 and 10 μ g/mL of preussilides (preussilide B was not tested due to sample limitation) for 18 h upon spreading. The cells were then harvested by trypsination and fixed with

2% PFA/PBS. After rehydration with PBS, cell pellets were collected by centrifugation at 500g, resuspended in ice cold methanol, and kept on ice for 30 min. Afterward, the cells were centrifuged and resuspended in FACS-buffer and stained with a mixture of anti-tubulin/anti-lamin antibodies as above in combination with RNase A and propidium iodide (PI) to stain DNA. As secondary antibodies, antibody goat anti-rat Alexa488 and goat anti-mouse Alexa647 (A-21235) were used. For detection of apoptosis, cells were incubated with the fluorescent substrate Cell Event caspase-3/7 green detection reagent C10723 (ThermoFisher) for 10 min prior to fixation. Staurosporine was used to induce apoptosis in U2OS as a positive control (250 nM for 16 h). Cells were analyzed using a FACS Canto (BD Biosciences). Data were analyzed using DIVA 6.1 software.

■ ASSOCIATED CONTENT

Supporting Information

The Supporting Information is available free of charge on the ACS Publications website at DOI: [10.1021/acs.jnatprod.7b00064](https://doi.org/10.1021/acs.jnatprod.7b00064).

Experimental procedures, 1D and 2D NMR data, LCMS data, morphological and phylogenetic details of the producing organism (PDF)

■ AUTHOR INFORMATION

Corresponding Author

*Tel: +49 531 6181-4240. Fax: +49 531 6181 9499. E-mail: marc.stadler@helmholtz-hzi.de.

ORCID

Marc Stadler: [0000-0002-7284-8671](https://orcid.org/0000-0002-7284-8671)

Notes

The authors declare no competing financial interest.

■ ACKNOWLEDGMENTS

S.R.N. acknowledges the Ministry of Higher Education and Scientific Research (MESRS) of Algeria for the financial support. S.E.H. is grateful for financial support from the Alexander von Humboldt Foundation. We are grateful to W. Collisi for conducting the bioassays, C. Kakoschke and C. Schwager for recording NMR and HPLC-MS data, A. Otto for excellent technical assistance in cell biology experiments, and M. Rohde for support with electron microscopy. Moreover, we thank C. Plaza for kindly providing the fluorescent substrate Cell Event caspase 3/7 and staurosporine.

■ REFERENCES



- (1) Bills, G. F.; Gloer, J. B. *Microbiol. Spectrum*, **2016**, *4*, [10.1128/microbiolspec.FUNK-0009-2016](https://doi.org/10.1128/microbiolspec.FUNK-0009-2016).
- (2) Schulz, B.; Haas, S.; Junker, C.; Andrée, N.; Schobert, M. *Curr. Sci.* **2015**, *109*, 39–45.
- (3) Ahmed, S. I.; Cain, R. F. *Can. J. Bot.* **1972**, *50*, 419–477.
- (4) Arenal, F.; Platas, G.; Peláez, F. *Fungal Divers.* **2005**, *20*, 1–15.
- (5) Arenal, F.; Platas, G.; Peláez, F. *Fungal Divers.* **2007**, *25*, 1–17.
- (6) Mapperson, R. R.; Kotiw, M.; Davis, R. A.; Dearnaley, J. D. W. *Curr. Microbiol.* **2014**, *68*, 30–37.
- (7) Abdullah, S. K.; Al-Saadoon; Abdullah, H.; Guarro, J. *Nova Hedw* **1999**, *69*, 211–216.
- (8) Krøys, Å.; Wedin, M. *Syst. Biodivers.* **2009**, *7*, 465–478.
- (9) Krøys, Å. *Phytotaxa* **2015**, *234*, 143–150.
- (10) Du, L.; King, J. B.; Morrow, B. H.; Shen, J. K.; Miller, A. N.; Cichewicz, R. H. *J. Nat. Prod.* **2012**, *75*, 1819–1823.
- (11) Du, L.; Robles, A. J.; King, J. B.; Mooberry, S. L.; Cichewicz, R. H. *J. Nat. Prod.* **2014**, *77*, 1459–1466.
- (12) Rangel-Grimaldo, M.; Rivero-Cruz, I.; Madariaga-Mazón, A.; Figueroa, M.; Mata, R. *J. Nat. Prod.* **2017**, *80*, 582.

- (13) Khan, R.; Cain, R. F. *Can. J. Bot.* **1979**, *57*, 1174–1186.
- (14) Arenal, F.; Platas, G.; Peláez, F. *Mycotaxon* **2004**, *89*, 137–151.
- (15) Weber, H. A.; Swenson, D. C.; Gloer, J. B.; Malloch, D. *Tetrahedron Lett.* **1992**, *33*, 1157–1160.
- (16) Weber, H. A.; Baenziger, N. C.; Gloer, J. B. *J. Am. Chem. Soc.* **1990**, *112*, 6718–6719.
- (17) Stadler, M.; Tichy, H.; Katsiou, E.; Hellwig, V. *Mycol. Prog.* **2003**, *2*, 95–122.
- (18) Karwehl, S.; Stadler, M. *Curr. Top. Microbiol. Immunol.* **2016**, *398*, 303–338.
- (19) Shiono, Y.; Seino, Y.; Koseki, T.; Murayama, T.; Kimura, K. I. *Z. Naturf.* **2008**, *63b*, 909–914.
- (20) Breinholt, J.; Kjoer, A.; Olsen, C. E.; Rassing, B. R.; Rosendahl, C. N. *Acta Chem. Scand.* **1997**, *51*, 1241–1244.
- (21) Harada, N.; Nakanishi, K. *Acc. Chem. Res.* **1972**, *5*, 257–263.
- (22) Boiadjev, S. E.; Lightner, D. A. *Monatsh. Chem.* **2005**, *136*, 489–508.
- (23) Stierle, D. B.; Stierle, A. A.; Ganser, B. K. *J. Nat. Prod.* **1999**, *62*, 1147–1150.
- (24) Lodge, D. J.; Fisher, P. J.; Sutton, B. C. *Mycologia* **1996**, *88*, 733–738.
- (25) Kusari, S.; Lamshöft, M.; Zühlke, S.; Spiteller, M. *J. Nat. Prod.* **2008**, *71*, 159–162.
- (26) Stadler, M.; Asakawa, Y.; Hashimoto, T.; Rogers, J. D.; Ju, Y.; Wetzstein, H. *Mycol. Res.* **2001**, *105*, 1191–1205.
- (27) White, T. J.; Bruns, T. D.; Lee, S. B. In *PCR Protocols: A Guide to Methods and Applications*; Academic Press: New York, 1990; pp 315–322.
- (28) Vilgalys, R.; Hester, M. *J. Bacteriol.* **1990**, *172*, 4238–4246.
- (29) Carbone, I.; Kohn, L. M. *Mycologia* **1999**, *3*, 553–556.
- (30) Kuhnert, E.; Surup, F.; Wiebach, V.; Bernecker, S.; Stadler, M. *Phytochemistry* **2015**, *117*, 116–122.
- (31) Surup, F.; Thongbai, B.; Kuhnert, E.; Sudarman, E.; Hyde, K. D.; Stadler, M. *J. Nat. Prod.* **2015**, *78*, 934–938.
- (32) Anke, H.; Zähler, H. *Arch. Microbiol.* **1978**, *116*, 253–257.
- (33) Stadler, M.; Anke, H.; Bergquist, K. E.; Sterner, O. *J. Antibiot.* **1993**, *46*, 968–971.
- (34) Anke, H.; Hillen-Maske, E.; Steglich, W. *Z. Naturforsch.* **1989**, *44C*, 7–11.
- (35) Wittstein, K.; Rascher, M.; Rupcic, Z.; Löwen, E.; Winter, B.; Köster, R. W.; Stadler, M. *J. Nat. Prod.* **2016**, *79*, 2264–2269.
- (36) Schindelin, J.; Arganda-Carreras, I.; Frise, E.; Kaynig, V.; Longair, M.; Pietzsch, T.; Preibisch, S.; Rueden, C.; Saalfeld, S.; Schmid, B.; Tinevez, J.-Y. J.-Y.; White, D. J.; Hartenstein, V.; Eliceiri, K.; Tomancak, P.; Cardona, A.; Liceiri, K.; Tomancak, P.; A, C. *Nat. Methods* **2012**, *9*, 676–682.

Paper II

Article

Furanones and Anthranilic Acid Derivatives from the Endophytic Fungus *Dendrothyrium variisporum*

Rémy B. Teponno^{1,2,†}, Sara R. Noumeur^{1,3,4,†}, Soleiman E. Helaly^{1,5} , Stephan Hüttel¹, Daoud Harzallah³ and Marc Stadler^{1,*} 

¹ Department of Microbial Drugs, Helmholtz Centre for Infection Research and German Centre for Infection Research (DZIF), partner site Hannover/Braunschweig, Inhoffenstrasse 7, 38124 Braunschweig, Germany; remyteponno@gmail.com (R.B.T.); noumeur.sara@gmail.com (S.R.N.); soleiman.helaly@aswu.edu.eg (S.E.H.); Stephan.Huettel@helmholtz-hzi.de (S.H.)

² Department of Chemistry, Faculty of Science, University of Dschang, P.O. Box 67, Dschang, Cameroon

³ Laboratory of Applied Microbiology, Department of Microbiology, Faculty of Natural and Life Sciences, University Sétif 1 Ferhat Abbas, 19000 Sétif, Algeria; harzallahdaoud@univ-setif.dz

⁴ Department of Microbiology-Biochemistry, Faculty of Natural and Life Sciences, University of Batna 2, 05000 Batna, Algeria

⁵ Department of Chemistry, Faculty of Science, Aswan University, 81528 Aswan, Egypt

* Correspondence: marc.stadler@helmholtz-hzi.de; Tel.: +49-531-6181-4240; Fax: +49-531-6181-9499

† These authors contributed equally to this work.

Received: 18 September 2017; Accepted: 6 October 2017; Published: 9 October 2017

Abstract: Extracts from an endophytic fungus isolated from the roots of the Algerian plant *Globularia alypum* showed prominent antimicrobial activity in a screening for novel antibiotics. The producer organism was identified as *Dendrothyrium variisporum* by means of morphological studies and molecular phylogenetic methods. Studies on the secondary metabolite production of this strain in various culture media revealed that the major components from shake flasks were massarilactones D (1) and H (2) as well as two new furanone derivatives for which we propose the trivial names (5*S*)-*cis*-gregatin B (3) and graminin D (4). Scale-up of the fermentation in a 10 L bioreactor yielded massarilactone D and several further metabolites. Among those were three new anthranilic acid derivatives (5–7), two known anthranilic acid analogues (8 and 9) and three cyclopeptides (10–12). Their structures were elucidated on the basis of extensive spectroscopic analysis (1D- and 2D-NMR), high-resolution mass spectrometry (HRESIMS), and the application of the modified Mosher's method. The isolated metabolites were tested for antimicrobial and cytotoxic activities against various bacteria, fungi, and two mammalian cell lines. The new Metabolite 5 and Compound 9 exhibited antimicrobial activity while Compound 9 showed cytotoxicity activity against KB3.1 cells.

Keywords: Montagnulaceae; *Dendrothyrium variisporum*; fermentation; furancarboxylic acid derivatives; anthranilic acid derivatives; antimicrobial activity; cytotoxicity

1. Introduction

Fungi are a rich source of secondary metabolites that may serve as leads for the development of badly needed novel antibiotics and anticancer agents. In particular, certain ecological groups of fungi like the endophytes have recently been proven to yield a plethora of novel metabolites exhibiting a variety of biological activities [1]. During the course of our studies on endophytic strains derived from plants collected in Algeria, we have encountered various interesting organisms that produced new chemical entities, such as the preussilides from *Preussia similis* [2]. The current study deals with the evaluation of the taxonomy and intensive studies on the secondary metabolite production of another

interesting strain *Dendrothyrium variisporum*, a coniothyrium-like fungus that was isolated during the same campaign from *Globularia alypum* Linn. (Plantaginaceae). This is the first report describing the secondary metabolites profile of the genus *Dendrothyrium* Verkley, Göker & Stielow, which was described recently as a new coelomycete genus belonging to the family Montagnulaceae [3].

2. Results and Discussion

Dendrothyrium variisporum was shown to produce in flasks mainly the polyketide massarilactone D (1) and as well as massarilactone H (2) and two new minor furanone derivatives 3 and 4. However, HPLC-MS analysis of the crude extracts revealed the presence of numerous minor constituents that could not be isolated in sufficient quantities to allow for their complete structure elucidation. To increase the amount of biologically active products, a fully controlled bioreactor experiment on a 10 L scale was conducted. A small amount of the culture medium was collected after each 24 h, extracted and analyzed using HPLCAD-MS for the estimation of metabolite production. After 8 days, the free glucose was completely depleted as determined by commercial glucose test strips, and the cultures were harvested as previously described [4]. From the resulting extracts, Metabolites 5–12 were isolated in addition to massarilactone D (Figure 1).

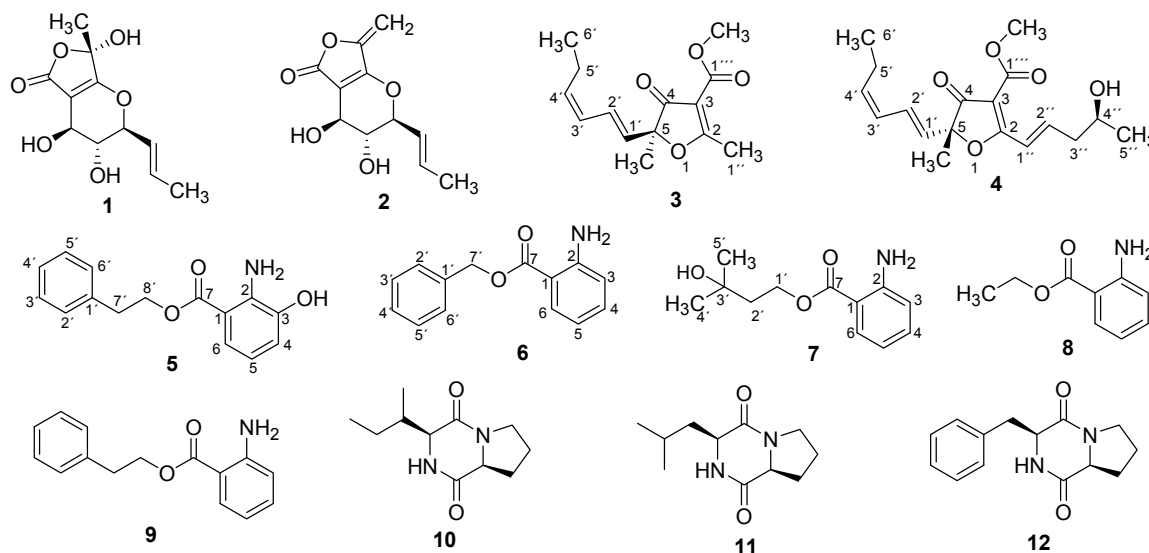


Figure 1. Structures of secondary metabolites isolated from *Dendrothyrium variisporum*.

Compound 3, isolated as colorless oil, was assigned the molecular formula $C_{14}H_{18}O_4$ (six double-bond equivalents) on the basis of HRESIMS ion cluster $[M + H]^+$ at m/z 251.1276 (Calcd. 251.1278). Its UV spectrum showed intense absorption maxima at 220 and 265 nm. The 1H -NMR spectrum exhibited resonances attributed to two tertiary methyl groups at δ_H 1.56 (s, Me-5) and 2.66 (s, H-1''), one primary methyl group at δ_H 1.01 (t, $J = 7.3$ Hz, H-6'), one methoxyl at δ_H 3.88 (s), and four olefinic proton signals at δ_H 6.59 (ddd, $J = 15.5$ Hz, 11.2 Hz, 1.3 Hz, H-2'), 5.90 (t, $J = 11.2$ Hz, H-3'), 5.63 (d, $J = 15.5$ Hz, H-1'), and 5.53 (dt, $J = 10.8$ Hz, 7.7 Hz, H-4') (Table 1). The ^{13}C -NMR showed the characteristic signals of furancarboxylic acid derivatives at δ_C 197.8 (C-4), 195.6 (C-2), 163.4 (C-1'''), 106.8 (C-3), and 91.4 (C-5) [5,6]. Other important signals were those of olefinic carbons at δ_C 136.9 (C-4'), 127.6 (C-1'), 126.5 (C-2'), and 126.2 (C-3'). The *E* geometry was assigned to the $\Delta^{1',2'}$ double bond based on the existence of a coupling constant of 15.5 Hz between H-1' and H-2', whereas a coupling constant of 10.8 Hz between H-3' and H-4' was in favor of the *Z* configuration for the $\Delta^{3',4'}$ double bond [5]. Careful examination of the 1H - 1H COSY, HSQC, and HMBC spectra (Figure 2) proved that 3 was similar to *cis*-gregatin B recently isolated from the ascomycete *Pulvinula* sp. 11120 [6]. The configuration at C-5 was proposed to be *S* based on the negative optical rotation of 3 (-36.67) by opposition to that

of (*R*)-*cis*-gregatin B (+168). Furthermore, the negative Cotton effect observed in the 255–265 nm region of the electronic circular dichroism (ECD) curves of Compound **3** in EtOH (Figure 3), when compared to the ECD spectra of aspertetronin A, was indicative of the *S* configuration [7]. The new natural furanone was finally elucidated as methyl (5*S*)-5-[(1'*E*,3'*Z*)-hexa-1,3-dienyl]-5-methyl-4-oxo-2-methyl-4,5-dihydrofuran-3-carboxylate ((5*S*) *cis*-gregatin B).

Table 1. ¹³C- and ¹H-NMR spectroscopic data of Compounds **3** and **4** (175 and 700 MHz, resp.; CDCl₃; δ in ppm).

Position	3		4	
	δ _C , Type	δ _H (J in Hz)	δ _C , Type	δ _H (J in Hz)
2	195.6, C	/	184.3, C	/
3	106.8, C	/	104.3, C	/
4	197.8, C	/	198.2, C	/
5	91.4, C	/	90.7, C	/
1'	127.6, CH	5.63, d (15.5)	128.2, CH	5.65, d (15.5)
2'	126.5, CH	6.59, ddd (15.5, 11.2, 1.3)	126.5, CH	6.59, ddd (15.5, 11.2, 1.3)
3'	126.2, CH	5.90, t (11.2)	126.3, CH	5.90, t (11.2)
4'	136.9, CH	5.53, d (10.8, 7.7)	136.7, CH	5.52, dt (10.8, 7.7)
5'	21.2, CH ₂	2.21, m	21.1, CH ₂	2.19, m
6'	14.1, CH ₃	1.01, t (7.3)	14.1, CH ₃	1.00, t (7.3)
1''			121.6, CH	7.41, dt (15.9, 1.7)
2''			145.1, CH	7.21, dt (15.9, 7.3)
3''			42.9, CH ₂	2.55, m
4''			67.0, CH	4.08, m
5''			23.6, CH ₃	1.31, d (6.2)
1'''	163.4, C	/	163.4, C	/
Me-5	22.5, CH ₃	1.56, s	22.5, CH ₃	1.58, s
OMe	51.6, CH ₃	3.83, s	51.7, CH ₃	3.85, s

The molecular formula of Metabolite **4**, also isolated as colorless oil, was deduced to be C₁₈H₂₄O₅ from the HRESIMS which showed ion clusters [M + H]⁺ at *m/z* 321.1690 (Calcd. 321.1697) and [2M + Na]⁺ at *m/z* 663.3130 (Calcd. 663.3140). The UV spectrum showed in addition to the absorption maxima at 216 and 255 nm as in Compound **3**, another band at 310 nm indicative of an extensive conjugated system. The ¹H-NMR spectrum showed signals attributed to a tertiary methyl group at δ_H 1.58 (s, Me-5), a secondary methyl group at δ_H 1.31 (d, *J* = 6.2 Hz, H-5''), a primary methyl group at δ_H 1.00 (t, *J* = 7.3 Hz, H-6'), an oxymethine proton at δ_H 4.08 (m, H-4'') and one methoxyl (δ_H 3.88 (s)). The resonances of six olefinic protons at δ_H 7.41 (dt, *J* = 15.9 Hz, 1.7 Hz, H-1''), 7.21 (dt, *J* = 15.9 Hz, 7.3 Hz, H-2''), 6.59 (ddd, *J* = 15.5 Hz, 11.2 Hz, 1.3 Hz, H-2'), 5.90 (t, *J* = 11.2 Hz, H-3'), 5.65 (d, *J* = 15.5 Hz, H-1'), and 5.52 (dt, *J* = 10.8 Hz, 7.7 Hz, H-4') were also observed (Table 1). Its ¹³C-NMR spectrum exhibited the characteristic signals of furancarboxylic acid derivatives at δ_C 198.2 (C-4), 184.3 (C-2), 163.4 (C-1'''), 104.3 (C-3), and 90.7 (C-5). The downfield shift of C-2 (δ_C 184.3) in Compound **4**, compared to **3** (δ_C 195.6) was in favor of the fixation of an olefinic carbon at C-2, which was evidenced by carbon signals at δ_C 121.6 (C-1'') and 145.1 (C-2''). This was further confirmed by the HMBC correlation observed between H-1'' (δ_H 7.41) and C-2 and between H-2'' (δ_H 7.21) and C-2. The ¹H- and ¹³C-NMR data of **4** were almost identical with those of graminin C [6] with the same chain attached to C-5. The only difference was the presence of one hydroxyl in the fragment attached to C-2. This hydroxyl group was located at C-4'' as evidenced not only by the ¹H-¹H COSY correlation depicted between the secondary methyl signal at δ_H 1.31 (d, *J* = 6.2 Hz, H-5'') and the proton at δ_H 4.08 (m, H-4''), but also by HMBC correlations observed between H-3'' (δ_H 2.55 (m)) and C-4'' (δ_C 67.0) and between H-2'' (δ_H 7.21 (dt, *J* = 15.9 Hz, 7.3 Hz)) and C-4'' (δ_C 67.0) (Figure 2). The *E* geometry was assigned to the Δ^{1',2'} double bond based on the existence of a coupling constant of 15.5 Hz between H-1' and H-2', whereas a coupling constant of 10.8 Hz

between H-3' and H-4' was in favor of the *Z* configuration for the $\Delta^{3',4'}$ double bond. The geometry of the $\Delta^{1'',2''}$ double bond was determined from the coupling constant $J_{1'',2''} = 15.9$ Hz, indicating an *E*-configuration. The configuration at C-5 was assigned by comparison of its CD characteristics (Figure 3) with those of Compound 3. The CD spectrum of 4 showed a positive Cotton effect in the 255–265 nm region (opposite to that of 3), so a *5R* configuration was concluded. The *S* configuration was assigned to C-4'' based on the analysis of the $\Delta\delta^{SR}$ values of the MTPA esters prepared from 4 [8]. The $\Delta\delta^{SR}$ differences of the MTPA esters revealed a negative value of -0.17 for H-5'', while the $\Delta\delta^{SR}$ value for H-3'' was $+0.05$ ppm (Figure 4) (Table S1). The structure of 4 was finally concluded as (5*R*)-5-[(1'*E*,3'*Z*)-hexa-1,3-dienyl]-5-methyl-4-oxo-2-[(4*S*,1*E*)-4-hydroxypent-1-enyl]-4,5-dihydrofuran-3-carboxylate, trivially named graminin D in agreement with the known compound graminin C without the hydroxyl group at C-4'' [6]. Compounds 3 and 4 are furancarboxylic acid derivatives, a structural class of natural oxygenated heterocycles that have been reported only from fungi of the genera *Aspergillus*, *Cephalosporium* (*Acremonium*), *Paraconiothyrium*, *Penicillium*, and *Pulvinula* [5,6]. Their core structure after several revisions was finally elucidated to 4-(methoxycarbonyl)furan-3(2*H*)-one from degradation reactions and total synthesis [9].

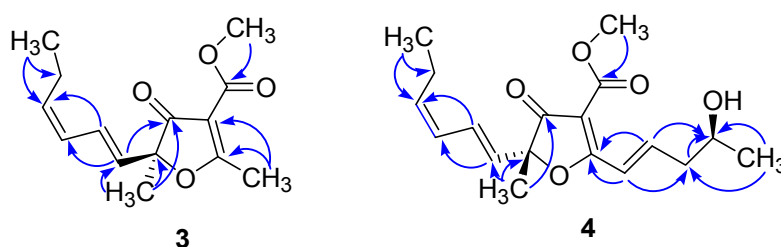


Figure 2. Selected HMBC correlations for Compounds 3 and 4.

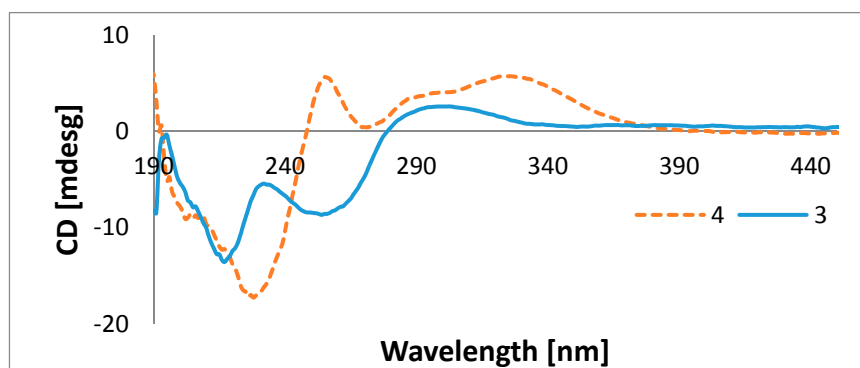


Figure 3. ECD spectra of Compounds 3 and 4 in ethanol.

Compound 5 was isolated as a brown gum. Its molecular formula $C_{15}H_{15}NO_3$ was established by the positive ion mode HRESIMS, which showed ion clusters at m/z 258.1128 $[M + H]^+$ (calcd. for $C_{15}H_{16}NO_3^+$: 258.1125) and 280.0946 $[M + Na]^+$ (calcd. for $C_{15}H_{15}NNaO_3^+$: 280.0944). The absorption maxima observed in the UV spectrum at λ_{max} 226, 260, and 342 nm suggested that 5 might be an anthranilic acid derivative [10]. The 1H -NMR spectrum exhibited three signals at δ_H 7.35 (dd, $J = 8.1$ Hz, 1.4 Hz, H-6), 6.90 (dd, $J = 7.8$ Hz, 1.4 Hz, H-4), and 6.66 (t, $J = 7.9$ Hz, H-5), indicating the presence of a system of three vicinal aromatic protons (Table 3). The two triplets (integrating for two protons each) located at δ_H 3.06 (t, $J = 6.9$ Hz, H-7') and 4.48 (t, $J = 6.9$ Hz, H-8') together with the signal integrating for four protons centered at δ_H 7.30 (H-2', H-3', H-5' and H-6') and the multiplet at δ_H 7.22 (H-4') were characteristic of a 2-phenylethyl group. The ^{13}C -NMR and DEPT NMR spectra showed 15 signals, including those of the 3-hydroxyanthranilic acid moiety at δ_C 169.2 (C-7), 147.8 (C-3), 137.5 (C-2), 122.8 (C-6), 119.5 (C-4), 119.0 (C-5), and 115.0 (C-1) [11]. The presence of the phenylethyl

group was evidenced by resonances of two methylenes at δ_C 36.3 (C-7'), 66.5 (C-8'), and aromatic carbon signals at δ_C 139.7 (C-1'), 130.2 (C-2' and C-6'), 129.7 (C-3' and C-5'), and 127.7 (C-7') (Table 2). The gross structure of **5** was determined by a combination of ^1H - ^1H COSY, HSQC, and HMBC spectra. The correlations shown by the HMBC spectrum (Figure 5) from H-6 (δ_H 7.35 (dd, $J = 8.1$ Hz, 1.4 Hz)) to C-7 (δ_C 169.2), C-2 (δ_C 137.5), and C-1 (δ_C 115.0) and from H-8' (δ_H 4.48 (t, $J = 6.9$ Hz)) to C-7 (δ_C 169.2), C-7' (δ_C 36.3), and C-1' (δ_C 139.6) confirmed the structure of the previously unreported Metabolite **5** as 2-phenylethyl 3-hydroxyanthranilate.

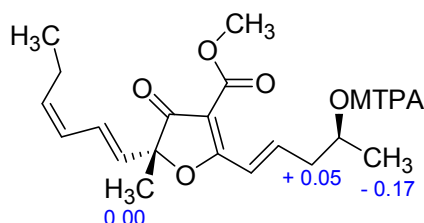


Figure 4. $\Delta\delta^{SR}$ values (ppm) for the C-4'' MTPA esters of Compound **4**.

Metabolite **6** was also obtained as a brown gum. Its HRESIMS exhibited an ion cluster at m/z 228.1018 $[\text{M} + \text{H}]^+$ corresponding to the molecular formula $\text{C}_{14}\text{H}_{13}\text{NO}_2^+$ (calcd. for $\text{C}_{14}\text{H}_{14}\text{NO}_2^+$: 228.1019). The UV spectrum displayed strong absorptions at 218, 246, and 336 nm. Its ^1H -NMR spectrum showed four signals at δ_H 7.83 (dd, $J = 8.1$ Hz, 1.6 Hz, H-6), 7.25 (ddd, $J = 8.5$ Hz, 7.0 Hz, 1.6 Hz, H-4), 6.77 (dd, $J = 8.3$ Hz, 1.0 Hz, H-3), and 6.60 (ddd, $J = 8.1$ Hz, 7.1 Hz, 1.1 Hz, H-5), indicating the presence of a system of four vicinal aromatic protons. The presence of the phenylmethyl (benzyl) moiety instead of a phenylethyl group as in Metabolite **5** was evidenced by a two protons singlet located at δ_H 5.31 (H-7') and five aromatic protons at δ_H 7.44 (dd, $J = 8.0$ Hz, 0.9 Hz, H-2' and H-6'), 7.38 (td, $J = 7.1$ Hz, 1.6 Hz, H-3' and H-5'), and 7.31 (m, H-4') (Table 2). Comparison of the ^1H - and ^{13}C -NMR/DEPT data of **6** with those of **5** indicated that the structures of these two compounds are very similar, except the absence of the hydroxyl group at C-3 in **6** and the substitution of the phenylethyl group by the benzyl moiety. This was confirmed by a comprehensive analysis of the 2D-NMR data, particularly ^1H - ^1H COSY, HSQC, and HMBC spectra. The HMBC correlation depicted between the benzylic proton at δ_H 5.31 (H-7') and the carbon at δ_C 169.3 (C-7) further confirmed the structure (Figure 5). Consequently, Compound **6** was elucidated as phenylmethyl anthranilate. Although it was previously reported as a synthetic compound with a fish anesthetic effect [12], this is the first report on its isolation from the natural source to the best of our knowledge. Furthermore, its NMR data have not yet been reported.

Compound **7** was isolated as a brown gum with the molecular formula $\text{C}_{12}\text{H}_{17}\text{NO}_3$ deduced from the HRESIMS which exhibited ion clusters $[\text{M} + \text{H}]^+$ at m/z 224.1279 (calcd. for $\text{C}_{12}\text{H}_{18}\text{NO}_3^+$: 224.1281) and $[\text{M} + \text{Na}]^+$ at 246.1098 (calcd. for $\text{C}_{12}\text{H}_{17}\text{NO}_3\text{Na}^+$: 246.1101). Its UV spectrum showed absorptions at 218, 255, and 334 nm. Detailed analysis of the ^1H - and ^{13}C -NMR spectra, DEPT as well as 2D-NMR data of **7** suggested that the molecule might possess the same anthranilic acid moiety as Compound **6**. This was further supported by the aromatic proton connectivities (H-3/H-4/H-5/H-6) observed in the ^1H - ^1H COSY spectrum and the HMBC correlations from H-6 (δ_H 7.81) to C-1 (δ_C 112.3), C-2 (δ_C 151.9), and C-7 and from H-3 (δ_H 6.78) to carbons C-1 (δ_C 112.3) and C-2 (δ_C 151.9) (Figure 5). The remaining proton signals were those of two methylenes at δ_H 1.94 (t, $J = 7.0$ Hz, H-2') and 4.41 (t, $J = 7.0$ Hz, H-1') and a singlet integrating for six protons at δ_H 1.28 (s). The ^{13}C -NMR and DEPT spectra of this part revealed signals for two symmetrical methyl groups at δ_C 29.8 (C-5' and C-6'), an oxygenated quaternary carbon at δ_C 70.6 (C-3'), two methylenes including an oxygen-bearing one at δ_C 62.4 (C-1') (Table 2). The HMBC correlation from H-4'/H-5' (δ_H 1.28) to carbons C-3' (δ_C 70.6) and C-2' (δ_C 43.0), then from H-1' (δ_H 4.41) to C-3' (δ_C 70.6) and C-2' (δ_C 43.0) confirmed the residue to be 3-hydroxy-3-methylbutyl (Figure 5). Furthermore, the HMBC correlation observed between the

oxymethylene protons at δ_{H} 4.41 (H-1') and the anthranilic acid carbonyl proved the structure of **7** to be the previously undescribed 3-hydroxy-3-methylbutyl anthranilate.

From spectroscopic analysis and by comparison with literature data, Compounds **1** and **2** were identified to massarilactone D [13] and massarilactone H [14], respectively. Ethyl anthranilate **8** was previously detected by GC-MS as one of the aroma-active compounds in Pinot Noir wines [15], while 2-phenylethyl anthranilate (**9**) is a fragrance ingredient present in the essential oils from the leaves of *Cinnamomum zeylanicum* Blume collected in India [16]. As far as we know, their ^1H - and ^{13}C -NMR data are reported in the present work for the first time (Table S2). The ^1H - and ^{13}C -NMR data of Compounds **10–12** were in agreement with those reported in the literature for cyclo-(L-pro-L-isoleu) [17], cyclo-(L-pro-L-leu) [17,18] and cyclo-(L-pro-L-phe) [18], respectively.

Table 2. ^{13}C - and ^1H -NMR spectroscopic data of Compounds **5–7** in CD_3OD .

Position	5 ^a		6 ^a		7 ^c	
	δ_{C}	δ_{H} (J in Hz)	δ_{C}	δ_{H} (J in Hz)	δ_{C}	δ_{H} (J in Hz)
1	115.0, C	/	111.7, C	/	112.3, C	/
2	137.5, C	/	152.5, C	/	151.9, C	/
3	147.8, C	/	118.2, CH	6.77, dd (8.3, 1.0)	118.4, CH	6.78, dd (8.3, 1.0)
4	119.5, CH	6.90, dd (7.8, 1.4)	135.4, CH	7.25, ddd (8.5, 7.0, 1.6)	135.2, CH	7.26, ddd (8.5, 7.1, 1.6)
5	119.0, CH	6.66, t (7.9)	117.2, CH	6.60, ddd (8.1, 7.1, 1.1)	117.5, CH	6.62, ddd (8.2, 7.1, 1.1)
6	122.8, CH	7.35, dd (8.1, 1.4)	132.2, CH	7.83, dd (8.1, 1.6)	132.2, CH	7.81, dd (8.1, 1.6)
7	169.2, C	/	169.3, C	/	169.6, C	/
1'	139.7, C	/	138.2, C	/	62.4, CH ₂	4.41, t (7.0)
2'	130.2, CH	7.30, m ^b	129.2, CH	7.44, dd (8.0, 0.9)	43.0, CH ₂	1.94, t (7.0)
3'	129.7, CH	7.30, m ^b	129.7, CH	7.38, td (7.1, 1.6)	70.6, C	/
4'	127.7, CH	7.22, m	129.3, CH	7.31, m	29.8, CH ₃	1.28, s
5'	129.7, CH	7.30, m ^b	129.7, CH	7.38, td (7.1, 1.6)	29.8, CH ₃	1.28, s
6'	130.2, CH	7.30, m ^b	129.2, CH	7.44, dd (8.0, 0.9)		
7'	36.3, CH ₂	3.06, t (6.9)	67.1, CH ₂	5.31, s		
8'	66.5, CH ₂	4.48, t (6.9)				

^a 175 and 700 MHz, resp.; ^b Overlapped; ^c 125 and 500 MHz, resp.

Since the crude extracts showed prominent antimicrobial activity, the isolated metabolites were screened against various bacteria and fungi. The minimum inhibitory concentration (MIC) values showed that only the new Metabolite **5** and Compound **9** were active, whereas the remaining compounds were inactive against the organisms tested (Table 3). Compound **5** showed the strongest activity against *Bacillus subtilis* and *Micrococcus luteus* with MIC values of 8.33 and 16.66 $\mu\text{g}/\text{mL}$, respectively, while the MIC value of Compound **9** against *Mucor hiemalis* (16.66 $\mu\text{g}/\text{mL}$) was the same as that of nystatin used as positive control. The two active metabolites are anthranilic acid derivatives with a phenylethyl core. Since Metabolite **6**, which contains a phenylmethyl group instead of a phenylethyl residue, was not active, it was concluded that the phenylethyl moiety in Compounds **5** and **9** is essential for their antimicrobial activity. Furthermore, the ability of some of the isolated compounds to inhibit the proliferation of two mammalian cell lines including HeLa cells KB3.1 and mouse fibroblasts L929 was examined. Only 2-phenylethyl anthranilate (**9**) showed moderate cytotoxic activity against HeLa cells KB3.1 with an IC_{50} value of 8.8 $\mu\text{g}/\text{mL}$ (Table 4).

Table 3. MIC [$\mu\text{g}/\text{mL}$] values of Compounds 1, 2, 4–12 against the tested microorganisms.

Test Organism	MIC ($\mu\text{g}/\text{mL}$)											References
	1	2	4	5	6	7	8	9	10	11	12	
<i>Schizosaccharomyces pombe</i> DSM 70572	n.a.	n.a.	n.a.	n.a.	n.a.	n.a.	n.a.	n.a.	n.a.	n.a.	n.a.	16.66 ⁿ
<i>Pichia anomala</i> DSM 6766	n.a.	n.a.	n.a.	n.a.	n.a.	n.a.	n.a.	n.a.	n.a.	n.a.	n.a.	8.33 ⁿ
<i>Mucor hiemalis</i> DSM 2656	n.a.	n.a.	n.a.	33.33	n.a.	n.a.	n.a.	16.66	n.a.	n.a.	n.a.	16.66 ⁿ
<i>Candida albicans</i> DSM 1665	n.a.	n.a.	n.a.	n.a.	n.a.	n.a.	n.a.	n.a.	n.a.	n.a.	n.a.	16.66 ⁿ
<i>Rhodoturula glutinis</i> DSM 10134	n.a.	n.a.	n.a.	66.67	n.a.	n.a.	n.a.	33.33	n.a.	n.a.	n.a.	2.08 ⁿ
<i>Micrococcus luteus</i> DSM 1790	n.a.	n.a.	n.a.	16.66	n.a.	n.a.	n.a.	n.a.	n.a.	n.a.	n.a.	0.40 ^o
<i>Bacillus subtilis</i> DSM 10	n.a.	n.a.	n.a.	8.33	n.a.	n.a.	n.a.	66.67	n.a.	n.a.	n.a.	4.16 ^o
<i>Escherichia coli</i> DSM 1116	n.a.	n.a.	n.a.	n.a.	n.a.	n.a.	n.a.	n.a.	n.a.	n.a.	n.a.	3.33 ^o
<i>Staphylococcus aureus</i> DSM 346	n.a.	n.a.	n.a.	66.67	n.a.	n.a.	n.a.	66.67	n.a.	n.a.	n.a.	0.10 ^o
<i>Mycobacterium smegmatis</i> DSM ATCC 700084	n.a.	n.a.	n.a.	n.a.	n.a.	n.a.	n.a.	n.a.	n.a.	n.a.	n.a.	2.08 ^k
<i>Chromobacterium violaceum</i> DSM 30191	n.a.	n.a.	n.a.	n.a.	n.a.	n.a.	n.a.	n.a.	n.a.	n.a.	n.a.	0.40 ^o
<i>Pseudomonas aeruginosa</i> DSM PA14	n.a.	n.a.	n.a.	n.a.	n.a.	n.a.	n.a.	n.a.	n.a.	n.a.	n.a.	0.52 ^g

n.a.: No Activity, ^g Gentamycin 1 mg/mL, ^k Kanamycin 10 mg/mL, ⁿ Nystatin 1 mg/mL, ^o Oxytetracyclin 1 mg/mL.

Table 4. Cytotoxic effect (IC_{50}) of Compounds 1, 2, and 4–12 against two cancer cell lines.

Cell Line	IC_{50} ($\mu\text{g}/\text{mL}$)											IC_{50} (ng/mL)
	1	2	4	5	6	7	8	9	10	11	12	Epithilone B
KB3.1	n.a.	n.a.	18	18	n.a.	n.a.	n.a.	8.8	n.a.	n.a.	n.a.	0.052
L929	n.a.	n.a.	19	no	n.a.	n.a.	n.a.	n.o.	n.a.	n.a.	n.a.	1.4

n.a.: Not active; no: IC_{50} not obtained.

3. Materials and Methods

3.1. General Experimental Procedures

Optical rotations were determined with a Perkin Elmer (Überlingen, Germany) 241 MC polarimeter (using the sodium D line and a quartz cuvette with a 10 cm path length and 0.5 mL volume). CD spectra were recorded on a JASCO spectropolarimeter, model J-815 (JASCO, Pfungstadt, Germany). NMR spectra were recorded on a Bruker (Bremen, Germany) 500 MHz Avance III spectrometer with a BBFO (plus) SmartProbe (^1H 500 MHz, ^{13}C 125 MHz) and a Bruker 700 MHz Avance III spectrometer with a 5 mm TCI cryoprobe (^1H 700 MHz, ^{13}C 175 MHz), locked to the deuterium signal of the solvent. Chemical shifts are given in parts per million (ppm), and coupling constants in hertz (Hz). Spectra were measured in methanol- d_4 and deuterated chloroform; chemical shifts were referenced to the solvent signals. HPLCAD MS analysis was performed using an amaZon speed ETD ion trap mass spectrometer (Bruker Daltonics) in positive and negative ionization modes. The mass spectrometer was coupled to an Agilent 1260 series HPLC-UV system (Agilent Technologies) (Santa Clara, CA, USA) [column 2.1×50 mm, $1.7 \mu\text{m}$, C18 Acquity uPLC BEH (Waters), solvent A: H_2O + 0.1% formic acid; solvent B: acetonitrile (ACN) + 0.1% formic acid, gradient: 5% B for 0.5 min, increasing to 100% B in 20 min, maintaining isocratic conditions at 100% B for 10 min, flow = 0.6 mL/min, UV-vis detection 200–600 nm]. HRESIMS spectra were recorded on a maXis ESI TOF mass spectrometer (Bruker Daltonics) [scan range m/z 100–2500, rate 2 Hz, capillary voltage 4500 V, dry temperature 200 °C], coupled to an Agilent 1200 series HPLC-UV system [column 2.1×50 mm, $1.7 \mu\text{m}$, C18 Acquity uPLC BEH (Waters), solvent A: H_2O + 0.1% formic acid; solvent B: ACN + 0.1% formic acid, gradient: 5% B for 0.5 min, increasing to 100% B in 19.5 min, maintaining 100% B for 5 min, FR = 0.6 mL/min, UV-vis detection 200–600 nm]. The molecular formulas were calculated including the isotopic pattern (Smart Formula algorithm). Preparative HPLC purification was performed at room temperature on an Agilent 1100 series preparative HPLC system [ChemStation software (Rev. B.04.03 SP1); binary pump system; column: Kinetex 5u RP C18, dimensions 250×21.20 mm; mobile phase: ACN + 0.05%

trifluoroacetic acid (TFA) and water + 0.05% TFA; flow rate 20 mL/min; diode-array UV detector; 226 fraction collector].

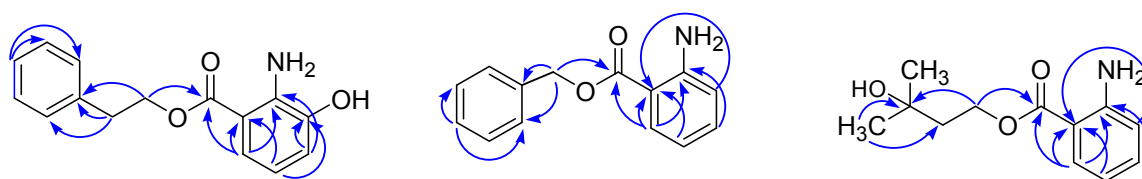


Figure 5. Selected HMBC correlations for Compounds 5–7.

3.2. Fungal Material

The endophytic fungus *Dendrothyrium variisporum* was isolated from fresh healthy roots of *Globularia alypum* Linn. (Plantaginaceae). The plant samples were collected in June 2015 from Ain Touta, Batna 05000 (Algeria). The isolation of the endophyte was achieved following a previously reported method [19,20]. Genomic DNA was extracted from fungal colonies growing on YMG using the EZ-10 Spin Column Genomic DNA Miniprep kit (Bio Basic Canada Inc., Markham, Ontario, Canada) following the manufacturer's protocol. The internal transcribed spacer (ITS) regions including the 3'-end of 18S rRNA gene, 5.8S rRNA gene, and the 5'-end of the 28S rRNA gene were amplified using ITS1F/ITS4 primer [21]. The ITS sequence of the endophytic fungus was deposited with GenBank under the accession number MG018984. The producer organism was identified as *Dendrothyrium variisporum* on the basis of ITS sequencing and morphology (see Supporting Information).

3.3. Fermentation and Extraction

For fermentation in flasks, the submerged culture were raised in 30 × 500 mL Erlenmeyer flasks, each containing 200 mL of YMG medium: 1.0% malt extract, 0.4% glucose, 0.4% yeast extract, pH 6.3 [20]. The flasks were inoculated with five mycelial plugs from actively growing yeast-malt-glucose-agar (YMG) plates and incubated at 23 °C under constant shaking at 140 rpm on a rotary shaker for 12 days. After separation from fungal mycelia by vacuum filtration, the supernatant was treated with 2% (v/v) of Amberlite XAD-16 resin. The latter was extracted with acetone by sonication at 40 °C for 30 min. The acetone extract was evaporated in vacuo, and the residual aqueous solution was re-extracted with EtOAc. The ethyl acetate extract was dried on Na₂SO₄ and concentrated by evaporation to yield 1.4 g of crude extract.

For the scale up, a seed culture of the strain with a total volume of 1000 mL was prepared in YMG medium incubated at 23 °C and 140 rpm for 5 days and homogenized with a Heidolph Silent Crusher. A 15 L in-situ autoclavable bioreactor (bbi Germany) was prepared with 10 L of YMG medium and inoculated with 1000 mL of the seed culture. The temperature was set at 23 °C, agitation with a Rushton-impeller was set to 150 rpm, and the aeration rate was set to 1.5 L/min (0.15 vvm) and remained constant during fermentation. The culture was harvested after 8 days as the glucose was depleted, and a stagnation of secondary metabolite production was observed by analytical HPLC. The mycelium was separated from the culture fluid (supernatant) by centrifugation in a Dupont Instrument (Sorvall RC-5B Refrigerated Superspeed Centrifuge) followed by vacuum filtration and was extracted three times with acetone, then with methanol in an ultrasonic bath at 40 °C for 30 min. The acetone and methanol extracts were filtered, combined and evaporated to yield an aqueous phase, which was further extracted with 3 × 500 mL EtOAc in a separating funnel. The ethyl acetate fraction was dried over anhydrous Na₂SO₄, filtered, and concentrated under vacuum to yield 373.7 mg of oily mycelial crude extract. The supernatant was treated with 2% adsorber resin Amberlite XAD-16 resin over 2 h at room temperature. The XAD was separated by filtration and extracted three times with acetone, then with methanol in an ultrasonic bath at 40 °C for 30 min. The extract was evaporated to yield an aqueous phase, which was further extracted with ethyl acetate (3 × 500 mL). After drying

over anhydrous Na₂SO₄, the ethyl acetate fraction was concentrated under vacuum to yield 508.2 mg of crude extract.

3.4. Isolation of Compounds 1–12

The crude supernatant extract from the fermentation in flasks (858.7 mg) was subjected to flash chromatography (GRACE Reveleris X2 flash system) with silica gel (40 g) as stationary phase. The column was eluted with the mixture of CH₂Cl₂ (solvent A) and acetone (solvent B); gradient: 100% A in 5 min, 0–100% B in 35 min, and finally 100% B for 5 min; flow rate: 40 mL/min; UV detection: 254, 280, and 380 nm. Three fractions were collected: Fraction 1 (32.4 mg, *t*_R = 8.5–10.1 min), Fraction 2 (32.0 mg, *t*_R = 11.5–13.5 min) and Fraction 3 (708.7 mg, *t*_R = 14.5–17.1 min), which was pure massarilactone D 1. Fraction 1 was further purified by preparative HPLC using a gradient of 25–60% solvent B in 40 min, 60–100% B for 5 min, and 100% B for 5 min. The fractions were combined according to UV absorption at 220, 280, and 325 nm and concurrent HPLC-MS analyses. Compound 3 (0.4 mg) was eluted at *t*_R = 12.80 min, and Compound 4 (1.8 mg) was eluted at *t*_R = 9.30 min. Fraction 2 was purified using the same preparative HPLC conditions as for Fraction 1 to yield Compound 2 (9.1 mg) at *t*_R = 5.88 min.

The mycelial extract from the bioreactor (373.7 mg) was purified by preparative HPLC (3 runs) using a gradient of 45–80% solvent B in 40 min, 80–100% B for 10 min, and 100% B for 10 min. The fractions were combined according to UV absorption at 220, 240, and 342 nm and concurrent HPLC-MS analyses. Compounds 5 (1.7 mg, *t*_R = 11.11 min), 6 (1.6 mg, *t*_R = 15.96 min), and 9 (6.1 mg, *t*_R = 17.50 min) were obtained. The supernatant extract from the bioreactor (508.2 mg) was submitted to preparative HPLC (4 runs) using a gradient of 15–55% solvent B in 40 min, 55–100% B for 10 min, and 100% B for 10 min (UV absorption at 220, 240, and 342 nm) to yield Compounds 1 (53.6 mg, *t*_R = 5.76 min), 7 (3.8 mg, *t*_R = 20.87 min), 9 (3.7 mg, *t*_R = 44.18 min), 10 (16.4 mg, *t*_R = 7.22 min), 11 (24.7 mg, *t*_R = 8.12 min), and 12 (7.8 mg, *t*_R = 9.77 min).

(5*S*) *cis*-gregatin B (3): colorless oil; [α]_D²⁵ −36.67 (*c* 0.0006, CHCl₃); UV (*c* 0.5 mg/mL, EtOH) λ_{\max} 220, 265 nm; CD (*c* 0.5 mg/mL, EtOH) λ_{\max} 260 (+) nm; HRESIMS *m/z* 251.1276 [M + H]⁺ (calcd. for C₁₄H₁₉O₄⁺, 251.1278); ¹H-NMR (CDCl₃, 700 MHz) and ¹³C-NMR (CDCl₃, 175 MHz) data: see Table 1.

Graminin D (4): colorless oil; [α]_D²⁵ +49.55 (*c* 0.001, CHCl₃); UV (*c* 1 mg/mL, EtOH) λ_{\max} 216, 255, 310 nm; CD (*c* 1 mg/mL, EtOH) λ_{\max} 260 (−) nm; HRESIMS *m/z* 321.1690 [M + H]⁺ (calcd. for C₁₈H₂₅O₅⁺, 321.1697); ¹H-NMR (CDCl₃, 700 MHz) and ¹³C-NMR (CDCl₃, 175 MHz) data: see Table 1.

2-Phenylethyl 3-hydroxyanthranilate (5): brown gum; UV λ_{\max} 226, 260, 342 nm; HRESIMS *m/z* 258.1128 [M + H]⁺ (calcd. for C₁₅H₁₆NO₃⁺, 258.1125), 280.0946 [M + Na]⁺ (calcd. for C₁₅H₁₅NNaO₃⁺, 280.0944); ¹H-NMR (CD₃OD, 700 MHz) and ¹³C-NMR (CD₃OD, 175 MHz) data: see Table 2.

Phenylmethyl anthranilate (6): brown gum; UV λ_{\max} 218, 246, 336 nm; HRESIMS *m/z* 228.1016 [M + H]⁺ (calcd. for C₁₄H₁₄NO₂⁺, 228.1019) ¹H-NMR (CD₃OD, 700 MHz) and ¹³C-NMR (CD₃OD, 175 MHz) data: see Table 2.

3-Hydroxy-3-methylbutyl anthranilate (7): brown gum; UV λ_{\max} 218, 255, 334 nm; HRESIMS *m/z* 224.1279 [M + H]⁺ (calcd. for C₁₂H₁₈NO₃⁺, 224.1281), 246.1098 [M + Na]⁺ (calcd. for C₁₂H₁₇NaNO₃⁺, 246.1101); ¹H-NMR (CD₃OD, 500 MHz) and ¹³C-NMR (CD₃OD, 125 MHz) data: see Table 2.

3.5. Preparation of the S- and R-MTPA Esters of 4

R(−)-MTPA-Cl (4 μ L) was added to a stirred solution of 4 (0.2 mg) and dry pyridine (5 μ L) in dry CDCl₃ (100 μ L) at room temperature. After 1 h, the reaction mixture was diluted by the addition of 100 μ L of CDCl₃. The produced S-MTPA ester of 4 was submitted to NMR spectroscopy. In an entirely

analogous fashion, the *R*-MTPA ester of **4** was prepared using *S*-(+)-MTPA-Cl. The ¹H-NMR data of the *R* and *S* derivatives are presented in the supporting information (Table S2).

3.6. Biological Activities

The MIC and the in vitro cytotoxicity (IC₅₀) were determined according to our previously reported procedures [2,22,23]. Briefly, minimum inhibitory concentrations (MICs) in µg/mL of the isolated compounds were determined by serial dilution assay against *Schizosaccharomyces pombe* DSM 70572, *Pichia anomala* DSM 6766, *Mucor hiemalis* DSM 2656, *Candida albicans* DSM 1665, *Rhodoturula glutinis* DSM 10134, *Micrococcus luteus* DSM 1790, *Bacillus subtilis* DSM 10, *Escherichia coli* DSM 1116, *Staphylococcus aureus* DSM 346, *Mycobacterium smegmatis* DSM ATCC 700084, *Chromobacterium violaceum* DSM 30191, and *Pseudomonas aeruginosa* DSM PA14. The assays were carried out in 96-well microtiter plates in YMG media for filamentous fungi and yeast and EBS for bacteria. Gentamycin, kanamycin, nystatin, and oxytetracyclin were used as positive control, and the negative control was methanol. The cytotoxicity against HeLa cells KB3.1 and mouse fibroblasts L929 cells was determined by using the MTT (2-(4,5-dimethylthiazol-2-yl)-2,5-diphenyltetrazolium bromide) method in 96-well microplates. The cell lines were cultured in DMEM (Gibco). Briefly, 60 µL aliquots of serial dilutions from an initial stock of 1 mg/mL in MeOH of the test compounds were added to 120 µL aliquots of a cell suspension (5 × 10⁴ cells/mL) in 96-well microplates. After 5 days incubation, an MTT assay was performed, and the absorbance measured at 590 nm using an ELISA plate reader (Victor). The concentration at which the growth of cells was inhibited to 50% of the control (IC₅₀) was obtained from the dose–response curves. Epothilone B was used as a positive control, while methanol was used as a negative control.

4. Conclusions

During the course of our studies on endophytic strains derived from plants collected in Algeria for the discovery of new antibiotics, 12 metabolites, including five new compounds, were isolated from the fungus *Dendrothyrium variisporum* harbored in *Globularia alypum* Linn. (Plantaginaceae). The anthranilic acid derivatives **5** and **9** exhibited antimicrobial activity, whereas the remaining compounds were inactive against the organisms tested.

Supplementary Materials: The description of the producer organism, LC-MS spectra, HRESIMS, ¹H- and ¹³C-NMR, ¹H-¹H COSY, HSQC, and HMBC spectra are available as Supplementary Material.

Acknowledgments: R.B.T. and S.E.H. are grateful for financial support from the Alexander von Humboldt Foundation. S.R.N. acknowledges the Ministry of Higher Education and Scientific Research (MESRS) of Algeria for the financial support. We thank Heitkämper S. for technical assistance, Collisi W. for conducting the bioassays, Kakoschke C. for recording NMR spectra and Karwehl S. for HRESIMS measurements.

Author Contributions: R.B.T. contributed to fermentation, isolation of compounds, structure elucidation, and manuscript writing; S.R.N. contributed to fungal specimen collection, species identification, fermentation, isolation of some compounds, and manuscript writing; S.E.H. contributed to guiding the experiments, structure elucidation, and manuscript preparation; S.E.H. contributed to the scaling-up of fermentation; D.H. contributed to fungal specimen collection and species identification; M.S. contributed to the selection of the producer strain and its characterisation and edited the subfinal manuscript.

Conflicts of Interest: The authors declare no conflict of interest.

References

1. Karwehl, S.; Stadler, M. Exploitation of fungal biodiversity for discovery of novel antibiotics. *Curr. Top. Microbiol. Immunol.* **2016**, *398*, 303–338. [PubMed]
2. Noumeur, S.R.; Helaly, S.E.; Jansen, R.; Gereke, M.; Stradal, T.E.B.; Harzallah, D.; Stadler, M. Preussilides A–F, bicyclic polyketides from the endophytic fungus *Preussia similis* with antiproliferative activity. *J. Nat. Prod.* **2017**, *80*, 1531–1540. [CrossRef] [PubMed]
3. Verkley, G.J.M.; Dukik, K.; Renfurm, R.; Göker, M.; Stielow, J.B. Novel genera and species of the coniothyrium-like fungi in Montagnulaceae (Ascomycota). *Persoonia* **2014**, *32*, 25–51. [CrossRef] [PubMed]

4. Chepkirui, C.; Richter, C.; Matasyoh, J.C.; Stadler, M. Monochlorinated calocerins A–D and 9-oxostrobilurin derivatives from the basidiomycete *Favolaschia calocera*. *Phytochemistry* **2016**, *132*, 95–101. [[CrossRef](#)] [[PubMed](#)]
5. Almeida, C.; El Aouad, N.; Martín, J.; Perez-Victoria, I.; Gonzalez-Menendez, V.; Platas, G.; De la Cruz, M.; Monteiro, M.C.; De Pedro, N.; Bills, G.F.; et al. Graminin B, a furanone from the fungus *Paraconiothyrium* sp. *J. Antibiot.* **2014**, *67*, 421–423. [[CrossRef](#)] [[PubMed](#)]
6. Wijeratne, E.M.K.; Xu, Y.; Arnold, A.E.; Gunatilaka, A.A.L. Graminin C, and *cis*-Gregatin B–New natural furanones from *Pulvinula* sp. 11120, a fungal endophyte of *Cupressus arizonica*. *Nat. Prod. Commun.* **2015**, *10*, 107–111. [[PubMed](#)]
7. Tang, H.-Y.; Zhang, Q.; Gao, Y.-Q.; Zhang, A.-L.; Gao, J.-M. Miniolins A–C, novel isomeric furanones induced by epigenetic manipulation of *Penicillium minioluteum*. *RSC Adv.* **2015**, *5*, 2185–2190. [[CrossRef](#)]
8. Hoye, T. R.; Jeffrey, C. S.; Shao, F. Mosher ester analysis for the determination of absolute configuration of stereogenic (chiral) carbinol carbons. *Nat. Protoc.* **2007**, *2*, 2451–2458. [[CrossRef](#)] [[PubMed](#)]
9. Burghart-Stoll, H.; Brückner, R. Total syntheses of the gregatins A–D and aspertetrinin A: Structure revisions of these compounds and of aspertetrinin B, together with plausible structure revisions of gregatin E, cyclogregatin, graminin A, the penicilliolis A and B, and the huaspenones A and B. *Eur. J. Org. Chem.* **2012**, 3978–4017.
10. Li, C.-S.; Li, X.-M.; Gao, S.-S.; Lu, Y.-H.; Wang, B.-G. Cytotoxic anthranilic acid derivatives from deep sea sediment-derived fungus *Penicillium paneum* SD-44. *Mar. Drugs* **2013**, *11*, 3068–3076. [[CrossRef](#)] [[PubMed](#)]
11. Miltojević, A.B.; Radulović, N.S. Complete assignment of ¹H- and ¹³C-NMR spectra of anthranilic acid and its hydroxyl derivatives and salicylic acid and its amino derivatives. *FU Phys. Chem. Technol.* **2015**, *13*, 121–132. [[CrossRef](#)]
12. Hirata, M.; Isoda, S.; Kanao, M.; Shimizu, H.; Inoue, S. Anesthetics for fish. *Nippon Suisan Gakk.* **1970**, *36*, 1127–1135. [[CrossRef](#)]
13. Kock, I.; Krohn, K.; Egold, H.; Draeger, S.; Schulz, B.; Rheinheimer, J. New massarilactones, massarigenin E, and coniothyrenol, isolated from the endophytic fungus *Coniothyrium* sp. from *Carpobrotus edulis*. *Eur. J. Org. Chem.* **2007**, 2186–2190.
14. Zhang, G.F.; Han, W.B.; Cui, J.T.; Ng, S.W.; Guo, Z.K.; Tan, R.X.; Ge, H.M. Neuraminidase inhibitory polyketides from the marine-derived fungus *Phoma herbarum*. *Planta Med.* **2012**, *78*, 76–78. [[CrossRef](#)] [[PubMed](#)]
15. Fang, Y.; Qian, M.C. Quantification of selected aroma-active compounds in Pinot Noir wines from different grape maturities. *J. Agric. Food Chem.* **2006**, *54*, 8567–8573. [[CrossRef](#)] [[PubMed](#)]
16. Raina, V.K.; Srivastava, S.K.; Aggarwal, K.K.; Ramesh, S.; Kumar, S. Essential oil composition of *Cinnamomum zeylanicum* Blume leaves from Little Andaman, India. *Flavour Frag. J.* **2001**, *16*, 374–376. [[CrossRef](#)]
17. Ren, S.; Ma, W.; Xu, T.; Lin, X.; Yin, H.; Yang, B.; Zhou, X.-F.; Yang, X.-W.; Long, L.; Lee, K.J.; et al. Two novel alkaloids from the South China Sea marine sponge *Dysidea* sp. *J. Antibiot.* **2010**, *63*, 699–701. [[CrossRef](#)] [[PubMed](#)]
18. Sansinenea, E.; Salazar, F.; Jiménez, J.; Mendoza, A.; Ortiz, A. Diketopiperazines derivatives isolated from *Bacillus thuringiensis* and *Bacillus endophyticus*, establishment of their configuration by X-ray and their synthesis. *Tetrahedron Lett.* **2016**, *57*, 2604–2607. [[CrossRef](#)]
19. Kusari, S.; Lamshöft, M.; Zühlke, S.; Spittler, M. An endophytic fungus from *Hypericum perforatum* that produces hypericin. *J. Nat. Prod.* **2008**, *71*, 159–162. [[CrossRef](#)] [[PubMed](#)]
20. Richter, C.; Helaly, S.E.; Thongbai, B.; Hyde, K.D.; Stadler, M. Pyristriatins A and B: Pyridino-cyathane antibiotics from the basidiomycete *Cyathus cf. striatus*. *J. Nat. Prod.* **2016**, *79*, 1684–1688. [[CrossRef](#)] [[PubMed](#)]
21. White, T.J.; Bruns, T.D.; Lee, S.B.; Taylor, J.W. Amplification and direct sequencing of fungal ribosomal RNA genes for phylogenetics. In *PCR Protocols: A Guide to Methods and Applications*; Innis, M.A., Gelfand, D.H., Sninsky, J.J., White, T.J., Eds.; Academic Press: New York, NY, USA, 1990; pp. 315–322.

22. Sudarman, E.; Kuhnert, E.; Hyde, K.D.; Esteban Benjamin Sir, E.B.; Surup, F.; Stadler, M. Truncatones A–D, benzo[*j*]fluoranthenes from *Annulohyphoxylon* species (Xylariaceae, Ascomycota). *Tetrahedron* **2016**, *72*, 6450–6454. [[CrossRef](#)]
23. Wittstein, K.; Rascher, M.; Rupcic, Z.; Löwen, E.; Winter, B.; Köster, R.W.; Stadler, M. Corallocins A–C, Nerve growth and brain-derived neurotrophic factor inducing metabolites from the Mushroom *Hericium coralloides*. *J. Nat. Prod.* **2016**, *79*, 2264–2269. [[CrossRef](#)] [[PubMed](#)]

Sample Availability: Samples of the compounds **1**, **2**, **10–12** are available from the authors.



© 2017 by the authors. Licensee MDPI, Basel, Switzerland. This article is an open access article distributed under the terms and conditions of the Creative Commons Attribution (CC BY) license (<http://creativecommons.org/licenses/by/4.0/>).

ملخص

تعتبر الفطريات الداخلية مصدرا غنيا بالمركبات الطبيعية اكتسبتها من خلال العلاقة التكافئية بينها وبين النبات العائل، تم خلال هذه الدراسة معرفة التنوع البيولوجي للفطريات الداخلية المعزولة من جذور نبتة *Globularia alypum* (Plantaginaceae, Scrophulariales) التي تم جمعها من ولاية باتنة (الجزائر). أدت الدراسة الى عزل 17 سلالة فطرية والتي عرفت إلى مستوى النوع باستخدام خصائص مورفولوجية وتحليل النشوء والتطور حيث مكنت هذه الأخيرة إلى انتماء الفطريات المعزولة إلى ثلاث فئات في شعبة Ascomycota: Eurotiomycetes، Dothideomycetes و Sordariomycetes و المتمثلة في تسعة أجناس: *Aspergillus*، *Alternaria*، *Chaetomium*، *Dendrothyrium*، *Diaporthe*، *Fusarium*، *Macrophomina*، *Penicillium* و *Preussia*. تم اختيار من بين الفطريات المعزولة ثمانية للتخمير على نطاق صغير في ثلاثة اوساط غذائية مختلفة. أثبتت المستخلصات المتحصل عليها نشاطا ضد ميكروبيبا. بعدها تم تخمير خمسة فطريات: ثلاث سلالات من *Preussia similis*، *Dendrothyrium variisporum* و *Chaetomium madrasense* على نطاق اكبر. أدى هذا التخمير إلى عزل 28 مستقلب ثانوي من بينها 12 مركبا جديدا. تم التعرف على صيغة المركبات الكيميائية المعزولة بواسطة طرق طيفية 1D و 2D NMR spectroscopy، high-resolution mass spectrometry و CD spectroscopy. درست النشاطات البيولوجية للمركبات المعزولة سواء الجديدة منها أو المعروفة بشكل واسع. تم عزل 13 مركب من المعقد *Preussia similis* من بينها ستة مركبات جديدة: بوليكتايد ثنائية الحلقة تم تسميتها A-F preussilides ومركب جديد dimer of 2-amino benzoid acid moieties بالإضافة إلى مركبات أخرى معروفة مثل الساييتوكالازين ومشتقات الغزانتون. أظهرت A و C preussilide و C preussilide في اختبار A-F preussilides نشاطا مثبطا انتقائيا ضد حقيقيات النواة، تأثيرا على مورفولوجيا خلايا سرطان العظام. كما يستهدف هذا البوليكيتايد إنزيم مسؤول على تنسيق دورة إنقسام الخلايا. أسفرت الدراسات التي أجريت على انتاج المستقلبات الثانوية من فطر *Dendrothyrium variisporum* عن عزل 12 مركب، منها H و D Massarilactones كمركيين رئيسيين و 2 من المشتقات الجديدة للفيرانون التي تم تسميتها B (5S)-cis-gregatin و D graminin بالإضافة إلى 3 مشتقات جديدة من حمض الأونتراليك، اثنين من نظائر حمض الأونتراليك المعروفة وثلاثة سيكلوبيبتيدس. أظهرت تجارب النشاط ضد ميكروبي أن للمركبين 2-phenylethyl-3-hydroxyanthranilate و 2-phenylethylanthranilate نشاطية تثبيطية ضد ميكروبية واسعة، في حين اظهر المركب تثبيطه لتكاثر الخلايا السرطانية HeLa. أخيرا تم عزل 3 مركبات معروفة من *Chaetomium madrasense*: A1، A3 xanthoquinodins و N-acetytryptamin.

كلمات مفتاحية: الفطريات الداخلية، التنوع البيولوجي، المستقلبات الثانوية، تعريف الصيغة الكيميائية، *Chaetomium madrasense*، *Preussia similis*، *Dendrothyrium variisporum*.

Abstract

The endophytic mycobiota constitute a prolific source of bioactive natural products that has evolved during the symbiotic endophyte-plant relationship. The diversity of fungal endophytes isolated from the roots of the plant *Globularia alypum* (Plantaginaceae, Scrophulariales) collected in Batna (Algeria) were studied in the present thesis. In total, seventeen fungal strains were isolated and identified to species level by means of morphological and molecular phylogenetic methods. The phylogenetic analysis of these fungal endophytes revealed their affinities to three classes of the phylum of Ascomycota: Eurotiomycetes, Dothideomycetes and Sordariomycetes representing nine genera: *Alternaria*, *Aspergillus*, *Chaetomium*, *Dendrothyrium*, *Diaporthe*, *Fusarium*, *Macrophomina*, *Penicillium* and *Preussia*. Among the isolated fungal endophytes, eight were selected for small scale fermentation in three different liquid media. Their extracts showed prominent antimicrobial activity in a screening for novel antibiotics by the serial dilution assay. A scale-up of fermentation of selected five fungi including three strains of *Chaetomium madrasense*, *Dendrothyrium variisporum* and *Preussia similis*, yielded twenty eight secondary metabolites, twelve of which turned out to be novel natural products. The structures of the isolated metabolites were elucidated using a combination of spectral methods, including 1D and 2D NMR spectroscopy, high-resolution mass spectrometry, and CD spectroscopy. The biological activities of both, the known and new compounds were extensively studied. Thirteen metabolites were isolated from the *Preussia similis* complex including six new bicyclic polyketides 1-6 (for which the trivial names preussilides A-F are proposed) and one new dimer of 2 amino benzoid acid moieties, along with several known cytochalasins and xanthenes derivatives. The preussilides were tested for antimicrobial and antiproliferative effects, and, in particular, preussilides A and C showed selective activities against eukaryotes. Subsequent studies on their influence on the morphology of human osteosarcoma cells (U2OS) suggest that these polyketides might target an enzyme involved in coordination of the cell division cycle. Hence, they might, for instance, affect timing or spindle assembly mechanisms, leading to defects in chromosome segregation and/or spindle geometry. Studies on the secondary metabolite production of *Dendrothyrium variisporum* in various culture media led to the isolation of twelve compounds. Massarilactones D and H were isolated as the major components as well as two new furanone derivatives for which we propose the trivial names (5S)-cis-gregatin B and graminin D, three new anthranilic acid derivatives, two known anthranilic acid analogues and three cyclopeptides. The new anthranilic acid derivatives, 2-phenylethyl-3-hydroxyanthranilate and 2-phenylethyl anthranilate exhibited antimicrobial activity while 2-phenylethyl anthranilate showed cytotoxicity against HeLa cells. Finally, from cultures of *Chaetomium madrasense*, three known compounds, xanthoquinodins A1, A3 and N-acetytryptamin were isolated.

Keywords: Fungal endophytes, biodiversity, *Globularia alypum*, secondary metabolites, *Preussia similis*, *Dendrothyrium variisporum* *Chaetomium madrasense*, structure elucidation.